

University of Alberta

Oxidation of 2-propanol in alkaline electrolytes using platinum and ruthenium-based catalysts:
prototype fuel cells and electrokinetics studies

by

Matthew Eugene Paul Markiewicz

A thesis submitted to the Faculty of Graduate Studies and Research
in partial fulfillment of the requirements for the degree of

Doctor of Philosophy

Department of Chemistry

©Matthew Eugene Paul Markiewicz
Fall 2011
Edmonton, Alberta

Permission is hereby granted to the University of Alberta Libraries to reproduce single copies of this thesis and to lend or sell such copies for private, scholarly or scientific research purposes only. Where the thesis is converted to, or otherwise made available in digital form, the University of Alberta will advise potential users of the thesis of these terms.

The author reserves all other publication and other rights in association with the copyright in the thesis and, except as herein before provided, neither the thesis nor any substantial portion thereof may be printed or otherwise reproduced in any material form whatsoever without the author's prior written permission.

Abstract

Alcohols are an attractive alternative to hydrogen fuel in fuel cells. They are energy dense, easy to store, transport, and they are readily available. Alkaline fuel cells have several kinetic advantages over acidic fuel cells, but they are sensitive to carbon dioxide. The fuel most studied in direct alcohol fuel cells is methanol. The oxidation of methanol, however, produces carbon dioxide that will gradually carbonate alkaline electrolytes, degrading their performance.

Investigations into the electrochemical oxidation of 2-propanol to acetone in alkaline electrolytes over platinum, platinum-ruthenium, and ruthenium catalysts were performed in three-electrode experiments. At the low anodic potentials that are required for efficient direct alcohol fuel cell, the oxidation of 2-propanol gives higher current densities than methanol over platinum. In contrast with the oxidation of methanol, which forms a stable carbon monoxide or similar surface poisoning intermediate, the oxidation of 2-propanol to acetone is believed to occur in the absence of a strongly adsorbed intermediate that hinders the reaction. Consistent with the behaviour in three-electrode experiments, prototype fuel cells operating on 2-propanol gave higher power densities than when operated on methanol, and they were also more stable.

The oxidation of 2-propanol at low potentials is enhanced by surface ruthenium. Multidimensional regression of the potential-temperature-current relationship found that ruthenium reduces the activation enthalpy by an amount consistent with hydrogen bonding (9 kJ mol^{-1}). A new transition state complex where an adsorbed oxygen species on ruthenium hydrogen bonds to the alcoholic proton of an intermediate formed during the oxidation of 2-propanol is proposed to account for this stabilization. This new mode of the bifunctional mechanism is believed to be responsible for the increased rate observed dur-

ing the oxidation of 2-propanol at low potentials using platinum-ruthenium catalysts.

In an operating fuel cell, ruthenium was found to increase the kinetics of the reaction and reduce its onset potential. Both these factors increase the power density of prototype alkaline direct 2-propanol fuel cells when a platinum-ruthenium anode is used as the catalysts compared to when platinum is used.

Acknowledgements

First, I would like to thank Prof. Steven Bergens for providing me with a challenging project, as well as for his advice and guidance throughout the course of my degree. I feel fortunate to have been given the opportunity to work side-by-side with the most amazing people during my time with the Bergens group; Dr. Robin Hamilton, Dr. Satoshi Takebayashi, Lise Menard, Andrew Sullivan, Mike Hass, Sonja Francis, Jeremy John, Elizabeth Corkum, and Suneth Kalapugama. Without their constant support over the years, the work described within this dissertation would never have been completed. This group of people managed to make even the most stressful days enjoyable. I particularly want to extend my gratitude to Lise Menard for being a great friend, and for listening to me rant when the stress of the job weighed heavily on me. I wish them all the best, and look forward to the day that our paths cross again.

There are too many friends I need to thank, and cannot possibly name them all individually. They know who they are, and I extend my humblest appreciation. However, I want to single-out Dr. Melissa Gajewski and Sara Bonderoff. These two people have been a kind of support system for me within the department, and I appreciate everything they have done for me, and the time that we spent together. We may not have been the best influence on each other from time to time, yet we still managed to get everything that needed to be done, done.

I've had several mentors over the years who helped me develop into the person that I am today, and I cannot continue these acknowledgments without thanking Dr. Anna Jordan and Jen Landry. Both of these women are amazingly strong people, whom I greatly respect. Dr. Anna Jordan took the additional

role of being a kind of surrogate mother, or at least she tried her best to fatten me up whenever she was given the opportunity.

Last, but surely not least, I wish to thank my parents, Val and Brian Boudreau. Their unyielding support got me through this, and I would never have been able to survive the trials of grad school if it were not for their words of support and comfort. They have seen me at my best and at my worst; they elevated me when I was down, and supported me when I was on the verge of collapse. I cannot think of words that are meaningful enough to express my gratitude for everything they have done. I love them both, and am blessed to have them in my life.

Contents

1	Introduction	1
1.1	Fuel Cells	2
1.1.1	Basic thermodynamics & operating principles	2
1.1.2	Types & classification schemes	4
1.1.3	Energy density	12
1.2	Efficiency	12
1.2.1	Intrinsic Maximum efficiency	14
1.2.2	Faradaic Efficiency	15
1.2.3	Voltage efficiency	16
1.3	Alcohol Oxidation in acid	22
1.3.1	Methanol oxidation	23
1.3.2	Ethanol oxidation	27
1.3.3	2-propanol oxidation	32
1.4	Direct alcohol Fuel Cells	44
1.5	Research Proposal	47
	References	48
2	Oxidation of 2-propanol in alkaline electrolytes using platinum catalysts	56
2.1	Introduction	56

2.1.1	Methanol oxidation in base	57
2.1.2	Ethanol oxidation in base	60
2.1.3	2-Propanol oxidation in base	62
2.2	Experimental	64
2.2.1	General	64
2.2.2	Preparation and characterization of the electrodes	65
2.2.3	Electrochemical oxidations	68
2.3	Results and discussion	68
2.4	Conclusion	83
	References	84
3	A prototype alkaline direct 2-propanol fuel cell using platinum electrodes	88
3.1	Introduction	88
3.2	Experimental	92
3.2.1	General	92
3.2.2	3-electrode experiments	93
3.2.3	Fuel cell experiments	93
3.3	Results and discussion	94
3.4	Conclusion	105
	References	105
4	Oxidation of 2-propanol in alkaline electrolytes using platinum, ruthenium, and platinum-ruthenium nanoparticle catalysts	110
4.1	Introduction	110
4.1.1	Methanol Oxidation	111
4.1.2	Ethanol Oxidation	115

4.1.3	2-propanol oxidation	116
4.2	Experimental	118
4.3	Results and discussion	120
4.4	Conclusion	130
	References	131
5	On the influences of ruthenium in the oxidation of 2-propanol in alkaline electrolytes	136
5.1	Introduction	136
5.2	Experimental	140
5.2.1	General	140
5.2.2	Preparation of platinum-ruthenium adatom catalysts .	140
5.2.3	Working electrode preparation, conditioning, and char- acterization	141
5.2.4	Multidimensional regression	145
5.3	Results and discussion	147
5.3.1	X-ray Photoelectron Spectroscopy	147
5.3.2	Ultraviolet Photoelectron Spectroscopy	151
5.3.3	Surface Composition	155
5.3.4	Variable temperature oxidations of 2-propanol	157
5.4	Conclusion	170
	References	173
6	Prototype alkaline direct 2-propanol fuel cell using platinum- ruthenium adatom catalyst	178
6.1	Introduction	178
6.2	Experimental	180

6.2.1	General	180
6.2.2	Preparation of platinum-ruthenium adatom electrodes . .	181
6.2.3	Electrochemical characterization of platinum ruthenium adatom electrodes	182
6.2.4	Operation of alkaline direct 2-propanol fuel cell using a platinum-ruthenium adatom anode	182
6.3	Results and discussion	183
6.4	Conclusion	191
	References	192
7	Conclusions and future work	195
7.1	Future Work	198

List of Tables

Chapter 1

1.1	Summary of the major difference between Fuel Cell types, and their representative anodic and cathodic reactions	5
1.2	Thermal and physical constants for a few typical Fuel Cell reactions	13
1.3	Summary of the peak current density and potential for the oxidation of methanol over low index platinum single crystals .	25
1.4	Steady-state current as a function of potential and surface step density for the oxidation of methanol on Pt[n(1 1 1)×(1 1 0)]-type electrodes.	26
1.5	Summary of the peak current density and potential for the oxidation of ethanol over low index platinum single crystals . .	30
1.6	Total anodic charge passed, and the fraction of this charge associated with the formation of acetic acid, during the bulk electrolysis of ethanol as a function of applied potential, and step density	32
1.7	Summary of the peak current density and potential for the oxidation of 2-propanol over low index platinum single crystals	35

1.8	Summary of the maximum kinetic rate of acetone and carbon dioxide formation on various Pt terraces, and stepped single crystals electrodes	37
1.9	Charge required to oxidize the strongly and weakly adsorbed intermediates formed during the oxidation of 2-propanol, as a function of adsorption potential	39
1.10	Potentials corresponding to peak carbon dioxide production rates from the oxidation of adsorbates formed from 2-propanol as a function of adsorption potential	40
1.11	Changes in adsorbate coverage, and stripping behaviour, as a function of incursion into the surface hydride potential region .	41

Chapter 2

2.1	Peak current density, and potential, for the oxidation of methanol over Pt(111), Pt(110), and Pt(100) as a function of electrolyte composition	59
2.2	A comparison of the activity of Pt(111), Pt(110), and Pt(100) toward the oxidation of ethanol in acidic and basic electrolytes .	61
2.3	Stripping charge associated with adsorbate formed on Pt(111), Pt(110), and Pt(100)	62
2.4	Peak current density, and potential, for the oxidation of 2-propanol over single crystal electrodes as a function of electrolyte composition and surface structure	63

Chapter 5

5.1	Summary of the ruthenium x-ray photoelectron spectra component fittings with different amounts of ruthenium-adatom on the surface.	149
5.2	Summary of the platinum x-ray photoelectron spectra component fittings with different amounts of ruthenium-adatom on the surface	150
5.3	Summary of the platinum and platinum-ruthenium Cu_{UPD} stripping component analysis	156
5.4	Summary of the kinetic parameters obtained from the three-dimensional regression analysis as a function of ruthenium surface composition	163

List of Figures

Chapter 1

1.1	General schematic representation of a hydrogen-oxygen Fuel Cell	3
1.2	Model Proton Exchange Membrane Fuel Cell polarization curve and a breakdown of the contributions of η_r , η_Ω , and η_d to η_{total}	18
1.3	Potential energy surface for a ne^- transfer event at E^0 , and E assuming that $\frac{[Ox]}{[Red]} = 1$	19
1.4	Representative atomic arrangements of some typical platinum surfaces.	25

Chapter 2

2.1	Illustration of the three-electrode setup used for the characterization of the electrochemical activity of platinum gauzes	66
2.2	Voltammogram of a blacked platinum gauze in H_2SO_4 , illustrating the H_{UPD} potential region used for the determination of the electrode's real area	67
2.3	Stabilized cyclic voltammograms of a blacked platinum gauze in $0.5 \text{ mol dm}^{-3} \text{ NaOH}$, and 1 mol dm^{-3} 2-propanol in $0.5 \text{ mol dm}^{-3} \text{ NaOH}$	70

2.4	Stabilized cyclic voltammograms of a blacked platinum gauze in 1, 2, 3, and 4 mol dm ⁻³ 2-propanol in 1 mol dm ⁻³ NaOH	71
2.5	Stabilized cyclic voltammograms of a blacked platinum gauze in 1 mol dm ⁻³ 2-propanol in 0.5, 1, and 3 mol dm ⁻³ NaOH	73
2.6	Current vs. time plot for the oxidation of 1 mol dm ⁻³ 2-propanol in 1 mol dm ⁻³ NaOH over a blacked platinum gauze at 0.1, 0.162, 0.25, and 0.55 V	74
2.7	Current at the end of a 15 min oxidation vs. potential for 1, 2, 3, and 4 mol dm ⁻³ 2-propanol in 1 mol dm ⁻³ NaOH over a blacked platinum gauze. 1 mol dm ⁻³ methanol in 1 mol dm ⁻³ NaOH is supplied for comparison	75
2.8	Current at the end of a 15 min oxidation vs. potential for 1 mol dm ⁻³ 2-propanol in 0.5, 1, and 3 NaOH over a blacked platinum gauze	78
2.9	Current at the end of a 15 min oxidation vs. potential for 1 mol dm ⁻³ 2-propanol, and 1 mol dm ⁻³ acetone in 1 mol dm ⁻³ NaOH over a blacked platinum gauze	79
2.10	Current vs. time plot for the oxidation of 4 mol dm ⁻³ 2-propanol in 1 mol dm ⁻³ NaOH over a blacked platinum gauze at 0.15, 0.30, and 0.5 V	81
2.11	Current at the end of a 15 min oxidation vs. potential for 1 mol dm ⁻³ 2-propanol in 1 mol dm ⁻³ NaOH, and 0.5 mol dm ⁻³ H ₂ SO ₄ over a blacked platinum gauze	82

Chapter 3

3.1	Exploded representation of the liquid electrolyte fuel cell used in this study	94
3.2	(a) Current-time-potential profile for the half-cell oxidation of 1 mol dm^{-3} 2-propanol / 1 mol dm^{-3} KOH over a $0.6 \text{ mg}_{\text{Pt}} \text{ cm}^{-2}$ ESNS electrode. (b) Sampled current voltammogram at 0.5, 3, 7.5, and 15 min from Figure 3.2a	96
3.3	Plot of the current density obtained at 15 min for the oxidation of 1 mol dm^{-3} 2-propanol / 1 mol dm^{-3} KOH over a $0.6 \text{ mg}_{\text{Pt}} \text{ cm}^{-2}$ ESNS electrode, and the percentage of the current changed prior to the reported current	97
3.4	Polarization curves for the same alkaline fuel cell operating on hydrogen, 100% 2-propanol, and 100% methanol	99
3.5	(a) Current-time-potential profile for the half-cell oxidation of 1 mol dm^{-3} 2-propanol / 1 mol dm^{-3} KOH over a 0.6 and $1.5 \text{ mg}_{\text{Pt}} \text{ cm}^{-2}$ ESNS electrode. (b) Sampled current voltammogram at 0.5, 3, 7.5, and 15 min from Figure 3.2a	101
3.6	Polarization curves for the alkaline direct 2-propanol fuel cell with differing anode and cathode catalyst-loading.	102
3.7	Polarization and power curves for the first and second polarization cycles of the alkaline direct 2-propanol fuel cell to 0 V. . .	104

Chapter 4

4.1	Carbon monoxide stripping voltammograms of Pt_{Black} , $\text{PtRu}_{\text{Black}}$, and Ru_{Black} , with the anodic charge due to the oxidation of carbon monoxide highlighted	120
-----	--	-----

4.2	Stabilized voltammogram of Pt _{Black} in 1 mol dm ⁻³ NaOH, 4 mol dm ⁻³ 2-propanol / 1 mol dm ⁻³ NaOH, and in 1 mol dm ⁻³ acetone / 1 mol dm ⁻³ NaOH electrolytes.	122
4.3	Stabilized voltammograms of Pt _{Black} , PtRu _{Black} , and Ru _{Black} in 1 mol dm ⁻³ NaOH, and in either 4 mol dm ⁻³ 2-propanol / 1 mol dm ⁻³ NaOH or 1 mol dm ⁻³ acetone / 1 mol dm ⁻³ NaOH electrolytes.	124
4.4	UPD cyclic voltammograms of platinum, platinum-ruthenium, and ruthenium blacks in sodium hydroxide	126
4.5	Sampled current voltammograms ($t = 15$ min) of Pt _{Black} , PtRu _{Black} , and Ru _{Black} in either 4 mol dm ⁻³ 2-propanol / 1 mol dm ⁻³ NaOH, or 1 mol dm ⁻³ acetone / 1 mol dm ⁻³ NaOH electrolytes	128

Chapter 5

5.1	Ruthenium x-ray photoelectron spectra, and component fitting, for platinum and platinum-ruthenium catalysts with different amounts of ruthenium-adatom on the surface. The results of this component analysis are summarized in Table 5.1.	147
5.2	Platinum x-ray photoelectron spectra, and component fitting, for platinum and platinum-ruthenium catalysts with different amounts of ruthenium-adatom on the surface. The results of this component analysis are summarized in Table 5.2.	151
5.3	Ultraviolet photoelectron spectra of platinum and platinum-ruthenium catalysts, with different amounts of ruthenium-adatom on the surface.	153

5.4	Stripping voltammetry of a underpotentially-deposited copper monolayer on platinum and platinum-ruthenium catalysts, with different amounts of ruthenium-adatom on the surface	155
5.5	Active areas of platinum and ruthenium as determined by the stripping of underpotentially deposited copper for platinum-ruthenium adatom catalysts with varying degrees of ruthenium coverage.	157
5.6	Linear sweep voltammetry of platinum and platinum-ruthenium adatom catalysts with and without 0.1 mol dm^{-3} 2-propanol in 1 mol dm^{-3} KOH as a function of temperature. $\omega = 50 \text{ s}^{-1}$, $\nu = 5 \text{ mV s}^{-1}$	159
5.7	Three-dimensional regression analysis of the variable temperature linear sweep voltammetry of platinum and platinum-ruthenium adatom catalysts with and without 0.1 mol dm^{-3} 2-propanol in 1 mol dm^{-3} KOH. $\omega = 50 \text{ s}^{-1}$, $\nu = 5 \text{ mV s}^{-1}$	162
5.8	Apparent kinetic rate constant as a function of the fractional composition of the platinum-ruthenium adatom catalysts. $T = 298 \text{ K}$	165
5.9	Activation enthalpy as a function of the fractional composition of the platinum-ruthenium adatom catalysts. $T = 298 \text{ K}$	167

Chapter 6

6.1	(a) Current-time-potential profiles for the half-cell oxidation of 2-propanol / KOH over a platinum ESNS electrode, and (b) the same study with progressively increasing amounts of ruthenium adatoms on the surface of the electrode.	184
-----	--	-----

6.2	Sampled current voltammograms for (a) the platinum electrode shown in Figure 6.1a, and (b) the platinum-ruthenium adatom electrodes shown in Figure 6.1b.	188
6.3	Polarization and power curves for the same alkaline fuel cell running on 100% 2-propanol with either a $1.5 \text{ mg}_{\text{Pt}} \text{ cm}^{-2}$ ESNS anode, or with the PtRu_3 additions anode	189

List of Schemes

Chapter 1

- 1.1 Representative reactions for the reforming of hydrocarbon fuels into hydrogen. 7
- 1.3 Generally accepted reaction scheme for the electrochemical oxidation of methanol on metal electrodes 28
- 1.4 General reaction scheme for the electrochemical oxidation of ethanol on metal electrodes 29
- 1.5 Generally accepted mechanism for the oxidation of 2-propanol over platinum catalysts. 43

Chapter 2

- 2.1 Electrochemical oxidation of 2-propanol to acetone in alkaline media. 77

Chapter 3

- 3.1 Alkaline oxidation of hydrogen, and reduction of oxygen . . . 88

Chapter 4

- 4.1 The bifunctional mechanism for the oxidation of carbon monoxide or metal electrodes 111

Chapter 5 135

- 5.1 Generally accepted mechanism for the oxidation of 2-propanol over platinum catalysts. 137
- 5.2 Proposed reaction scheme for the preparation of platinum-ruthenium adatom catalysts 147
- 5.3 Elementary steps for the oxidation of 2-propanol to acetone on metal electrodes. 169
- 5.4 Proposed transition state complex for the rate determining step during the oxidation of 2-propanol over platinum-ruthenium adatom catalysts. 170

Chapter 6 177

- 6.1 Electrochemical oxidation of 2-propanol to acetone in alkaline media. 178
- 6.2 Proposed transition state complex for the rate determining step during the oxidation of 2-propanol over platinum-ruthenium adatom catalysts. 185

List of Abbreviations

AD2PFC	Alkaline Direct 2-Propanol Fuel Cell
AD AFC	Alkaline Direct Alcohol Fuel Cell
ADEFC	Alkaline Direct Ethanol Fuel Cell
ADMFC	Alkaline Direct Methanol Fuel Cell
AFC	Alkaline Fuel Cell
CV	Cyclic Voltammogram
D2PFC	Direct 2-propanol Fuel Cell
DAFC	Direct Alcohol Fuel Cell
DEFC	Direct Ethanol Fuel Cell
DEMS	Differential Electrochemical Mass Spectrometry
DMFC	Direct Methanol Fuel Cell
EIS	Electrochemical Impedance Spectroscopy
FC	Fuel Cell
FTIR	Fourier Transform Infrared Spectroscopy
HPLC	High Pressure Liquid Chromatography
LHV	Low Heating Value
LSV	Linear Sweep Voltammogram
MCFC	Molten Carbonate Fuel Cell
NASA	National Aeronautics and Space Administration
NHE	Normal Hydrogen Electrode
NIST	National Institute of Standards and Technology

OCV	Open Circuit Voltage
OLEMS	Online Electrochemical Mass Spectroscopy
PAFC	Phosphoric Acid Fuel Cell
PBI	Polybenzimidazole
PEMFC	Proton Exchange Membrane Fuel Cell
PTFE	Polytetrafluoroethylene
RDE	Rotating Disk Electrode
RHE	Reference Hydrogen Electrode
RRDE	Rotating Ring Disk Electrode
SERS	Surface Enhanced Raman Spectroscopy
SNIFTIR	Subtractively Normalized Interfacial Fourier Transform Infrared Spectroscopy
SOFC	Solid Oxide Fuel Cell
SPAIRS	Single Potential Alteration Infrared Spectroscopy
STM	Scanning Tunneling Microscope
UHV	Ultra High Vacuum
UPS	Ultraviolet Photoelectron Spectroscopy
XPS	X-ray Photoelectron Spectroscopy

List of Symbols

Symbol	Meaning	Usual Units
A	Surface area	cm^2
A	Pre-exponential Factor	None
C^*	Bulk solution concentration	mol dm^{-3}
$C_{ox}(0, t)$	Concentration of oxidant at the electrode surface	mol dm^{-3}
$C_{red}(0, t)$	Concentration of reductant at the electrode surface	mol dm^{-3}
D	Diffusion coefficient	$\text{cm}^2 \text{s}^{-1}$
E	Potential	V
E^0	Standard Potential	V
E_{cell}	Cell Potential	V
F	Faraday's constant	$9.64853 \times 10^4 \text{ C mol}^{-1}$
f_s	Fractional Coverage	None
ΔG	Gibbs energy of reaction	kJ mol^{-1}
ΔG^\ddagger	Gibbs energy of activation	kJ mol^{-1}
ΔH	Enthalpy of reaction	kJ mol^{-1}
ΔH^\ddagger	Enthalpy of activation	kJ mol^{-1}
ΔH_{vap}	Enthalpy of vaporization	kJ mol^{-1}
I	Current	A
I_m	Theoretical maximum current	A
j	Current Density	A cm^{-2}
k^0	Potential Independent Rate Constant	cm s^{-1}

k_a	Anodic Rate Constant	cm s^{-1}
k_c	Cathodic Rate Constant	cm s^{-1}
n	Number of electrons	mol
n_{surf}	Number of surface atoms	mol
R	Resistance	Ω
s	Standard deviation	Variable
ΔS	Entropy of reaction	$\text{J mol}^{-1} \text{K}^{-1}$
ΔS^\ddagger	Entropy of activation	$\text{J mol}^{-1} \text{K}^{-1}$
T	Temperature	$^\circ\text{C}, \text{K}$
t	Time	s
T_H	Temperature of the high temperature reservoir	K
T_L	Temperature of the low temperature reservoir	K
$W_{electrical}$	Electrical work	W
Q_{Ap}	Charge Density	C cm^{-2}
Q_{BL}	Baseline charge	C
Q_{CO}	Charge from the oxidation of carbon monoxide	C
Q_H	H_{UPD} charge	C
$Q_{\text{Ru-Cu}_{\text{UPD}}}$	Cu_{UPD} charge from ruthenium	C
$Q_{\text{Pt-Cu}_{\text{UPD}}}$	Cu_{UPD} charge from platinum	C
w	Weight percent	%
α	Transfer coefficient	None
δ	Diffusion layer thickness	cm
ε_e	Voltage efficiency	None
ε_f	Faradaic efficiency	None
ε_i	Intrinsic maximum efficiency	None
$\varepsilon_{i,HE}$	Intrinsic maximum efficiency of a heat engine	None

$\varepsilon_{i,FC}$	Intrinsic maximum efficiency of a fuel cell	None
$\varepsilon_{overall}$	Overall efficiency	None
η	Overpotential ($E - E^0$)	V
η_{anode}	Anodic Overpotential	V
$\eta_{cathode}$	Cathodic Overpotential	V
η_d	Diffusion Overpotential	V
η_r	Reaction Overpotential	V
η_{Ω}	Resistance Overpotential	V

Chapter 1

Introduction

Galvanic cells are electrochemical devices that transform the free energy of a chemical reaction directly into electrical power. Examples include Fuel Cells (FCs), and primary and secondary batteries. The chemical oxidant and reductant are physically separated by an ionic conducting medium (the electrolyte), and are each in contact with an electronically conducting medium (the electrodes). When a current is drawn from the cell, electrons are lost by the reductant to its electrode, the anode. These electrons travel through an external circuit, providing electrical work, and arrive at the cathode where they are accepted by the oxidant. The oxidant is thereby reduced and the reductant is oxidized. Localized charge buildup at the anode and cathode is dissipated by the migration of ions through the electrolyte. The chemical nature of the migrating ions depends upon the makeup of the cell.

1.1 Fuel Cells

1.1.1 Basic thermodynamics & operating principles of Fuel Cells

A FC is a type of galvanic cell that does not store its oxidant or reductant within the cell. Rather, the oxidant and reductant are supplied to the FC, which only contains the components necessary to facilitate the electrochemical reactions. In principle, electrical work can be obtained from a FC as long as it is supplied with an oxidant and reductant. In contrast, electrical work can only be produced by batteries until the internal oxidant and/or reductant are consumed. Once discharged, primary cells must be replaced, and secondary cells must be recharged in order to replenish the spent oxidant/reductant.

Figure 1.1 illustrates the general schematic of a hydrogen-oxygen FC. The balanced reduction and oxidation half cell reactions, and the overall cell reaction, are also provided. Hydrogen is supplied to the anode compartment, and oxygen is supplied to the cathode compartment, at standard ambient temperature and pressure. At the anode, and with an acidic electrolyte, hydrogen is oxidized to protons and electrons. The protons migrate through the electrolyte to the cathode, and electrical work is obtained from the conduction of electrons through an external circuit. At the cathode, oxygen is reduced by the electrons and combines with the migrated protons to produce water. The net chemical reaction is the hydrogen combustion reaction.

The maximum amount of electrical work ($W_{electrical}$) obtained from a galvanic cell is equal to the change in Gibbs free energy of the reaction (ΔG) as shown in equation 1.1. The driving force to move an electron from the anode to the cathode, also known as the electromotive force (E_{cell}), is related to ΔG

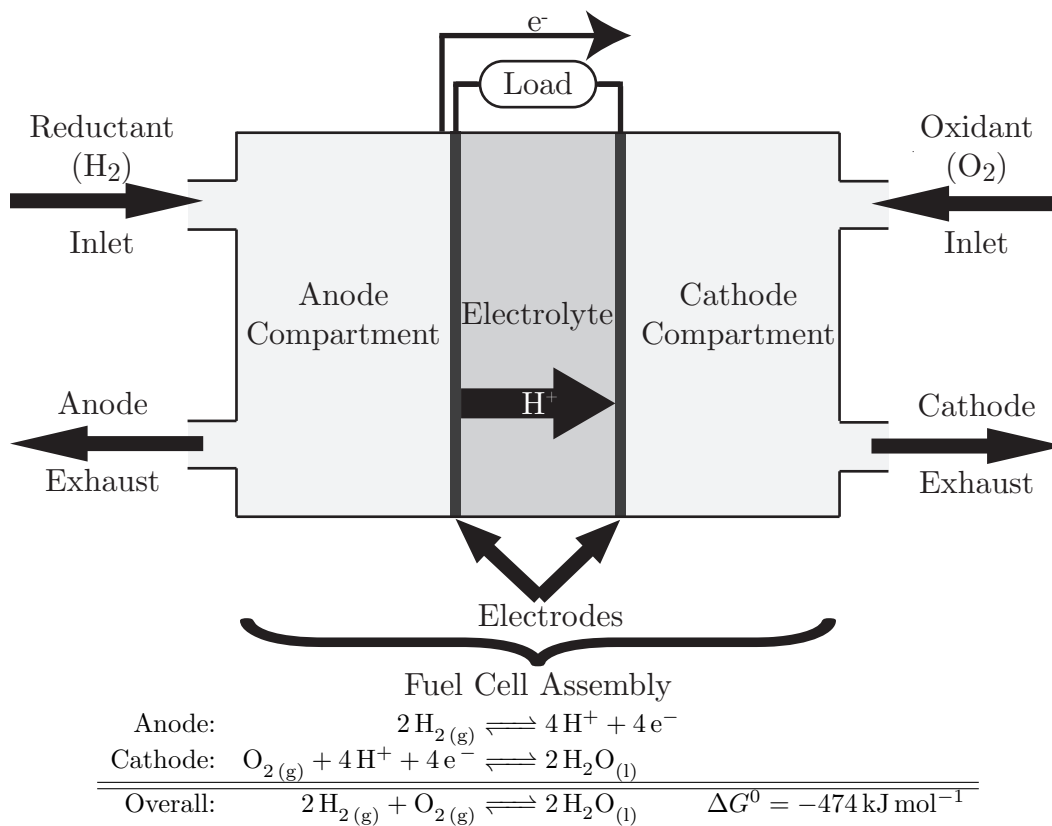


Figure 1.1: A general schematic representation of a hydrogen-oxygen Fuel Cell, identifying its basic components.

by equation 1.2,

$$\Delta G = -W_{\text{electrical}} \quad (1.1)$$

$$\Delta G = -nFE_{\text{cell}} \quad (1.2)$$

where n is the number of electrons in the balanced cell reaction, and F is Faraday's constant ($9.64853 \times 10^4 \text{ C mol}^{-1}$).

1.1.2 Fuel Cell types & classification schemes

The chemical reactions occurring in a FC, and the identity of the charge carriers, depends on the architecture of the cell. Typically, a FC is categorized by the nature of its electrolyte:

1. Alkaline Fuel Cell (AFC),
2. Phosphoric Acid Fuel Cell (PAFC),
3. Molten Carbonate Fuel Cell (MCFC),
4. Solid Oxide Fuel Cell (SOFC), and
5. Proton Exchange Membrane Fuel Cell (PEMFC).

Alternatively, a FC can be categorized by its operating temperature range:

1. High-temperature Fuel Cell (SOFC & MCFC),
2. Medium-temperature Fuel Cell (PAFC & AFC), and
3. Low-temperature Fuel Cell (PEMFC & AFC).

Table 1.1 summarizes the general differences between these FC types, along with a few representative anodic and cathodic reactions. Each type will be further discussed in §§1.1.2.1–1.1.2.5.

Table 1.1: Summary of the major difference between Fuel Cell types, and their representative anodic and cathodic reactions. [1-3]

Cell type	Temp (°C)	Anode		Cathode		ϵ^b
		Catalyst	Representative reaction(s) ^a	Catalyst	Reaction ^a	
PEMFC	50-80	Pt	$\text{H}_2 \rightleftharpoons 2\text{H}^+ + 2\text{e}^-$	Pt	$\frac{1}{2}\text{O}_2 + 2\text{H}^+ + 2\text{e}^- \rightleftharpoons \text{H}_2\text{O}$	45-60%
	60-90	Ni/Ag metal oxides, & noble metals	$\text{H}_2 + 2\text{OH}^- \rightleftharpoons 2\text{H}_2\text{O} + 2\text{e}^-$	FeCo, Ni/Ag metal oxides & noble metals	$\frac{1}{2}\text{O}_2 + \text{H}_2\text{O} + 2\text{e}^- \rightleftharpoons 2\text{OH}^-$	40-60%
PAFC	160-220	Pt	$\text{H}_2 \rightleftharpoons 2\text{H}^+ + 2\text{e}^-$	Pt	$\frac{1}{2}\text{O}_2 + 2\text{H}^+ + 2\text{e}^- \rightleftharpoons \text{H}_2\text{O}$	55%
MCFC	600-700	Ni	$\text{H}_2 + \text{CO}_3^{2-} \rightleftharpoons \text{H}_2\text{O} + \text{CO}_2 + 2\text{e}^-$	NiO	$\frac{1}{2}\text{O}_2 + \text{CO}_2 + 2\text{e}^- \rightleftharpoons \text{CO}_3^{2-}$	60-65%
			$\text{CO} + \text{CO}_3^{2-} \rightleftharpoons 2\text{CO}_2 + 2\text{e}^-$ etc.			
SOFC	800-1000	Pt,	$\text{H}_2 + \text{O}^{2-} \rightleftharpoons \text{H}_2\text{O} + 2\text{e}^-$	Pt,	$\frac{1}{2}\text{O}_2 + 2\text{e}^- \rightleftharpoons \text{O}^{2-}$	55-60%
		Co-ZrO ₂ or Ni-ZrO ₂	$\text{CO} + \text{O}^{2-} \rightleftharpoons \text{CO}_2 + 2\text{e}^-$ $\frac{1}{4}\text{CH}_4 + \text{O}^{2-} \rightleftharpoons \frac{1}{4}\text{CO}_2 + \frac{1}{2}\text{H}_2\text{O} + 2\text{e}^-$ $\frac{1}{3}\text{CH}_3\text{OH} + \text{O}^{2-} \rightleftharpoons \frac{1}{3}\text{CO}_2 + \frac{2}{3}\text{H}_2\text{O} + 2\text{e}^-$ etc.	Sr-LaMnO ₃		

^a Embolden species are the electrolyte charge carriers.

^b ϵ : Operating efficiency of the hydrogen-oxygen FC, when gaseous water is the final product of the combustion and the thermal energy stored as $\Delta H_{\text{vap}}(\text{H}_2\text{O})$ is not recovered.

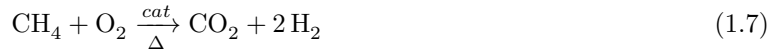
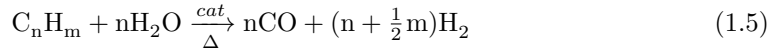
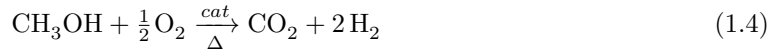
1.1.2.1 Proton Exchange Membrane Fuel Cells^[3-5]

The PEMFC has several advantages over other FC variants. They operate at low temperatures with high efficiencies, and have relatively short start-up times. The proton conducting membrane is typically made of polytetrafluoroethylene sulfonic acid, commercially sold under the trade-name NafionTM, and consists of three regions:

1. a hydrophobic polytetrafluoroethylene backbone,
2. side chains of $-O-CF_2-CF_2-O-CF_2-CF_2-$ connecting the first and third regions, and
3. ionic clusters containing sulfonic acid anions.

The hydrogen-oxygen PEMFC is capable of producing power densities (power output per unit area of the electrodes) as high as $6-8 \text{ kW m}^{-2}$, and has demonstrated lifetimes of $10-100 \times 10^3 \text{ h}$. The hydrogen fuel can be stored in a tank, or generated as needed directly from common fuels using a reformer (Scheme 1.1). Reformate gas generally contains mixtures of hydrogen, carbon dioxide, and a small amount of carbon monoxide. The electrodes are typically made from carbon-supported platinum, or binary and ternary platinum-based alloys. A considerable problem associated with the use of platinum catalysts is that they are susceptible to poisoning by carbon monoxide.^[2] The majority of the carbon monoxide in the reformate must therefore be removed, adding system cost and complexity. Other than catalyst poisoning, some of the challenges associated with PEMFCs arise from their poor thermal and water management properties.

Today, PEMFC research is mostly directed towards the advancement of polymer electrolyte materials^[6], improving water management and mass trans-



Scheme 1.1: Representative reactions for the reforming of hydrocarbon fuels into hydrogen.

port, and reducing the loading of noble metals. This includes improving the electrolytes thermal stability, chemical resistance, water retention at elevated temperatures, and reducing their capital cost. Phosphoric acid doped Polybenzimidazole (PBI) is one material that has attracted considerable attention, and has demonstrated^[7] stable operation at high temperatures (200 °C) without gas humidification. These high temperature cells are also more tolerant to gas impurities.

Another research goal is to reduce the platinum-loading in the electrodes by identifying new catalysts that are more active than platinum, and more tolerant to gaseous impurities.^[8] To this end, ternary PtRuM alloy anode catalysts (M = WO_x, W₂C, Mo, Ir, Ni, Co, Rh, Os, and V) have demonstrated improved carbon monoxide tolerance compared to commercial PtRu. Similarly, binary and ternary cathode catalysts such as PtNi, PtCr, PtCo, PtCoCr, PtCuFe, PtGaCr, PtRhFe, PtCrCu, and PtCuFe have demonstrated improved oxygen reduction kinetics relative to platinum. The activities of these ternary materials are, however, difficult to directly compare.^[8]

1.1.2.2 Phosphoric Acid Fuel Cells^[9–11]

The PAFC uses a concentrated phosphoric acid electrolyte, $w_{\text{H}_3\text{PO}_4} \simeq 0.99$, and operates at 160–220 °C. Because of these high operating temperatures, the PAFC is more tolerant than the PEMFC to gaseous impurities, such as carbon monoxide, but also has a longer start-up time. The PAFC produces good-quality waste heat which, if recovered for co-generation, can raise its overall efficiency to more than 80%. Their major limitation is that the oxygen reduction reaction is slow, resulting in low power densities. The poor performance of the cathode is further exacerbated by dissolution of the noble metal cathodic catalyst and corrosion of its support.

Despite the demonstration of more than 500 commercial PAFC units, some having lifetimes greater than 230 000 h, significant advancements are required before the technology can be widely adopted.^[10] As mentioned above, there has recently been considerable interest in phosphoric acid doped PBI. These solid state electrolytes can contain as high as 20-40 mol H_3PO_4 per monomer unit, and should not only be viewed as the next generation PEMFC, but also the next generation PAFC. As such, many of the technological advancements in the field are the same as those discussed in §1.1.2.1. Recent research activities, however, are also focusing on combined heat and power generation.^[9] Additionally, dilution of the electrolyte by product water, mitigation of catalyst sintering, and reduction of capital costs remain key challenges that must be addressed.^[10]

1.1.2.3 Alkaline Fuel Cells^[9,12–16]

The AFC is the oldest FC technology to be put into commercial use, and was the primary power sources used during the National Aeronautics and Space Administration (NASA) space flights between the 1960s and 1970s.^[2] They

use an aqueous KOH electrolyte, typically 30–45% by weight, and operate between 60 and 90 °C, and with electrical efficiencies that are between ca. 40 and 60%. The reduction of oxygen is more facile in an alkaline electrolyte, and non-noble metal cathode catalysts can be used.^[13] The performance of the AFC is influenced by carbon dioxide due to the gradual carbonation of the electrolyte. Carbonation reduces the electrolyte's conductivity, and precipitation of carbonate salts within the porous electrodes hinders the mass transport of reactants. Further, these precipitates can damage the electrodes by inducing mechanical strain.^[2]

Recent advances in anion exchange membranes^[17] has lead to a resurgence in AFC research. The use of polymer immobilized cations, rather than mobile solution phase cations, precludes the formation of carbonate precipitates. Typically, the immobile cation is a quaternary ammonium group. Promisingly, Lu et al. have reported^[18] a polymer electrolyte AFC that is free of noble metals, significantly reducing the cost of the catalyst layers. Further, such anion exchange membranes have shown excellent utility in Alkaline Direct Alcohol Fuel Cells (ADAFCs).^[19] Some key advantages afforded by the polymer electrolyte include:

1. Improved oxidation / reduction kinetics,
2. reduced alcohol crossover from the anode to the cathode,
3. potentially simplified water management, and
4. potentially reduced corrosion.

These advantages will be discussed in more detail in Chapter 3.

1.1.2.4 Molten Carbonate Fuel Cells^[9,11,20-23]

The electrolyte used in the MCFC is a eutectic melt of $\text{Li}_2\text{CO}_3\text{-K}_2\text{CO}_3$, or $\text{Li}_2\text{CO}_3\text{-Na}_2\text{CO}_3$. The cell operates at 923–1123 K, with efficiencies as high as 50%; however, this efficiency can be increased to ca. 86% if the exhaust heat is used for co-generation. Their high operating temperature makes them carbon monoxide tolerant; however, they are not tolerant to sulphurous compounds. Another interesting advantage of their high operating temperature is that they can reform hydrocarbon fuels internally, simplifying ancillary components. The high operating temperature also enables the use of non-noble metal catalysts such as Ni anodes and NiO cathodes, but significantly lengthens start-up times, and enhances the corrosion and breakdown of cell components. Additionally, start-stop cycling results in thermal fatigue of the components, and can lead to cracking. The cathode gas stream must also contain a mixture of carbon dioxide and oxygen, which complicates the make-up of the oxidant stream.

The MCFC is highly regarded as being a promising stationary power source, but efforts must be made to prolong their lifetime.^[23] In lower temperature systems that use a liquid electrolyte, such as the PAFC and AFC, stable gas/liquid interfaces can be established using Polytetrafluoroethylene (PTFE). At high temperatures, however, the only method to control this interface is through control of the electrode's porous structure. Leaked electrolyte can redistribute within the FC stack,^[24,25] resulting in decreased performance over time. Additionally, dissolution of the cathode, and corrosion of components are significant hindrances towards commercialization of the MCFC.^[25]

1.1.2.5 Solid Oxide Fuel Cells^[9,11,26–32]

The SOFC uses ceramic electrolytes such as $(\text{ZrO}_2)_{0.92}(\text{Y}_2\text{O}_3)_{0.08}$, ceria-based electrolytes, $\text{Ce}_x\text{Zr}_{0.82-x}\text{Gd}_{0.18}\text{O}_{1.91}$, and a variety of mixed metal oxides typically of the perovskite structure type.^[30] The cell must be operated at elevated temperatures, as the ceramic electrolyte is not ionically conductive at low temperatures. These high temperatures make the SOFC relatively insensitive to poisons (such as sulphur and carbon monoxide), capable of reforming hydrocarbon fuels internally, and, in principle, not reliant on the use of noble metal catalysts. The high temperature is also beneficial from the stance of co-generation of heat and power which increases cell efficiencies to 85%. Although the high temperature FCs enhance the kinetics of the electrochemical reactions, they also enhances corrosion processes and solid state reactions at the cathode/electrolyte interface, which form a low conducting phase. The high temperatures also require long start-up times, while repeated start-stop cycles results in thermal fatigue and cracking of parts.

State of the art research in SOFC is, in part, focused on reducing the operating temperature. These intermediate temperature (770–1070 K) FCs will reduce component corrosion, and thereby increase the lifetime of the cells and well as afford cell construction using cheaper cell components. One drawback of using a lower operating temperature, however, is that the reaction kinetics at the anode and cathode can begin to become critical. A significant and rich body of work towards reducing the operating temperature of SOFCs is available, and has been recently reviewed by Tsipis and Kharton.^[33]

1.1.3 Energy density

A fuel's energy density is the *maximum* amount of energy that can be produced from the fuel, normalized by unit mass (gravimetric energy density) or by unit volume (volumetric energy density). Equation 1.1 states that $-\Delta G^0$ is the maximum amount of electrical work that can be obtained from a chemical reaction. Using constants tabulated in the CRC handbook of chemistry and physics,^[34-36] and Hess's law, ΔG^0 , ΔH^0 , and ΔS^0 can be calculated for many typical FC reactions. Table 1.2 summarizes some volumetric energy densities for hydrogen and low molecular weight alcohols that were calculated in this way.

The volumetric energy density of an alcohol is several orders of magnitude higher than hydrogen gas, and is also more energy dense than liquid hydrogen. In fact, the volumetric energy density of liquid hydrogen at its triple point (ca. -240°C and 12.7 atm) is only about half that of methanol. The high volumetric energy density of alcohols is one of the primary driving force towards their utilization in FCs. Further, they are readily available, and exist in a liquid phase under ambient conditions, allowing their easy integration into existing transportation infrastructure. The actual amount of energy obtained from a fuel is a product of its energy density and the overall efficiency of the FC. The following sections will discuss the factors that influence how efficiently this chemical energy is converted into electrical energy.

1.2 Energy conversion efficiency

The overall efficiency ($\varepsilon_{\text{overall}}$) for the conversion of chemical energy into electrical work is the product of several independent efficiencies, as shown in

Table 1.2: Thermal and physical constants for a few typical Fuel Cell reactions.

Overall Cell Reaction	$\Delta G_r^{0,a}$ (kJ mol ⁻¹)	$\Delta H_r^{0,a}$ (kJ mol ⁻¹)	$\Delta S_r^{0,a}$ (J mol ⁻¹ K ⁻¹)	Molar Volume (cm ³ mol ⁻¹)	Energy Density ^b (Wh cm ⁻³) ^c
$H_{2(g)} + \frac{1}{2} O_{2(g)} \rightleftharpoons H_2O_{(l)}$	-237.8	-268.8	-163.3	26.19 ^d	2.515
$CH_3OH_{(l)} + \frac{3}{2} O_{2(g)} \longrightarrow CO_{2(g)} + 2 H_2O_{(l)}$	—	—	—	64.37 ^e	1.023
$CH_3CH_2OH_{(l)} + 3 O_{2(g)} \longrightarrow 2 CO_{2(g)} + 3 H_2O_{(l)}$	—	—	—	2.447×10^4 ^f	2.692×10^{-3}
$(CH_3)_2CHOH_{(l)} + \frac{9}{2} O_{2(g)} \longrightarrow 3 CO_{2(g)} + 4 H_2O_{(l)}$	-703.3	-727.4	-80.8	40.49 ^g	4.825
$(CH_3)_2CHOH_{(l)} + \frac{9}{2} O_{2(g)} \longrightarrow 3 CO_{2(g)} + 4 H_2O_{(l)}$	-1 325.4	-1 366.8	-138.7	58.37 ^g	6.388
$(CH_3)_2CHOH_{(l)} + \frac{1}{2} O_{2(g)} \rightleftharpoons (CH_3)_2CO_{(l)} + H_2O_{(l)}$	-1 967.3	-2 025.6	-195.6	76.96 ^g	7.101
	-223.7	-231.6	-26.4	76.96 ^g	0.808

^a Calculated from thermodynamic constants tabulated in the CRC Handbook of Chemistry and Physics.^[34]

^b Energy density represents the *maximum* volumetric energy content of a fuel, that has not been diluted, at 20 °C and 1 atm pressure. Actual electrical energy obtained from a FC using these fuels is a function of the overall efficiency of the electrical conversion process(see §1.2 for details).

^c 1 Wh = 3.6 kJ.

^d Liquid phase para-hydrogen at its triple point. Temperature = 13.8 K, pressure = 0.0069 atm, $\rho = 76.98$ kg m⁻³.^[35]

^e Liquid phase para-hydrogen at its critical point. Temperature = 32.94 K, pressure = 12.7 atm, $\rho = 31.32$ kg m⁻³.^[35]

^f Gas phase hydrogen at standard ambient temperature and pressure.

^g Calculated from physical constants tabulated in the CRC Handbook of Chemistry and Physics.^[36]

equation 1.9. They are:

1. the intrinsic maximum efficiency (ε_i),
2. the Faradaic efficiency (ε_f), and
3. the voltage efficiency (ε_e).

$$\varepsilon_{\text{overall}} = \varepsilon_i \varepsilon_f \varepsilon_e \quad (1.9)$$

The underlying sources of each of these efficiency losses will be briefly discussed in this section, in order to understand the practical implications of each component.

1.2.1 Intrinsic Maximum efficiency (ε_i): The Fuel Cell versus the Heat Engine^[37]

The intrinsic maximum efficiency of a FC, $\varepsilon_{i,FC}$, is defined as

$$\varepsilon_{i,FC} = \frac{\Delta G}{\Delta H} \quad (1.10)$$

or by substituting $\Delta G = \Delta H - T\Delta S$,

$$\varepsilon_{i,FC} = 1 - \frac{T\Delta S}{\Delta H} \quad (1.11)$$

where ΔG , ΔH , and ΔS are the Gibbs energy, enthalpy, and entropy changes for the net reaction occurring in the FC. $\varepsilon_{i,FC}$ is the maximum energy conversion efficiency based on thermodynamic considerations, and results from the loss of thermal energy during the oxidation-reduction processes. It is specific for each set of oxidation-reduction reactions in a FC, and it is also known as the

reversible efficiency. For the hydrogen-oxygen FC illustrated in Figure 1.1, $\varepsilon_{i,FC}$ is 83%.

The intrinsic maximum efficiency of a heat engine ($\varepsilon_{i,HE}$), such as a gas turbines or a combustion engine, is derived from the Carnot cycle. It is defined as

$$\varepsilon_{i,HE} = 1 - \frac{T_L}{T_H} \quad (1.12)$$

where T_L and T_H are the temperatures of the low and high temperature reservoirs, respectively. As explained by Zhao and Van Nguyen,^[37] in a “perfect” combustion reaction the flame temperature (T_H) is above 3000 K. In practice, however, a perfect combustion is not achieved due to incomplete combustion, and product dissociation, which lowers T_H . Metallurgical considerations resulting from insufficient mechanical strength requires further cooling of T_H to ca. 1000 K. Ideally T_L is at room temperature; however, inefficient heat rejection raises this value to ca. 550 K. These limitations give practical ε_i values around 45%; however, values close to ca. 33% are typical of the internal combustion engines used in automobiles.^[37]

1.2.2 Faradaic Efficiency (ε_f)

The faradaic efficiency, ε_f , is the number of electrons removed from a mole of reactant relative to its theoretical maximum. It is defined as

$$\varepsilon_f = I/I_m \quad (1.13)$$

where I and I_m are the observed and the theoretical maximum currents (determined by fuel supply rate), respectively. In a well designed FC, ε_f is ca. unity; however, several chemical factors can result in smaller values, including:

1. parallel reactions yielding fewer electrons per mole of reactant,
2. non-electrochemical reactions that are catalyzed by the electrode, and
3. direct chemical reactions between the oxidant and reductant (e.g., cross-over).

1.2.3 Voltage efficiency (ε_e)

The voltage of an electrochemical cell while it is under load is lower than E^0 . The voltage efficiency is defined as

$$\varepsilon_e = \frac{E}{E^0} \quad (1.14)$$

where E is the potential of the FC while under load.

The magnitude that the potential deviates from E^0 is a function of the current drawn through the cell, and is known as the overpotential (η).

$$\eta = E - E_{\text{cell}}^0 \quad (1.15)$$

Several physical phenomena contribute this deviation from E^0 , including:

1. reaction overpotential (η_r),
2. resistance overpotential (η_Ω), and
3. diffusion overpotential (η_d).

The total overpotential for a reaction (η_{total}) can be viewed as the algebraic sum of these components.

$$\eta_{\text{total}} = \eta_r + \eta_\Omega + \eta_d \quad (1.16)$$

In a FC, both the anodic and cathodic reactions contribute their η_r and η_d to the observed overpotential of the cell; η_Ω is common to both reactions, and arises from the total ionic current flowing through the cell.

$$\eta_{total,cell} = \eta_{anode} + \eta_{cathode} \quad (1.17)$$

$$\eta_{total,cell} = \eta_{r,anode} + \eta_{r,cathode} + \eta_{d,anode} + \eta_{d,cathode} + \eta_\Omega \quad (1.18)$$

Figure 1.2 illustrates a typical FC polarization curve. Although $\eta_{r,anode}$, $\eta_{r,cathode}$, $\eta_{d,anode}$, $\eta_{d,cathode}$, and η_Ω operate simultaneously, their relative contributions to η_{total} are a function of the current density (j). The underpinning mechanisms for each of these overpotentials, and the interpretation of Figure 1.2, will be discussed in detail in the proceeding sections.

1.2.3.1 Reaction overpotential (η_r)

At low current densities, η_r is the main source of overpotential, and is linked to the activation energy barriers (ΔG^\ddagger) for the anodic and cathodic reactions. Figure 1.3 illustrates the potential energy surface for a n electron transfer event, assuming that $[Ox] = [Red]$. At equilibrium, and in the absence of a net faradaic current, the free energy of the electrode exactly counterbalances ΔG such that the free energy of the reactants and products are equal (solid lines in Figure 1.3). The potential energy surfaces of the reactants and products intersect at the transition state, and the activation energy (ΔG^\ddagger) for the forward and reverse process are equal.

When a potential is applied to the electrode the free energy of the electrons changes by $nF(E - E^0)$, and the activation energy for the cathodic and anodic

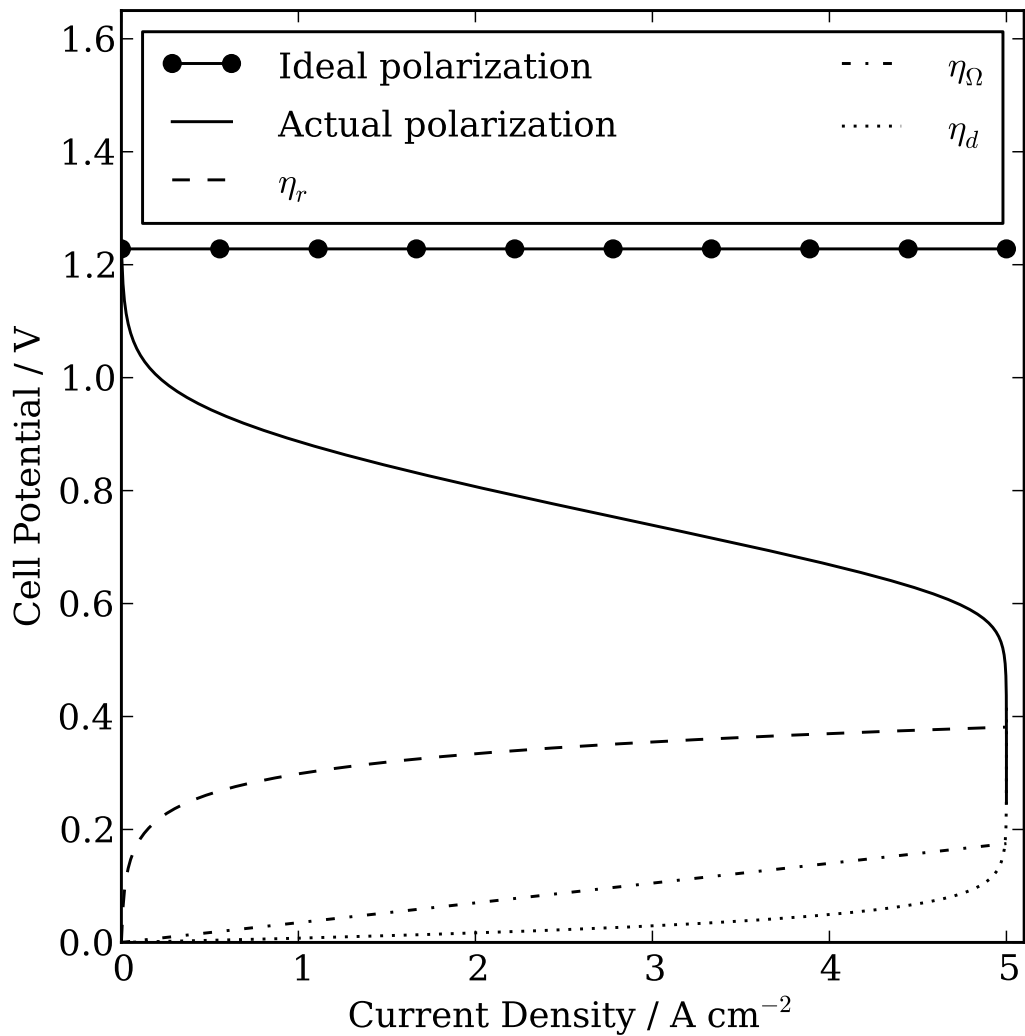


Figure 1.2: Model hydrogen-oxygen Proton Exchange Membrane Fuel Cell polarization curve(—), and its nonpolarizable analogue (●). η_r (—) and η_Ω (- · -) are calculated from the i_0 and R values reported by Gu et al., and η_d (···) is calculated using an estimated i_l value, obtained by extrapolating the i_l data also reported by Gu et al. to 20% oxygen in nitrogen.^[38]

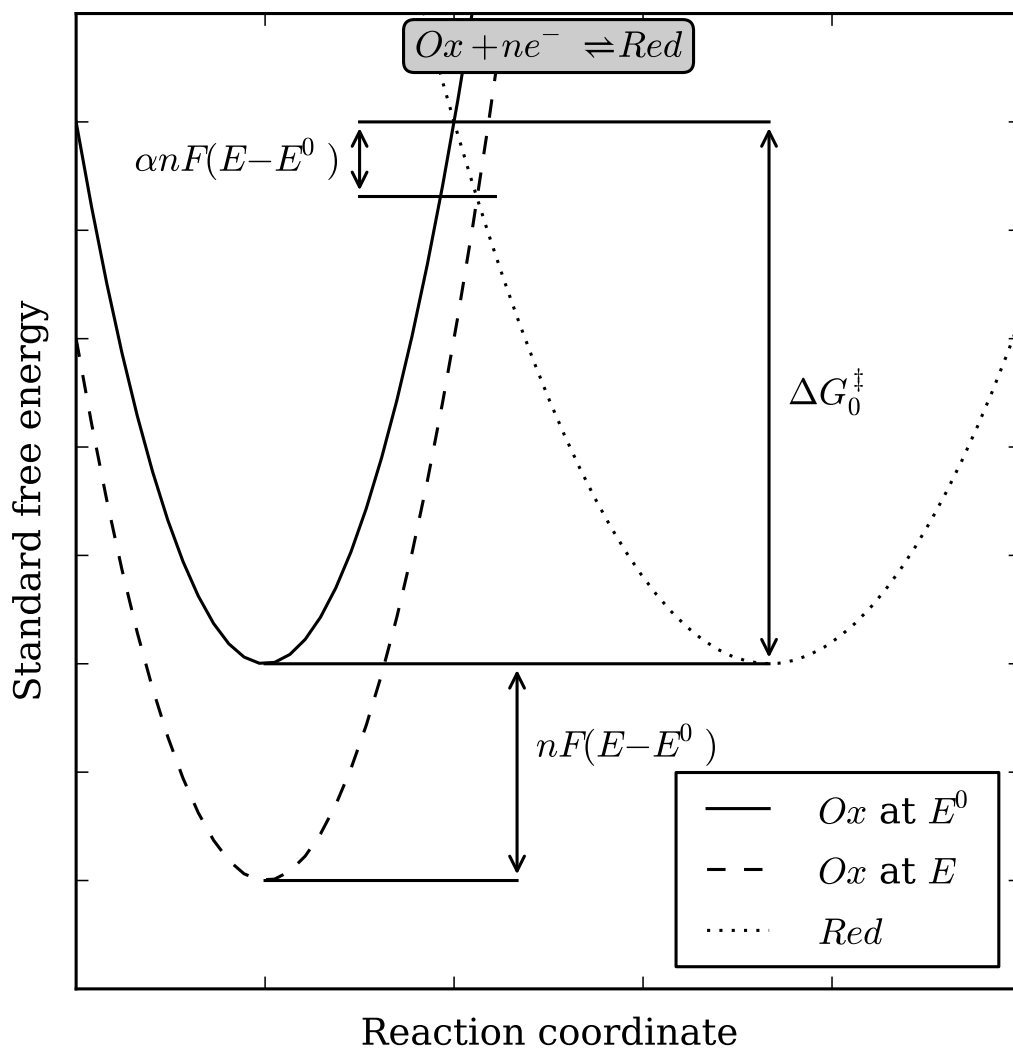


Figure 1.3: Potential energy surface for a ne^- transfer event at E^0 , and E assuming that $[Ox] = [Red]$.

directions become

$$\Delta G_a^\ddagger = \Delta G_0^\ddagger - (1 - \alpha)F(E - E^0) \quad (1.19)$$

$$\Delta G_c^\ddagger = \Delta G_0^\ddagger + \alpha F(E - E^0) \quad (1.20)$$

The rate constants for the cathodic and anodic reactions have an Arrhenius form,

$$k_c = Ae^{-\frac{\Delta G_0^\ddagger}{RT}} e^{-\frac{-\alpha F(E-E^0)}{RT}} \quad (1.21)$$

$$k_a = Ae^{-\frac{\Delta G_0^\ddagger}{RT}} e^{\frac{(1-\alpha)F(E-E^0)}{RT}} \quad (1.22)$$

They share the common factor $Ae^{-\frac{\Delta G_0^\ddagger}{RT}}$, which is known as the *standard rate constant* (k^0).

The potential-dependant current density is simply the difference between the rates of the forward and reverse reactions,

$$j = nFk^0 \left[C_{ox}(0, t) e^{-\frac{-\alpha F(E-E^0)}{RT}} - C_{red}(0, t) e^{\frac{(1-\alpha)F(E-E^0)}{RT}} \right] \quad (1.23)$$

This derivation is known as the *Butler-Volmer* formulation of electron transfer kinetics, and is the fundamental model describing the current-overpotential relationship. Continuing to assume that $\frac{[Ox]}{[Red]} = 1$, at E^0 no net current is observed; however, the reaction proceeds in the forward and reverse directions with equal velocities. The “current” of this process can be defined as

$$j_0 = nFk^0 C_{ox}^{*(1-\alpha)} C_{red}^{*\alpha} \quad (1.24)$$

and is known as the exchange current density. Combining equations 1.15,

1.23, and 1.24, and expressing the result in a logarithmic form gives the Tafel equation,

$$\eta_r = \frac{RT}{\alpha F} \ln j_0 - \frac{RT}{\alpha F} \ln j \quad (1.25)$$

which describes the relationship between η_r and the activation energy barrier (through j_0). Smaller values of ΔG_0^\ddagger yield smaller η_r , and thereby a smaller η_{total} . This can be accomplished by carefully tailoring the catalyst for the reduction/oxidation reaction of interest, and is a key goal in electrocatalysis.

1.2.3.2 Ohmic overpotential (η_Ω)

η_Ω occurs whenever a current flows, and results from the resistances associated with the movement of charge carriers:

$$\eta_\Omega = jR \quad (1.26)$$

where j is the current density, and R is the total resistance. R is the series/parallel summation of the cell's individual resistance elements, including:

1. the conduction of electrons through the cell components,
2. the migration of ions through the electrolyte, and
3. contact resistances.

η_Ω is minimized by optimizing the cell construction and minimizing the resistance of its components.

1.2.3.3 Concentration overpotential (η_d)

Concentration overpotential arises from the diffusion of species from the bulk solution to the electrode surface, and is therefore intimately linked to the

species diffusion coefficient. Analytically, η_d is expressed as

$$\eta_d = -\frac{RT}{nF} \ln \left(1 - \frac{j}{j_l} \right) \quad (1.27)$$

where j_l is the limiting current density (i.e., the current density at the maximum rate of diffusion). Many formula are used to describe j_l , and all are derived on the basis of Fick's law of diffusion. The solution to the diffusion problem is dependant on the geometry of the electrode (i.e., sphere, plane, band etc.). In the case of semi-infinite linear diffusion, the limiting current for an oxidation reaction is given by

$$j_l = \frac{nFDC^*}{\delta} \quad (1.28)$$

where n is the number of electrons transferred, D is the diffusion coefficient of the reactant, and δ is the thickness of the diffusion layer.

1.3 Alcohol oxidation mechanisms in acid

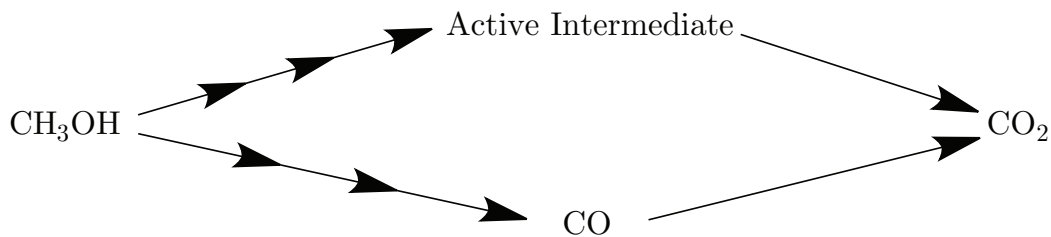
In 1975, Sokolova^[39] found that the electrochemical behaviour of alcohols with different numbers of carbon atoms, and structures, depended strongly on the number of hydrogen atoms connected to the α -carbon. All other structural properties were found to be less important. This finding leads to natural divisions in the broad topic of alcohol oxidation, and categorizes all monohydric alcohols into four groups: methanol, primary, secondary, and tertiary alcohols. With the exception of the tertiary alcohols, which do not show appreciable reactivity at low temperature, the proceeding sections will discuss the generally accepted mechanisms of their oxidation. To highlight the differences between these groups, only the simplest examples will be discussed: methanol, ethanol, and 2-propanol, focusing on the use of platinum catalysts an acidic electrolyte.

Particular emphasis will be placed on the oxidation of 2-propanol, as it is a topic that has not received much attention in reviews, and it is also the main reaction investigated throughout the remainder of this dissertation. Changes with electrolyte pH will be discussed in Chapter 2, and the use of alloyed catalysts will be discussed in Chapter 4.

1.3.1 Methanol oxidation

The simplest and possibly the most studied alcohol for use in a Direct Alcohol Fuel Cell (DAFC) is methanol. A significant body of work has been dedicated to understanding the mechanism of its oxidation, and many comprehensive reviews are available.^[40–42] For the purpose of this discussion, only investigations using platinum single crystals will be discussed, specifically focusing on the effects of structure on reactivity. Methanol oxidation to carbon dioxide, involving the transfer of six e^- and the addition of an oxygen atom from water, is inevitably complex and involves several intermediates. In general, there is a consensus that the oxidation follows a dual-pathway mechanism (Scheme 1.2). In this mechanism, carbon dioxide is formed through either an “active” intermediate, or through a carbon monoxide intermediate.^[43,44] The formation of carbon monoxide occurs under open circuit conditions, and the maximum coverage is similar to that observed from the decomposition of formic acid. The oxidation of formic acid and of methanol, however, behave very differently; Willsau and Heitbaum^[45] showed that the onset of carbon dioxide production from the oxidation of a pre-adsorbed carbon monoxide monolayer and from methanol occurs simultaneously, while formic acid is oxidized before pre-adsorbed carbon monoxide. Specifically, a $^{13}\text{CO}_2$ saturated platinum electrode was used to oxidize $^{12}\text{CH}_3\text{OH}$ or $^{12}\text{CHOOH}$, and the car-

bon dioxide products were monitored by Differential Electrochemical Mass Spectrometry (DEMS). Signals for $^{13}\text{CO}_2$ and $^{12}\text{CO}_2$ occurred simultaneously during oxidation of methanol, while $^{12}\text{CO}_2$ was observed before $^{13}\text{CO}_2$ during the oxidation of formic acid. This behaviour shows that carbon monoxide must be removed from the catalyst surface before methanol can be oxidized, while oxidation of formic acid can occur on the carbon monoxide saturated platinum catalyst. This difference in behaviour is believed to result from a higher steric requirement for the oxidation of methanol, which is proposed^[46,47] to require three contiguous surface sites.



Scheme 1.2: The duel-pathway mechanism for the methanol oxidation reaction.

Herrero et al.^[48] studied the oxidation of methanol on clean, well-defined platinum single crystal electrodes. Table 1.3 summarizes the initial activity of these surfaces towards the oxidation of methanol (0.2 M methanol in 0.1 M HClO_4), and Figure 1.4 illustrates the atomic arrangements of these surfaces. The rate of methanol oxidation is significantly influenced by the atomic arrangement of the surface atoms, i.e., the reaction is surface structure sensitive. In the case of Pt(111) and Pt(100), significant hysteresis is observed due to the formation of poisoning species at low potentials. Hysteresis during alcohol oxidation indicate the formation of strongly adsorbed intermediates that hinder the catalytic reaction during the anodic sweep. These intermediates are oxidized at high potentials, yielding a clean platinum surface during the cathodic sweep. During the cathodic sweep, fewer or no adsorbed intermediates

remain on the electrode surface, leading to higher current densities. In the case of Pt(110), Herrero et al.^[48] attributed the low current density during the cathodic sweep to an increase in the oxidation potential for carbon monoxide; i.e., carbon monoxide adsorbents were still present.

Table 1.3: Summary of the peak current density and potential for the oxidation of methanol over Pt(111), Pt(110), and Pt(100).^[48]

Surface	Anodic Sweep ^a		Cathodic Sweep ^a	
	j_{peak} (mA cm ⁻²)	E_{peak} (V)	j_{peak} (mA cm ⁻²)	E_{peak} (V)
Pt(111)	1.91	0.69	1.30	0.65
Pt(110)	33.80	0.87	6.15	0.74
Pt(100)	4.21	0.78	3.55	0.76

^a Values are estimated from the curves published by Herrero et al.^[48]

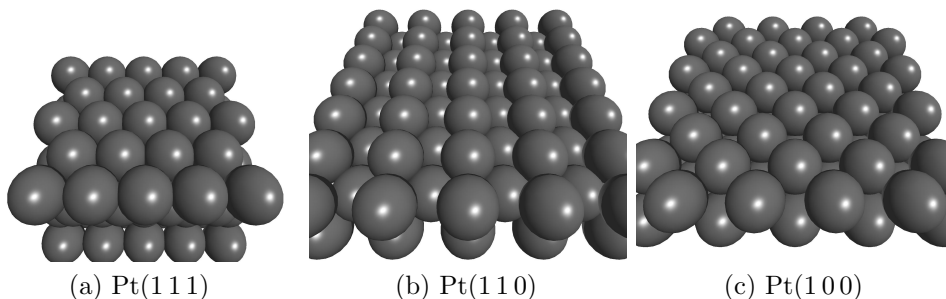


Figure 1.4: Representative atomic arrangements of some typical platinum surfaces.

As is the case for the oxidation of carbon monoxide,^[49] the oxidation of methanol^[50] is enhanced by the presence of steps and surface defects. Table 1.4 summarizes the steady-state current as a function of potential and surface atomic arrangement, determined after a 15 min oxidation using Pt(111) and Pt[n(111)×(110)]-type electrodes (Pt(554), n = 9, and Pt(553), n = 4). A

stark increase in the stabilized current density occurs as the number of Pt(110) steps increases.

Table 1.4: Steady-state current as a function of potential and surface step density for the oxidation of methanol on Pt[n(111)×(110)]-type electrodes.^[50]

E (V)	$j_{t=15\ min}^{Pt(111)}$ ($\mu\text{A cm}^{-2}$)	$j_{t=15\ min}^{Pt(554)}$ ($\mu\text{A cm}^{-2}$)	$j_{t=15\ min}^{Pt(553)}$ ($\mu\text{A cm}^{-2}$)
0.4	0.0	0.5	1.5
0.5	0.5	3.6	2.5
0.6	2.5	49.1	120.6
0.7	20.0	140.4	370.0

A kinetic analysis of the chronoamperometric transients was also carried out to determine the decomposition rate of methanol, the oxidation rate of carbon monoxide, the time-dependant surface coverage of carbon monoxide, and a general expression for the direct pathway, as a function of the applied potential. Although the model used is somewhat simplistic in nature, good fitting of the current-time transients was achieved. Housmans and Koper found that not only is the oxidation rate of carbon monoxide enhanced by step edges, but so is the decomposition rate of methanol. For the three catalyst surfaces studied, at potentials below 0.55 V the rate of oxidation of carbon monoxide is slower than the decomposition rate of methanol, and at potentials above 0.55 V the rate of oxidation of carbon monoxide is faster than decomposition. The latter scenario has important implications, as it predicts a rising current-time transient, which is the case for Pt(111). Further, the authors also found that step edges facilitate the direct oxidation pathway.

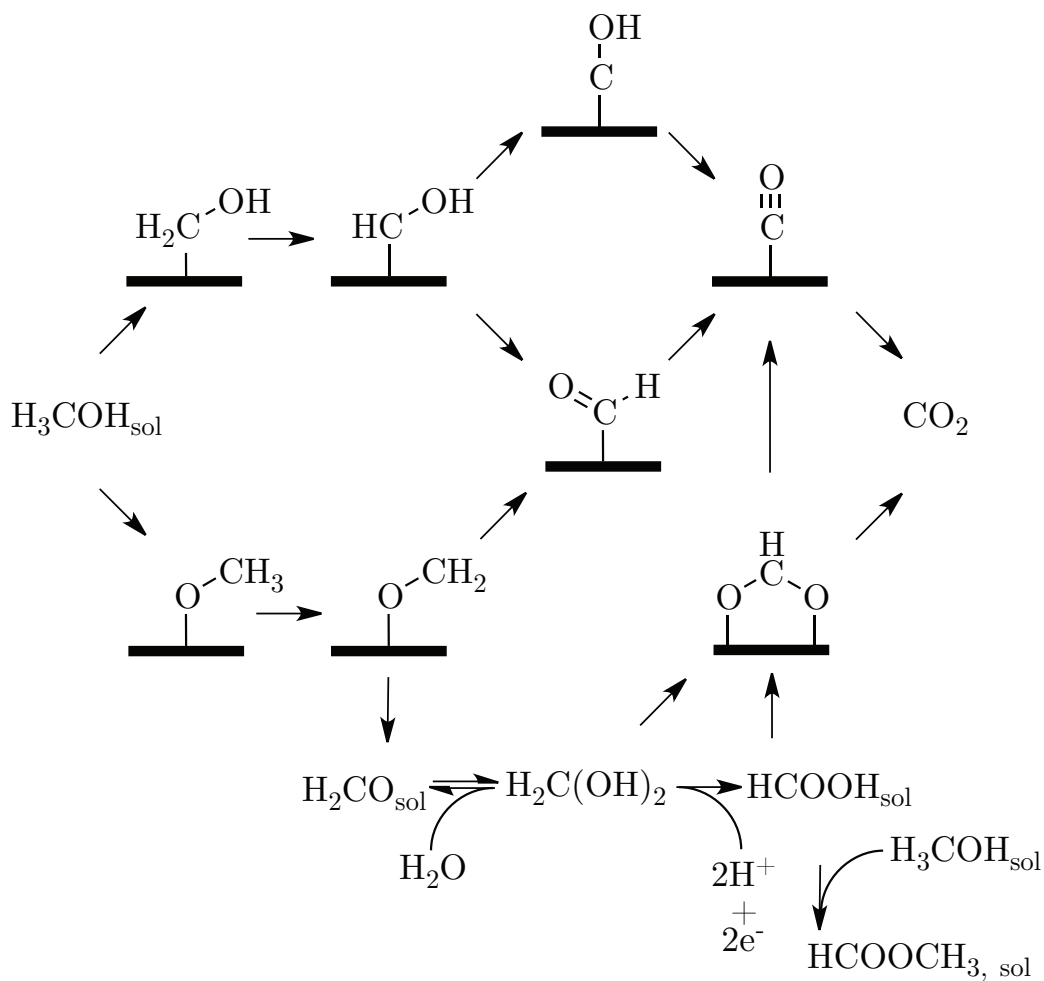
Aside from carbon monoxide, several solution phase intermediates have been observed experimentally, including formic acid,^[51,52] formaldehyde,^[51-53] and methylformate.^[54] Scheme 1.3 depicts the commonly accepted pathway for the oxidation of methanol on platinum that accounts for the presence of

the observed solution phase species. As can be seen from this mechanism, the decision between the carbon monoxide-forming pathway, and the active intermediate pathway, is made during the first activation step (i.e., cleavage of a CH or the OH bond). Results from Online Electrochemical Mass Spectroscopy (OLEMS) suggest that the choice to cleave either the CH or the OH band depends on the arrangements of the surface atoms, as well as the electrolyte.^[54] Further, consistent with activities tabulated in Table 1.3, it was found that the carbon monoxide-forming pathway plays a predominant role on Pt(111), while the pathway through the active intermediate (solution phase formic acid in Scheme 1.3) is more pronounced on Pt(100) and Pt(110).

1.3.2 Ethanol oxidation

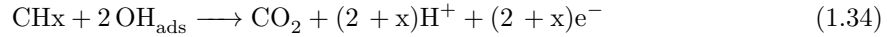
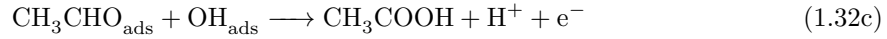
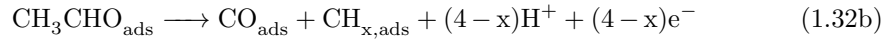
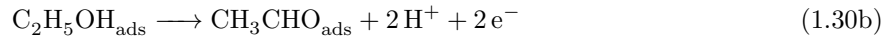
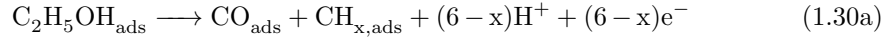
Ethanol, being the simplest monohydric alcohol containing a C–C bond, is regarded as a model molecule in probing the electrooxidative cleavage of C–C bonds. Further, its high energy density (Table 1.2), and the fact that it can be viewed as being renewable when made from biomass, has attracted considerable interest from the scientific community.^[40] Its complete oxidation, requiring the transfer of 12 e⁻ and the addition of three O atoms, is complex and not fully understood.

The oxidation of ethanol, rather than proceeding completely to carbon dioxide, produces acetaldehyde and acetic acid as the major products of the reaction.^[40] These two and four e⁻ transfer products are unwanted, as they yield only a fraction of ethanol's energy density and, perhaps more importantly in the case of acetic acid, produce a strongly coordinating acetate ion which can poison the catalyst.^[55] Scheme 1.4 presents the commonly accepted reactions that occur during the oxidation of ethanol using a platinum catalyst. It should



Scheme 1.3: Generally accepted reaction scheme for the electrochemical oxidation of methanol on metal electrodes.^[54] Note that loss of H from adsorbed species to form H_{ad} or H^+ is not differentiated, so charge transfer events have not been included (i.e., concerted proton transfer to a nearby water molecule coupled with electron transfer, vs stepwise deprotonation to form $\text{Pt}-\text{H}$ followed by its oxidation).

be emphasized that these are not the elementary steps of the reaction, and do not represent a complete mechanism. They do, however, represent a generalized set of reactions that account for the formation of all the experimentally observed products.



Scheme 1.4: General reaction scheme for the electrochemical oxidation of ethanol on metal electrodes.^[40]

The current density observed during the oxidation of ethanol shows a significant dependence on the arrangement of the surface atoms.^[56–58] Table 1.5 summarizes the voltammetric activity of several low index platinum single crystal electrodes (Figure 1.4) in a 0.1 M ethanol solution with a 0.1 M HClO_4 supporting electrolyte. Similar trends were also reported by Morin et al.^[57] As was the case observed with the oxidation of methanol, the oxidation of ethanol is surface structure sensitive (i.e., the reaction rate strongly depends on the arrangement of surface atoms). In situ Fourier Transform Infrared Spectroscopy (FTIR) identified the presence of acetaldehyde, acetic acid and, to a limited extent, carbon dioxide and carbon monoxide. Carbon monoxide acts as a surface poisoning species during the oxidation of ethanol,^[57] similar to the poisoning effect observed in the oxidation of methanol. The formation of adsorbed carbon monoxide begins at low potentials (ca. 0.2 V for all three

surface) indicating that, although only to a small extent, C–C bond cleavage has occurred. Carbon dioxide formation commences at ca. 0.5 V. Even after the removal of all the carbon monoxide from the surface, the FTIR band due to carbon dioxide continues to grow. Such behaviour is indicative of other adsorbents that are not observed by FTIR, such as adsorbed CH_x fragments. Supporting this conclusion, Shin et al.^[55] have demonstrated that the $\alpha - C$ of ethanol is more efficiently oxidized to carbon dioxide at lower potentials. Specially, carbon dioxide isotopomers produced from the oxidation of $^{13}\text{CH}_3^{12}\text{CHOH}$ and $^{12}\text{CH}_3^{13}\text{CHOH}$ over a polycrystalline platinum catalyst were studied as a function of applied potential using DEMS. At potentials between 0.44 and 0.84 V, up to three times more $^{13}\text{CO}_2$ is produced from $^{12}\text{CH}_3^{13}\text{CHOH}$ than from $^{13}\text{CH}_3^{12}\text{CHOH}$.

Table 1.5: Summary of the peak current density and potential for the oxidation of ethanol over Pt(1 1 1), Pt(1 1 0), and Pt(1 0 0).^[56]

Surface	Anodic Sweep ^a		Cathodic Sweep ^a	
	j_{peak} (mA cm ⁻²)	E_{peak} (V)	j_{peak} (mA cm ⁻²)	E_{peak} (V)
Pt(1 1 1)	0.64	0.53	0.87	0.82
Pt(1 1 0)	1.13	0.74	1.62	0.70
Pt(1 0 0)	1.29	0.79	1.07	0.71

^a Values are estimated from the curves published by Xia et al.^[56]

Chang et al.^[58] also studied the oxidation of ethanol on Pt(1 1 1), Pt(1 1 0), and Pt(1 0 0), by voltammetry and FTIR, with a particular emphasis on the selectivity of these surfaces towards the formation of the three products discussed previously. It was found that the onset for the formation of acetaldehyde was 0.54–0.64 V, regardless of crystallographic orientation. The onset of the oxidation to form acetic acid, however, occurs at the same potential as acetaldehyde over Pt(1 1 1), at ca. 0.7 V over Pt(1 0 0), and at ca. 0.64 V over

Pt(110). Further, the onset to form acetic acid, and the onset to form carbon dioxide, behave very similarly. This similarity in behaviour between the four e^- pathway to form acetic acid, and the 12 e^- pathway to form carbon dioxide, as well as the activity dependence on surface structure, is explained by the activity of these surface towards formation of adsorbed oxygen species.^[58] These species then act as the oxygen source to form acetic acid and carbon dioxide. In all cases, acetic acid was the most dominant species observed by FTIR at the end of the potential sweep, indicating a strong preference of these surfaces towards the four e^- pathway.

The influence of steps on the selectivity towards acetic acid production during ethanol oxidation over platinum was studied by Tarnowski and Korzeniowski.^[59] Specifically, Pt(111), Pt(557) (Pt[6(111) × (100)]), and Pt(335) (Pt[4(111) × (100)]) electrodes were used to oxidize a ca. 40 μ L drop of 0.3 M ethanol in 0.1 M HClO₄ for a duration of 60 s. An aliquot of this solution was then analyzed by ion chromatography, and was compared to the total charge passed during the 60 s electrolysis experiment. Table 1.6 summarizes the results of this study. As the density of steps and defects increases, the total charge transferred during the bulk electrolysis of ethanol increases, despite a decrease in acetic acid yield. The authors attributed this counter-intuitive behaviour to the higher activity of these sites towards the formation of acetaldehyde and/or carbon dioxide, in agreement with previous reports^[55] on the higher catalytic activity of steps towards C–C bond cleavage. The authors note that although CO₃²⁻ was observed by ion chromatography, quantifiable concentrations could not be determined due to background CO₃²⁻ from atmospheric carbon dioxide.

Table 1.6: Total anodic charge passed, and the fraction of this charge associated with the formation of acetic acid, during the bulk electrolysis of ethanol as a function of applied potential, and step density.^[59]

E (V)	Pt(1 1 1)		Pt(5 5 7)		Pt(3 3 5)	
	Q_{anodic}^a (mC cm ⁻²)	% <i>Acetate</i> ^a (%)	Q_{anodic}^a (mC cm ⁻²)	% <i>Acetate</i> ^a (%)	Q_{anodic}^a (mC cm ⁻²)	% <i>Acetate</i> ^a (%)
0.44	15.6	30.8	15.6	14.0	10.0	8.4
0.54	90.0	24.1	59.6	21.7	38.0	9.7
0.64	64.4	14.7	86.0	9.1	66.8	9.5
0.74	48.0	6.6	44.8	5.2	56.4	6.3
0.84	10.0	13.3	25.5	8.0	28.7	7.4

^a Values are estimated from the plots published by Tarnowski and Korzeniowski.^[59]

1.3.3 2-propanol oxidation

In 1975, Sokolova^[39] found that there are three essential differences between the voltammograms of secondary and primary alcohols, using a smooth polycrystalline platinum electrode:

1. the hydrogen desorption maxima (ca. 0–0.3 V vs. RHE) are not suppressed in the presence of the secondary alcohol,
2. they are electrochemically active in the double-layer region (ca. 0.3–0.8 V vs. RHE) during the anodic sweep, and
3. they are inactive at potentials between ca. 0.8 and 1.0 V vs. RHE, but are active at higher potentials (ca. 1.0–1.6 V vs. RHE).

The retention of the hydrogen desorption maxima during the first anodic sweep indicates that no carbon containing poisons form at the beginning of the sweep. This behaviour contrasts that of methanol, which decomposes under open circuit conditions to form adsorbed carbon monoxide,^[40] and suppresses the hydrogen desorption maxima. Succeeding potential sweeps in the presence of secondary alcohols also do not suppress the hydrogen desorption

maxima, indicating that poisoning intermediates, if formed, do not remain on the electrode, or that they are susceptible to reductive elimination.

The electrochemical activity in the double-layer region, indicating the onset of electrochemical oxidation, supports Sokolova's conclusion that destructive chemisorption occurs at these potentials. The proposed intermediate of this chemisorption is RRC^*OH (where the * denotes the atom that is bonded to the surface). The loss in activity near 1.0 V indicates a change in mechanism due to the oxidation of the platinum surface to form weakly bound oxygen species. However, the fact that the platinum is active at potentials exceeding 1.0 V, where more strongly bound oxygen species form, indicates that the oxidation also occurs through a pathway involving the oxygen covered platinum surface.

Gao et al.^[60] also studied the oxidation of 2-propanol in aqueous, and non-aqueous environments. In neat 2-propanol, using LiClO_4 as an electrolyte, acetone is the only product observed by Single Potential Alteration Infrared Spectroscopy (SPAIRS). Its onset potential is 0.9 V; in an aqueous environment, however, the onset potential for the formation of acetone is significantly depressed, and begins to form at 0.1 V. Such drastic changes in the electrochemical behaviour of 2-propanol illustrates the extreme influence that the solution environment can play on electrochemical reaction kinetics.

During the oxidation of 2-propanol, only acetone and carbon dioxide have been observed by in situ IR spectroscopy,^[60-65] and gas chromatography^[66] (note that carbon dioxide was observed by first converting it to the carbonate anion). Further, the current densities observed^[67] during the half cell oxidation of 2-propanol are significantly higher than those for methanol, at potentials lower than 0.9 V in acid. Additionally, the current densities observed^[68] during the half cell oxidation of 2-propanol are also significantly higher than those for

ethanol, at potentials lower than 0.8 V in acid.

1.3.3.1 Oxidation using well defined platinum electrodes

Leung et al.^[65] was the first to study the oxidation of 2-propanol on well defined platinum single crystals in 0.1 mol dm⁻³ HClO₄. Supplementing their voltammetric studies, SPAIRS was used to identify the molecular species present in solution, and on the surface of the electrode, during the oxidation. On an ordered Pt(111) electrode, acetone is the major product of the oxidation; only a small amount of carbon dioxide (ca. 6×10^{-10} mol cm⁻³) is observed at potentials between 0.64 and 1.04 V. On a disordered Pt(111) electrode, acetone is still the major product, however, slightly larger quantities of carbon dioxide are produced. In both cases, no IR adsorption bands indicative for Pt–CO are observed, indicating that carbon monoxide is not an intermediate of the oxidation pathway, or it exists at concentrations below detection limits ($\theta \leq 0.05$).

These results were later corroborated by Sun and Lin,^[63] who also expanded the oxidation of 2-propanol studies to Pt(110) and Pt(100) surface. S-polarized IR spectroscopy was used to identify the species present in solution during the oxidation (adsorbed species are IR inactive under these conditions^[69]). At potentials lower than 0.44 V, a single alkene band occurs at 1600 cm⁻¹, presumably due to the dehydration of 2-propanol to form CH₃–CH=CH₂. This band quickly disappears above 0.54 V, and new bands at 3010 and 1700 cm⁻¹ begin to grow in, signifying the onset of 2-propanol dehydrogenation to form acetone, and are assigned to the C–H and C=O stretches of acetone, respectively. Above 0.74 V, a new absorption band at 2345 cm⁻¹ appears, signifying the formation of carbon dioxide; the onset of carbon dioxide formation

correlates well with the formation of oxygen species on platinum. Even at potentials exceeding 1.24 V, however, acetone is the major product of 2-propanol oxidation.

There are two significant differences between the behaviours of Pt(111), Pt(110), and Pt(100) during the oxidation of 2-propanol. First, their catalytic activities differ significantly, that is to say that the reaction is surface structure sensitive. Table 1.7 summarizes the activity of these surfaces, represented by the oxidation peak potential and current density. The oxidation of 2-propanol is significantly favoured over the (110) facet of platinum. Sun and Lin, however, also observed that Pt(110) is the least stable to potential cycling. Armand and Clavilier^[70] previously demonstrated that Pt(110) surfaces reconstruct upon oxidation ($E \geq 0.8$ V). The symmetry of the reconstructed Pt(110) surface is essentially the same as Pt(111). The apparent instability of the Pt(110) surface towards the oxidation of 2-propanol is thereby believed to result from this reconstruction.

Table 1.7: Summary of the peak current density and potential for the oxidation of 2-propanol over Pt(111), Pt(110), and Pt(100).^[63]

Pt Surface	j_{peak} (mA cm ⁻²)	E_{peak} (V)
Pt(111)	3.63	0.68
Pt(110)	10.11 ^a 0.63 ^b	0.72
Pt(100)	1.97	0.88

^a First cycle.

^b 10th cycle.

The second major difference between the facets is that only Pt(100) shows significant hysteresis (i.e., current densities during the cathodic sweep are higher than during the anodic sweep). The absence of hysteresis on Pt(111) and Pt(110) indicate that fewer, or no poisons are formed on these crystal facets.

Interestingly for Pt(110), when the low-potential limit of the voltammogram is decreased from 0.24 to -0.01 V, less hysteresis occurs, and the product distribution changes. Specifically, the amount of product carbon dioxide decreases, and the amount of product acetone increases. Consistent with the findings of Sokolova,^[39] Sun and Lin concluded that molecular adsorption of 2-propanol occurs at 0.24 V. They further proposed that the resulting unidentified adsorbate is the source of hystereses during the oxidation on Pt(110). Further, this adsorbate enhances the production of carbon dioxide, and it inhibits the production of acetone. They concluded that at potentials below 0.24 V the unidentified species desorbs, freeing surface sites for 2-propanol dehydrogenation, and lessening the hysteresis between the anodic and cathodic sweeps. Further, this unidentified species appears to be linked with the formation of carbon dioxide.

Previously, Housmans and Koper^[50] demonstrated that the oxidative decomposition of methanol on platinum to form Pt-CO is enhanced by step edges. Further, Lebedeva et al.^[49] demonstrated that the rate of carbon monoxide oxidation increased linearly with platinum step density. Step edges are more active towards water oxidation, forming oxygen-containing species at lower potentials than terraces. These oxygen-containing species are the oxygen source during the oxidation of carbon monoxide to carbon dioxide. The lowered onset potential for their formation on step edges, explains the linear relationship between step density and activity towards carbon monoxide oxidation. Sun and Lin^[62] also studied the kinetics of acetone and carbon dioxide formation during the oxidation of 2-propanol on the stepped platinum surfaces, Pt(610) and Pt(210). Table 1.8 summarizes the peak rates and potentials for the formation of acetone and carbon dioxide.

Table 1.8: Summary of the maximum kinetic rate of acetone and carbon dioxide formation on various Pt terraces, and stepped single crystals electrodes. [62]

Surface	$k_{\text{C=O}}^{\text{peak}} \times 10^3$ ($\text{s}^{-1} \text{cm}^{-2}$)	$E_{\text{peak}}(\text{C=O})$ (V)	$k_{\text{CO}_2}^{\text{peak}} \times 10^3$ ($\text{s}^{-1} \text{cm}^{-2}$)	$E_{\text{peak}}(\text{CO}_2)$ (V)
Pt(111)	1.50	0.30	6.12	0.90
	10.40	1.00		
Pt(110)	0.96	0.40	1.54	1.10
	12.83	1.00		
Pt(100)	26.04	0.60	4.06	1.00
	8.06	0.90		
Pt(610)	25.73	0.60	7.95	1.00
	5.09	1.10		
Pt(211)	5.65	0.50	2.13	1.10
	8.65	1.00		

According to the terrace-ledge-kink model, Pt(610) is viewed as a six atom wide Pt(100) terraces with monoatomic Pt(110) steps, and Pt(210) is viewed as a three atom wide Pt(111) terraces with monoatomic Pt(100) steps. Contrary to the behaviour of methanol^[50] and carbon monoxide, the activity of stepped platinum surfaces towards the 2-propanol does not scale with step density (i.e., $k_{\text{CO}_2}^{\text{Pt}(211)} < k_{\text{CO}_2}^{\text{Pt}(610)}$). The activities of these stepped surfaces, however, does closely resemble that of the terraces (i.e., $k_{\text{C=O}}^{\text{Pt}(610)} \simeq k_{\text{C=O}}^{\text{Pt}(110)}$ and the behaviour of $k_{\text{C=O}}^{\text{Pt}(211)}$ is between $k_{\text{C=O}}^{\text{Pt}(111)}$ and $k_{\text{C=O}}^{\text{Pt}(100)}$). Further, in the case of Pt(610), the step edges do appear to enhance the activity of the surface towards carbon dioxide formation relative to Pt(100). This trend, however, does not apply to the Pt(210) surface (i.e., $k_{\text{C=O}}^{\text{Pt}(210)} < k_{\text{C=O}}^{\text{Pt}(111)}$ or $k_{\text{C=O}}^{\text{Pt}(100)}$).

The selectivity of these surfaces towards the formation of acetone vs. carbon dioxide is determined by comparing the maximum values of $k_{\text{C=O}}$ and k_{CO_2} . As can be seen from Table 1.8, the ordering of $k_{\text{C=O}}$ and k_{CO_2} as a function of surface atomic arrangement is different. It appears that the surface atomic arrangement that is optimum for acetone formation may not be optimum for carbon dioxide formation.

1.3.3.2 Investigations of the nature and reactivity of adsorbed intermediates

The nature of the adsorbates formed during the oxidation of 2-propanol was first studied by Sumodjo et al.^[71] The adsorbates were first formed at 0.35 V for 10 mins. The electrolyte was then exchanged with a H₂SO₄ electrolyte, and the adsorbates were stripped by voltammetry. Sweeping the electrode in either initial directions gives a peak at 1.12 V. The amount of charge transferred during the stripping, however, decreases when the potential is swept in the cathodic direction first. Thus the weakly adsorbed intermediates are susceptible to reductive elimination at potentials below 0.35 V, while the strongly adsorbed intermediate(s) remain on the electrode.

The charge required to oxidize the weakly- and strongly-bound intermediates was used to study their relative predominance as a function of adsorption potential. Table 1.9 summarizes the approximate distribution of these charges. At adsorption potentials between 0.15 and 0.6 V, the charge for stripping the strongly adsorbed intermediate is ca. 20–35% of the total charge. In contrast, greater than 50% of the total charge is required to oxidize the strongly adsorbed intermediates formed from n-propanol, 1,2-propandiol, and 1,3-propandiol.^[71] As the adsorption potential is increased, the amount of strongly adsorbed intermediate increases at the expense of the weakly adsorbed intermediate. In addition, the total oxidative stripping charge decreases as the adsorption potential increases from 0.3 to 0.6 V. These results show most of the adsorbates formed during the oxidation of 2-propanol are weakly adsorbed, and that the nature and distribution of the adsorbates is significantly influenced by the adsorption conditions.

Pastor et al.^[64] later investigated the chemical nature of the adsorbed

Table 1.9: Charge required to oxidize the strongly and weakly adsorbed intermediates formed during the oxidation of 2-propanol, as a function of adsorption potential.^[71]

Adsorption Potential (V)	Q_{weak}^a (mC cm ⁻²)	Q_{strong}^a (mC cm ⁻²)	% _{weak}
0.15	0.31	0.08	79
0.20	0.38	0.09	80
0.25	0.38	0.10	79
0.30	0.38	0.11	78
0.35	0.36	0.13	73
0.40	0.34	0.13	72
0.45	0.32	0.14	70
0.50	0.29	0.15	66
0.55	0.26	0.14	65
0.60	0.24	0.13	65

^a Values are estimated from the curves published by Sumodjo et al.^[71]

intermediates using FTIR and DEMS. First, adsorbates were formed by oxidizing 2-propanol on a polycrystalline platinum electrode at either 0.25 or 0.35 V. During adsorption at 0.35 V, a residual current remains after five mins, resulting from bulk electrolysis; no residual current is observed at 0.25 V after two mins.

The intermediates formed were then stripped in a 2-propanol free HClO₄ electrolyte, and the products were analyzed by DEMS. The onset potential for oxidation of the adsorbates is 0.55 V, and the volatile product is carbon dioxide. As illustrated in Table 1.10, the stripping behaviour of the adsorbates formed at 0.25 and 0.35 V is different during the first anodic sweep. Specifically, carbon dioxide production peaks at two potentials for adsorbates formed at 0.35 V, and only at one potential for adsorbates formed at 0.25 V. Thus the number and the nature of the adsorbates is potential dependent, with the appearance of a second intermediate at higher potentials. During the first cathodic sweep, after the anodic week and regardless of adsorption potential, a single carbon dioxide peak is observed by DEMS, following the reduction of Pt–O, just as

free platinum surface domains begin to appear.

Table 1.10: Potentials corresponding to peak carbon dioxide production rates from the oxidation of adsorbates formed from 2-propanol as a function of adsorption potential.^[64]

E_{ad} (V)	$E_{peak}(\text{CO}_2)$	
	Anodic sweep (V)	Cathodic sweep (V)
0.25	1.04	0.73
0.35	0.69	0.73
	1.04	

The chemical nature of the adsorbates formed was investigated with FTIR. Using a flow-cell, such that the electrode potential could be continuously maintained while also avoiding its exposure to air, adsorbates were formed at 0.3 V, and the electrolyte was then replaced with a 2-propanol-free HClO_4 electrolyte. The adsorption potential was chosen in order to avoid significant contribution of the oxidation and reduction processes discussed previously. A reference spectrum was collected, and the adsorbates were then oxidized at 1.5 V. IR bands at 2962 and 1262 cm^{-1} were assigned to CH_3 and C–OH moieties, respectively. These bands are absent using s-polarized light, confirming that they result from an adsorbed species. No bands consistent with carbon monoxide are observed. Pastor et al. thereby concluded that adsorption at 0.3 V proceeds via cleavage of the $\alpha\text{-C-H}$ bond to produce $(\text{CH}_3)_2\text{C}^*\text{OH}$, consistent with the findings of Sokolova,^[39] and Sun and Lin.^[62,63]

Similar to the findings of Sumodjo et al.,^[71] Pastor et al.^[64] found that cycling the adsorbates into the hydride region significantly reduces the stripping charge; Table 1.11 summarizes these results. At potentials below 0.2 V propane is detected by DEMS, and is consistent with a loss of an adsorbate and with its dehydration. The preservation of the adsorbate’s C_3 backbone during this

process indicates that cleavage of the C–C bonds does not occur at potentials below 0.35 V. This reduction to form propane is, however, more difficult for adsorbates formed at 0.35 V than at 0.25 V.

Table 1.11: Changes in adsorbate coverage, and stripping behaviour, as a function of incursion into the surface hydride potential region.^[64]

Adsorption potential (V)	Number of sweeps in Pt–H region	Anodic CO ₂ peak potential (V)	Total stripping charge (C)
0.25	0	1.04	3.85
	4	0.66	0.75
0.35	0	1.04	3.03
		0.69	
	4	1.04	1.05
		0.65	
		1.03	
10	0.67	0.92	
		1.04	

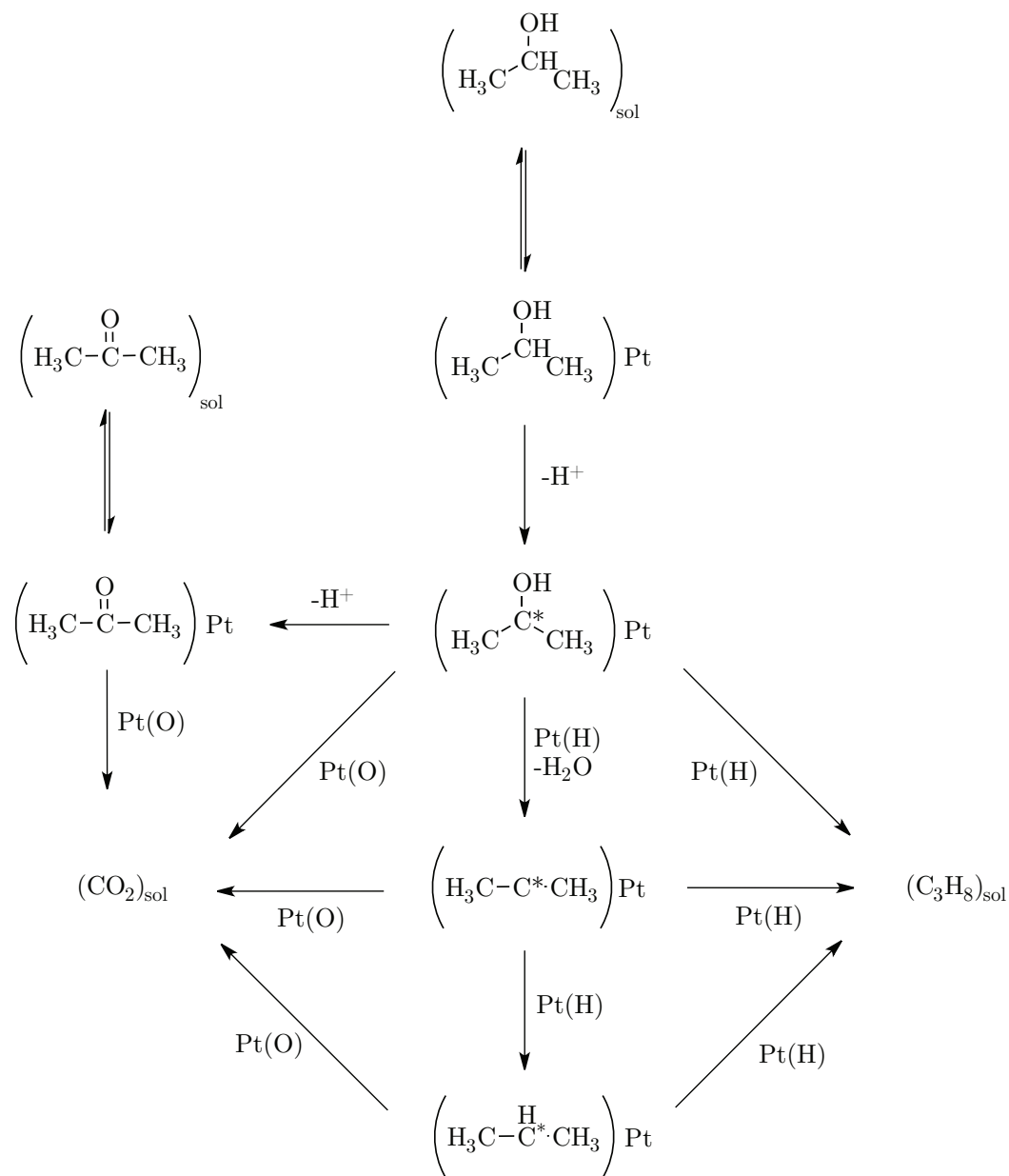
In summary of the above investigations, the most complete mechanism for the oxidation of 2-propanol over platinum catalysts in acid was proposed by Pastor et al.^[64] (Scheme 1.5). A similar mechanism was proposed by Sun and Lin.^[63] Firstly, 2-propanol is destructively chemisorbed onto platinum via cleavage of the α -C-H bond to form $(\text{CH}_3)_2\text{C}^*\text{OH}$. Once adsorbed, the oxidative mechanism diverges into parallel pathways; the dominant pathway is dictated by the coverage of the platinum surface by adsorbed hydrogen. At high coverages of Pt-H, hydrogenolysis to produce either $(\text{CH}_3)_2\text{C}^*$ or $(\text{CH}_3)_2\text{C}^*\text{H}$ must be considered. These σ -bound adsorbates are highly susceptible to reductive elimination in the presence of Pt-H, generating propane as the product of their reduction.

At higher potentials, i.e., lower Pt-H coverage, dehydrogenation of adsorbed $(\text{CH}_3)_2\text{C}^*\text{OH}$ forms acetone that is adsorbed on the surface via a π -bonding interaction. This intermediate can desorb from the surface, giving acetone

as the oxidation product. Pastor et al.^[64] proposed that $\eta^2\text{-(CH}_3)_2\text{CO}$ is the adsorbate that remains of the electrode surface after cycling the electrode in the hydride region. Indeed, the adsorbates formed at higher potentials are more difficult to reduce than those formed at lower potentials (Table 1.11), and it is expected that the dehydrogenation of $(\text{CH}_3)_2\text{C}^*\text{OH}$ should be favoured over its hydrogenolysis as the adsorption potential is increased, as a result of the decreasing coverage of adsorbed hydrogen. It should be noted that the absence of a ketone absorption band in the IR spectra can be explained for $\eta^2\text{-(CH}_3)_2\text{CO}$, as only IR stretching modes that have a component that is perpendicular to the surface are IR active.^[72] All of the adsorbed species: $(\text{CH}_3)_2\text{C}^*\text{OH}$, $(\text{CH}_3)_2\text{C}^*$, $(\text{CH}_3)_2\text{C}^*\text{H}$, and $\eta^2\text{-(CH}_3)_2\text{CO}$ can potentially be oxidized to carbon dioxide in the presence of adsorbed oxygen-species; however, the pathway to form carbon dioxide is, at this time, unknown.

In contrast to the results of Pastor et al., Gootzen et al.^[73] observed a small Pt–CO IR absorption band at 2010 cm^{-1} for adsorbed formed from the oxidation of 2-propanol. In their study, 2-propanol was adsorbed onto a rough, electrodeposited-platinum electrode at 0.4 V, and then a reference IR spectrum as collected in a 2-propanol free HClO_4 electrolyte. The adsorbates were either: 1) stripped voltammetrically, between 0 and 1.4 V, by sweeping in the anodic or cathodic direction first, and collecting the resulting DEMS spectrum of the oxidized products, or 2) oxidized at 1.4 V, and collecting the resulting IR spectrum upon returning the electrode to the adsorption potential.

Consistent with the previously discussed reports,^[64,71] oxidation peaks at 0.65 and 1.02 V were observed during the stripping of the adsorbents, and both give carbon dioxide mass signals in DEMS. In contrast with Pastor et al., Gootzen et al. proposed that the oxidative peak at 0.65 V was due to



Scheme 1.5: Generally accepted mechanism for the oxidation of 2-propanol over platinum catalysts.^[64]

the oxidation adsorbed carbon monoxide to carbon dioxide. This conclusion, however, appears to be inconsistent with the single crystal studies reported by Sun and Lin^[62] (Table 1.8, p.37), as this peak appears to result from the production of acetone. Sweeping the electrode in the cathodic direction results in a loss of adsorbates, and the formation of propane and propene; no ethane, ethene, or methane was observed which is consistent with the retention to the C₃ backbone of the adsorbate.

The average number of electrons required to produce carbon dioxide from the adsorbates, as quantified by DEMS, was found to be $3.8 \frac{e^-}{CO_2}$ when swept in the anodic direction first, and $5.2 \frac{e^-}{CO_2}$ when swept in the cathodic direction. The fact that more electrons are required to oxidize the adsorbents upon sweeping to potentials below 0.4 V indicate that the adsorbents are, at least partially, susceptible to reductive hydrogenation. On the basis of their experimental $\frac{e^-}{CO_2}$, Gootzen et al.^[73] proposed that their adsorbates have either C₃HO or C₃H₂O molecular formulas. These adsorbates are similar to those proposed by Pastor et al., in that they have retained the C₃ backbone, but they are significantly more dehydrogenated. Although it was not mentioned by Gootzen et al., $5.2 \frac{e^-}{CO_2}$ is close to what is expected for the oxidation of acetone ($5.7 \frac{e^-}{CO_2}$). It is reasonable to conclude that the degree of protonation of the adsorbed species is potential dependant.

1.4 Direct alcohol Fuel Cells

As previously discussed in §1.1.3, the high energy density of alcohols is one of the largest motivations for the development of a DAFC. The efficiency (§1.2) at which this chemical energy is transformed into electrical power is contingent on the mechanism of its oxidation, or more specifically its reaction

kinetics (§1.2.3). As discussed in §1.3, the mechanisms of oxidation for the simplest monohydric alcohols — methanol, ethanol, and 2-propanol — using platinum as a catalyst differ significantly. This section cannot hope to envelope the richness and diversity of the DAFC literature; rather, it will highlight a few *comparative studies* of DAFCs when operated on these three model fuels under comparable conditions. Moreover, subtle differences in the electrolyte, electrode composition, and operating conditions can have large influences on the operating characteristics of a DAFC, and makes comparison between reports challenging. The interested reader, however, is directed to a few recent and comprehensive reviews on the topic.^[74–77]

Aricò et al.^[78] reported a comparison between their methanol and ethanol in a FC using a composite membrane, a platinum-ruthenium anode, and operating at 145 °C. The maximum power density of the Direct Methanol Fuel Cell (DMFC) was twice that of the Direct Ethanol Fuel Cell (DEFC) (110 mW cm⁻² versus 240 mW cm⁻²). Further, the cell potential at peak power was ca. 0.1 V higher in the case of ethanol, denoting that the oxidation was more efficient for methanol. Methanol was completely oxidized to carbon dioxide, and ethanol was oxidized to a mixture of carbon dioxide, and a small amount of acetaldehyde. This product distribution is quite different from that reported by Wang et al.^[79] using either platinum or platinum-ruthenium, who found that their major product was acetaldehyde. It was proposed that the differences in the product distribution resulted from difference in the alcohol:water ratios; Aricò et al.^[78] used a mole ratio of 53:1, and Wang et al.^[79] ratios between two and five. Wang et al. found that increasing the water:ethanol ratio increases the yield of carbon dioxide, from 19.5 to 32.1%. Aricò et al. proposed that the high selectivity of their fuel cell operating on ethanol resulted from the

low ethanol content of the fuel, and that the low performance of their DEFC resulted from the formation of strongly adsorbed intermediates that hindered the reaction.

The rate of alcohol crossover through the membrane was studied by Song et al.^[80] for the DMFC and the DEFC. Crossover^[81] of fuel from the anode to the cathode results in cell depolarization, loss of fuel by evaporation at the cathode. The rate of crossover is known to increase with temperature, with concentration of alcohol in the fuel stream. In order to avoid the negative effects resulting from fuel crossover, dilute fuel solutions in water are generally used. This dilution of the fuel, however, decreases the volumetric energy content of the fuel mixture. Song et al. found that ethanol was less susceptible to crossover than methanol, however, the DMFC performance was higher than the DEFC. The low performance of the DEFC was attributed to activation losses from the oxidation of ethanol.

Somewhat conflicting results appear for the use of 2-propanol in a fuel cell. For example, Wang et al. found that ethanol performed better than 2-propanol at 170 °C when using a platinum-ruthenium anode catalyst, while Cao and Bergens^[82] found that their fuel cell operated at higher potentials (i.e., electrical efficiencies) when operated on 2-propanol than when operated on methanol. Similar performance characteristics were reported by Qi and Kaufman.^[83,84] The performance of the Direct 2-propanol Fuel Cell (D2PFC) showed promisingly high voltage efficiencies at peak power, with values of 60% for 2-propanol, and 30% for methanol. The peak power density of the D2PFC, however, was 75% that of the DMFC.

In addition to the high efficiency of the D2PFC, the crossover of 2-propanol was also found to be less than methanol under comparable conditions.^[82,84] For

example, Qi and Kaufman quantified the rate of 2-propanol crossover and found that it was $\frac{1}{7}$ that of methanol crossover. The low rate of 2-propanol affords the use of higher concentrations of 2-propanol in the fuel mixture, increasing its gravimetric energy density. Promisingly, a D2PFC operating on 100% 2-propanol that achieved good performance has been reported.^[83]

1.5 Research Proposal

As discussed thus far, the mechanisms for the oxidation for methanol, ethanol, and 2-propanol differ significantly from one another. The efficiency of a fuel cell operating on these fuels is highly influenced by the mechanism of oxidation. As will be discussed in more detail in the following chapters, the oxidation of alcohols and the reduction of oxygen is enhanced in alkaline media (see Chapter 2). This enhancement in the rate of reaction should enhance the efficiency of the fuel cell. Further, the lack of carbon monoxide during the oxidation of 2-propanol is an attractive result, and has been used to explain the high activity of the D2PFC.^[82,84]

My research mission is, first, to compare the activity of platinum towards the oxidation of 2-propanol in acidic and alkaline electrolytes and to determine if any kinetic advantages do indeed exist for 2-propanol in base. Further, the activity of this system will be compared with that of methanol. This investigation will then be extended to a real prototype ADAFC, as a proof-of-concept study for comparison with other ADAFC systems.

Little is known about the reaction mechanism of 2-propanol in base, nor about what metals promote the reaction. My second goal will be to conduct a survey of commercially available platinum and platinum-ruthenium alloy catalysts, and compare their real activities in alkaline electrolyte (i.e., nor-

malized to the active area of the catalyst). Additionally, platinum-ruthenium adatom catalysts that have controlled ratios of platinum and ruthenium on the surface will also be evaluated to see the effects of surface ruthenium on the rate of 2-propanol oxidation. Detailed kinetic studies of these catalysts will be described, in hopes to clarify some of the uncertainties in the rate determining step during the oxidation of 2-propanol to acetone. Such knowledge is necessary if rational design of FC catalysts for the oxidation of 2-propanol is ever to be realized.

The final stage of this investigation was to tie together the kinetic studies performed in the three-electrode configuration, and correlate these results with the activity of platinum-ruthenium adatom catalysts within an operating Alkaline Direct 2-Propanol Fuel Cell (AD2PFC). The goal was a proof-of-concept study, to see if the conclusion reached during the three-electrode investigations can be extended to a real operating FC.

References

- [1] Mench, M. M., *Fuel Cell Engines*. Wiley, **2008**.
- [2] Viswanathan, B.; Scibioh, M. A., *Fuel Cells: Principles and Applications*. CRC Press, **2008**, 1st edition.
- [3] Liu, H.; Song, C.; Zhang, L.; Zhang, J.; Wang, H.; Wilkinson, D., A review of anode catalysis in the direct methanol fuel cell. *J Power Sources* **2006**, *155* (2), pp. 95–110.
- [4] Serov, A.; Kwak, C., Review of non-platinum anode catalysts for DMFC and PEMFC application. *Appl Catal, B* **2009**, *90* (3-4), pp. 313–320.
- [5] de Bruijn, F. A.; Dam, V. A. T.; Janssen, G. J. M., Review: Durability and Degradation Issues of PEM Fuel Cell Components. *Fuel Cells* **2008**, *8* (1), pp. 3–22.
- [6] Peighambardoust, S. J.; Rowshanzamir, S.; Amjadi, M., Review of the proton exchange membranes for fuel cell applications. *Int J Hydrogen Energ* **2010**, *35* (17), pp. 9349–9384.

- [7] Li, Q.; Jensen, J.; Savinell, R., High temperature proton exchange membranes based on polybenzimidazoles for fuel cells. *Progress in Polymer Science* **2009**, *5* (34), pp. 449–477.
- [8] Antolini, E., Platinum-based ternary catalysts for low temperature fuel cells Part II. Electrochemical properties. *Appl Catal, B* **2007**, *74*, pp. 337–350.
- [9] Kirubakaran, A.; Jain, S.; Nema, R. K., A review on fuel cell technologies and power electronic interface. *Renewable Sustainable Energy Rev.* **2009**, *13* (9), pp. 2430–2440.
- [10] Sammes, N.; Bove, R.; Stahl, K., Phosphoric acid fuel cells: Fundamentals and applications. *Curr Opin Solid State Mater Sci* **2004**, *8* (5), pp. 372–378.
- [11] Appleby, A., Fuel cell technology: Status and future prospects. *Energy* **1996**, *21* (7-8), pp. 521–653.
- [12] Yu, E. H.; Krewer, U.; Scott, K., Principles and Materials Aspects of Direct Alkaline Alcohol Fuel Cells. *Energies* **2010**, *3* (8), pp. 1499–1528.
- [13] Bidault, F.; Brett, D. J. L.; Middleton, P. H.; Brandon, N. P., Review of gas diffusion cathodes for alkaline fuel cells. *J Power Sources* **2009**, *187* (1), pp. 39–48.
- [14] Gülzow, E., Alkaline fuel cells: A critical view. *J Power Sources* **1996**, *61* (1-2), pp. 99–104.
- [15] McLean, G.; Niet, T.; Prince-Richard, S.; Djilali, N., An assessment of alkaline fuel cell technology. *Int J Hydrogen Energ* **2002**, *27* (5), pp. 507–526.
- [16] Wang, Y.; Li, L.; Hu, L.; Zhuang, L.; Lu, J.; Xu, B., A feasibility analysis for alkaline membrane direct methanol fuel cell: thermodynamic disadvantages versus kinetic advantages. *Electrochem Commun* **2003**, *5* (8), pp. 662–666.
- [17] Varcoe, J.; Slade, R., Prospects for alkaline anion-exchange membranes in low temperature fuel cells. *Fuel Cells* **2005**, *5* (2), pp. 187–200.
- [18] Lu, S.; Pan, J.; Huang, A.; Zhuang, L.; Lu, J., Alkaline polymer electrolyte fuel cells completely free from noble metal catalysts. *Proc Natl Acad Sci* **2008**, *105* (52), pp. 20611–20614.
- [19] Antolini, E., Alkaline direct alcohol fuel cells. *J Power Sources* **2010**, *195* (11), pp. 3431–3450.

- [20] Wee, J.-H.; Roh, J.; Kim, J., A comparison of solar photovoltaics and molten carbonate fuel cells as commercial power plants. *Renewable Sustainable Energy Rev.* **2011**, *15* (1), pp. 697–704.
- [21] Frusteri, F.; Freni, S., Bio-ethanol, a suitable fuel to produce hydrogen for a molten carbonate fuel cell. *J Power Sources* **2007**, *173* (1), pp. 200–209.
- [22] Dicks, A., Molten carbonate fuel cells. *Curr Opin Solid State Mater Sci* **2004**, *8* (5), pp. 379–383.
- [23] Dicks, A.; Siddle, A., Assessment of commercial prospects of molten carbonate fuel cells. *J Power Sources* **2000**, *86* (1), pp. 316–323.
- [24] Kunz, H. R., Transport of Electrolyte in Molten Carbonate Fuel Cells. *J Electrochem Soc* **1987**, *134* (1), p. 105.
- [25] Perry, M. L.; Fuller, T. F., A Historical Perspective of Fuel Cell Technology in the 20th Century. *J Electrochem Soc* **2002**, *149* (7), pp. S59–S67.
- [26] Howe, K.; Thompson, G.; Kendall, K., Micro-tubular solid oxide fuel cells and stacks. *J Power Sources* **2011**, *196* (4), pp. 1677–1686.
- [27] Fabbri, E.; Pergolesi, D.; Traversa, E., Materials challenges toward proton-conducting oxide fuel cells: a critical review. *Chem Soc Rev* **2010**, *39* (11), pp. 4355–4369.
- [28] Shearing, P. R.; Brett, D. J. L.; Brandon, N. P., Towards intelligent engineering of SOFC electrodes: a review of advanced microstructural characterisation techniques. *Int Mater Rev* **2010**, *55* (6), pp. 347–363.
- [29] Mahapatra, M. K.; Lu, K., Seal glass for solid oxide fuel cells. *J Power Sources* **2010**, *195* (21), pp. 7129–7139.
- [30] Malavasi, L.; Fisher, C. A. J.; Islam, M. S., Oxide-ion and proton conducting electrolyte materials for clean energy applications: structural and mechanistic features. *Chem Soc Rev* **2010**, *39* (11), pp. 4370–4387.
- [31] Ettler, M.; Timmermann, H.; Malzbender, J.; Weber, A.; Menzler, N. H., Durability of Ni anodes during reoxidation cycles. *J Power Sources* **2010**, *195* (17), pp. 5452–5467.
- [32] Tucker, M. C., Progress in metal-supported solid oxide fuel cells: A review. *J Power Sources* **2010**, *195* (15), pp. 4570–4582.
- [33] Tsipis, E. V.; Kharton, V. V., Electrode materials and reaction mechanisms in solid oxide fuel cells: a brief review. III. Recent trends and selected methodological aspects. *J Solid State Electrochem* **2011**, *15* (5), pp. 1007–1040.

- [34] Standard Thermodynamic Properties of Chemical Substances. In *CRC Handbook of Chemistry and Physics*, Haynes, W. M., ed., Boca Raton, FL: CRC Press/Taylor and Francis, **2010**.
- [35] Thermophysical Properties of Fluids. In *CRC Handbook of Chemistry and Physics*, Haynes, W. M., ed., Boca Raton, FL: CRC Press/Taylor and Francis, **2010**.
- [36] Physical Constants of Organic Compounds. In *CRC Handbook of Chemistry and Physics*, Haynes, W. M., ed., Boca Raton, FL: CRC Press/Taylor and Francis, **2010**.
- [37] Zhao, T. S.; Van Nguyen, T., *Advances in fuel cells*. Elsevier Science, **2007**.
- [38] Gu, W.; Baker, D. R.; Liu, Y.; Gasteiger, H. A., Proton exchange membrane fuel cell (PEMFC) down-the-channel performance model. In *Handbook of Fuel Cells: Fundamentals, Technology, and Applications*, Vielstich, W.; Yokokawa, H.; Gasteiger, H. A., eds., John Wiley & Sons Ltd., **2009**.
- [39] Sokolova, E., Einfluss der natur der alkohole auf den mechanismus ihrer elektrooxidation. *Electrochim Acta* **1975**, *20* (5), pp. 323–330.
- [40] Koper, M. T. M.; Lai, S. C. S.; Herrero, E., Mechanisms of the Oxidation of Carbon Monoxide and Small Organic Molecules at Metal Electrodes. In *Fuel Cell Catalysis: A Surface Science Approach*, Koper, M. T. M., ed., Wiley, **2009**, pp. 159–208.
- [41] Markoví, N.; Ross Jr, P., Surface science studies of model fuel cell electrocatalysts. *Surf Sci Rep* **2002**, *45* (4-6), pp. 117–229.
- [42] Wasmus, S.; Küver, A., Methanol oxidation and direct methanol fuel cells: A selective review. *Journal of Electroanalytical Chemistry* **1999**, *461* (1-2), pp. 14–31.
- [43] Leung, L.-W. H.; Weaver, M. J., Influence of adsorbed carbon monoxide on electrocatalytic oxidation of simple organic molecules at platinum and palladium electrodes in acidic solution: a survey using real-time FTIR spectroscopy. *Langmuir* **1990**, *6* (2), pp. 323–333.
- [44] Ren, B., Surface Raman spectroscopy as a versatile technique to study methanol oxidation on rough Pt electrodes. *Electrochim Acta* **2000**, *46* (2-3), pp. 193–205.
- [45] Willsau, J.; Heitbaum, J., Analysis of Adsorbed Intermediates and Determination of Surface-Potential Shifts by Dems. *Electrochim Acta* **1986**, *31* (8), pp. 943–948.

- [46] Cuesta, A., At Least Three Contiguous Atoms Are Necessary for CO Formation during Methanol Electrooxidation on Platinum. *J Am Chem Soc* **2006**, *128* (41), pp. 13 332–13 333.
- [47] Cuesta, A.; Escudero, M.; Lanova, B.; Baltruschat, H., Cyclic Voltammetry, FTIRS, and DEMS Study of the Electrooxidation of Carbon Monoxide, Formic Acid, and Methanol on Cyanide-Modified Pt(111) Electrodes. *Langmuir* **2009**, *25* (11), pp. 6500–6507.
- [48] Herrero, E.; Franaszcuk, K.; Wieckowski, A., Electrochemistry of Methanol at Low-Index Crystal Planes of Platinum - an Integrated Voltammetric and Chronoamperometric Study. *J Phys Chem* **1994**, *98* (19), pp. 5074–5083.
- [49] Lebedeva, N.; Koper, M.; Feliu, J. M.; Van Santen, R., Role of crystalline defects in electrocatalysis: Mechanism and kinetics of CO adlayer oxidation on stepped platinum electrodes. *J Phys Chem B* **2002**, *106* (50), pp. 12 938–12 947.
- [50] Housmans, T.; Koper, M., Methanol oxidation on stepped Pt[n(111) (110)] electrodes: A chronoamperometric study. *J Phys Chem B* **2003**, *107* (33), pp. 8557–8567.
- [51] Jusys, Z.; Behm, R. J., Methanol Oxidation on a Carbon-Supported Pt Fuel Cell Catalyst A Kinetic and Mechanistic Study by Differential Electrochemical Mass Spectrometry. *J Phys Chem B* **2001**, *105* (44), pp. 10 874–10 883.
- [52] Wang, H.; Baltruschat, H., DEMS Study on Methanol Oxidation at Poly- and Monocrystalline Platinum Electrodes: The Effect of Anion, Temperature, Surface Structure, Ru Adatom, and Potential. *J Phys Chem C* **2007**, *111* (19), pp. 7038–7048.
- [53] Korzeniewski, C.; Childers, C. L., Formaldehyde Yields from Methanol Electrochemical Oxidation on Platinum. *J Phys Chem B* **1998**, *102* (3), pp. 489–492.
- [54] Housmans, T. H. M.; Wonders, A. H.; Koper, M. T. M., Structure Sensitivity of Methanol Electrooxidation Pathways on Platinum: An On-Line Electrochemical Mass Spectrometry Study. *J Phys Chem B* **2006**, *110* (20), pp. 10 021–10 031.
- [55] Shin, J.; Tornquist, W. J.; Korzeniewski, C.; Hoaglund, C. S., Elementary steps in the oxidation and dissociative chemisorption of ethanol on smooth and stepped surface planes of platinum electrodes. *Surf Sci* **1996**, *364* (2), pp. 122–130.

- [56] Xia, X. H.; Liess, H.-D.; Iwasita, T., Early stages in the oxidation of ethanol at low index single crystal platinum electrodes. *Journal of Electroanalytical Chemistry* **1997**, *437* (1-2), pp. 233–240.
- [57] Morin, M. C.; Lamy, C.; Leger, J. M.; Vasquez, J. L.; Aldaz, A., Structural effects in electrocatalysis: Oxidation of ethanol on platinum single crystal electrodes. Effect of pH. *Journal of Electroanalytical Chemistry* **1990**, *283* (1-2), pp. 287–302.
- [58] Chang, S. C.; Leung, L. W. H.; Weaver, M. J., Metal crystallinity effects in electrocatalysis as probed by real-time FTIR spectroscopy: electrooxidation of formic acid, methanol, and ethanol on ordered low-index platinum surfaces. *J Phys Chem* **1990**, *94* (15), pp. 6013–6021.
- [59] Tarnowski, D. J.; Korzeniewski, C., Effects of Surface Step Density on the Electrochemical Oxidation of Ethanol to Acetic Acid. *J Phys Chem B* **1997**, *101* (2), pp. 253–258.
- [60] Gao, P.; Chang, S.-C.; Zhou, Z.; J Weaver, M., Electrooxidation pathways of simple alcohols at platinum in pure nonaqueous and concentrated aqueous environments as studied by real-time ftir spectroscopy. *Journal of Electroanalytical Chemistry* **1989**, *272* (1-2), pp. 161–178.
- [61] Reis, R.; Martins, C.; Camara, G., The Electrooxidation of 2-Propanol: An Example of an Alternative Way to Look at In Situ FTIR Data. *Electrocatal* **2010**, *1* (2-3), pp. 1–6.
- [62] Sun, S.-G.; Lin, Y., Kinetics of isopropanol oxidation on Pt(111), Pt(110), Pt(100), Pt(610) and Pt(211) single crystal electrodes - Studies of in situ time-resolved FTIR spectroscopy. *Electrochim Acta* **1998**, *44* (6-7), pp. 1153–1162.
- [63] Sun, S.; Lin, Y., FTIR spectroscopic investigations of reaction mechanism of isopropanol oxidation on platinum single crystal electrodes. *Electrochim Acta* **1996**, *41* (5), pp. 693–700.
- [64] Pastor, E.; Gonzalez, S.; Arvia, A. J., Electroreactivity of Isopropanol on Platinum in Acids Studied by DEMS and FTIRS. *J Electroanal Chem* **1995**, *395* (1-2), pp. 233–242.
- [65] Leung, L.-W. H.; Chang, S.-C.; Weaver, M. J., Real-time FTIR spectroscopy as an electrochemical mechanistic probe. Electrooxidation of ethanol and related species on well-defined Pt (111) surfaces. *Journal of Electroanalytical Chemistry* **1989**, *266* (2), pp. 317–336.
- [66] Card, J.; Lyke, S.; Langer, S., Electrogenative oxidation of model alcohols at packed bed anodes. *J Appl Electroche* **1990**, *20* (2), pp. 269–280.

- [67] Santasalo, A.; Vidal-Iglesias, F.; Solla-Gullón, J.; Berná, A.; Kallio, T.; Feliu, J. M., Electrooxidation of methanol and 2-propanol mixtures at platinum single crystal electrodes. *Electrochim Acta* **2009**, *54* (26), pp. 6576–6583.
- [68] Sen Gupta, S.; Datta, J., An investigation into the electro-oxidation of ethanol and 2-propanol for application in direct alcohol fuel cells (DAFCs). *J Chem Sci* **2005**, *117* (4), pp. 337–344.
- [69] Dignam, M. J.; Fedyk, J., Infrared Ellipsometric Spectroscopy of Adsorbed Species. *Appl Spectrosc Rev* **1978**, *14* (2), pp. 249–285.
- [70] Armand, D.; Clavilier, J., Quantitative analysis of the distribution of the hydrogen adsorption states at platinum surfaces. Part II. Application to Pt (110), stepped and polyoriented platinum surfaces in sulphuric acid medium. *Journal of Electroanalytical Chemistry* **1987**, *233* (1-2), pp. 251–265.
- [71] Sumodjo, P.; da Silva, E.; Rabockai, T., Electrosorption of hydroxylated compounds: a comparative study of molecules with three carbon atoms. *Journal of Electroanalytical Chemistry* **1989**, *271* (1-2), pp. 305–317.
- [72] Sheppard, N.; Erkelens, J., Vibrational Spectra of Species Adsorbed on Surfaces: Forms of Vibrations and Selection Rules for Regular Arrays of Adsorbed Species. *Appl. Spectrosc.* **1984**, *38* (4), pp. 471–485.
- [73] Gootzen, J.; Wonders, A.; Visscher, W.; Van Veen, J., Adsorption of C3 alcohols, 1-butanol, and ethene on platinized platinum as studied with FTIRS and DEMS. *Langmuir* **1997**, *13* (6), pp. 1659–1667.
- [74] Legar, J. M.; Coutanceau, C.; Lamey, C., Electrocatalysis for the Direct Alcohol Fuel Cell. In *Fuel Cell Catalysis: A Surface Science Approach*, Koper, M. T. M., ed., Wiley, **2009**, pp. 343–374.
- [75] Jesys, Z.; Behm, R. J., Methanol, Formaldehyde, and Formic Acide Adsorption/Oxidation on Carbon-Supported Pt Nanoparticle Fuel Cell Catalyst: A Comparative Quantitative DEMS Study. In *Fuel Cell Catalysis: A Surface Science Approach*, Koper, M. T. M., ed., Wiley, **2009**, pp. 411–464.
- [76] Kamarudin, S. K.; Achmad, F.; Daud, W. R. W., Overview on the application of direct methanol fuel cell (DMFC) for portable electronic devices. *Int J Hydrogen Energy* **2009**, *34* (16), pp. 6902–696916.
- [77] Neburchilov, V.; Martin, J.; Wang, H.; Zhang, J., A review of polymer electrolyte membranes for direct methanol fuel cells. *J Power Sources* **2007**, *169* (2), pp. 221–238.

- [78] Aricò, A. S.; Creti, P.; Antonucci, P. L.; Antonucci, V., Comparison of Ethanol and Methanol Oxidation in a Liquid-Feed Solid Polymer Electrolyte Fuel Cell at High Temperature. *Electrochem Solid-State Lett* **1999**, *1* (2), pp. 66–68.
- [79] Wang, J.; Wasmus, S.; Savinell, R. F., Evaluation of Ethanol, 1-Propanol, and 2-Propanol in a Direct Oxidation Polymer-Electrolyte Fuel Cell. *J Electrochem Soc* **1995**, *142* (12), pp. 4218–4224.
- [80] Song, S.; Zhou, W.; Liang, Z.; Cai, R.; Sun, G.; Xin, Q.; Stergiopoulos, V.; Tsiakaras, P., The effect of methanol and ethanol cross-over on the performance of PtRu/C-based anode DAFCs. *Appl Catal, B* **2005**, *55* (1), pp. 65–72.
- [81] Heinzl, A., A review of the state-of-the-art of the methanol crossover in direct methanol fuel cells. *J Power Sources* **1999**, *84* (1), pp. 70–74.
- [82] Cao, D.; Bergens, S. H., A direct 2-propanol polymer electrolyte fuel cell. *J Power Sources* **2003**, *124* (1), pp. 12–17.
- [83] Qi, Z.; Kaufman, A., Liquid-feed direct oxidation fuel cells using neat 2-propanol as fuel. *J Power Sources* **2003**, *188* (1-2), pp. 54–60.
- [84] Qi, Z.; Kaufman, A., Performance of 2-propanol in direct-oxidation fuel cells. *J Power Sources* **2002**, *122* (1), pp. 121–129.

Chapter 2

Oxidation of 2-propanol in alkaline electrolytes using platinum catalysts*

2.1 Introduction

As discussed in §1.3, the proposed mechanisms for the oxidation of methanol, ethanol, and 2-propanol differ substantially, and they are sensitive to the surface atomic arrangement of the catalyst. The following chapter will discuss how these reactions proceed in an alkaline electrolyte. In order to facilitate comparisons between the oxidations in base and in acid, all potentials in this chapter will be reported on the Reference Hydrogen Electrode (RHE) scale. This scale is pH dependent, as shown in equation 2.1.

$$E_{RHE}^0 = -0.0592 \text{ V} \times \text{pH} \quad (2.1)$$

*A version of this chapter had been previously published:

Markiewicz, M.; Hebert, D.; Bergens, S., Electro-oxidation of 2-propanol on platinum in alkaline electrolytes. *J Power Sources* **2006**, *161* (2), pp. 761–767

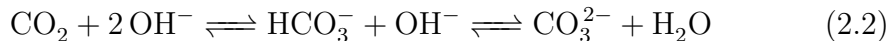
2.1.1 Methanol oxidation in base

Similar to the oxidation of methanol in acidic electrolyte, the oxidation of methanol in alkaline electrolytes produces carbon monoxide as a surface stable poison.^[2-5] The oxidation of carbon monoxide in alkaline electrolytes has been recently reviewed,^[6] and will not be discussed in detail here. The oxidation of methanol is faster, however, in alkaline electrolytes.^[5] In fact, the onset potential^[7] is 0.2 V lower, and the rate is enhanced^[8] by a factor of 30. It is generally accepted that this enhancement results from the absence of poisoning species other than carbon monoxide,^[9] and ubiquitous adsorbed hydroxide that facilitates its oxidation.^[10,11] At elevated potentials, sites that would otherwise be catalytically active are blocked by strongly bound oxygen species.^[7,12,13] This inhibition at high potentials is stronger in base than in acid. To investigate the catalytic oxidation of methanol in alkaline electrolytes under well defined conditions, the following discussion will focus on investigations using single crystal electrodes. Although these surfaces are an idealized model of the catalysts used in the Direct Alcohol Fuel Cell (DAFC), strong correlations between their activity, and the activity of actual DAFC catalysts, have been reported.^[14]

The oxidation of methanol on single crystal electrodes has been studied by voltammetry^[3,11-17] and Fourier Transform Infrared Spectroscopy (FTIR).^[3] These investigations propose that, similar to the oxidation of methanol in acid, the oxidation of methanol in base proceeds through the dual pathway mechanism (Scheme 1.2, p. 24). Indeed, Morallon et al.^[3] found that formate is the major oxidation product, leading to the conclusion that the direct pathway, through weakly adsorbed intermediates, predominates over the carbon monoxide forming pathway.^[12] The onset potential for the formation of formate

is 0.47 V on Pt(1 1 0) and Pt(1 0 0), and 0.7 V on Pt(1 1 1). The onset of carbon dioxide formation is 0.72 V, and results from the oxidation of adsorbed carbon monoxide and from the oxidation of formate. The rate of oxidation is enhanced by platinum steps,^[14] which is believed to result from their higher activity towards to adsorption of oxygen species, resulting in “well balanced coverage[s] by methanol and [adsorbed hydroxide]”.^[14] By this the authors mean that the steps provide the adsorbed oxygen species necessary to oxidize the intermediates formed during the oxidation of methanol to carbon dioxide.

The oxidation of methanol to carbon dioxide in an alkaline medium will inevitably result in carbonation of the electrolyte through equation 2.2.



The influence of (bi)carbonate on the oxidation of methanol was investigated by Tripković et al.^[15–17] using voltammetry. Table 2.1 summarizes the activity of Pt(1 1 1), Pt(1 1 0), and Pt(1 0 0) as a function of the base electrolyte. Similar to findings of Herrero et al.^[18] in acid (Table 1.3, p. 25), Tripković et al. found that Pt(1 1 0) is the most active in base. The activity of the Pt(1 1 1), however, shows the highest enhancement in base.

A clear decrease in the peak current density is observed in (bi)carbonate electrolytes, relative to hydroxide, indicating an inhibitory effect. The voltammograms of the base electrolyte shows that (bi)carbonate inhibits the formation of adsorbed hydroxide, and that the rate of methanol oxidation at 0.55 V is linearly dependent on the coverage of the surface by weakly bound hydroxide.^[17] These two dependencies provide convincing evidence that (bi)carbonate inhibits the oxidation of methanol by decreasing the amount of surface hydroxides. This inhibition has been proposed as the source of the reduction in the current

Table 2.1: Peak current density, and potential, for the oxidation of methanol over Pt(111), Pt(110), and Pt(100) as a function of electrolyte composition.^[15–17]

Surface	Electrolyte	Anodic		Cathodic	
		E_{peak} (V)	j_{peak} (mA cm ⁻²)	E_{peak} (V)	j_{peak} (mA cm ⁻²)
Pt(111)	0.1 mol dm ⁻³ NaOH	0.90	10.67	0.86	7.79
	0.1 mol dm ⁻³ NaHCO ₃	0.75	0.49	0.75	0.37
	0.1 mol dm ⁻³ Na ₂ CO ₃	0.83	2.32	0.83	1.66
Pt(110)	0.1 mol dm ⁻³ NaOH	0.55	1.45	0.59	0.76
		0.95	11.68	0.74	0.87
	0.1 mol dm ⁻³ NaHCO ₃	0.85	1.03	0.77	0.40
		1.05	1.07		
Pt(100)	0.1 mol dm ⁻³ Na ₂ CO ₃	0.85	5.28	0.71	1.38
	0.1 mol dm ⁻³ NaOH	0.73	2.59	0.65	2.06
		0.76	2.92	0.71	2.87
	0.1 mol dm ⁻³ NaHCO ₃	0.68	0.60	0.72	0.41
		0.74	0.40		
	0.1 mol dm ⁻³ Na ₂ CO ₃	0.71	1.47	0.69	1.14
	0.77	1.58			

density observed during the oxidation of methanol in carbonate electrolytes.

Forced convection methods have shown^[19] that the product selectivity (i.e., carbonate vs formate) is changed in carbonate electrolytes. Specifically, Rotating Disk Electrode (RDE) experiments using a polycrystalline platinum electrode showed that the voltammetric response is highly influenced by the rate of electrode rotation. Higher rotation rates remove solution phase products (such as carbonates and formic acid) from the electrode/electrolyte interface, and supply it with methanol. During the cathodic sweep, the oxidation peak immediately following the reduction of platinum oxides is proportional to the amount of carbon monoxide on the catalyst. The ratio of the peak heights during the anodic and cathodic sweeps can therefore be used as a measure of the indirect pathway through carbon monoxide, versus the direct pathway through formic acid. As would be expected from increased diffusion, faster rotation rates increase $\frac{j_{peak, anodic}}{j_{peak, cathodic}}$; however, this ratio is lower in carbonate electrolytes. This lower ratio indicates that carbonates increase the prevalence

of the indirect pathway, through carbon monoxide.

2.1.2 Ethanol oxidation in base

The oxidation of ethanol in alkaline electrolytes is also enhanced^[20,21] relative to its oxidation in acid. Similar to the oxidation of ethanol in acid (§1.3.2), Lopez-Atalaya et al.^[22] found that acetate is the main solution phase product in base, and that carbon monoxide is a surface poisoning intermediate. It should be noted that the formation of acetaldehyde should not be discarded as a possible intermediate, as it is known to readily convert into the geminal diol^[23] in alkaline solutions. This diol has been proposed^[20] as an intermediate during the formation of the acetate product. High Pressure Liquid Chromatography (HPLC) studies found^[24] small amounts of acetaldehyde; however, the amount of acetaldehyde formed is significantly less than acetate.

Morin et al.^[21] found that Pt(110) is the most active crystal face for the oxidation of ethanol in alkaline electrolytes (Table 2.2). The trends in activity are similar to those reported by Xia et al.^[25] for the oxidation of ethanol in acidic electrolyte (§1.3.2). The rate of oxidation over Pt(111) and Pt(110), however, is significantly enhanced in base. Pt(100) is slightly less active in alkaline electrolytes, initially, but its activity does not decay as significantly in base. A similar trend in activity was reported by Lai and Koper.^[26]

The amount of adsorbates formed in an alkaline electrolyte was rigorously investigated by Lopez-Atalaya et al.^[22] Subtractively Normalized Interfacial Fourier Transform Infrared Spectroscopy (SNIFTIR) identified carbon monoxide as a poisoning species, indicating that the carbon-carbon bond is cleaved during their production. The quantity of the adsorbates changes with the arrangement of the platinum surface atoms, indicating that the cleavage of the carbon-

Table 2.2: A comparison of the activity of Pt(111), Pt(110), and Pt(100) toward the oxidation of ethanol (0.1 mol dm^{-3}) in acidic and basic electrolytes.^[21]

Surface	Sweep Number	$0.15 \text{ mol dm}^{-3} \text{ NaOH}$		$0.1 \text{ mol dm}^{-3} \text{ HClO}_4$	
		E_{peak} (V)	j_{peak} (mA cm^{-2})	E_{peak} (V)	j_{peak} (mA cm^{-2})
Pt(111)	1	0.87	25.5	0.45	1.5
	2		15.5		0.6
	5		4.8		0.4
Pt(110)	1	0.82	34.0	0.74	3.8
	2		15.1		2.1
	5		8.0		1.4
Pt(100)	1	0.71	4.6	0.73	6.2
	2		4.2		4.2
	5		3.6		2.8

carbon bond is surface structure sensitive. Table 2.3 summarized the charges associated with the oxidative stripping of these adsorbates, formed at 0.3 V for 2 min in either a hydroxide or a (bi)carbonate electrolyte, and also includes the voltammetric activity of these surfaces towards the oxidation of ethanol. As can be seen from the stripping charges, Pt(100) is the most active towards the cleave of the carbon-carbon bond in either electrolyte. With the exception of Pt(100), carbonates do not appear to significantly influence the amount of adsorbed carbon monoxide formed during the oxidation of ethanol.

Table 2.3: Stripping charge associated with adsorbate formed on Pt(111), Pt(110), and Pt(100) at 0.3 V for 2 min.^[22]

Surface	$0.1 \text{ mol dm}^{-3} \text{ Na}_2\text{CO}_3$		$0.1 \text{ mol dm}^{-3} \text{ NaOH}$	
	Q_{strip} ($\mu\text{C cm}^{-2}$)	E_{peak} (V)	Q_{strip} ($\mu\text{C cm}^{-2}$)	E_{peak} (V)
Pt(111)	170.0	0.78	152.4	0.80
Pt(110)	113.3	0.69	109.3	0.67
Pt(100)	191.6	0.64	265.4	0.62
		0.74		0.99

Lai and Koper used Surface Enhanced Raman Spectroscopy (SERS) to study the intermediates formed during the oxidation of ethanol on stepped platinum

surfaces with the Pt[n(111) × (110)] structure type. It was found that the oxidation of partially dehydrogenation C₁ intermediates (CH_x, 3 ≤ x ≤ 0) plays a significant role on the overall rate of the oxidation of ethanol. Specifically, the low activity of Pt(111) relative to Pt(110) was found to result from difference in the activity of these surfaces towards the oxidation of CH_x fragments. In fact, it was found that the oxidation of CH_x fragments to carbon monoxide occurs at potentials that are nearly 0.45 V higher on Pt(111), and it is slower than to the oxidation of carbon monoxide to carbon dioxide. The current densities obtained using stepped surfaces, Pt(553) (n = 4), Pt(554) (n = 9) and Pt(151514) (n = 29), were more stable than Pt(111), presumably due to an increase in the rate of the oxidation of CH_x fragments (i.e., less CH_x accumulates on the stepped surfaces). Additionally, increasing the density of the step lowers the onset potential for the oxidation of ethanol. Pt(111) also formed the least amount of C₁ intermediates, indicating that step edges are more active than the Pt(111) terrace planes towards carbon-carbon bond cleavage.

2.1.3 2-Propanol oxidation in base

Since the original publication date of the paper that this chapter is based on (2006), several new investigations on 2-propanol oxidation over platinum have been reported. In keeping with the structure of the discussion, however, only studied on single crystals, the differences between acidic and basic electrolytes, and product distribution, will be discussed here. The use of catalysts other than pure platinum will be discussed in Chapter 4.

Table 2.4 summarizes the voltammetric activity of Pt(111), Pt(110), and Pt(100) towards the oxidation of 2-propanol in acidic and alkaline elec-

trolytes.^[27] Contrasting methanol and ethanol, the oxidation of 2-propanol gives higher peak currents in acidic media. The onset potential and the peak current potential, however, occur at lower potentials in alkaline electrolytes. The magnitude of the hysteresis is also less in alkaline electrolytes, indicating that fewer surface poisons are formed in alkaline electrolytes.

Table 2.4: Peak current density, and potential, for the oxidation of 2-propanol over single crystal electrodes as a function of electrolyte composition and surface structure.^[27]

Surface	Electrolyte	E_{onset} (V)	Anodic		Cathodic	
			E_{peak} (V)	j_{peak} (mA cm ⁻²)	E_{peak} (V)	j_{peak} (mA cm ⁻²)
Pt(111)	0.5 mol dm ⁻³ NaOH	0.53	0.9 ^a	18.0	—	—
	0.5 mol dm ⁻³ H ₂ SO ₄	0.21	0.41	4.2	0.41	4.1
Pt(110)	0.5 mol dm ⁻³ NaOH	0.19	0.35	1.3	0.44	1.3
			0.53	2.0	0.68	1.0
			0.73	2.5	—	—
Pt(100)	0.5 mol dm ⁻³ H ₂ SO ₄	0.35	0.67	6.2	0.69	11.5
	0.5 mol dm ⁻³ NaOH	0.32	0.54	1.2	0.54	1.2
			0.76	0.4	0.76	0.2
	0.5 mol dm ⁻³ H ₂ SO ₄	0.42	—	—	0.72	2.3
					0.88	4.6

^a Not a true peak, but rather the maximum observed current.

Santasalo-Aarnio et al.^[24] studied the products formed during the oxidation of 2-propanol by HPLC. Acetone is the only product observed; however, the use of an acidic eluent may have resulted in the loss of (bi)carbonates from the analyte. In situ FTIR studies^[28] have shown adsorption bands indicative of carbonates at potentials exceeding 1.4 V[†].

This chapter will describe a comparison of the oxidation of 2-propanol in acidic and in alkaline electrolytes, and compares this activity to that of methanol. Particular emphasis is placed on chronoamperometric oxidations, such that the steady-state rate of these reactions can be more equitably compared under

[†]Note: This value does seem to be unusually high. The authors originally cite 0.4 V vs SCE, in a 0.1 mol dm⁻³ NaOH electrolyte. 1.4 V vs RHE is calculated assuming pH = 13, and therefor RHE(0.1 mol dm⁻³ NaOH) = -1.014 V vs SCE.

conditions which are more representative of operating fuel cells. Further, the influence of acetone on the rate of 2-propanol oxidation was investigated. The goal of this investigation is to investigate if any significant catalytic enhancement for the oxidation of 2-propanol occurs in alkaline electrolytes, under conditions that represent an operating fuel cell more accurately (i.e., steady-state power generation).

2.2 Experimental

2.2.1 General

Nitrogen (Praxair, prepurified), NaOH (Alfa Aesar, 99.99%, semiconductor grade), H₂SO₄ (Alfa Aesar, 99.9999%), H₂O₂ (EM Science, ACS Grade), H₂PtCl₆·6H₂O (Alfa Aesar, 99.9% metal basis), and platinum gauze (Alfa Aesar, ca. 25 × 25 mm, 52 mesh woven from 0.1 mm diameter wire, 99.9% metal basis) were used as received from supplier. The water was deionized, distilled, and distilled again from alkaline KMnO₄ (Fisher Scientific) before use. Methanol (Fisher, ACS grade) was distilled over Mg(OMe)₂, 2-propanol (Fisher Scientific, suitable for electronic use) was freshly distilled, and acetone (Caledon, ACS grade) was distilled over molecular sieves (Caledon, 3Å) before use.

Electrochemical experiments were performed in a typical three-electrode glass cell using an EG&G Princeton Applied Research Potentiostat/Galvanostat (model 273) controlled with the supplied EG&G PAR electrochemistry software. Electrolytes were purged with nitrogen for 15 min prior to measurements, and protected by a nitrogen atmosphere at bubbler pressure during experiments. The counter electrode was a blacked platinum gauze behind a 10 μm

sintered glass frit, and the working electrode was the same without the glass frit. Figure 2.1 illustrates this setup. The preparation of these blacked gauzes is described below. The openings to the electrochemical glass cell were sealed using septa that had been extracted with toluene and punched with holes to fit the electrodes/frit. The electrochemical cell was equipped with a dry ice/acetone condenser to minimize loss of 2-propanol by evaporation. A constant temperature bath (IKA Labortenchnik, RCT basic) equipped with a temperature probe/controller (IKA Labortechnik, ETS-D4 fuzzy) was used to maintain the cell temperature at 60 °C.

2.2.2 Preparation and characterization of the electrodes

The working and counter electrodes were prepared by first cleaning a platinum gauze with 1% H_2O_2 , followed by platinum deposition from 2 wt.% $\text{H}_2\text{PtCl}_6 \cdot 6\text{H}_2\text{O}$ in 1 mol dm^{-3} HCl at 0.050 V versus Normal Hydrogen Electrode (NHE) for 3 h, with stirring.

The active area of the electrode was determined daily, using the method of Biegler et al.^[29] Specifically, using a voltammogram recorded in 1 mol dm^{-3} H_2SO_4 , the charge associated with the formation of a H_{UPD} monolayer (Q_H) was determined by integrating the area between the double layer region, and the onset of hydrogen evolution. Figure 2.2 illustrates this region of the voltammogram. The fractional coverage (f_s) is assumed to be 0.77, and the charge associated with the monolayer (Q_{Ap}) is assumed to be $210 \mu\text{C cm}^{-2}$ (i.e., the atomic packing density is 1.51×10^{15} atoms cm^{-2}). Equation 2.4 was then used to determine the real number of surface atoms, and to normalize the

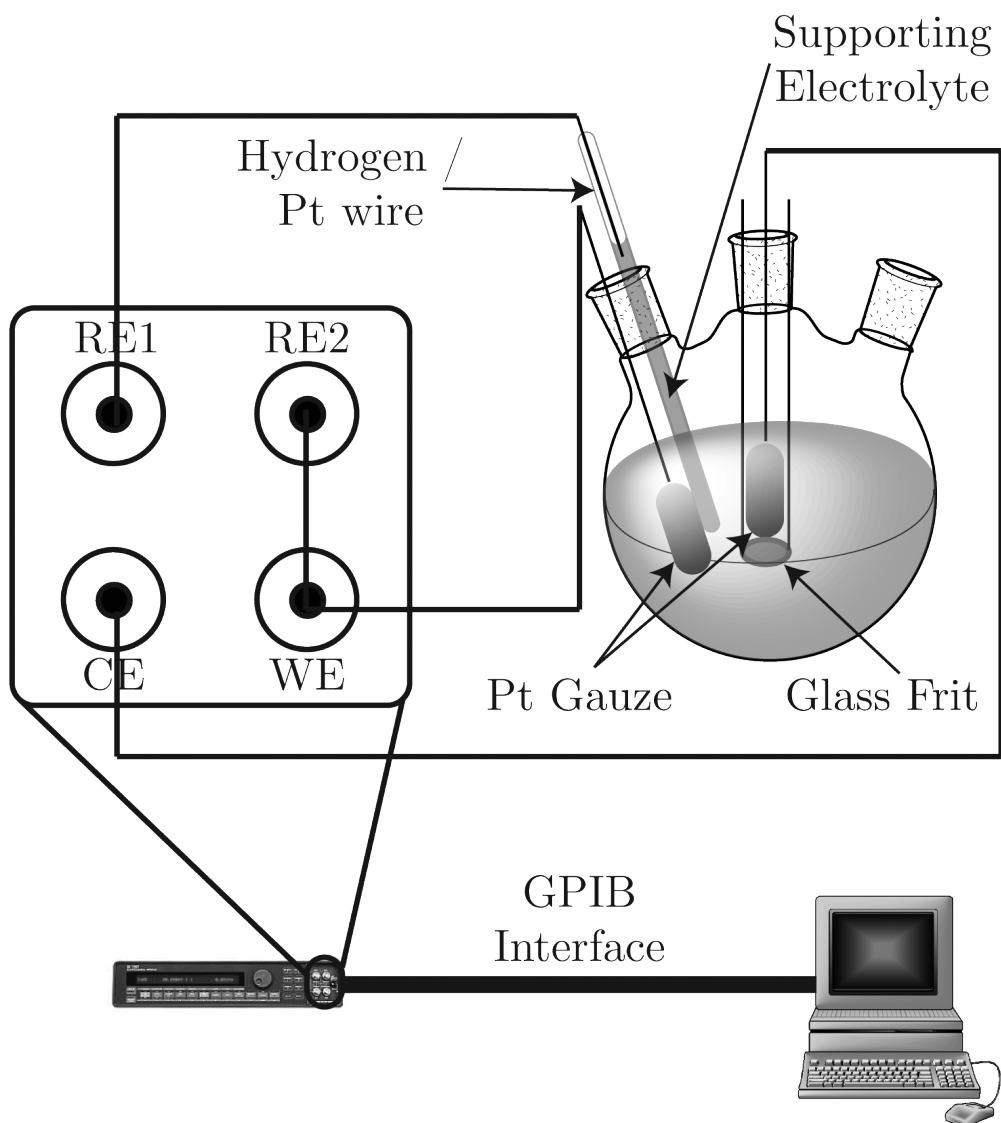


Figure 2.1: Illustration of the three-electrode setup used for the characterization of the electrochemical activity of platinum gauzes. Note that the reference electrode was placed as close as possible to the working electrode, and that the reference hydrogen electrode was prepared using the supporting electrolyte without any alcohol. The dry ice/acetone condenser, and the temperature bath have been omitted for clarity.

reported current densities.

$$A_{real} = \frac{Q_H}{f_s \times Q_{Ap}} \quad (2.3)$$

$$n_{Pt \text{ surface}} = \frac{Q_H}{74.334 \times 10^3 \text{ C mol}_{\text{surface}}^{-1}} \quad (2.4)$$

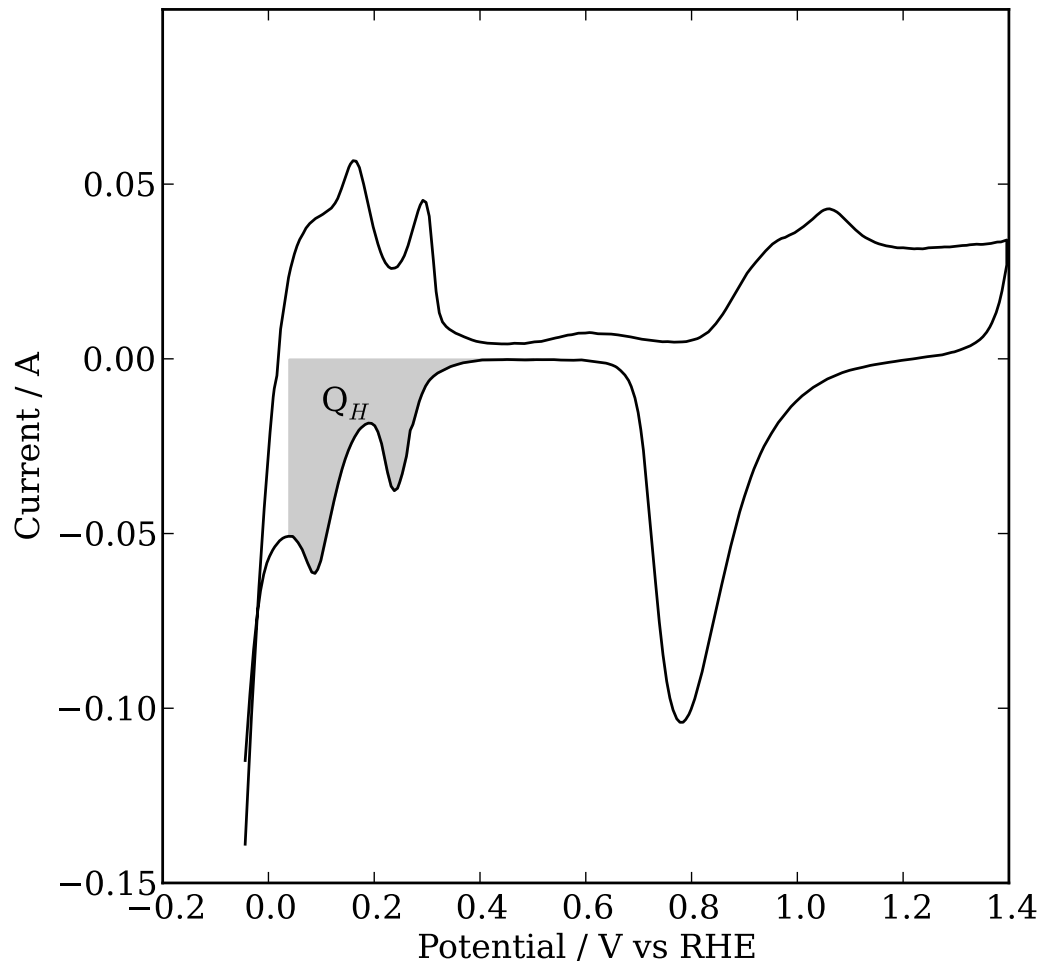


Figure 2.2: Voltammogram of a blacked platinum gauze in $1 \text{ mol dm}^{-3} \text{ H}_2\text{SO}_4$, illustrating the H_{UPD} potential region used for the determination of the electrode's real area.

2.2.3 Electrochemical oxidations

All potentials were recorded versus a RHE made from the alcohol-free supporting electrolyte. All potentials are also reported versus this RHE, unless stated otherwise. Current densities were normalized to the active area of the electrode, measured daily. Measurements are not iR compensated.

Cyclic voltammetry and chronoamperometry was performed using the setup described in §2.2.1. Prior to each experiment, the working electrode was conditioned at 1.2 V for 60 s, and then at -0.1 V for 60 s. The potential limits of the cyclic voltammograms are discussed in the text. Chronoamperometry experiments were performed for a duration of 15 min; sampled current voltammograms were constructed from the chronoamperometry data by averaging the last 5 s of the experiment, and plotting the resulting value against the applied potential.

2.3 Results and discussion

Figure 2.3 shows the voltammogram of a blackened platinum gauze obtained in the presence of 2-propanol in 0.5 mol dm^{-3} NaOH electrolyte at 60°C . The figure also shows the voltammogram obtained without 2-propanol. All currents reported in this paper are normalized to the real surface area of the platinum electrode measured before the experiment. The voltammetric response in the absence of 2-propanol is typical of polycrystalline platinum in NaOH. The hydride region of the stabilized voltammogram obtained in the presence of 2-propanol retains elements of structure that are present in its absence. This similarity in structure indicates that the hydride region is not significantly poisoned by repeated sweeps with 2-propanol in alkaline electrolyte over the

period of these experiments. The currents in the hydride regions of the anodic and cathodic sweeps are higher, however, in the presence of 2-propanol. This increase of current in the hydride region shows that the oxidation of 2-propanol occurs at these low potentials. There is also a significant, rapid increase in current for the oxidation of 2-propanol in the cathodic sweeps that occurs when the oxides are reduced from the surface. This rapid increase in current during the cathodic sweep shows that surface oxides impede the oxidation. This property is a well-known phenomenon for most reported oxidations of alcohols over platinum in acidic or basic electrolytes, as has been discussed previously (see §§1.3 and 2.1).

Figure 2.4 shows the stabilized voltammograms obtained with 1, 2, 3, and 4 mol dm⁻³ solutions of 2-propanol in 1 mol dm⁻³ NaOH. Attempts to use higher concentrations of 2-propanol were prevented by the formation of biphasic electrolyte mixtures. Increasing the concentration of 2-propanol resulted in an increase in current in the hydride-, double layer-, and oxide regions of the voltammograms. The shapes of the voltammograms did not change significantly upon increasing the 2-propanol concentration. A second oxidation peak did appear, however, centred at ca. 0.93 V in the cathodic sweeps when the concentration of 2-propanol was increased from 1 to 2 mol dm⁻³ or higher. The origins of this new peak are unclear at this time, but may be associated with a carbon dioxide precursor.

Figure 2.5 shows the stabilized voltammograms obtained in 0.5, 1, and 3 mol dm⁻³ solutions of NaOH in 1 mol dm⁻³ 2-propanol. Increasing the hydroxide concentration from 0.5 to 3 mol dm⁻³ decreased the current for the oxidation in the oxide region of the voltammogram. Increasing the hydroxide concentration did not change the current in the hydride region to the extent that it decreased

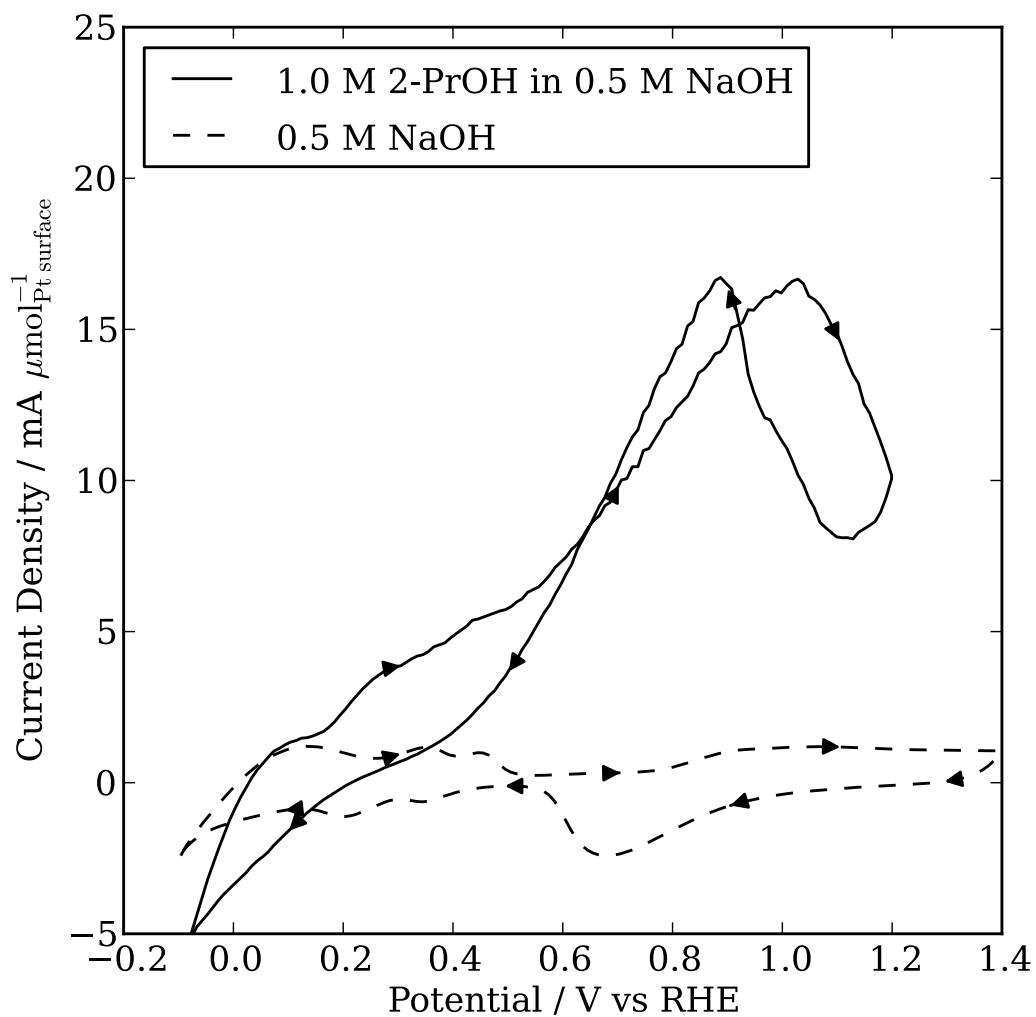


Figure 2.3: Stabilized cyclic voltammograms of a blacked platinum gauze in 0.5 mol dm^{-3} NaOH (---), and 1 mol dm^{-3} 2-propanol in 0.5 mol dm^{-3} NaOH(—). $T = 60^\circ\text{C}$, $v = 5 \text{ mV s}^{-1}$.

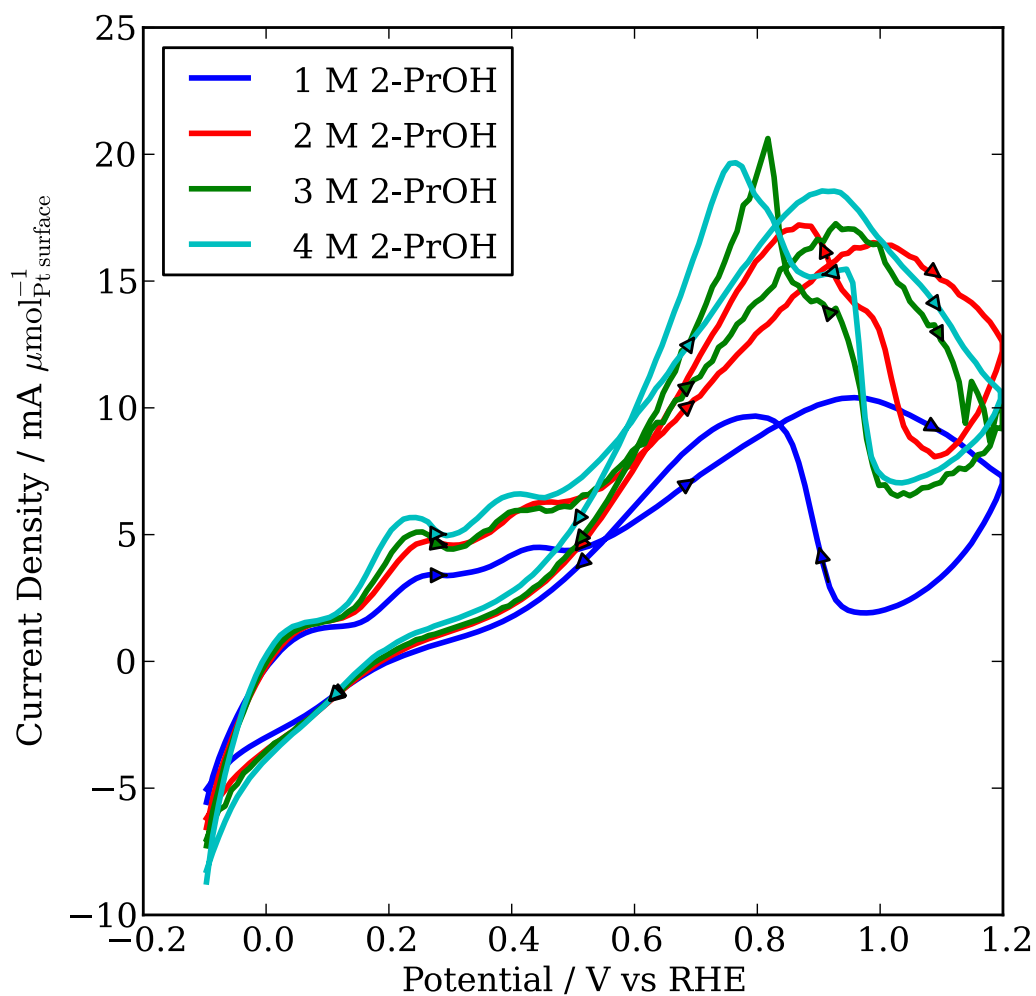


Figure 2.4: Stabilized cyclic voltammograms of a blacked platinum gauze in 1 (blue), 2 (red), 3 (green), and 4 mol dm^{-3} (cyan) 2-propanol in 1 mol dm^{-3} NaOH. $T = 60^\circ\text{C}$, $v = 5 \text{ mV s}^{-1}$.

the current in the oxide region of the voltammogram. Increasing the hydroxide concentration did, however, change the relative peak heights in the hydride region of the anodic sweeps. Specifically the second oxidation peak at lower potentials increased relative to the first peak at high NaOH concentrations. These differences in response to hydroxide concentration indicate that the oxidation of 2-propanol in the hydride region occurs by a different mechanism than the oxidation in the oxide region. Chronoamperometric oxidations of 2-propanol were carried out over platinum in base to further investigate this system under conditions that better approximate an operating fuel cell.

Figure 2.6 shows the current-time plot for the chronoamperometric oxidations of 2-propanol in 1 mol dm^{-3} NaOH at a few selected potentials. The platinum was conditioned before each oxidation by holding the potential at 1.2 V for 1 min, then at -0.1 V for 1 min, followed by a jump to the desired potential. After the jump to the desired potential, there typically occurred an initial, rapid decrease in current followed by a region of more stable currents that decreased slowly during the remainder of the oxidation. The oxidation of 2-propanol occurred even at 0.1 V. Further, comparison of the stabilized current at increasing potentials reveals an unexpected and substantive current maximum that occurred at low potentials. Figure 2.7 shows the sampled current voltammogram, measured at 15 min, that shows the large current maximum centred at approximately 0.17 V, and ranging from approximately 0.17 to 0.3 V. To the best of my knowledge, no such maximum in stabilized current at low potentials has been reported previously for the chronoamperometric oxidation of an alcohol over a platinum-based catalyst. For comparison, Figure 2.7 also shows the sampled current voltammogram for the oxidation of methanol under identical conditions. As is typical for alcohols, the oxidation of methanol

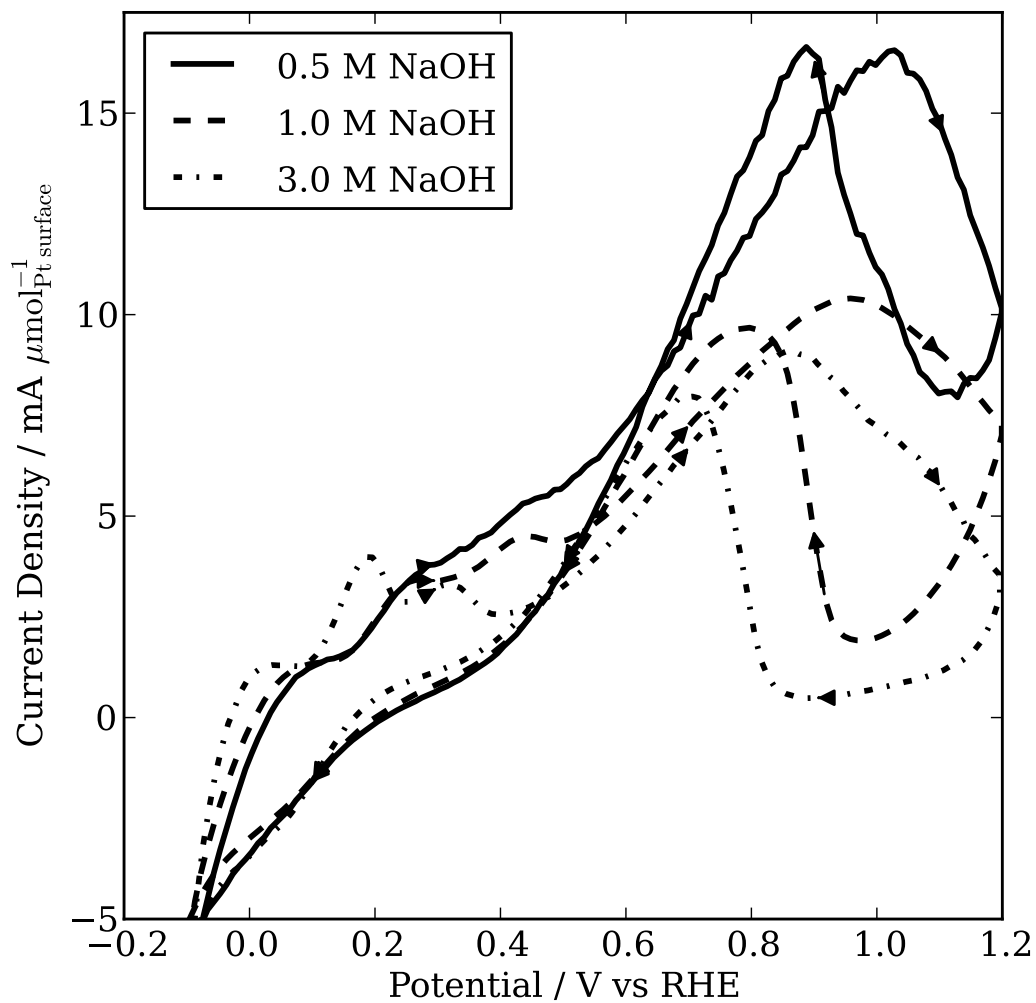


Figure 2.5: Stabilized cyclic voltammograms of a blacked platinum gauze in 1 mol dm⁻³ 2-propanol in 0.5 (—), 1 (---), and 3 mol dm⁻³ (-·-) NaOH. RHEs were prepared with the corresponding NaOH electrolyte. $T = 60\text{ }^{\circ}\text{C}$, and $v = 5\text{ mV s}^{-1}$.

produces only negligible stabilized currents at low potentials.

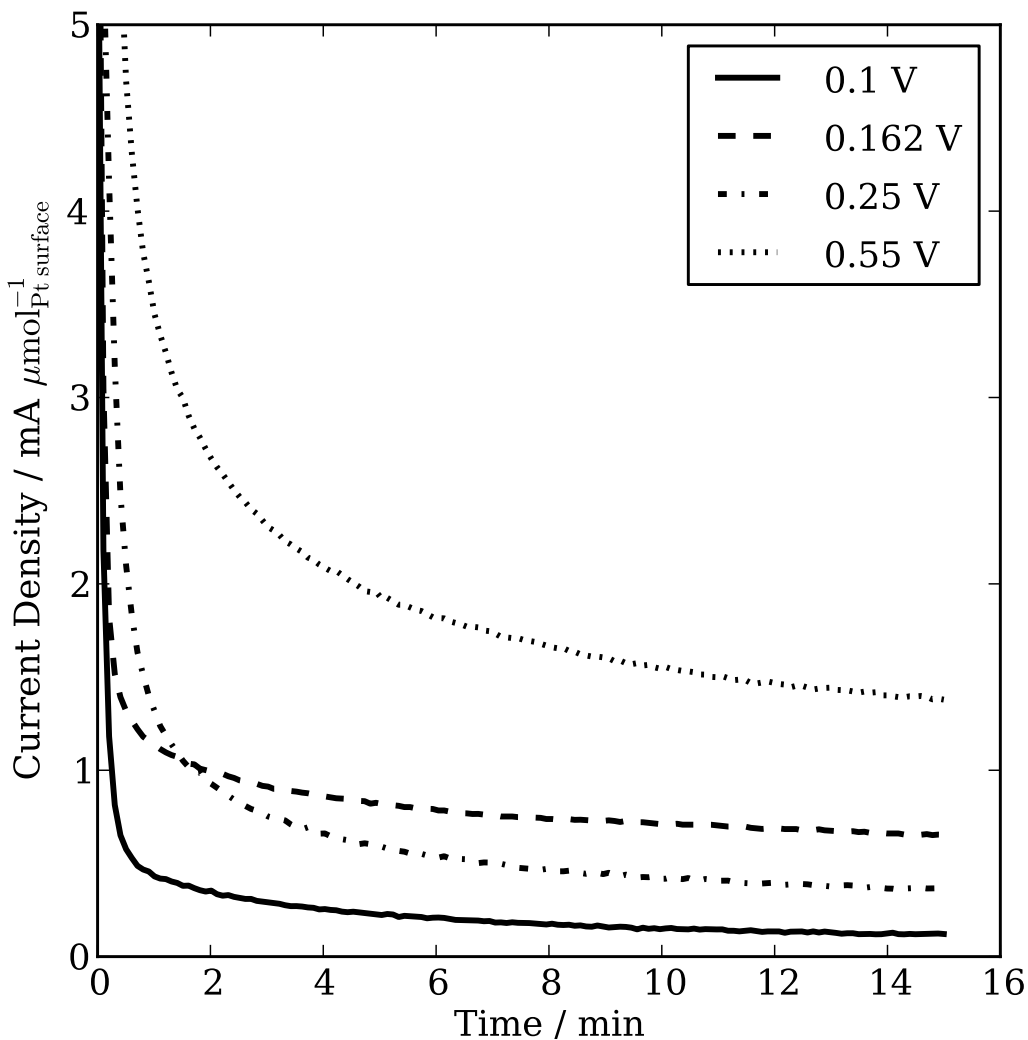


Figure 2.6: Current vs. time plot for the oxidation of 1 mol dm^{-3} 2-propanol in 1 mol dm^{-3} NaOH over a blacked platinum gauze at 0.1 (—), 0.162 (---), 0.25 (— · —), and 0.55 V (····). $T = 60^\circ\text{C}$.

The current maximum at low potentials confirms the evidence from the cyclic voltammetry experiments that at least two mechanisms operate in basic electrolytes. One mechanism predominates at low potentials, while the other, or perhaps both, mechanisms operate at higher potentials. Figure 2.7 also shows plots of the stabilized current versus potential in 1, 2, 3, and 4 mol dm^{-3} 2-propanol. Increasing the concentration of 2-propanol from 1

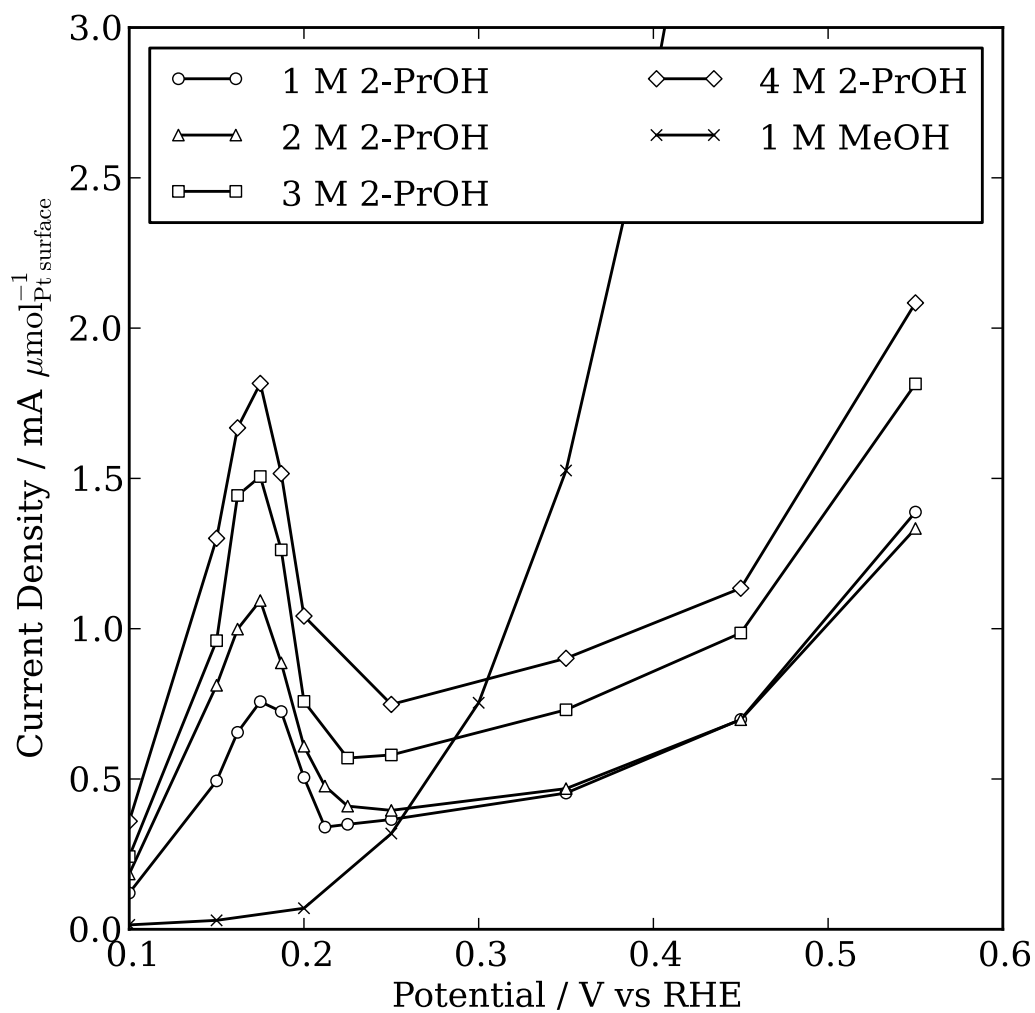


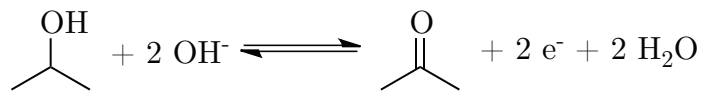
Figure 2.7: Current at the end of a 15 min oxidation vs. potential for 1 (\circ), 2 (\triangle), 3 (\square), and 4 mol dm^{-3} (\diamond) 2-propanol in 1 mol dm^{-3} NaOH over a blacked platinum gauze. 1 mol dm^{-3} methanol (\times) in 1 mol dm^{-3} NaOH is supplied for comparison. $T = 60^\circ\text{C}$.

to 4 mol dm^{-3} increased the current maximum at low potentials by a factor of ca. 2.4. This substantial increase in current shows that the oxidation at potentials below, or near the current maximum is not limited by saturation kinetics over this concentration range of 2-propanol. That the oxidation is not limited by saturation kinetics in 2-propanol at low potentials, and that the low-potential current maximum is quite large, both show that 2-propanol and the intermediates involved in its oxidation in this potential range do not strongly poison platinum. As would be expected if different mechanisms were in operation, the increases in current with the concentration of 2-propanol were less at higher potentials than they were at low potentials.

Figure 2.8 shows the sampled current voltammograms for the oxidations of 1 mol dm^{-3} 2-propanol in 0.5, 1, and 3 mol dm^{-3} solutions of NaOH. The size of the current maximum increased with the concentration of NaOH. Increasing the concentration of NaOH from 0.5 to 3 mol dm^{-3} increased the low-potential current maximum by a factor of ca. 1.6. The current in the potential range from ca. 0.23 to 0.45 V also increased with increasing NaOH concentration, but to a lesser extent than the current increased at the low-potential maximum. Conversely, the currents at potentials greater than 0.45 V decreased with increasing NaOH concentration. This behaviour is also consistent with one mechanism operating for the oxidation of 2-propanol at low potentials, with another mechanism, or combination of mechanisms operating at high potentials.

We propose that the mechanism up to the current maximum at low potentials involves the oxidation of 2-propanol to acetone (Scheme 2.1). Taking into consideration the reported observations made in acid (§1.3.3) and in base (§2.1.3) electrolytes, it is reasonable to assume that the oxidation of 2-propanol to acetone proceeds at high currents because it does not involve strongly

adsorbed intermediates that poison the platinum surface. We propose that the current drop after the low-potential current maximum is caused by the onset of acetone oxidation. Taking into consideration the reported observations made in acid and in base electrolytes, the oxidation of acetone in base appears to proceed through strongly adsorbed intermediates. We investigated this possibility by carrying out the chronoamperometric oxidation of acetone over platinum in base.



Scheme 2.1: Electrochemical oxidation of 2-propanol to acetone in alkaline media.

Figure 2.9 shows the sampled current voltammograms for the oxidations of 1 mol dm^{-3} 2-propanol and 1 mol dm^{-3} acetone under identical conditions in 1 mol dm^{-3} NaOH. Comparison of the plots at low potentials shows that negligible currents are produced by the oxidation of acetone up to the low-potential current maximum for the oxidation of 2-propanol. The low-potential current maximum for the 2-propanol oxidation, and the onset of acetone oxidation occur at nearly the same potential. This coincidence in potentials is further, strong evidence that the oxidation of acetone proceeds through strongly adsorbed intermediates that impede the rapid oxidation of 2-propanol to acetone at low potentials. The cathodic current that occurs in 1 mol dm^{-3} acetone at potentials below approximately 0.17 V is likely due to the reduction of acetone, perhaps to produce 2-propanol.

Gradual declines after the initial, rapid decrease in current are often observed during chronoamperometric oxidations of alcohols over platinum-based catalysts in acid. Figure 2.10 shows the current versus time plots we obtained for the

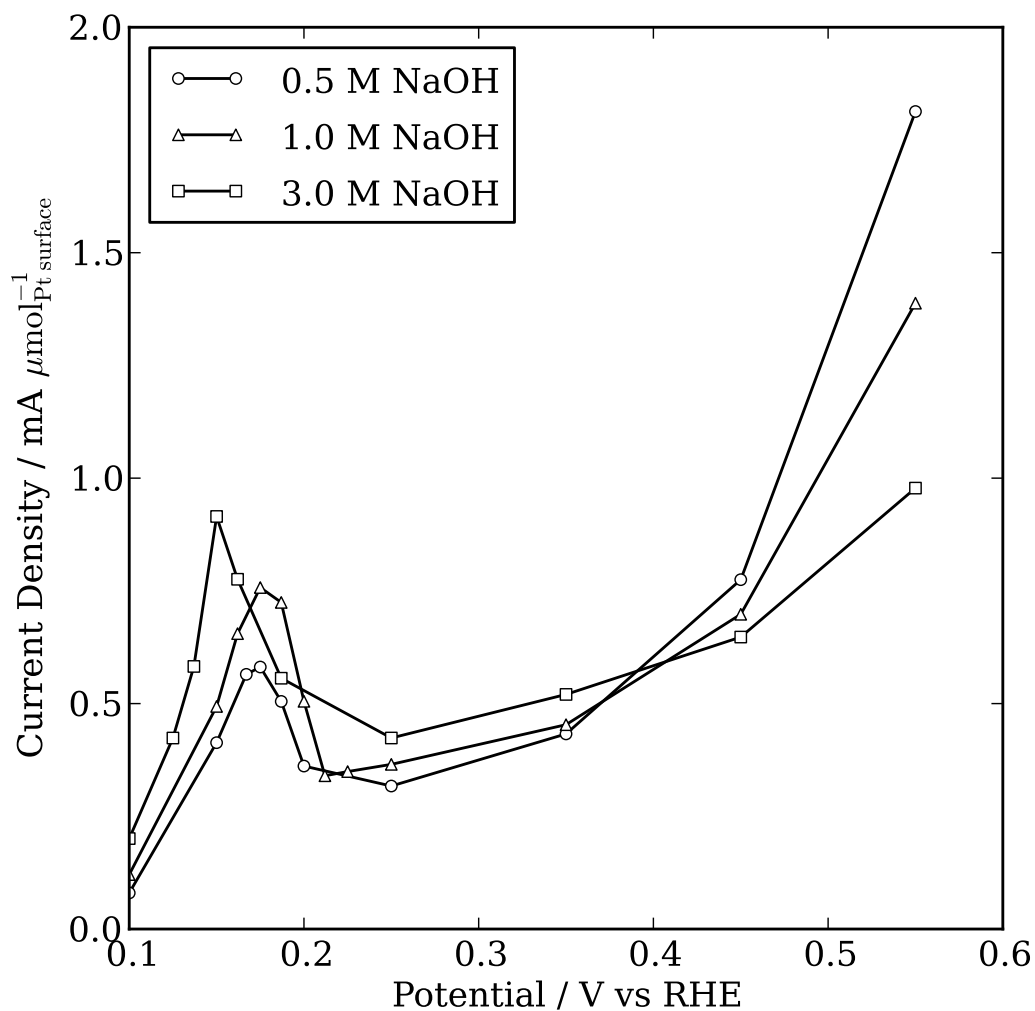


Figure 2.8: Current at the end of a 15 min oxidation vs. potential for 1 mol dm^{-3} 2-propanol in 0.5 (\circ), 1 (\triangle), and 3 mol dm^{-3} (\square) NaOH over a blacked platinum gauze. RHEs were prepared with the corresponding NaOH electrolyte and had potentials of: 0.5 mol dm^{-3} , $E = -0.779 \text{ V}$; 1 mol dm^{-3} , $E = -0.828 \text{ V}$; 3 mol dm^{-3} , $E = -0.998 \text{ V}$ vs. NHE. $T = 60^\circ\text{C}$.

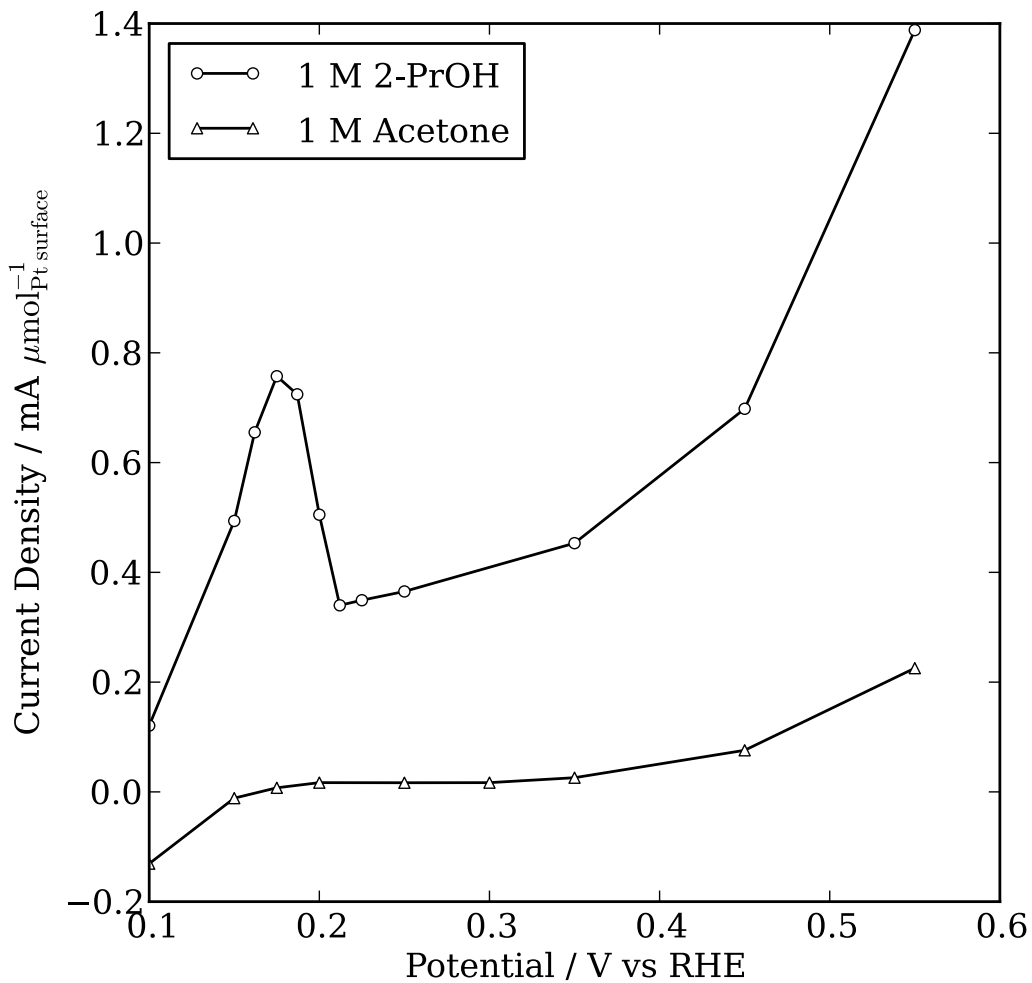


Figure 2.9: Current at the end of a 15 min oxidation vs. potential for 1 mol dm^{-3} 2-propanol (\circ), and 1 mol dm^{-3} acetone (\triangle) in 1 mol dm^{-3} NaOH over a blacked platinum gauze. $T = 60^\circ\text{C}$.

chronoamperometric oxidation of 2-propanol carried out over a 3 h period at 0.15, 0.30, and 0.55 V in 1 mol dm⁻³ NaOH. The current at 0.15 V, below the low-potential current maximum observed after 15 min, was the most stable of the potentials studied. The current at 0.30 V, a potential after the low-potential current maximum, was lower than the current at 0.15 V over most of the oxidation, and it drifted downwards faster as well. The decline of the current over the last hour of the oxidation at 0.55 V was the fastest of the potentials studied. In fact, the current for the oxidation at this higher potential drifted downward to a value below the current at 0.15 V by the end of the 3 h period, despite the 0.35 V difference between these two applied potentials. The current densities above the low-potential current maximum are therefore not under steady-state conditions; this behaviour is consistent with the change in mechanism proposed previously that involves a rapid oxidation of 2-propanol to acetone at low potentials, and a slower oxidation of acetone that occurs at higher potentials through an intermediate or intermediates that bind strongly to the platinum surface.

Figure 2.11 shows the sampled current voltammogram for the oxidation of 2-propanol in 0.5 mol dm⁻³ H₂SO₄ and in 1 mol dm⁻³ NaOH. The oxidation kinetics of 2-propanol in acid are faster at potentials higher than ca. 0.26 V and up to the maximum potential used for this experiment, 0.55 V. The oxidation kinetics in base, however, are substantially faster at low potentials, ranging from 0.1 through 0.26 V. The cathodic current observed in acid at potentials below 0.15 V is likely due to the reduction of 2-propanol to generate water and propane, as reported by Pastor et al.^[30] As demonstrated in Figure 2.11, such a reduction is not accessible within the potential range studied.

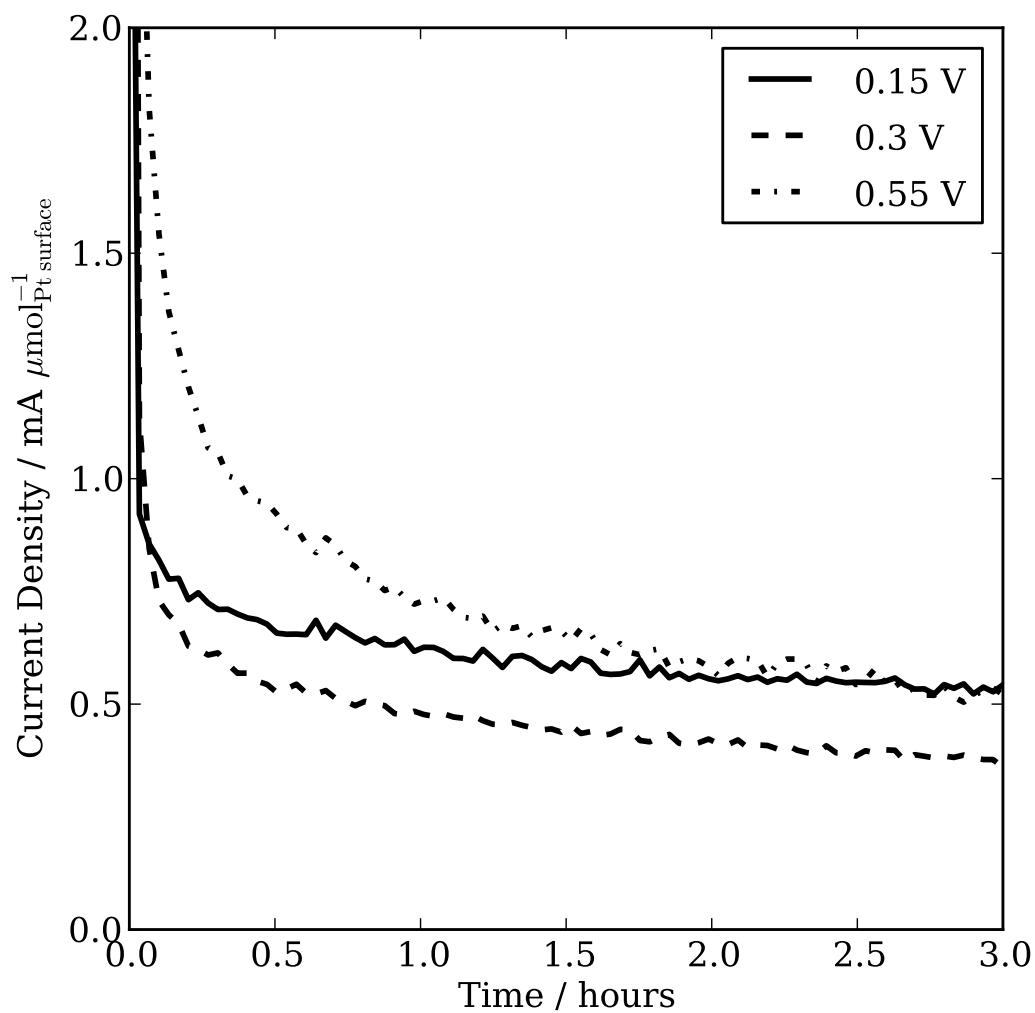


Figure 2.10: Current vs. time plot for the oxidation of 4 mol dm^{-3} 2-propanol in 1 mol dm^{-3} NaOH over a blacked platinum gauze at 0.15 (—), 0.30 (---), and 0.55 V (-.-) vs NHE. $T = 60^\circ\text{C}$.

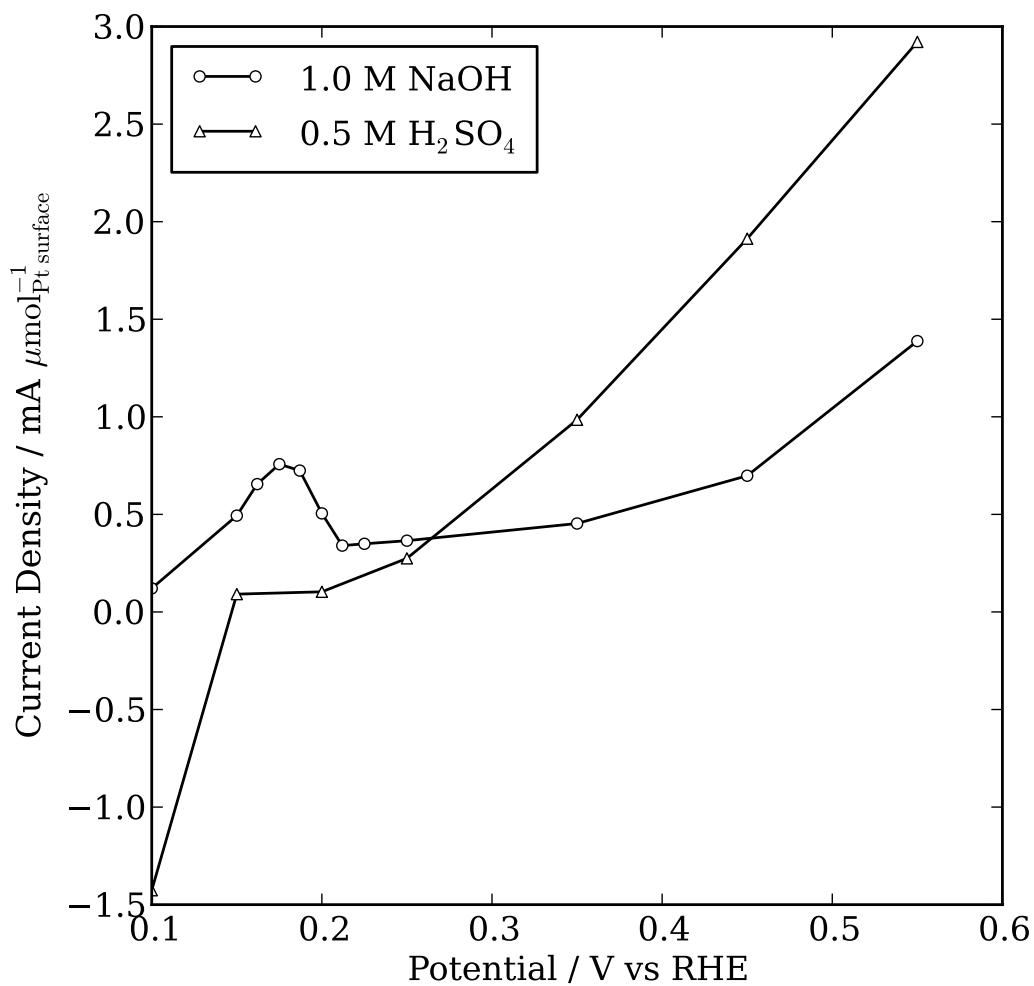


Figure 2.11: Current at the end of a 15 min oxidation vs. potential for 1 mol dm^{-3} 2-propanol in 1 mol dm^{-3} NaOH (\circ), and 0.5 mol dm^{-3} H_2SO_4 (\triangle) over a blacked platinum gauze. $T = 60^\circ\text{C}$.

2.4 Conclusion

The chronoamperometric oxidation of 2-propanol over platinum in base occurs with a large current maximum at low potentials. In comparison, current densities of $0.8 \text{ mA } \mu\text{mol}_{\text{surf}}^{-1}$ were obtained at low potentials using 2-propanol in base, whereas 2-propanol in acid, and methanol in base solutions provided only 0.2 and $0.05 \text{ mA } \mu\text{mol}_{\text{surf}}^{-1}$ respectively under comparable conditions and potentials. To the best of the authors knowledge, such a low-potential current maximum as observed herein with 2-propanol in base has not been observed previously. I suspect that similar behaviour will occur during the oxidation of other secondary alcohols over platinum in base. The evidence obtained during this investigation indicates that two or more mechanisms are in operation for this oxidation. At low potentials, the oxidation produces acetone at high currents without strongly adsorbed intermediates. At higher potentials, the oxidation of acetone commences via formation of strongly adsorbed intermediates that impede the oxidations. Detailed mechanistic experiments are required to confirm these suppositions.

As we reported previously,^[31] the cell voltage from open-circuit up to ca. 0.2 A cm^{-2} of an acid electrolyte (NafionTM) DAFC was ca. 0.22 V higher when it operated on 2-propanol than methanol. Unfortunately, the 2-propanol cell voltage dropped rapidly and became erratic at current densities higher than ca. 0.2 A cm^{-2} . Despite this drop at high currents, the higher cell voltage up to ca. 0.2 A cm^{-2} resulted in an electrical efficiency at peak power (max power per unit area of electrode) operating on 2-propanol that was nearly twice (60% vs 32%) that of the cell operating on methanol. The peak power of the 2-propanol cell was ca. 75% that of the methanol cell. The results obtained from the present investigation hold promise that an alkaline-based, 2-propanol

DAFC will operate at high cell voltages over larger current ranges than did the acid-based DAFC. Other potential advantages of such an alkaline, 2-propanol DAFC include: (1) that formation of carbon monoxide and carbonate would be minimized at high currents and cell voltages; (2) that anion flow from the cathode to the anode would impede 2-propanol crossover; (3) that such a system can, in principle be made regenerative by hydrogenating the acetone to produce 2-propanol.^[32]

References

- [1] Markiewicz, M.; Hebert, D.; Bergens, S., Electro-oxidation of 2-propanol on platinum in alkaline electrolytes. *J Power Sources* **2006**, *161* (2), pp. 761–767.
- [2] Caram, J. A.; Gutiérrez, C., Cyclic voltammetric and potential-modulated reflectance spectroscopic study of the electroadsorption of methanol and ethanol on a platinum electrode in acid and alkaline media. *Journal of Electroanalytical Chemistry* **1992**, *323* (1-2), pp. 213–230.
- [3] Morallon, E.; Rodes, A.; Vázquez, J. L.; Pérez, J. M., Voltammetric and in-situ FTIR spectroscopic study of the oxidation of methanol on Pt (hkl) in alkaline media. *J Electroanal Chem* **1995**, *391* (1-2), pp. 149–157.
- [4] Spendelow, J. S.; Goodpaster, J. D.; Kenis, P. J. A.; Wieckowski, A., Methanol Dehydrogenation and Oxidation on Pt(111) in Alkaline Solutions. *Langmuir* **2006**, *22* (25), pp. 10 457–10 464.
- [5] Christensen, P.; Hamnett, A.; Linares-Moya, D., Oxygen reduction and fuel oxidation in alkaline solution. *Phys Chem Chem Phys* **2011**, *13* (12), pp. 5206–5214.
- [6] Garcia, G.; Koper, M. T. M., Carbon Monoxide Oxidation on Pt Single Crystal Electrodes: Understanding the Catalysis for Low Temperature Fuel Cells. *Chemphyschem* **2011**, *12* (11), pp. 2064–2072.
- [7] Hayes, J. R.; Zeller, D.; Friesen, C., The Influence of Platinum Surface Morphology on the Electrooxidation of Methanol in Alkaline Solutions. In *ECS Trans*, ECS, **2008**, pp. 41–54.

- [8] Tripkovi, A.; Popovi, K.; Grgur, B.; Blizanac, B.; Ross, P.; Marković, N., Methanol electrooxidation on supported Pt and PtRu catalysts in acid and alkaline solutions. *Electrochim Acta* **2002**, *47* (22-23), pp. 3707–3714.
- [9] Parsons, R., The oxidation of small organic molecules: A survey of recent fuel cell related research. *Journal of Electroanalytical Chemistry* **1988**.
- [10] Spendelow, J. S.; Goodpaster, J. D.; Kenis, P. J. A.; Wieckowski, A., Mechanism of CO Oxidation on Pt(111) in Alkaline Media. *J Phys Chem B* **2006**, *110* (19), pp. 9545–9555.
- [11] Lamy, C., Electrocatalytic oxidation of organic compounds on noble metals in aqueous solution. *Electrochim Acta* **1984**, *29* (11), pp. 1581–1588.
- [12] Tripković, A. V.; Popović, K. D.; Lović, J. D., The influence of the oxygen-containing species on the electrooxidation of the C1–C4 alcohols at some platinum single crystal surfaces in alkaline solution. *Electrochim Acta* **2001**, *46* (20-21), pp. 3163–3173.
- [13] Hao Yu, E.; Scott, K.; Reeve, R. W., A study of the anodic oxidation of methanol on Pt in alkaline solutions. *Journal of Electroanalytical Chemistry* **2003**, *547* (1), pp. 17–24.
- [14] Tripković, A. V.; Popović, K. D.; Lović, J. D.; Jovanović, V. M.; Kowal, A., Methanol oxidation at platinum electrodes in alkaline solution: comparison between supported catalysts and model systems. *Journal of Electroanalytical Chemistry* **2004**, *572* (1), pp. 119–128.
- [15] Tripković, A. V.; Popovic, K. D.; Momčilović, J. D.; Dražić, D. M., Kinetic and mechanistic study of methanol oxidation on a Pt (111) surface in alkaline media. *J Electroanal Chem* **1996**, *418* (1-2), pp. 9–20.
- [16] Tripković, A. V.; Popović, K. .; Momčilović, J. D.; Dražić, D. M., Kinetic and mechanistic study of methanol oxidation on a Pt(110) surface in alkaline media. *Electrochim Acta* **1998**, *44* (6-7), pp. 1135–1145.
- [17] Tripković, A. V.; Popovic, K. D.; Momčilović, J. D.; Dražić, D. M., Kinetic and mechanistic study of methanol oxidation on a Pt (100) surface in alkaline media. *Journal of Electroanalytical Chemistry* **1998**, *448* (2), pp. 173–181.
- [18] Herrero, E.; Franaszcuk, K.; Wieckowski, A., Electrochemistry of Methanol at Low-Index Crystal Planes of Platinum - an Integrated Voltammetric and Chronoamperometric Study. *J Phys Chem* **1994**, *98* (19), pp. 5074–5083.
- [19] Vega, J. A.; Smith, S.; Mustain, W. E., Hydrogen and Methanol Oxidation Reaction in Hydroxide and Carbonate Alkaline Media. *J Electrochem Soc* **2011**, *158* (4), pp. B349–B354.

- [20] Lai, S. C. S.; Kleijn, S. E. F.; Öztürk, F. T. Z.; van Rees Vellinga, V. C.; Koning, J.; Rodriguez, P.; Koper, M. T. M., Effects of electrolyte pH and composition on the ethanol electro-oxidation reaction. *Catalysis Today* **2010**, *154* (1-2), pp. 92–104.
- [21] Morin, M. C.; Lamy, C.; Leger, J. M.; Vasquez, J. L.; Aldaz, A., Structural effects in electrocatalysis: Oxidation of ethanol on platinum single crystal electrodes. Effect of pH. *Journal of Electroanalytical Chemistry* **1990**, *283* (1-2), pp. 287–302.
- [22] Lopez-Atalaya, M.; Morallon, E.; Cases, F.; Vázquez, J. L.; Pérez, J. M., Electrochemical oxidation of ethanol on Pt(hkl) basal surfaces in NaOH and Na₂CO₃ media. *J Power Sources* **1994**, *52* (1), pp. 109–117.
- [23] Sibille, S.; Moiroux, J.; Marot, J.-C.; Deycard, S., Oxydation électrochimique des aldéhydes en solution aqueuse: I. Oxydation de solutions aqueuses basiques d'aldéhydes à des électrodes d'or et de platine. *J Electroanal Chem Interfacial Electrochem* **1978**, *88* (1), pp. 105–121.
- [24] Santasalo-Aarnio, A.; Kwon, Y.; Ahlberg, E.; Kontturi, K.; Kallio, T.; Koper, M. T. M., Comparison of methanol, ethanol and iso-propanol oxidation on Pt and Pd electrodes in alkaline media studied by HPLC. *Electrochem Commun* **2011**, *13* (5), pp. 466–469.
- [25] Xia, X. H.; Liess, H.-D.; Iwasita, T., Early stages in the oxidation of ethanol at low index single crystal platinum electrodes. *Journal of Electroanalytical Chemistry* **1997**, *437* (1-2), pp. 233–240.
- [26] Lai, S. C. S.; Koper, M. T. M., Ethanol electro-oxidation on platinum in alkaline media. *Phys Chem Chem Phys* **2009**, *11* (44), pp. 10 446–10 456.
- [27] Santasalo, A.; Vidal-Iglesias, F.; Solla-Gullón, J.; Berná, A.; Kallio, T.; Feliu, J. M., Electrooxidation of methanol and 2-propanol mixtures at platinum single crystal electrodes. *Electrochim Acta* **2009**, *54* (26), pp. 6576–6583.
- [28] Lin, H.; Chen, G.; Zheng, Z.; Zhou, J.; Chen, S.; Lin, Z., The adsorption and oxidation of isopropanol at platinum electrode in alkaline media. *Acta Phys-Chim Sin* **2005**, *21* (11), pp. 1280–1284.
- [29] Biegler, T.; Rand, D. A. J.; Woods, R., Limiting Oxygen Coverage on Platinized Platinum - Relevance to Determination of Real Platinum Area by Hydrogen Adsorption. *Journal of Electroanalytical Chemistry* **1971**, *29* (2), pp. 269–277.
- [30] Pastor, E.; Gonzalez, S.; Arvia, A. J., Electroreactivity of Isopropanol on Platinum in Acids Studied by DEMS and FTIRS. *J Electroanal Chem* **1995**, *395* (1-2), pp. 233–242.

- [31] Cao, D.; Bergens, S. H., A direct 2-propanol polymer electrolyte fuel cell. *J Power Sources* **2003**, *124* (1), pp. 12–17.
- [32] Ralph, C.; Bergens, S. H., A highly reusable catalyst for enantioselective ketone hydrogenation. Catalyst-organic frameworks by alternating ROMP assembly. *Organometallics* **2007**, *26* (7), pp. 1571–1574.

Chapter 3

A prototype alkaline direct 2-propanol fuel cell using platinum electrodes*

3.1 Introduction

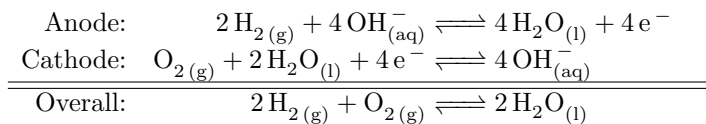
As discussed previously, the activation energies for the oxidation and reduction reactions occurring in a Fuel Cell (FC) are among the most important factors governing FC performance characteristics (§1.2.3.1). These activation energies are dependent on the mechanisms of the reactions, or more specifically, the kinetics of the rate determining steps. The mechanisms for the oxidation of methanol, ethanol, and 2-propanol, using a platinum catalyst, significantly differ from one another in both acidic (§1.3) and alkaline electrolytes (§2.1.3). §1.4 discussed how these mechanisms influence the activity of operating fuel cells in acid. This chapter will only discuss the performance of an Alkaline Fuel Cell (AFC) with platinum catalysts. Due to a lack of standardized testing condition, it is difficult to compare between reported fuel cell performances. Therefore, this section will only focus on comparative studies between different

*A version of this chapter had been previously published:

Markiewicz, M. E. P.; Bergens, S. H., A liquid electrolyte alkaline direct 2-propanol fuel cell. *J Power Sources* **2010**, *195* (21), pp. 7196–7201

fuels, specifically, between methanol, ethanol, and 2-propanol. However, the interested reader is directed to a recent and comprehensive review by Antolini.^[2]

The AFC has several advantages^[2,3] over the acidic electrolyte FC. First, alkaline electrolytes are less corrosive than acidic electrolytes; the less caustic nature of the electrolyte ensures greater longevity of the cell components, and allows the use of cheaper materials (such as stainless steel) in their fabrication. Second, the reduction kinetics of oxygen are more facile in base.^[4] This enhancement results from fewer specifically adsorbed anions on the catalyst that inhibit the reaction, such as sulfate and bisulfate (in sulphuric acid electrolytes). This increase in reaction kinetics enables the use of non-noble metal catalysts, lowering the cost of the catalyst layers. Third, the ionic current from the migration of ionic charge carrier flows from the cathode to the anode in the AFC.^[5] This is the opposite direction of the acidic FC ionic-current, and it reverses the electro-osmotic drag effect (i.e., water is dragged from the cathode to the anode). Flooding of the cathode with product water is a common problem in acidic FC systems, as it increases mass transport losses (§1.2.3.3) at the cathode. The AFC, however, has demonstrated greater tolerance to cathode flooding.^[5] This is in part due to the reversed direction of electro-osmosis, as well as the fact that water is a reactant at the cathode in alkaline electrolytes (Scheme 3.1).



Scheme 3.1: Alkaline oxidation of hydrogen, and reduction of oxygen

One of the problems associated with the alkaline systems is the gradual carbonation of the electrolyte.^[2,3,6] Carbon dioxide can be present in the gas streams, or it may be a product of a reaction, such as the oxidation of trace car-

bon monoxide impurities in reformat gas streams. Changes in the chemistry of the electrolyte resulting from carbonation alter its properties, such as its surface tension, conductivity, and viscosity, and results in performance degradation. Exemplifying this, Kiros et al.^[6] observed a gradual decay ($3.4 \mu\text{V h}^{-1}$) in the operating voltage of their hydrogen-oxygen AFC when small amounts of carbon monoxide, which is oxidized to carbon dioxide, were added to the gas streams. Addition of barium chloride to the liquid electrolyte, forming insoluble barium carbonate, confirmed the gradual buildup of (bi)carbonate in the electrolyte. Xing and Savadogo^[7] found that addition of potassium carbonate to their alkaline-doped Polybenzimidazole (PBI) electrolyte membranes decreased its conductivity by nearly an order of magnitude. Further, the precipitation of carbonate salts in the electrode layers can block mass transport within the catalyst layer.^[8,9]

By far the most studied Alkaline Direct Alcohol Fuel Cell (ADAFc) systems are the Alkaline Direct Methanol Fuel Cell (ADMFC),^[5,10–15] and the Alkaline Direct Ethanol Fuel Cell (ADEFC).^[16–23] Jayashree et al.^[10] compared the performance characteristics of an air-breathing laminar flow-based Direct Alcohol Fuel Cell (DAFC) when operated using either 1 mol dm^{-3} potassium hydroxide or 0.5 mol dm^{-3} sulphuric acid as an electrolyte. The peak power density was found to be 11.8 mW cm^{-2} with the acidic electrolyte, and 17.2 mW cm^{-2} with the alkaline electrolyte. In agreement with the previously discussed mechanistic data (§2.1.1), Jayashree et al. found that this enhancement was due to significantly enhanced kinetics of the anodic reaction, and a small enhancement of the cathodic reaction.

Verma and Basu^[24] compared the ADMFC and the ADEFC using unsupported, and carbon-supported platinum catalysts. They found that their

unsupported platinum catalysts outperformed their carbon-supported platinum catalysts, and that the unsupported particles were finer than the carbon supported particles. It seems likely that this difference in performance resulted from differences in the specific surface areas of the catalyst layers. With regard to the performances of the ADMFC and the ADEFC, Verma and Basu found that the ADMFC gave higher limiting current densities and higher power densities than the ADEFC.

The ADMFC oxidation products are a mixture of carbon dioxide and formic acid over platinum anode catalysts.^[25] The ADEFC also only produces partial oxidation products; specifically, acetic acid and acetaldehyde are the major products observed from the oxidation of ethanol over platinum.^[25] These products react in non-electrochemical acid/base reactions to consume hydroxide and thus require the use of hydroxide-alcohol fuel mixtures to replenish the hydroxide consumed at the anode (3.1–3.4).



As discussed in Chapter 2, it is proposed that the dehydrogenation of 2-propanol to acetone occurs at low anode potentials, and that a slower oxidation to form carbon dioxide occurs at higher potentials. Unlike carbon dioxide, formic acid, and acetic acid, acetone does not react in irreversible stoichiometric side reactions with hydroxide, and thus does not require added base. In 3-electrode experiments, the platinum-catalyzed oxidation of 2-propanol to acetone provides relatively high stabilized current densities at low anode poten-

tials (see §2.3). Despite this promising behaviour, Yang et al.^[26] reported poor performance for their Alkaline Direct 2-Propanol Fuel Cell (AD2PFC) relative to methanol and ethanol. Specifically, using a PtRu anode (2 mg cm^{-2}), Yang et al. reported a maximum power density of 5.46 mW cm^{-2} for the AD2PFC, and 9.25 and 8.00 mW cm^{-2} for their ADMFC and ADEFC, respectively. This ordering is contradicted by Santasalo-Aarnio et al.,^[14] who found that their AD2PFC significantly outperformed the ADMFC, and the ADEFC under similar conditions.

The goal of this study was to construct a prototype AD2PFC with a liquid KOH electrolyte, 100% alcohol fuel, and low-loading commercial platinum electrodes, in hopes of shedding light on the contradicting results presented in the literature. More specifically, the activity of the electrodes will be tested both in an operating fuel cell and in 3-electrode experiments, to investigate how the low-potential current maximum reported in Chapter 2 influences the performance characteristics of the operating AD2PFC.

3.2 Experimental

3.2.1 General

Nitrogen (Praxair, prepurified), hydrogen (Praxair, prepurified), oxygen (Praxair), KMnO_4 (Fisher, ACS grade) and KOH (Caledon, reagent grade) were used as received. Water from an in-house distilled water line was distilled a second time, and then distilled from alkaline KMnO_4 . 2-propanol (Fisher Scientific, suitable for electronic use) and methanol (Fisher, ACS grade) were freshly distilled before use. ESNS electrodes (silver plated nickel screen, 0.6 mg cm^{-2} platinum loading using 10% platinum on Vulcan XC-72, or 1.5 mg cm^{-2} plat-

inum loading using 20% platinum on Vulcan XC-72) were pretreated as outlined in §§3.2.2 and 3.2.3. All potentials are reported versus the Reference Hydrogen Electrode (RHE) unless stated otherwise. Solution resistance was not determined, and measurements are not iR compensated.

3.2.2 3-electrode experiments

Electrochemical experiments were performed using the setup described in §2.2.1. The working electrode was a 1 cm² ESNS electrode (0.6 or 1.5 mg_{Pt} cm⁻²); it was conditioned in 1 mol dm⁻³ KOH at 60 °C by potential cycling between -0.5 and 0.5 V at 5 mV s⁻¹ until a stable response was achieved (ca. 60 cycles). The electrode was then cleaned in 3% H₂O₂ at 0 °C for several hours, and then slowly warmed to room temperature until all the peroxide had been consumed. The electrode was immersed in a 1 mol dm⁻³ KOH / 1 mol dm⁻³ 2-propanol electrolyte at 60 °C, the electrode was then reduced at -0.1 V over a period of 5 mins. Potential step experiments were then performed for 15 min, with 2 min conditioning steps between potential step experiments ($E_{\text{conditioning}} = -0.1 \text{ V}$).

3.2.3 Fuel cell experiments

Commercial fuel cell hardware (QuickCellTM QC200) was purchased from Astris Energi; the cell hardware is illustrated in Figure 3.1. ESNS electrodes with a geometric area of 5 cm² were constructed by mounting the electrode material (0.6 mg_{Pt} cm⁻² or 1.5 mg_{Pt} cm⁻²) in Teflon frames that were fitted with a current collecting nickel wire. 0.2 dm³ of 5 M potassium hydroxide electrolyte was maintained at 70 °C within an external reservoir that was recirculated using a nitrogen gas lift pump. The volume of electrolyte between the electrodes was

ca. 7.5 cm^3 , and the volume of the anode/cathode chambers was ca. 5.0 cm^3 . When the cell was operated on alcohol fuels, the electrolyte was drained from an outlet between the anode and cathode at $2.5 \text{ cm}^3 \text{ min}^{-1}$, and fresh electrolyte was periodically added to the reservoir. Electrodes were first conditioned under hydrogen by sweeping between -0.5 and 0.5 V at 5 mV s^{-1} until a stable response was achieved (ca. 60 cycles). Experiments were performed using dry hydrogen ($600 \text{ cm}^3 \text{ min}^{-1}$, RT), 100% methanol ($0.5 \text{ cm}^3 \text{ min}^{-1}$, RT), 100% 2-propanol ($0.5 \text{ cm}^3 \text{ min}^{-1}$, RT), and dry oxygen ($300 \text{ cm}^3 \text{ min}^{-1}$, RT). Polarization curves were collected by stepping the current density using a logarithmic scale; the cell potential was allowed to equilibrate for 30 s at each current density before recording the cell potential.

3.3 Results and discussion

Figure 3.2a shows the 3-dimensional current-time-potential (j-t-E) profile for the oxidation of 2-propanol using a low loading commercial platinum electrode ($0.6 \text{ mg cm}^{-2} \text{ Pt/C}$). Figure 3.2b shows the sampled current voltammogram at 0.5, 3, 7.5, and 15 min versus the applied potential. The electrode was first reduced electrochemically at -0.1 V for 2 min, and then held at the desired oxidation potential for 15 min. The resulting current-time transients were then plotted against the applied potential to generate the 3-dimensional profile. The current maximum at 0.25 V (12.9 mA cm^{-2} or $21.5 \text{ mA mg}_{\text{Pt}}^{-1}$ at 15 min) is consistent with those we reported using platinum gauzes (see Chapter 2). To the knowledge of the author, they are the highest reported stabilized current densities for the oxidation of an alcohol at low anode potentials, e.g., at 0.25 V above the reversible hydrogen electrode. In Chapter 1, it was shown that this low-potential current maximum occurs near the onset of acetone oxidation;

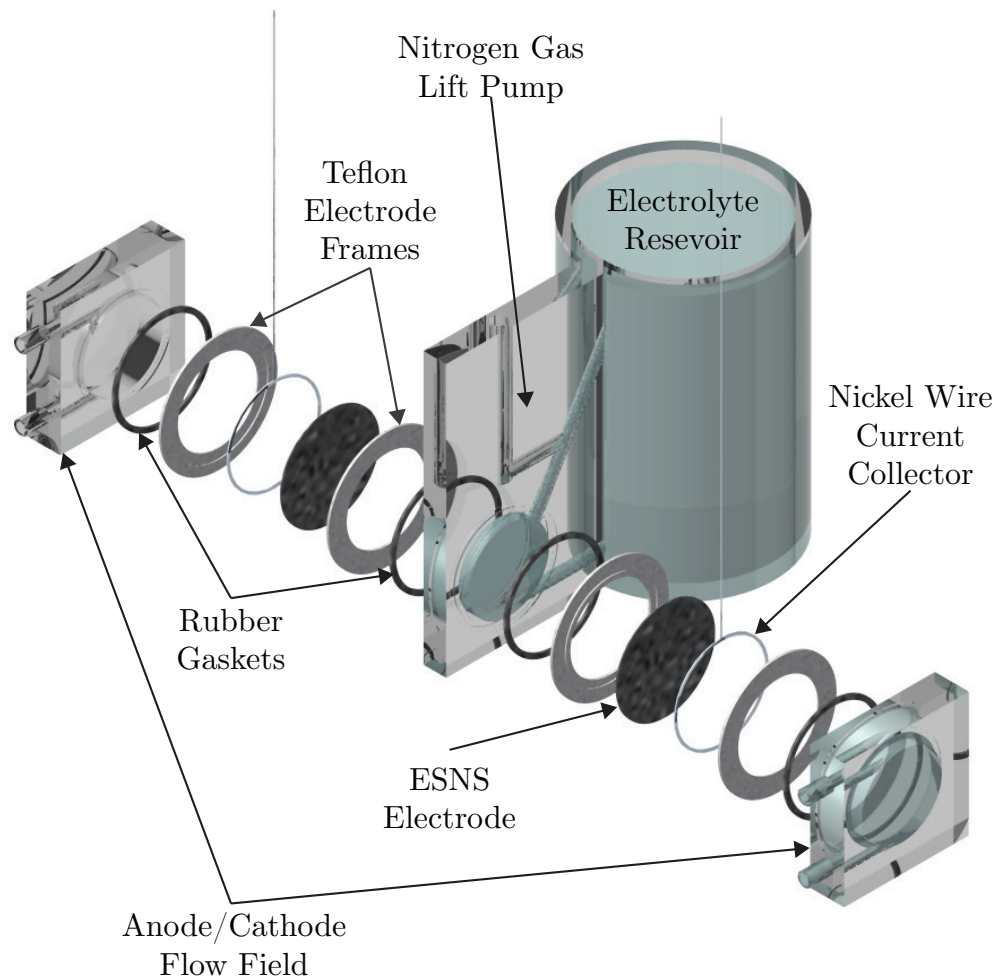
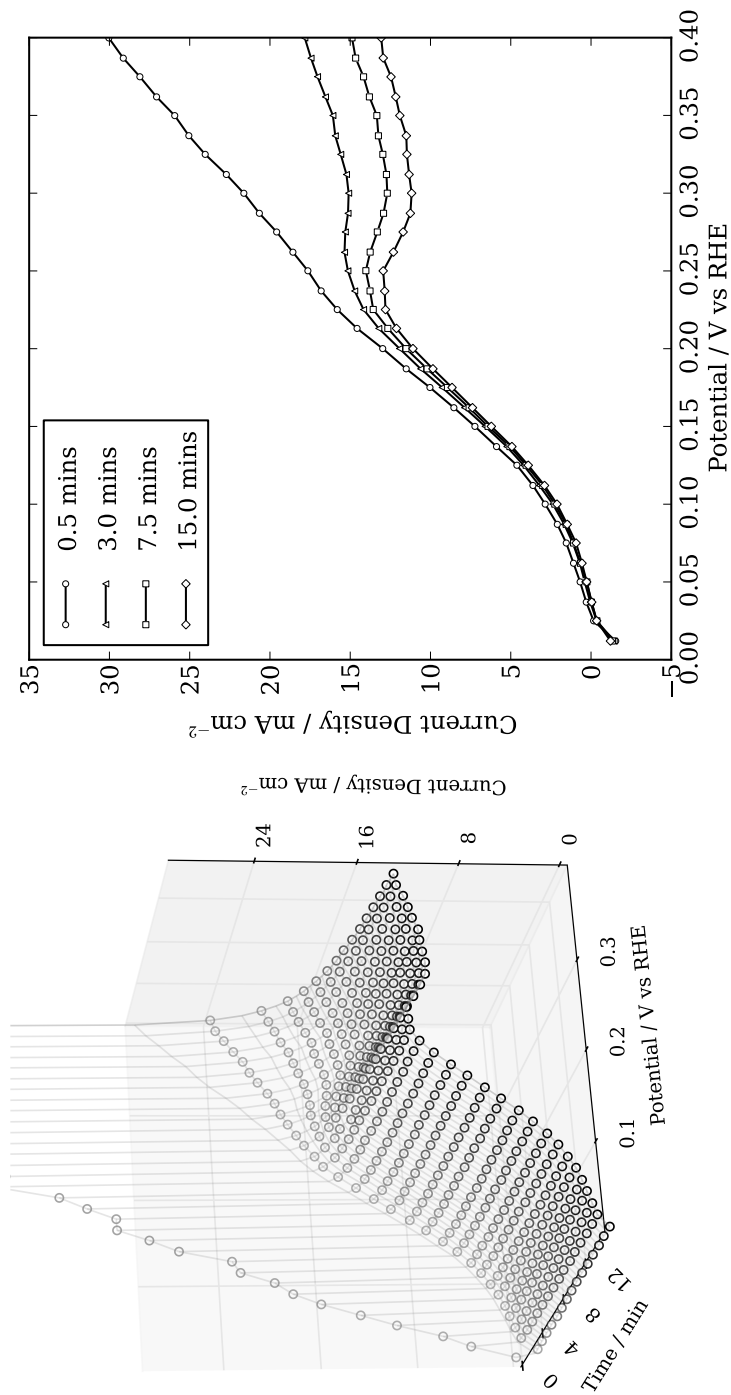


Figure 3.1: Exploded representation of the liquid electrolyte fuel cell (QuickCell™ QC200) used in this study. The active area of the electrodes was 5 cm^2 . The electrolyte reservoir contained ca. 0.2 dm^3 of the 5 mol dm^{-3} KOH and was maintained at 70°C . The volume of electrolyte between the electrodes was ca. 7.5 cm^3 , and the volume of the anode/cathode chambers was ca. 5.0 cm^3 .

here, it is also shown that this maximum is accompanied by a dramatic change in the stability of the current transients.

Figure 3.3 illustrates this change by plotting the percentage of the current lost over the final 10 min of the oxidation $[(j_{5 \text{ min}} - j_{15 \text{ min}}) \div j_{15 \text{ min}}] \times 100$ versus the step potential. The magnitude of the current density at each potential step (j_{15}) is also supplied for comparison. A pronounced change in the stability of the current transients occurs at 0.25 V, and two clearly resolved regions are observed, showing that 2-propanol is oxidized through different mechanisms at potentials below, and above, 0.25 V. This interpretation is consistent with previous studies that proposed that an oxidative dehydrogenation of 2-propanol to acetone occurs at low potentials, and that a slower oxidation to form carbon dioxide occurs at higher potentials (see §1.3.3). To investigate how these different mechanisms impact the performance of an AD2PFC, fuel cells were built and characterized using this electrode material as the anode and cathode.

Figure 3.4 shows the performance curves of the same ADAFC operating on 2-propanol, methanol, and hydrogen when polarized to a lower cell voltage limit of 0.5 V. The hydrogen cell is provided to gauge the performance of the cell hardware, and the low platinum loading electrodes. The Open Circuit Voltage (OCV) of the AD2PFC is ca. 0.16 V higher than the ADMFC, and maintains a higher cell potential (electrical efficiency, 1.2) at current densities up to 16 mA cm^{-2} . The performance of the ADMFC quickly degrades when the cell potential is cycled between its OCV and a lower cell voltage limit of 0.5 V. This degradation is presumably due to the accumulation of carbon monoxide-like intermediates, and/or carbonate species, that inhibit the catalyst. It is likely that the performance of the ADMFC can be recovered by either applying highly oxidizing potentials (i.e., $E_{\text{applied}} \geq 1.0 \text{ V}$) in an alcohol-free electrolyte,



(a) j - t - E profile

(b) j - E (t)

Figure 3.2: (a) Current-time-potential profile for the half-cell oxidation of 1 mol dm⁻³ 2-propanol / 1 mol dm⁻³ KOH over a 0.6 mg_{Pt} cm⁻² ESNS electrode at 60 °C. The electrode was first conditioned at -0.1 V for 2 min, then current-time transients were collected for 15 min every 12.5 mV and plotted against the applied potential. The electrode was conditioned at -0.1 V for 2 min between potential steps. (b) Sampled current voltammogram at 0.5 (○), 3 (△), 7.5 (□) and 15 min (◇) from Figure 3.2a.

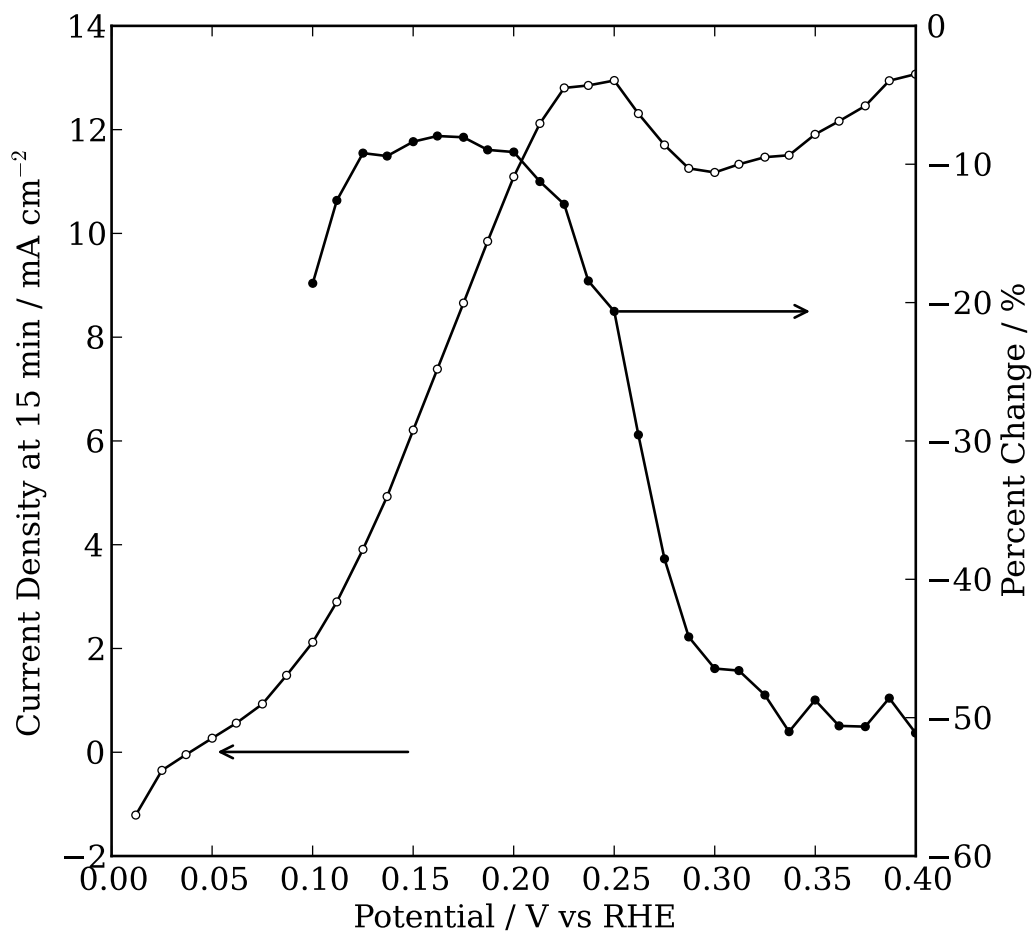


Figure 3.3: Plot of the current density obtained at 15 min for the oxidation of 1 mol dm^{-3} 2-propanol / 1 mol dm^{-3} KOH over a $0.6 \text{ mg}_{\text{Pt}} \text{ cm}^{-2}$ ESNS electrode at 60°C (○), and the percentage of the current changed prior to the reported current (●). Points below 0.1 V are omitted due to the large error associated with the small current density changes.

or by introducing oxygen to the anode compartment to oxidize adsorbates that were formed. In contrast, the AD2PFC is stable to potential cycling within this potential range, showing that 2-propanol does not significantly accumulate intermediates or carbonates that poison the catalyst under these conditions. The time that the cell was allowed to equilibrate at each potential ($t = 30\text{ s}$) is short; however, as shown in 3.2b, the current density is relatively stable at low anodic potentials. The magnitude of the potential steps are small, meaning that the steady-state reaction does not need to change significantly to re-establish the new steady state. Further, the stability of the AD2PFC to potential cycling suggests that there is no accumulation of surface poisoning intermediates. Taking these factors into account, the polarization curves at high cell voltages should be indicative of the stabilized cell performance. If the anode exceeds the low-potential current maximum, however, anode poisoning may reduce the current densities over time. To determine the contributions of the anodic and cathodic polarizations on the AD2PFCs polarization, the loadings of catalyst were increased and studied in the AD2PFC and in 3-electrode experiments.

Figure 3.5b shows the j - t - E profiles for the oxidation of 2-propanol in 3-electrode experiments with a commercial electrode having platinum loadings of 0.6 (10% platinum on Vulcan XC-72) and 1.5 mg cm^{-2} (20% platinum on Vulcan XC-72). Figure 3.5a shows the sampled current voltammogram at 0.5, 3, 7.5, and 15 min versus the applied potential for both electrodes. Somewhat higher current densities occurred at lower potentials over the higher loading electrode. At 15 min, the j - t - E profile peaks at 16.9 mA cm^{-2} and 0.2 V over the 1.5 mg cm^{-2} electrode, and at 12.9 mA cm^{-2} and 0.25 V over the 0.6 mg cm^{-2} electrode. The current densities were similar for both electrodes at higher potentials (i.e., above 0.3 V).

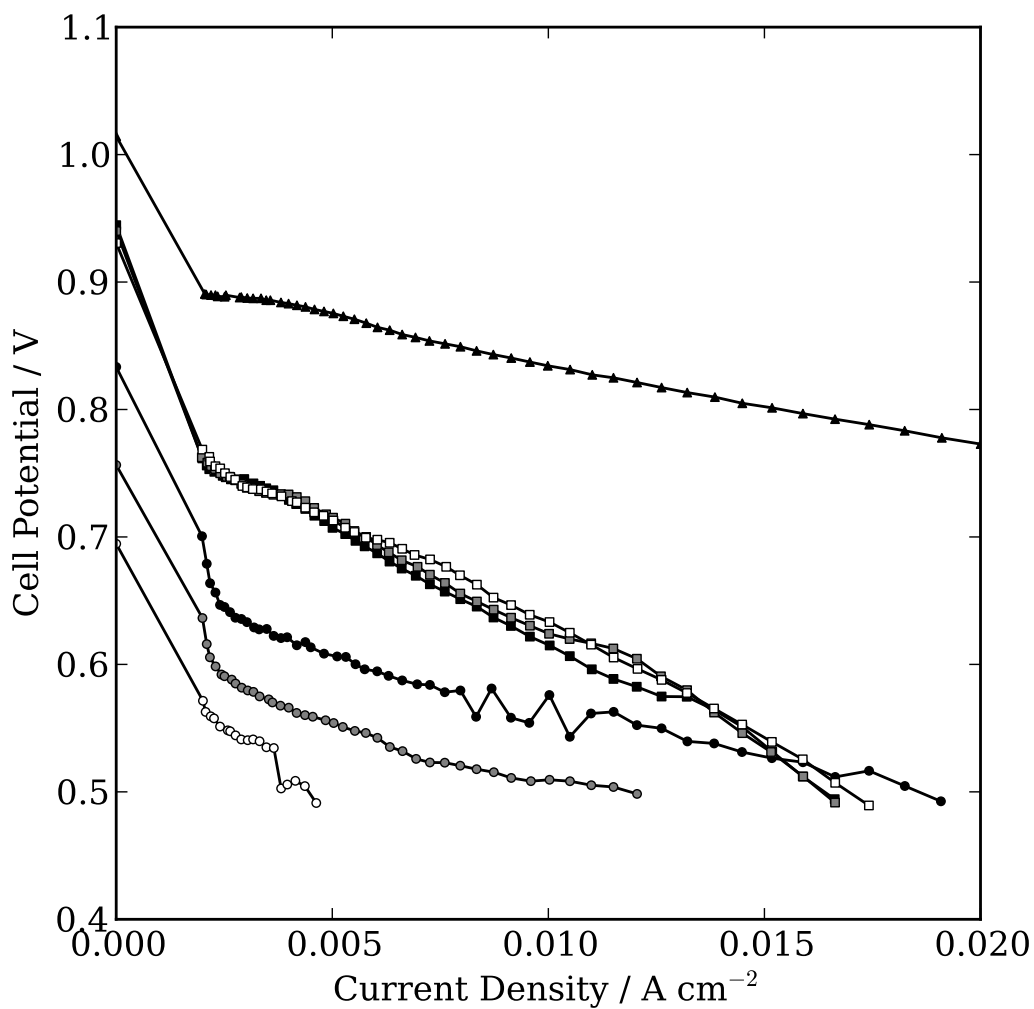
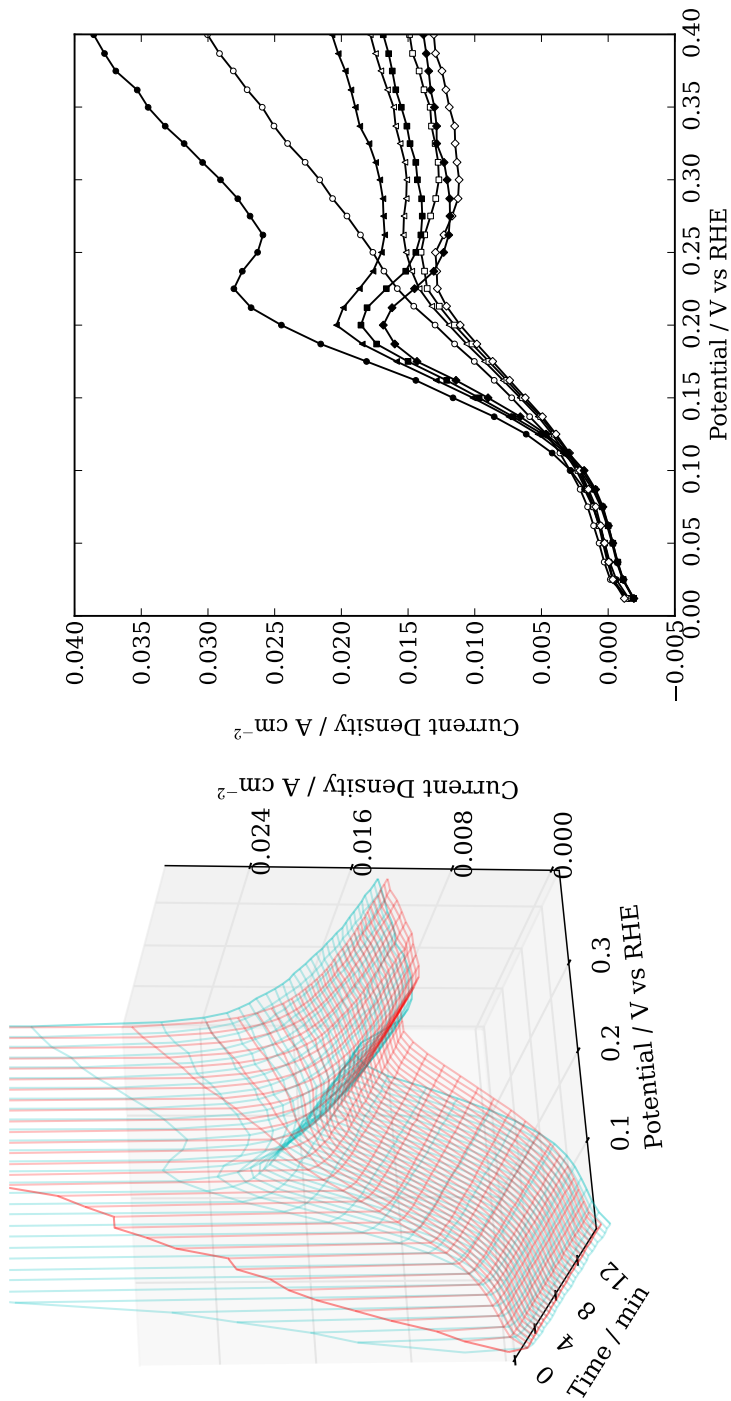


Figure 3.4: Polarization curves for the same alkaline fuel cell operating on hydrogen (▲), 100% 2-propanol (■ = first cycle, ◼ = second cycle, ◻ = third cycle), and 100% methanol (● = first cycle, ◐ = second cycle, ○ = third cycle). Temperature = 70 °C; alcohol flow rate = 0.5 mL min⁻¹ ; dry O₂ = 300 sccm; dry H₂ = 600 sccm; anode and cathode = 0.6 mg_{Pt} cm⁻² ESNS electrode.



(a) j-t-E profile

(b) j-E(t)

Figure 3.5: (a) Current-time-potential profile for the half-cell oxidation of 1 mol dm^{-3} 2-propanol / 1 mol dm^{-3} KOH over a 0.6 (red) and 1.5 mgPt cm^{-2} (cyan) ESNS electrode at 60°C . The electrode was first conditioned at -0.1 V for 2 min , then current-time transients were collected for 15 min every 12.5 mV and plotted against the applied potential. The electrode was conditioned at -0.1 V for 2 min between potential steps. (b) Sampled current voltammogram curves at 0.5 (\circ, \bullet), 3 ($\triangle, \blacktriangle$), 7.5 (\square, \blacksquare) and 15 min (\diamond, \blacklozenge) from Figure 3.2a; $0.6 \text{ mgPt cm}^{-2} = (\circ, \triangle, \square, \diamond)$, and $1.5 \text{ mgPt cm}^{-2} = (\bullet, \blacktriangle, \blacksquare, \blacklozenge)$.

Figure 3.6 shows the performance curves of the AD2PFC with different platinum loadings at the anode and cathode when the cell potential is scanned from its OCV to a lower cell voltage limit of 0.5 V. Increasing the catalyst loading at both the anode and cathode increases the current densities throughout this potential range. Decreasing the loading of the anode back to 0.6 mg cm^{-2} , while leaving the cathode unchanged at 1.5 mg cm^{-2} , did not adversely affect the cell performance at low current densities. Thus, the cathode is the dominant source of polarization under these conditions. The higher anode loading, however, did result in slightly higher current densities at cell voltages near 0.5 V. This increase is consistent with the 3-electrode experiments (Figure 3.5).

Figure 3.7 shows the performance curves for the AD2PFC when cycled from its OCV to a lower cell voltage limit of 0 V. During the first cycle the maximum power density was 13.4 mW cm^{-2} ; this power density is $2.4\times$ that previously reported for a AD2PFC with higher loadings of catalyst.^[26] Polarizing the cell to a lower cell voltage limit of 0 V does, however, result in considerable performance degradation with cycling; the second cycle has a maximum power density that is 60% of the first cycle. This loss in activity is similar to the performance degradation observed during the polarization of the ADMFC to a lower cell voltage limit of 0.5 V (Figure 3.4), and likely results from the accumulation of surface adsorbates. Note that the stable power density achieved when the cell was polarized to a lower cell voltage limit of 0.5 V was 13.1 mW cm^{-2} , that is, 98% of that achieved during the first polarization cycle to a lower cell voltage limit of 0 V. Thus, the change in mechanism at low and high anode potentials results in dramatic changes in the polarization characteristics of the AD2PFC. When the potential of the anode remains below the low-potential current maximum, the AD2PFC is capable of supplying

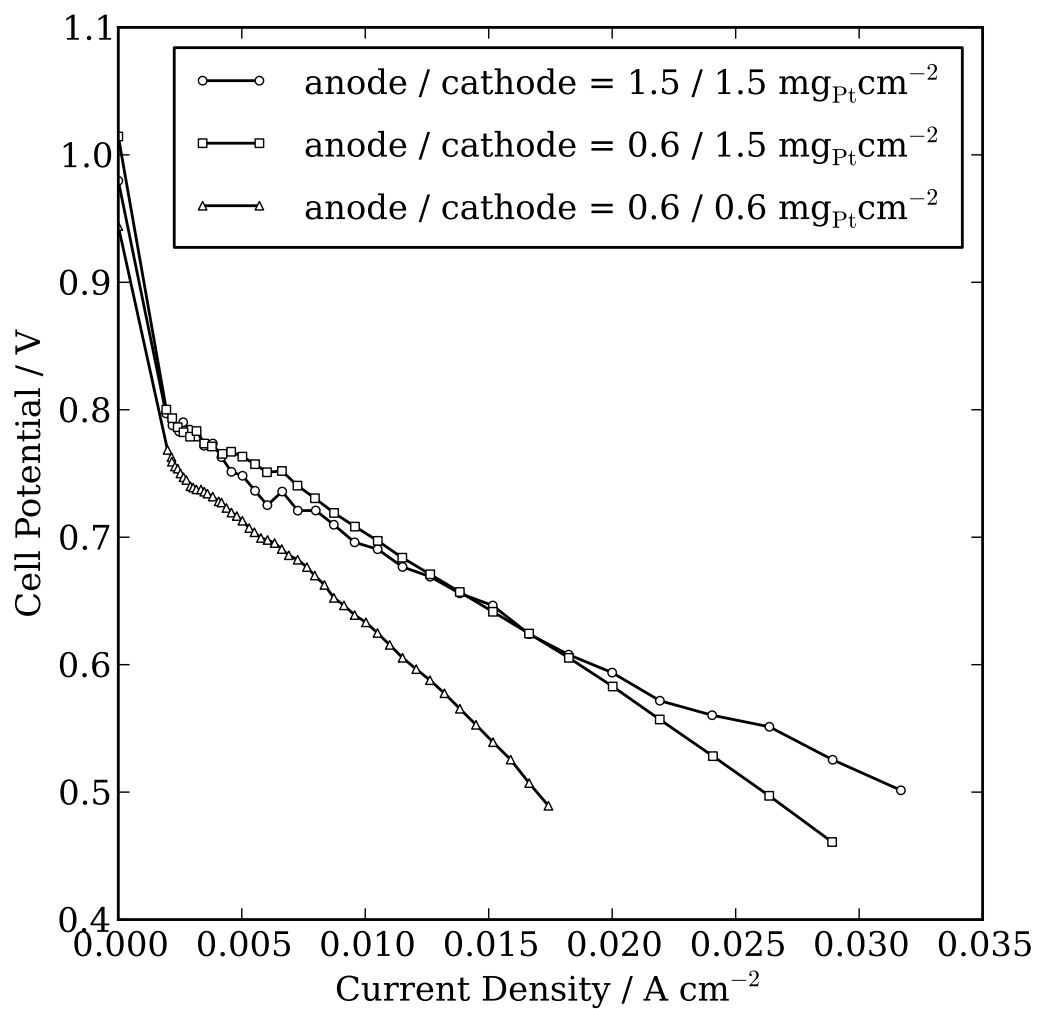


Figure 3.6: Polarization curves for the alkaline direct 2-propanol fuel cell with differing anode and cathode catalyst-loading. $\triangle = 0.6 / 0.6$, $\square = 0.6 / 1.5$, $\circ = 1.5 / 1.5 \text{ mg}_{\text{Pt}} \text{ cm}^{-2}$ (anode loading / cathode loading). Temperature = 70°C; alcohol flow rate = 0.5 mL min⁻¹; dry O₂ = 300 sccm.

relatively high power densities that are stable to potential cycling. When the cell is polarized to low cell potentials strongly bound intermediates form on the anode, and the performance of the AD2PFC declines. It is likely that the high performance of the AD2PFC can be recovered by either reducing the adsorbates, or by applying highly oxidizing potentials (i.e., $E_{applied} \geq 1.0\text{ V}$) in the absence of 2-propanol.

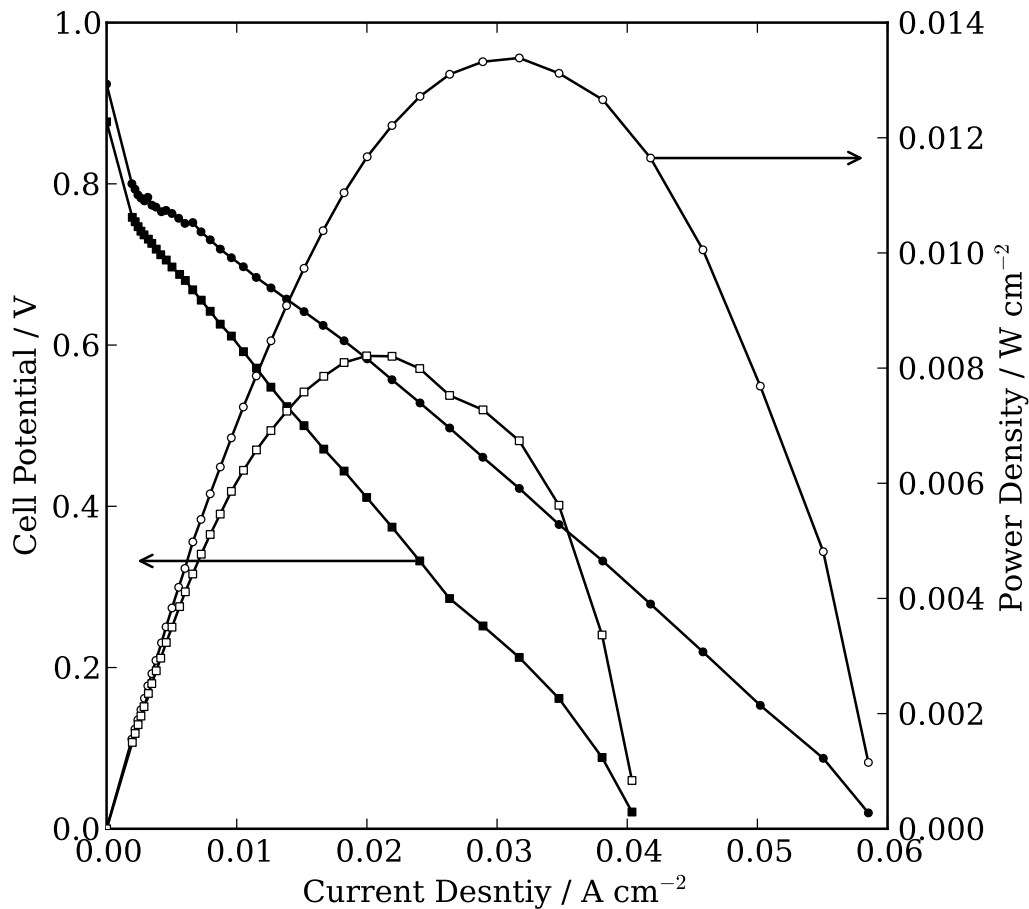


Figure 3.7: Polarization (\blacksquare, \bullet) and power (\square, \circ) curves for the first (\bullet, \circ) and second (\blacksquare, \square) polarization cycles of the alkaline direct 2-propanol fuel cell to 0 V. Temperature = 70°C ; dry $\text{O}_2 = 300\text{ sccm}$; 100% 2-propanol = 0.5 mL min^{-1} ; anode = $0.6\text{ mg}_{\text{Pt}}\text{ cm}^{-2}$ ESNS electrode; cathode = $1.5\text{ mg}_{\text{Pt}}\text{ cm}^{-2}$ ESNS electrode.

Table 3.1 provides a representative survey of recently reported ADAFCs

under comparable conditions. The catalyst-normalized AD2PFC performance is comparable to the state-of-the-art ADAFCs that operate on methanol or ethanol fuel. The AD2PFCs performance reported here is outperformed only by three recently reported ADEFs.

3.4 Conclusion

These proof-of-concept AD2PFC investigations show a good correlation between the activity of the anode in 3-electrode experiments and the activity of the cell. Specifically, the AD2PFC significantly outperformed the ADMFC, and it was more stable when the cell potential was kept above 0.5 V. At lower cell voltages, the maximum power density was only marginally higher, and the cell was unstable, presumably due to anode poisoning by carbonates or strongly adsorbed intermediates from acetone oxidation. The major source of polarization is likely the cathode when these cells operate reversibly at relatively high voltages. The performance of these cells is promising and suggests that a carefully optimized polymer based system will provide high power densities in the absence of carbonate formation.

References

- [1] Markiewicz, M. E. P.; Bergens, S. H., A liquid electrolyte alkaline direct 2-propanol fuel cell. *J Power Sources* **2010**, *195* (21), pp. 7196–7201.
- [2] Antolini, E., Alkaline direct alcohol fuel cells. *J Power Sources* **2010**, *195* (11), pp. 3431–3450.
- [3] McLean, G.; Niet, T.; Prince-Richard, S.; Djilali, N., An assessment of alkaline fuel cell technology. *Int J Hydrogen Energ* **2002**, *27* (5), pp. 507–526.
- [4] Markovic, N.; Gasteiger, H.; Ross, P., Kinetics of oxygen reduction on Pt(hkl) electrodes: Implications for the crystallite size effect with sup-

Table 3.1: Representative survey of Alkaline Direct Alcohol Fuel Cell performance under comparable conditions.

Fuel & Concentration (mol dm ⁻³)	Anode (mg cm ⁻²)	Cathode (mg cm ⁻²)	Pressure ^a (MPa)	Electrolyte	Max Power (mW mg _{anode} ⁻¹)	$E_{max\ power}^b$ (V)	Power at $E = 0.5 V^b$ (mW mg _{anode} ⁻¹)	Temp. (°C)	Reference
MeOH (2) / KOH (2)	PtRu/C (2.0)	Pt/C (1.0)	O ₂ (0.2)	PBI	15.5	0.50	16.0	90	[27]
EtOH (2) / KOH (2)	PtRu/C (2.0)	Pt/C (1.0)	O ₂ (0.2)	PBI	25.0	0.40	27.5	75	[19]
EtOH (3) / KOH (7)	HYPERMEC (2.0)	HYPERMEC (1.0)	99.7% O ₂	Tokuyama A201	30.0	0.25	12.5	40	[20]
EtOH (1) / KOH (0.5)	PtRu (3.0)	Pt (3.0)	O ₂	Tokuyama A201	20.0	0.25	4.2	60	[18]
EtOH (10%) / KOH (2)	Pd-(Ni-Zn)/C (1.0)	HYPERMEC (2.0)	O ₂	Tokuyama A201	80.0	0.40	50.0	80	[17]
MeOH (2) / NaOH (4)	Pt/Ti (1.24)	Pt (0.77)	Air (0.1)	Morgane-ADP	10.6	0.30	2.8	60	[28]
2-PrOH (2) / KOH (4)	PtRu (3.6)	MnO ₂ (3.6)	Air (0.1)	PVA/TiO ₂	1.5	0.30	16.0	25	[26]
MeOH (2) / KOH (2)	PtRu (3.6)	MnO ₂ (3.6)	Air (0.1)	PVA/TiO ₂	2.6	0.25	1.4	25	[26]
100% 2-PrOH	Pt/C (0.6)	Pt/C ^c (1.5)	O ₂ (0.1)	5 M KOH	22.3	0.42	22.0	70	This Work

^a Missing values are due to unspecified pressures.

^b Estimated values from published performance curves.

- ported Pt electrocatalysts. *J Electrochem Soc* **1997**, *144* (5), pp. 1591–1597.
- [5] Yu, E.; Scott, K., Development of direct methanol alkaline fuel cells using anion exchange membranes. *J Power Sources* **2004**, *137* (2), pp. 248–256.
- [6] Kiros, Y.; Myrén, C.; Schwartz, S.; Sampathrajan, A.; Ramanathan, M., Electrode R&D, stack design and performance of biomass-based alkaline fuel cell module. *Int J Hydrogen Energ* **1999**, *24* (6), pp. 549–564.
- [7] Xing, B.; Savadogo, O., Hydrogen/oxygen polymer electrolyte membrane fuel cells (PEMFCs) based on alkaline-doped polybenzimidazole (PBI). *Electrochem Commun* **2000**, *2* (10), pp. 697–702.
- [8] Al-Saleh, M. A.; Gültekin, S.; Al-Zakri, A. S.; Celiker, H., Effect of carbon dioxide on the performance of Ni/PTFE and Ag/PTFE electrodes in an alkaline fuel cell. *J. Appl. Electrochem.* **1994**, *24* (6), pp. 575–580.
- [9] Viswanathan, B.; Scibioh, M. A., *Fuel Cells: Principles and Applications*. CRC Press, **2008**, 1st edition.
- [10] Jayashree, R.; Egas, D.; Spendelow, J. S.; Natarajan, D.; Markoski, L.; Kenis, P. J. A., Air-breathing laminar flow-based direct methanol fuel cell with alkaline electrolyte. *Electrochem Solid-State Lett* **2006**, *9* (5), pp. A252–A256.
- [11] Tripathi, B. P.; Kumar, M.; Shahi, V. K., Organic-inorganic hybrid alkaline membranes by epoxide ring opening for direct methanol fuel cell applications. *J Membr Sci* **2010**, *360* (1-2), pp. 90–101.
- [12] Lue, S. J.; Wang, W. T.; Mahesh, K. P. O.; Yang, C. C., Enhanced performance of a direct methanol alkaline fuel cell (DMAFC) using a polyvinyl alcohol/fumed silica/KOH electrolyte. *J Power Sources* **2010**, *195* (24), pp. 7991–7999.
- [13] Pan, W. H.; Lue, S. J.; Chang, C. M.; Liu, Y. L., Alkali doped polyvinyl alcohol/multi-walled carbon nano-tube electrolyte for direct methanol alkaline fuel cell. *J Membr Sci* **2011**, *376* (1-2), pp. 225–232.
- [14] Santasalo-Aarnio, A.; Kallio, T.; Kontturi, K., Methanol, Ethanol and Iso-Propanol Performance in Alkaline Direct Alcohol Fuel Cell (ADAFC). *ECS Trans* **2010**, *33* (1), pp. 1701–1714.
- [15] Kim, J.-H.; Kim, H.-K.; Hwang, K.-T.; Lee, J.-Y., Performance of air-breathing direct methanol fuel cell with anion-exchange membrane. *Int J Hydrogen Energ* **2010**, *35* (2), pp. 768–773.

- [16] Bambagioni, V.; Bianchini, C.; Marchionni, A.; Filippi, J.; Vizza, F.; Teddy, J.; Serp, P.; Zhiani, M., Pd and Pt–Ru anode electrocatalysts supported on multi-walled carbon nanotubes and their use in passive and active direct alcohol fuel cells with an anion-exchange membrane (alcohol = methanol, ethanol, glycerol). *J Power Sources* **2009**, *190* (2), pp. 241–251.
- [17] Bianchini, C.; Bambagioni, V.; Filippi, J.; Marchionni, A.; Vizza, F.; Bert, P.; Tampucci, A., Selective oxidation of ethanol to acetic acid in highly efficient polymer electrolyte membrane-direct ethanol fuel cells. *Electrochem Commun* **2009**, *11* (5), pp. 1077–1080.
- [18] Fujiwara, N.; Siroma, Z.; Yamazaki, S.-i.; Iorori, T.; Senoh, H.; Yasuda, K., Direct ethanol fuel cells using an anion exchange membrane. *J Power Sources* **2008**, *185* (2), pp. 621–626.
- [19] Hou, H.; Sun, G.; He, R.; Wu, Z.; Sun, B., Alkali doped polybenzimidazole membrane for high performance alkaline direct ethanol fuel cell. *J Power Sources* **2008**, *182* (1), pp. 95–99.
- [20] Li, Y. S.; Zhao, T. S.; Liang, Z. X., Performance of alkaline electrolyte-membrane-based direct ethanol fuel cells. *J Power Sources* **2009**, *187* (2), pp. 387–392.
- [21] Li, Y. S.; Zhao, T. S.; Liang, Z. X., Effect of polymer binders in anode catalyst layer on performance of alkaline direct ethanol fuel cells. *J Power Sources* **2009**, *190* (2), pp. 223–229.
- [22] Modestov, A. D.; Tarasevich, M. R.; Leykin, A. Y.; Filimonov, V. Y., MEA for alkaline direct ethanol fuel cell with alkali doped PBI membrane and non-platinum electrodes. *J Power Sources* **2009**, *188* (2), pp. 502–506.
- [23] Yang, C.-C.; Lee, Y.-J.; Chiu, S.-J.; Lee, K.-T.; Chien, W.-C.; Lin, C.-T.; Huang, C.-A., Preparation of a PVA/HAP composite polymer membrane for a direct ethanol fuel cell (DEFC). *Journal of Electroanalytical Chemistry* **2008**, *38* (10), pp. 1329–1337.
- [24] Verma, A.; Basu, S., Direct alkaline fuel cell for multiple liquid fuels: Anode electrode studies. *J Power Sources* **2007**, *174* (1), pp. 180–185.
- [25] Spendelow, J. S.; Wieckowski, A., Electrocatalysis of oxygen reduction and small alcohol oxidation in alkaline media. *Phys Chem Chem Phys* **2007**, *9* (21), p. 2654.
- [26] Yang, C. C.; Chiu, S. J.; Lee, K. T.; Chien, W. C.; Lin, C. T.; Huang, C. A., Study of poly (vinyl alcohol)/titanium oxide composite polymer membranes and their application on alkaline direct alcohol fuel cell. *J Power Sources* **2008**, *184*, pp. 44–51.

- [27] Hou, H.; Sun, G.; He, R.; Sun, B.; Jin, W.; Liu, H.; Xin, Q., Alkali doped polybenzimidazole membrane for alkaline direct methanol fuel cell. *Int J Hydrogen Energ* **2008**, *33* (23), pp. 7172–7176.
- [28] Yu, E.; Scott, K., Direct methanol alkaline fuel cells with catalysed anion exchange membrane electrodes. *Journal of Electroanalytical Chemistry* **2005**, *35* (1), pp. 91–96.

Chapter 4

Oxidation of 2-propanol in alkaline electrolytes using platinum, ruthenium, and platinum-ruthenium catalysts*

4.1 Introduction

It is well known that bi- and multi-metallic catalysts can be more active than monometallic catalysts towards the oxidation of an alcohol. It is generally accepted that this enhancement can result from:^[2]

1. a structural effect, where addition of the second metal changes the local bonding geometry of the surface;
2. a bifunctional effect, where the two metals fulfill different functions in a cooperative manner;
3. an ensemble effect, where the addition of the second metal changes the distribution of active sites; and

*A version of this chapter had been previously published:

Markiewicz, M.; Bergens, S., Electro-oxidation of 2-propanol and acetone over platinum, platinum-ruthenium, and ruthenium nanoparticles in alkaline electrolytes. *J Power Sources* **2008**, *185* (1), pp. 222–225

4. an electronic effect, where the addition of the second metal changes the electronic structure of the catalyst in such a way that it enhances its reactivity.

The synthesis of carbon-supported bimetallic platinum-metal alloys has been reviewed.^[3,4] Such alloys are typically prepared by either the simultaneous reduction of both metal precursors on carbon, or by the deposition of platinum on carbon followed by alloying the second metal from a suitable precursor at high temperatures.

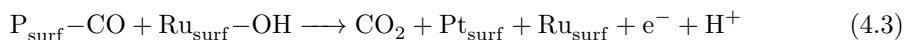
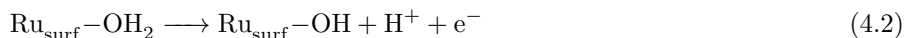
Herein, the behaviour of bi-metallic catalysts towards the oxidation of methanol, ethanol, and 2-propanol, relative to platinum, will be explored and compared.

4.1.1 Methanol Oxidation

As discussed previously, the major surface-poisoning species formed during the oxidation of methanol in acidic (§1.3.1) and in alkaline (§2.1.1) electrolytes is carbon monoxide. The oxidation of this adsorbate requires the formation of a surface oxygen species from the oxidation of water; on platinum, the potential at which these species forms depends on the symmetry of the crystal surface, as well as the nature of the electrolyte. Different metals, however, form surface oxygen species at different potentials, and thus have the propensity to facilitate the oxidation of adsorbed carbon monoxide at lower potentials. This effect was first observed by Petry et al.^[5] in 1965; today, it is known as the bifunctional mechanism (Scheme 4.1), and was originally elucidated by Watanabe and Motoo^[6] ten years after its original observation.

The elementary steps for the oxidation of methanol on platinum and on platinum ruthenium are the same.^[7] On platinum ruthenium, however, methanol

is oxidized on the platinum sites to form carbon monoxide, and ruthenium oxidizes water to form adsorbed surface oxygen species. These oxygen species then act as the oxygen source during the oxidation of carbon monoxide to carbon dioxide. Because ruthenium oxidizes water at lower potentials than platinum, catalysts with platinum and ruthenium on the surface are able to oxidize carbon monoxide at lower potentials than pure platinum, making these sites available for the oxidative adsorption of methanol. The net effect is an increase in the rate of the oxidation of methanol. The use of platinum-ruthenium as a catalyst for the oxidation of methanol has been extensively reviewed by Petrii,^[8] who discusses the work described in over 500 reports on platinum-ruthenium catalysts in methanol oxidation. Here, only a select few papers that demonstrate some of the key effects that enhance the activity of platinum will be discussed.



Scheme 4.1: The bifunctional mechanism for the oxidation of carbon monoxide or metal electrodes.^[9]

Gasteiger et al. showed that the activity of platinum-ruthenium alloys towards the oxidation of methanol is heavily dependent on temperature,^[10] and surface composition.^[11] They found that 10 atomic% ruthenium gave the most active catalyst at room temperature. This composition was explained by a statistical model based on the bifunctional mechanism (vide supra). At high ruthenium content the reaction is limited by dissociative adsorption of methanol, resulting from the dilution of the more active three-fold platinum site. This is known as the ensemble effect.

Alloying platinum with ruthenium has also been shown to change the bonding interactions between the surface and the carbon monoxide intermediate. Specifically, Iwasita et al.^[12] observed that the Fourier Transform Infrared Spectroscopy (FTIR) adsorption frequency for carbon monoxide shifts to higher values upon alloying platinum with ruthenium. This shift is believed to result from less electronic donation from the metal surface to the π^* orbitals of carbon monoxide, strengthening the carbon-oxygen bond and shifting its adsorption frequency to higher values. The reduced donation from the metal to the π^* orbitals of carbon monoxide weakens the metal-carbon bond. This weaker bond is then more easily oxidized, as compared with the oxidation of carbon monoxide on pure platinum. Similar conclusions have been made by Babu et al.^[13] using ^{195}Pt and ^{13}C NMR, and by Maillard et al.^[14] using FTIR. This change in the bonding interactions between the metal and the adsorbent is known as the electronic effect.

Alloys of platinum and ruthenium have also been found to facilitate the formation of adsorbed carbon monoxide from methanol.^[15] That is to say that ruthenium also increases the rate of the steps prior to the oxidation of carbon monoxide. It is believed that ruthenium causes an electronic deficiency at platinum, and this deficiency reduces the repulsive interactions between the metal surface and the electron rich methanol molecule. As a result, the energy barrier to adsorption is reduced, leading to a more facile production of carbon monoxide.

Other than carbon dioxide, small amounts of formaldehyde and formic acid have been observed during the oxidation of methanol.^[16] The distribution of products depends on the alloy composition, with formaldehyde and formic acid being more common with platinum-ruthenium catalysts that are rich in

platinum. The differences in the distribution of these products are believed^[16] to result from changes in the coverage of adsorbed hydroxide.

Platinum-ruthenium based catalysts are the most studied in regards to the oxidation of methanol; however, other metals have been found to enhance the activity of platinum. Extensive reviews on this topic are available,^[17-20] and will only be briefly discussed here. Tin-oxide supported platinum has shown increased resistance to carbon monoxide poisoning by a “chemical interaction” between platinum and tin-oxide.^[21] Platinum-tin alloys have also shown increased activity towards the oxidation of methanol, which has been explained by invoking the bifunctional mechanism,^[22] where tin acts as the oxophilic centre. Additionally, alloying platinum with tin expands the platinum lattice slightly, which is believed to favour methanol adsorption. This is the structural effect mentioned previously. Platinum-tin alloys, however, are less active than platinum-ruthenium towards the oxidation of methanol.^[19]

Oxides of cerium, nickel, cobalt, tungsten, titanium, and molybdenum have also shown positive effects on the oxidation of methanol.^[17] The activity of these catalysts have been attributed to the release of oxygen from the oxide, which then acts as an oxygen source during the oxidation of adsorbed carbon monoxide. Alloys of platinum with base metals, such as nickel, iron, cobalt, and molybdenum, as well as alloys of these types with other noble metal alternatives such as palladium, ruthenium, and osmium have also been investigated.^[18] The activity of many of these alternative catalysts, however, still remain inferior to that of platinum. Promisingly, reports^[23] of highly active catalysts that contain low loadings of platinum have been reported for quaternary alloys, such as $\text{Ni}_{31}\text{Zr}_{13}\text{Pt}_{33}\text{Ru}_{23}$.

4.1.2 Ethanol Oxidation

Several alloys of platinum have been investigated as catalysts for the oxidation of ethanol. The most pervasive of these are based on platinum-tin, which have been identified as the most active binary catalysts for the oxidation of ethanol,^[24] and are more active than either platinum, or platinum-ruthenium.^[25] Leger et al.^[26] reported that the formation of carbon dioxide coincides with the removal of adsorbed carbon monoxide from platinum-tin. Other than carbon dioxide, acetic acid and acetaldehyde are observed with platinum-ruthenium and platinum-tin electrodes.^[27] The ratio of these products depends on the metal ratio of that platinum-metal alloy, the potential, and the identity of the alloying metal. Specifically, platinum-tin alloys favour the formation of acetic acid, and platinum metal favours the formation of acetaldehyde.

Morimoto and Yeager^[28] have found that platinum-tin alloys are active towards the oxidation of carbon monoxide at lower potentials than platinum. Despite this activity, platinum-tin alloys produce less carbon dioxide than platinum during the oxidation of ethanol.^[29] The decrease in carbon dioxide yield indicates that the platinum-tin surface is less active towards the cleavage of the carbon-carbon bond in ethanol. The high current densities observed with platinum-tin alloys is therefore believed to be enhanced by factors other than only the bifunctional mechanism. First, the dilution of the platinum sites by tin reduces the amount of adsorbed carbon monoxide by reducing the number of adjacent platinum sites on the surface (i.e., the ensemble effect).^[29] Second, tin activates water at lower potentials than platinum, giving adsorbed hydroxides at lower potentials. These adsorbed hydroxides then act as the oxygen source for the production of acetic acid, enhancing the selectivity towards acetic acid (i.e., a bifunctional effect). Similar conclusions have been reached by Del Colle

et al.^[30] using platinum-tin adatom catalysts.

Other than tin and ruthenium, platinum alloys of tungsten, palladium, rhodium, rhenium, molybdenum, titanium, and cerium have been investigated.^[24] These catalysts are less active than either platinum-tin or platinum-ruthenium, but have shown enhanced performance relative to platinum. The main mechanism of enhancement is believed to result from an increase in the amount of bound surface oxygen species, that act as the oxygen source during either the production of acetic acid or carbon dioxide. A notable exception to this behaviour is that of platinum-rhodium, which significantly enhances the formation of carbon dioxide^[31] by increasing the catalysts activity towards the cleavage of the carbon-carbon bond.

Alternatives to platinum have namely focused on the use of palladium.^[32-36] In contrast with the behaviour of methanol, pure palladium is more active than platinum at oxidizing ethanol in alkaline electrolytes.^[37] Santasalo-Aarnio et al.^[34] found that acetate is the major product formed during the oxidation of ethanol over palladium, and acetaldehyde over platinum. The higher activity of palladium relative to platinum is believed to result from a decrease in the activity towards the cleavage of the carbon-carbon bond, forming carbon monoxide.

4.1.3 2-propanol oxidation

Very little work has been done on the oxidation of 2-propanol using catalysts other than platinum, or alloys with platinum. Rodrigues and Nart^[38] studied the oxidation of 2-propanol using alloys of platinum and rhodium. Rhodium was found to facilitate the cleavage of the carbon-carbon bonds of 2-propanol, increasing the yield of carbon dioxide. Increasing the rhodium content increases

the selectivity of the reaction towards the production of carbon dioxide.

Platinum-ruthenium catalysts were studied by Wang et al.^[39] at elevated temperatures (between 150 and 190 °C). They found that the oxidation of 2-propanol over platinum-ruthenium produced acetone, nearly exclusively. At these high temperatures, however, the rate of 2-propanol oxidation was found to be less than that of ethanol or methanol. Similar catalysts were studied by Rodrigues et al.;^[40] however, in contrast with the result of Wang et al., Rodrigues et al. concluded that their platinum-ruthenium catalysts increased the selectivity towards the formation of carbon dioxide. Rodrigues et al. also observed a high selectivity towards the formation of carbon dioxide using platinum only deposits prepared in the same fashion as their platinum-ruthenium catalysts. Rodrigues et al. concluded that it was not ruthenium that was influencing the selectivity of the reaction, but the high roughness of the deposit.

Palladium has been studied as an alternative to platinum by Liu et al..^[41] Palladium was found to have significant activity towards the oxidation of 2-propanol in alkaline media. Further, the onset potential for the 2-propanol over palladium is significantly lower than methanol. The onset potential for the oxidation of 2-propanol over palladium in alkaline media is also less than ethanol,^[42] and the activation energy for the rate-determining step for the oxidation of 2-propanol was found to be lower than for ethanol. The oxidation is promoted by gold,^[43] despite the low activity of gold towards the oxidation of 2-propanol.

In Chapter 2, we found a substantial maximum in the stabilized current density at low potentials during the oxidation of 2-propanol over platinum in alkaline electrolytes. In this potential region, the current density is significantly

higher in alkaline electrolytes than in acidic electrolytes, and is also significantly higher than the current densities observed for methanol. In Chapter 3, this maximum in the stabilized current density was found to correlate well with the performance of an operating Alkaline Direct 2-Propanol Fuel Cell (AD2PFC). When the cell was operated within current density ranges that are consistent with the maximum in stabilized current, the cell performance was stable due to the absence of strongly adsorbed species that accumulate on the electrode.

In this chapter, I present an investigation into the performance of some alternative catalyts at low potentials; specifically, ruthenium and platinum ruthenium blacks. To compare the real activity of these catalysts, the current densities are normalized to the active area of the electrode materials. The goal of this study was to determine if ruthenium enhances the catalytic activity within this low potential region, and determine if the use of platinum ruthenium black may improve the performance in a AD2PFC.

4.2 Experimental

Nitrogen (Praxair, prepurified), hydrogen (Praxair, prepurified), NaOH (Alfa Aesar, 99.99% semiconductor grade), H₂SO₄ (EMD, ACS Grade), Pt black (Johnson Matthey, HiSPECTM 1000), and PtRu black (Johnson Matthey, 50:50 at.%, HiSPEC 6000) were used as-received from the supplier. Ru black (Johnson Matthey) was reduced with hydrogen (1 atm) at 60 °C. The reduced catalyst was stored under nitrogen in a glove box until use. The ruthenium catalyst was slowly exposed to air at 0 °C prior to fabrication of the working electrode. Briefly, a glass vial containing the catalysts and sealed with a septum was cooled in an ice bath, air was allowed to slowly diffuse into the vial through an 18 gauge needle over a period of 1 h to oxidize the surface in a slow and

controlled fashion. Water from an in-house distilled water line was distilled once, then distilled again from alkaline KMnO_4 (Fisher Scientific) before use. 2-propanol (Fisher Scientific, suitable for electronic use) and acetone (Caledon, ACS grade) was freshly distilled before experiments.

Electrochemical experiments were performed using the setup described previously (§2.2.1). All potentials are reported versus the Reference Hydrogen Electrode (RHE), unless stated otherwise. The working electrode was a Pt foil with an adsorbed layer of nanoparticle catalyst. The foil was cleaned in solutions of Aqua Regia (3:1 $\text{HCl}:\text{HNO}_3$) for 15 min, Piranha (5:1 $\text{H}_2\text{SO}_4:\text{H}_2\text{O}_2$) for 15 min, rinsed with triply-distilled water, and then dried in an oven at 100°C . The catalysts (2.5 mg) were suspended in water (2 mL) by sonication for 1 h. $200\ \mu\text{L}$ of the suspension was dropped on a Pt foil, and then dried in air; the resulting physically adsorbed catalyst layer, ca. 0.25 mg, was then used as the working electrode.

All current densities reported in this chapter have been normalized to the real surface area of the catalyst measured prior to the experiment. The active area was determined by carbon monoxide stripping voltammetry.^[44] Briefly, a layer of carbon monoxide was adsorbed onto the catalyst in $1\ \text{mol dm}^{-3}\ \text{H}_2\text{SO}_4$ at 0.1 V (platinum and platinum-ruthenium blacks), and 0.075 V (ruthenium black) for 25 min. The electrolyte was purged with nitrogen while maintaining the electrode at its adsorption potential, followed by sweeping anodically. Assuming a fractional coverage of 0.69, the charge transferred during the oxidation of a pre-adsorbed monolayer of carbon monoxide can be used to estimate the mols of surface atoms (n_{surf}) by 4.4,

$$n_{surf} = \frac{Q_{CO} - Q_{BL}}{6.3040 \times 10^{-13}\ \text{C mol}^{-1}} \quad (4.4)$$

where Q_{CO} and Q_{BL} are the charges associated with the oxidation of the pre-adsorbed monolayer of carbon monoxide, and for the baseline within the same potential region, respectively.

Before potential cycling and chronoamperometry, the electrode was conditioned at -0.050 V versus RHE for 2 min. Potential limits were chosen as to avoid irreversible catalyst oxidation, and are outlined in the text. Potential sweeps were conducted at 50 mV s^{-1} . Potential step experiments were held for 15 min before returning to Open Circuit Voltage (OCV). The electrolyte was not stirred. The measurements are not iR compensated.

4.3 Results and discussion

Figure 4.1 show the carbon monoxide stripping voltammograms of platinum black, platinum-ruthenium black, and ruthenium black in $1 \text{ mol dm}^{-3} \text{ H}_2\text{SO}_4$ at room temperature. During the first anodic sweep, signals due to the oxidation of surface hydrides are completely suppressed, confirming the formation of the carbon monoxide monolayer. In the case of platinum black, a small pre-peak is observed at ca. 0.5 V. This pre-peak has been previously attributed to the oxidation of carbon monoxide that is adsorbed on defect sites (i.e., low coordination sites).^[45]

Consistent with previous reports,^[9,46] pronounced peaks occur at 0.76 , 0.56 , and 0.54 V for the oxidation of carbon monoxide on platinum, platinum-ruthenium, and ruthenium blacks, respectively. Upon addition of ruthenium to platinum, the potential for the oxidation of carbon monoxide stripping peak is decreased by ca. 0.2 V; this behaviour is consistent with the bi-functional mechanism for the oxidation of carbon monoxide. Specifically, ruthenium forms surface oxygen species at lower potentials than platinum, and these surface

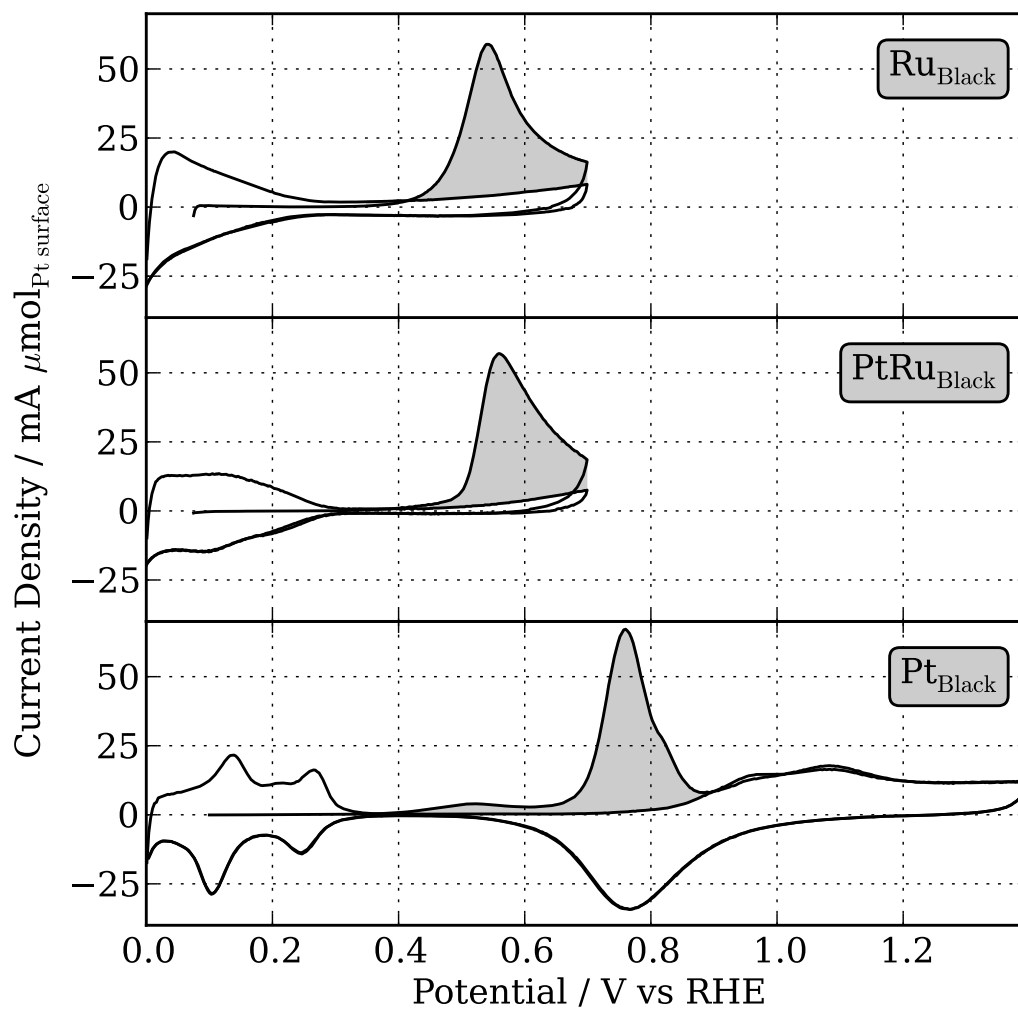


Figure 4.1: Carbon monoxide stripping voltammograms of Pt_{Black}, PtRu_{Black}, and Ru_{Black}, with the anodic charge due to the oxidation of carbon monoxide highlighted. All experiments were collected in 1 mol dm⁻³ H₂SO₄ at room temperature, and at 50 mV s⁻¹.

oxygen species then act as the oxygen source during the oxidation of carbon monoxide to carbon dioxide (Scheme 4.1).

Figure 4.2 shows the voltammograms of platinum black with and without 2-propanol in 1 mol dm^{-3} NaOH at 60°C . The current density has been normalized to the electrodes' number of active sites, and all potentials are reported versus the RHE. The onset potential for oxidation of 2-propanol was ca. 0.14 V , a potential that is within the surface hydride region. The current then increases throughout the double layer potential region, and reaches a maximum at 0.77 V . This current maximum occurs near the onset for surface oxide formation, demonstrating that strongly-bound oxides are less active towards the oxidation of 2-propanol. During the cathodic sweep, a rapid increase in current density occurs once these strongly-bound oxides are reduced; however, the current density in the anodic sweep remains higher than during the cathodic sweep throughout the potential scan. The fact that the current density is higher during the anodic sweep indicates that strongly-bound adsorbents do not form at low potentials in the voltammogram; however, the lower current densities during the cathodic sweep does indicate that some intermediates are formed at higher potentials. The H_{UPD} region of the voltammogram is not suppressed in the presence of 2-propanol; this behaviour suggests that the intermediates that are formed at elevated potentials during the cathodic sweep are susceptible to reductive elimination.

Figure 4.2, also shows the stabilized voltammogram for the oxidation of acetone over platinum black. These same experiments are also plotted in Figure 4.3; however, the scale of the y-axis is more conducive to visualizing the data. All acetone experiments were carried out under the same conditions as those for 2-propanol, with the exception that the concentration of acetone

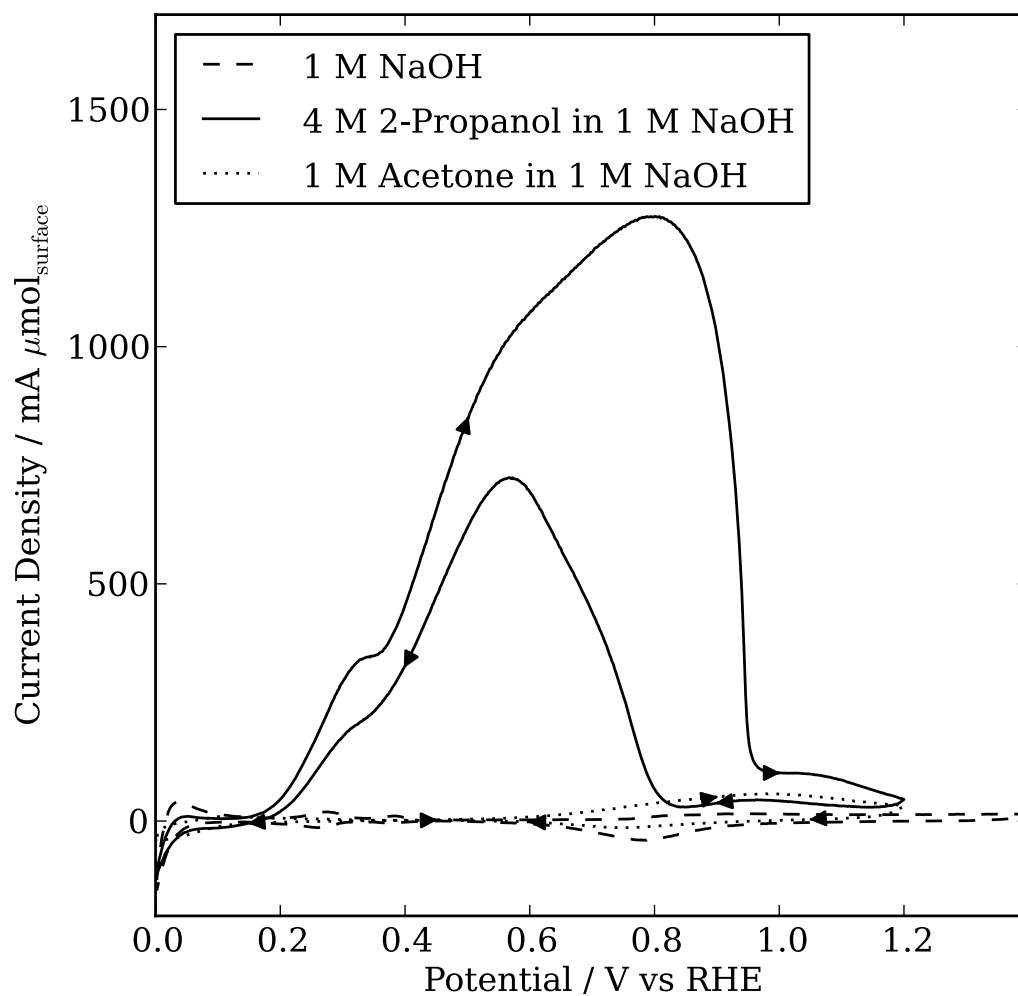


Figure 4.2: Stabilized voltammogram of Pt_{Black} in 1 mol dm^{-3} NaOH (---), 4 mol dm^{-3} 2-propanol / 1 mol dm^{-3} NaOH (—), and in 1 mol dm^{-3} acetone / 1 mol dm^{-3} NaOH (···) electrolytes. All experiments were collected at 60°C , and 50 mV s^{-1} .

was 1 mol dm^{-3} . Platinum is substantially less active towards acetone than 2-propanol. The onset potential for the oxidation of acetone is ca. 0.45 V , about 0.300 V higher than the onset of 2-propanol. The current densities within the surface hydride region are substantially suppressed in the presence of acetone, indicating that strongly bound intermediates are present on the catalyst surface. During the cathodic sweep, a small reductive shoulder occurs at ca. 0.03 V , which may be due to the reduction of acetone to 2-propanol or from the reductive elimination of an adsorbate.

Figure 4.3 also shows the voltammograms of ruthenium black in 1 mol dm^{-3} NaOH, in 1 mol dm^{-3} NaOH / 4 mol dm^{-3} 2-propanol, and in 1 mol dm^{-3} NaOH / 1 mol dm^{-3} acetone electrolytes. Before the voltammograms were collected, the as-received unsupported ruthenium black was reduced under hydrogen at 60°C and 1 atm pressure. The activity of ruthenium towards 2-propanol is substantially lower than platinum; however, ruthenium has some activity towards 2-propanol in the hydride region of the anodic sweep, lower than the onset potential over platinum. The activity of ruthenium towards the oxidation of acetone is very low. There are, however, strong reductive currents between 0.0 and 0.09 V in the anodic and cathodic sweeps for acetone. These currents are far higher than those over platinum, showing that ruthenium is quite active towards the reduction of acetone at low potentials. This electrochemical reduction likely produces 2-propanol as the final product; however, only small amounts of 2-propanol would be produced from these experiments and its presence was not verified. This proposal must be confirmed spectroscopically.

Figure 4.3 also shows the baseline, 2-propanol, and acetone voltammograms over unsupported platinum-ruthenium in 1 mol dm^{-3} NaOH. The onset potential for 2-propanol in the anodic sweep is 0.089 V , consistent with the calculated

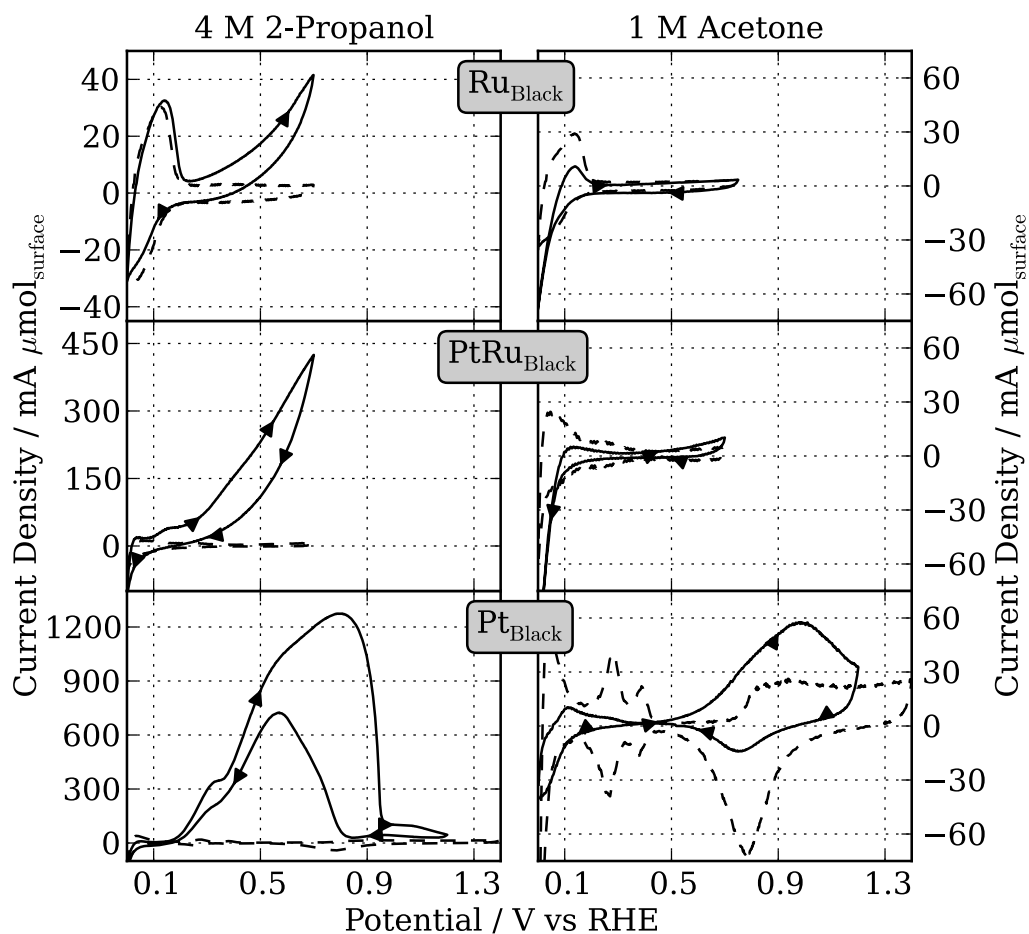


Figure 4.3: Stabilized voltammograms of Pt_{Black} , $\text{PtRu}_{\text{Black}}$, and Ru_{Black} in 1 mol dm^{-3} NaOH (---), and in either 4 mol dm^{-3} 2-propanol / 1 mol dm^{-3} NaOH or 1 mol dm^{-3} acetone / 1 mol dm^{-3} NaOH (—) electrolytes. Note that in the case of 2-propanol, the y-axis scale is different for all three catalysts. All experiments were collected at 60°C , and 50 mV s^{-1} .

2-propanol/acetone equilibrium potential (ca. 0.2 V vs RHE), and lower than the onset potential over platinum. At potentials greater than 0.33 V, platinum-ruthenium is at least $3\times$ more active than ruthenium, but $\frac{1}{3}$ as active as platinum. As was the case for ruthenium, platinum-ruthenium is very active towards the reduction of acetone at low potentials in both the anodic and cathodic sweeps. The normalized current for this reduction is larger than platinum or ruthenium; thus, the combination of these elements is more active than its individual components. Similar to the behaviour of ruthenium, platinum-ruthenium has low activity towards the oxidation of acetone.

Comparing the voltammetric activities of platinum, platinum-ruthenium, and ruthenium blacks towards to oxidation of 2-propanol and acetone shows that platinum is the most active of the three catalysts. This is consistent with an inhibition by adsorbed oxygen species, where addition of the oxophilic ruthenium metal to the catalyst increases the coverage of the surface by adsorbed oxygen species.^[47–49] However, it is also clear from the baseline voltammetry that addition of ruthenium to the catalyst results in the oxidation of H_{UPD} at lower potentials. Figure 4.4 shows the H_{UPD} potential regions for the three catalysts studied. A clear shift in the potential peaks for the oxidation of the H_{UPD} is observed upon addition of ruthenium; however it should be noted that this region may also have some contribution from the chemisorption of hydroxide on ruthenium.^[50] Such changes in the H_{UPD} characteristics of platinum-ruthenium have been well documented for platinum-ruthenium catalysts.^[50–52]

Vannice et al.^[53] has previously shown that 2-propanol does not decompose to acetone on hydride covered platinum surfaces in a Ultra High Vacuum (UHV) environment. Here and in Chapter 2, it was shown that the oxidation of 2-

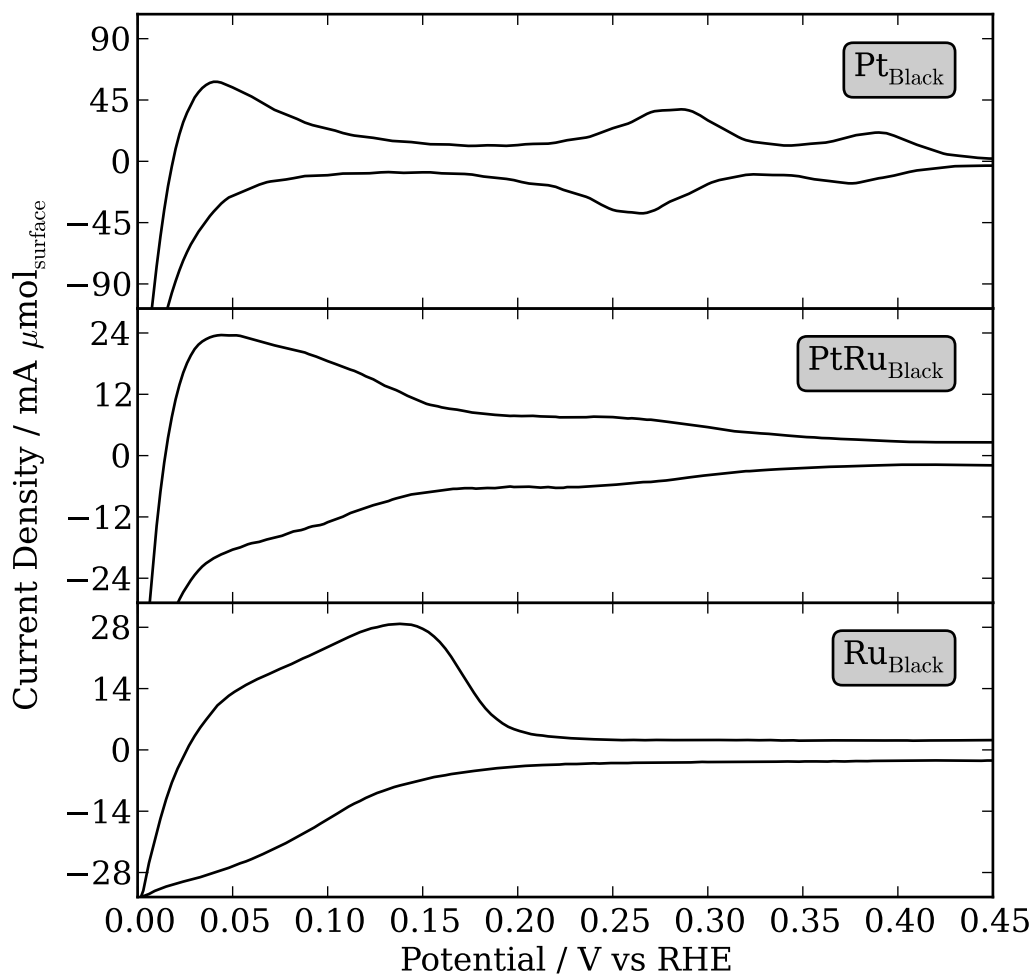


Figure 4.4: H_{UPD} cyclic voltammograms of platinum, platinum-ruthenium, and ruthenium blacks in 1 mol dm^{-3} sodium hydroxide at 60°C .

propanol proceeded through a well defined low-potential current maximum within the H_{UPD} potential region of platinum, platinum-ruthenium, and ruthenium blacks. The fact that addition of ruthenium lowers the potentials where the surface hydrides are oxidized, may also lower the onset potentials for the oxidation of 2-propanol in chronoamperometric experiments. To more thoroughly investigate this proposal, chronoamperometry was performed to investigate the steady-state activity of these catalysts.

Figure 4.5 shows the sampled current voltammogram ($t_{sample} = 15$ min) for oxidation of 2-propanol over the platinum, platinum-ruthenium, and ruthenium blacks. Before each experiment, the electrodes were conditioned for 2 min at -0.05 V to reduce the surface and form a H_{UPD} monolayer. The electrode was then stepped to the desired potential, and held for 15 min without stirring. A low-potential current maximum is observed for all three catalysts; the potential of the current maximum increases from ruthenium, to platinum-ruthenium, and is the highest for platinum. Interestingly, the onset potential for the oxidation of 2-propanol, and the coverages of the surface by H_{UPD} also follows this trend. The magnitude of the current maximum is slightly less for ruthenium than platinum, but it occurs at 0.130 V lower potential. To the best of the author's knowledge, this is the highest potentiostatic current density reported near the H_2/H^+ redox couple for an alcohol/catalyst system. The magnitude of the current maximum is approximately three times higher over platinum-ruthenium than it is over either platinum or ruthenium. These results suggest that, contrary to the behaviour of these catalysts in the voltammetric study, platinum ruthenium is superior to platinum at low potentials. The differences between the sampled current voltammograms and the cyclic voltammograms likely results from the timeframe of the experiments, where the chronoamperometric studies allow the

surface composition to evolve over a significantly longer period of time. The potential of the current maximum over platinum-ruthenium occurs at 0.14 V, a value between the maximums for ruthenium and platinum. Platinum-ruthenium is the most active of these catalysts at high potentials.

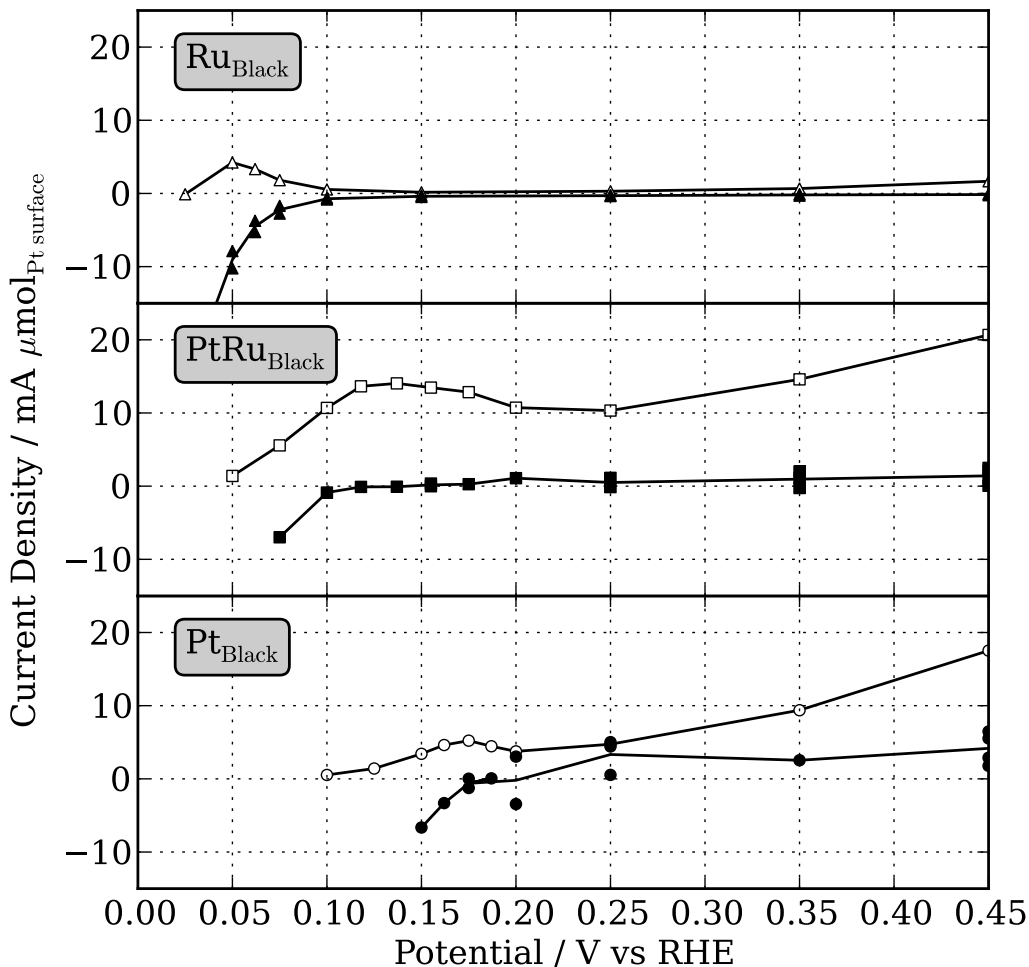


Figure 4.5: Sampled current voltammograms ($t = 15$ min) of Pt_{Black}, PtRu_{Black}, and Ru_{Black} in either 4 mol dm⁻³ 2-propanol / 1 mol dm⁻³ NaOH (○, □, △), or 1 mol dm⁻³ acetone / 1 mol dm⁻³ NaOH electrolytes (●, ■, ▲).

Figure 4.5 also shows the sampled current voltammogram ($t_{sample} = 15$ min) for oxidation of acetone over the three catalysts. All three catalysts possess poor activity towards the oxidation of acetone. Ruthenium, and platinum-ruthenium are highly active towards the reduction of acetone at low potentials. The onset

potentials for the reduction of acetone, however, also follow the H_{UPD} coverage trends discussed previously. It appears that the coverage of the surface by H_{UPD} plays a significant role in the oxidation of 2-propanol, and in the reduction of acetone. This result, combined with those from 2-propanol oxidation, shows that a highly reversible, low-potential 2-propanol/acetone redox couple exists over platinum-ruthenium electro-catalysts in alkaline electrolytes.

4.4 Conclusion

The results of this study show that there is a cooperative effect between platinum and ruthenium towards the oxidation of 2-propanol at the low potentials required for an efficient Direct Alcohol Fuel Cell (DAFC). Of the three catalyst surveyed in this study, platinum-ruthenium had the most favourable combination of onset potential and stabilized-current density at low potentials. The low-potential steady-state current maximum for the oxidation of 2-propanol is observed for all three catalysts.

Addition of ruthenium to the catalyst appears to have two effects. At moderate potentials the higher surface coverage by weakly adsorbed hydroxides inhibits the oxidation of 2-propanol. The effect is reversed at low potentials, where ruthenium catalysts have lower coverages of H_{UPD} , and consequently have a lower onset potential for the oxidation of 2-propanol. In regards to the reduction of acetone, the lower H_{UPD} coverages of the ruthenium surface significantly reduces the potential required for reduction. Ruthenium containing catalysts also appear to be less active towards the oxidation of acetone, with ruthenium being nearly completely inactive. These results suggest that an optimized catalyst for the oxidation of 2-propanol to acetone should have low coverages of adsorbed hydrides and oxygen containing species.

References

- [1] Markiewicz, M.; Bergens, S., Electro-oxidation of 2-propanol and acetone over platinum, platinum–ruthenium, and ruthenium nanoparticles in alkaline electrolytes. *J Power Sources* **2008**, *185* (1), pp. 222–225.
- [2] Stamenkovic, V. R.; Markovic, N. M., Electrochemistry at Well-Characterized Bimetallic Surfaces. In *Fuel Cell Catalysis: A Surface Science Approach*, Koper, M. T. M., ed., Wiley, **2009**, pp. 245–270.
- [3] Antolini, E., Formation of carbon-supported PtM alloys for low temperature fuel cells: a review. *Mater Chem Phys* **2003**, *78* (3), pp. 563–573.
- [4] Liu, H.; Song, C.; Zhang, L.; Zhang, J.; Wang, H.; Wilkinson, D., A review of anode catalysis in the direct methanol fuel cell. *J Power Sources* **2006**, *155* (2), pp. 95–110.
- [5] Petry, O. A.; Podlovch, B. I.; Frumkin, A. N.; Lal, H., Behaviour of Platinized-Platinum and Platinum-Ruthenium Electrodes in Methanol Solutions. *J Electroanal Chem Interfacial Electrochem* **1965**, *10* (4), pp. 253–289.
- [6] Watanabe, M.; Motoo, S., Electrocatalysis by ad-atoms part II. Enhancement of the oxidation of methanol on platinum by ruthenium ad-atoms. *Journal of Electroanalytical Chemistry* **1975**, *60* (3), pp. 267–273.
- [7] He, C.; Kunz, H. R.; Fenton, J., Evaluation of platinum-based catalysts for methanol electro-oxidation in phosphoric acid electrolyte. *J Electrochem Soc* **1997**, *144* (3), pp. 970–979.
- [8] Petrii, O. A., Pt–Ru electrocatalysts for fuel cells: a representative review. *J Solid State Electrochem* **2008**, *12* (5), pp. 609–642.
- [9] Yajima, T.; Uchida, H.; Watanabe, M., In-situ ATR-FTIR spectroscopic study of electro-oxidation of methanol and adsorbed CO at Pt-Ru alloy. *J Phys Chem B* **2004**, *108* (8), pp. 2654–2659.
- [10] Gasteiger, H. A.; Markovic, N.; Ross Jr, P. N.; Cairns, E. J., Temperature-dependent methanol electro-oxidation on well-characterized Pt-Ru alloys. *J Electrochem Soc* **1994**, *141* (7), pp. 1795–1803.
- [11] Gasteiger, H. A.; Markovic, N.; Ross Jr, P.; Cairns, E., Methanol electrooxidation on well-characterized Pt-Ru alloys. *J Phys Chem* **1993**, *97* (46), pp. 12 020–12 029.
- [12] Iwasita, T.; Nart, F.; Vielstich, W., FTIR study of the catalytic activity of a 85: 15 Pt. Ru alloy for methanol oxidation. *Ber Bunsen Phys Chem* **1990**, *94* (9), pp. 1030–1034.

- [13] Babu, P. K.; Kim, H. S.; Oldfield, E.; Wieckowski, A., Electronic Alterations Caused by Ruthenium in PtRu Alloy Nanoparticles as Revealed by Electrochemical NMR. *J Phys Chem B* **2003**, *107* (31), pp. 7595–7600.
- [14] Maillard, F.; Gloaguen, F.; Hahn, F.; Leger, J. M., Electrooxidation of Carbon Monoxide at Ruthenium-Modified Platinum Nano-particles: Evidence for CO Surface Mobility. *Fuel Cells* **2002**, *2* (34), pp. 143–152.
- [15] Waszczuk, P.; Wieckowski, A.; Zelenay, P.; Gottesfeld, S.; Coutanceau, C.; Leger, J. M.; Lamy, C., Adsorption of CO poison on fuel cell nanoparticle electrodes from methanol solutions: A radioactive labeling study. *Journal of Electroanalytical Chemistry and Interfacial Electrochemistry* **2001**, *511* (1-2), pp. 55–64.
- [16] Kabbabi, A.; Faure, R.; Durand, R.; Beden, B.; Hahn, F.; Leger, J.; Lamy, C., In situ FTIRS study of the electrocatalytic oxidation of carbon monoxide and methanol at platinum-ruthenium bulk alloy electrodes. *Journal of Electroanalytical Chemistry and Interfacial Electrochemistry* **1998**, *444* (1), pp. 41–53.
- [17] Yu, E. H.; Krewer, U.; Scott, K., Principles and Materials Aspects of Direct Alkaline Alcohol Fuel Cells. *Energies* **2010**, *3* (8), pp. 1499–1528.
- [18] Serov, A.; Kwak, C., Review of non-platinum anode catalysts for DMFC and PEMFC application. *Appl Catal, B* **2009**, *90* (3-4), pp. 313–320.
- [19] Antolini, E.; Gonzalez, E. R., The electro-oxidation of carbon monoxide, hydrogen/carbon monoxide and methanol in acid medium on Pt-Sn catalysts for low-temperature fuel cells: A comparative review of the effect of Pt-Sn structural characteristics. *Electrochim Acta* **2010**, *56* (1), pp. 1–14.
- [20] Legar, J. M.; Coutanceau, C.; Lamey, C., Electrocatalysis for the Direct Alcohol Fuel Cell. In *Fuel Cell Catalysis: A Surface Science Approach*, Koper, M. T. M., ed., Wiley, **2009**, pp. 343–374.
- [21] Okanishi, T.; Matsui, T.; Takeguchi, T.; Kikuchi, R.; Eguchi, K., Chemical interaction between Pt and SnO₂ and influence on adsorptive properties of carbon monoxide. *Appl Catal a-Gen* **2006**, *298* (1-2), pp. 181–187.
- [22] Frelink, T.; Visscher, W.; van Venn, J. A. R., On the role of Ru and Sn as promoters of methanol electro-oxidation over Pt. *Surf Sci* **1995**, *335*, pp. 353–360.
- [23] Whitacre, J. F.; Valdez, T.; Narayanan, S. R., Investigation of Direct Methanol Fuel Cell Electrocatalysts Using a Robust Combinatorial Technique. *J Electrochem Soc* **2005**, *152* (9), p. A1780.

- [24] Antolini, E., Catalysts for direct ethanol fuel cells. *J Power Sources* **2007**, *170* (1), pp. 1–12.
- [25] Colmati, F.; Antolini, E., Effect of temperature on the mechanism of ethanol oxidation on carbon supported Pt, PtRu and Pt₃Sn electrocatalysts. *J Power Sources* **2006**.
- [26] Leger, J.; Rousseau, S.; Coutanceau, C.; Hahn, F.; Lamy, C., How bimetallic electrocatalysts does work for reactions involved in fuel cells? Example of ethanol oxidation and comparison to methanol. *Electrochim Acta* **2005**, *50* (25-26), pp. 5118–5125.
- [27] Vigier, F.; Coutanceau, C.; Perrard, A.; Belgsir, E. M.; Lamy, C., Development of anode catalysts for a direct ethanol fuel cell. *J. Appl. Electrochem.* **2004**, *34* (4), pp. 439–446.
- [28] Morimoto, Y.; Yeager, E. B., CO oxidation on smooth and high area Pt, Pt-Ru and Pt-Sn electrodes. *Journal of Electroanalytical Chemistry* **1998**, *441* (1-2), pp. 77–81.
- [29] Rousseau, S.; Coutanceau, C.; Lamy, C.; Légera, J.-M., Direct ethanol fuel cell (DEFC): Electrical performances and reaction products distribution under operating conditions with different platinum-based anodes. *J Power Sources* **2006**, *158* (1), pp. 18–24.
- [30] Del Colle, V.; Souza-Garcia, J.; Tremiliosi-Filho, G.; Herrero, E.; Feliu, J. M., Electrochemical and spectroscopic studies of ethanol oxidation on Pt stepped surfaces modified by tin adatoms. *Phys Chem Chem Phys* **2011**, *13* (26), p. 12 163.
- [31] De Souza, J.; Queiroz, S. L.; Bergamaski, K.; Gonzalez, E. R.; Nart, F., Electro-Oxidation of Ethanol on Pt, Rh, and PtRh Electrodes. A Study Using DEMS and in-Situ FTIR Techniques. *J Phys Chem B* **2002**, *106* (38), pp. 9825–9830.
- [32] Antolini, E., Alkaline direct alcohol fuel cells. *J Power Sources* **2010**, *195* (11), pp. 3431–3450.
- [33] Wang, X.; Wang, W. W.; Qi, Z.; Zhao, C.; Ji, H.; Zhang, Z., Fabrication; microstructure and electrocatalytic property of novel nanoporous palladium composites. *J Alloys Compd* **2010**, *508* (2), pp. 463–470.
- [34] Santasalo-Aarnio, A.; Kwon, Y.; Ahlberg, E.; Kontturi, K.; Kallio, T.; Koper, M. T. M., Comparison of methanol, ethanol and iso-propanol oxidation on Pt and Pd electrodes in alkaline media studied by HPLC. *Electrochem Commun* **2011**, *13* (5), pp. 466–469.

- [35] Bambagioni, V.; Bianchini, C.; Filippi, J.; Oberhauser, W.; Marchionni, A.; Vizza, F.; Psaro, R.; Sordelli, L.; Foresti, M. L.; Innocenti, M., Ethanol Oxidation on Electrocatalysts Obtained by Spontaneous Deposition of Palladium onto Nickel-Zinc Materials. *ChemSusChem* **2009**, *2* (1), pp. 99–122.
- [36] Bagchi, J.; Bhattacharya, S. K., Electrocatalytic activity of binary Palladium Ruthenium anode catalyst on Ni-support for ethanol alkaline fuel cells. *Transition Met Chem* **2007**, *32* (1), pp. 47–55.
- [37] Antolini, E., Palladium in fuel cell catalysis. *Energy Environ. Sci.* **2009**, *2* (9), pp. 915–931.
- [38] Rodrigues, I.; Nart, F., 2-Propanol oxidation on platinum and platinum-rhodium electrodeposits. *Journal of Electroanalytical Chemistry* **2006**, *590* (2), pp. 145–151.
- [39] Wang, J.; Wasmus, S.; Savinell, R. F., Evaluation of Ethanol, 1-Propanol, and 2-Propanol in a Direct Oxidation Polymer-Electrolyte Fuel Cell. *J Electrochem Soc* **1995**, *142* (12), pp. 4218–4224.
- [40] Rodrigues, I.; De Souza, J.; Pastor, E.; Nart, F., Cleavage of the C-C bond during the electrooxidation of 1-propanol and 2-propanol: Effect of the Pt morphology and of codeposited Ru. *Langmuir* **1997**, *13* (25), pp. 6829–6835.
- [41] Liu, J.; Ye, J.; Xu, C.; Jiang, S.; Tong, Y., Electro-oxidation of methanol, 1-propanol and 2-propanol on Pt and Pd in alkaline medium. *J Power Sources* **2008**, *177* (1), pp. 67–70.
- [42] Su, Y.; Xu, C.; Liu, J.; Liu, Z., Electrooxidation of 2-propanol compared ethanol on Pd electrode in alkaline medium. *J Power Sources* **2009**, *194* (1), pp. 295–297.
- [43] Xu, C.; Tian, Z.; Chen, Z.; Jiang, S. P., Pd/C promoted by Au for 2-propanol electrooxidation in alkaline media. *Electrochem Commun* **2008**, *10* (2), pp. 246–249.
- [44] Lee, C. E., *Self-directing Organometallic Deposition of Ruthenium*. Ph.D. thesis, University of Alberta **2003**.
- [45] Koper, M. T. M.; Lai, S. C. S.; Herrero, E., Mechanisms of the Oxidation of Carbon Monoxide and Small Organic Molecules at Metal Electrodes. In *Fuel Cell Catalysis: A Surface Science Approach*, Koper, M. T. M., ed., Wiley, **2009**, pp. 159–208.

- [46] Kawaguchi, T.; Sugimoto, W.; Murakami, Y.; Takasu, Y., Temperature dependence of the oxidation of carbon monoxide on carbon supported Pt, Ru, and PtRu. *Electrochem Commun* **2004**, *6* (5), pp. 480–483.
- [47] Hayes, J. R.; Zeller, D.; Friesen, C., The Influence of Platinum Surface Morphology on the Electrooxidation of Methanol in Alkaline Solutions. In *ECS Trans*, ECS, **2008**, pp. 41–54.
- [48] Tripković, A. V.; Popović, K. D.; Lović, J. D., The influence of the oxygen-containing species on the electrooxidation of the C1–C4 alcohols at some platinum single crystal surfaces in alkaline solution. *Electrochim Acta* **2001**, *46* (20-21), pp. 3163–3173.
- [49] Hao Yu, E.; Scott, K.; Reeve, R. W., A study of the anodic oxidation of methanol on Pt in alkaline solutions. *Journal of Electroanalytical Chemistry* **2003**, *547* (1), pp. 17–24.
- [50] Conway, B., Electrochemical oxide film formation at noble metals as a surface-chemical process. *Prog Surf Sci* **1995**, *49* (4), pp. 331–452.
- [51] Hoster, H. E.; Behm, R. J., The Effect of Structurally Well-Depined Pt Modification on the Electrochemical and Electrocatalytic Properties of Ru(0001) Electrodes. In *Fuel Cell Catalysis: A Surface Science Approach*, Koper, M. T. M., ed., Wiley, **2009**, pp. 465–506.
- [52] Waszczuk, P.; Solla-Gullón, J.; Kim, H. S.; Tong, Y. Y.; Montiel, V.; Aldaz, A.; Wieckowski, A., Methanol Electrooxidation on Platinum/Ruthenium Nanoparticle Catalysts. *J Catal* **2001**, *203* (1), pp. 1–6.
- [53] Vannice, M. A.; Erley, W.; Ibach, H., A RAIRS and HREELS Study of Isopropyl-Alcohol on Pt(111). *Surf Sci* **1991**, *254* (1-3), pp. 12–20.

Chapter 5

On the influences of ruthenium in the oxidation of 2-propanol in alkaline electrolytes

5.1 Introduction

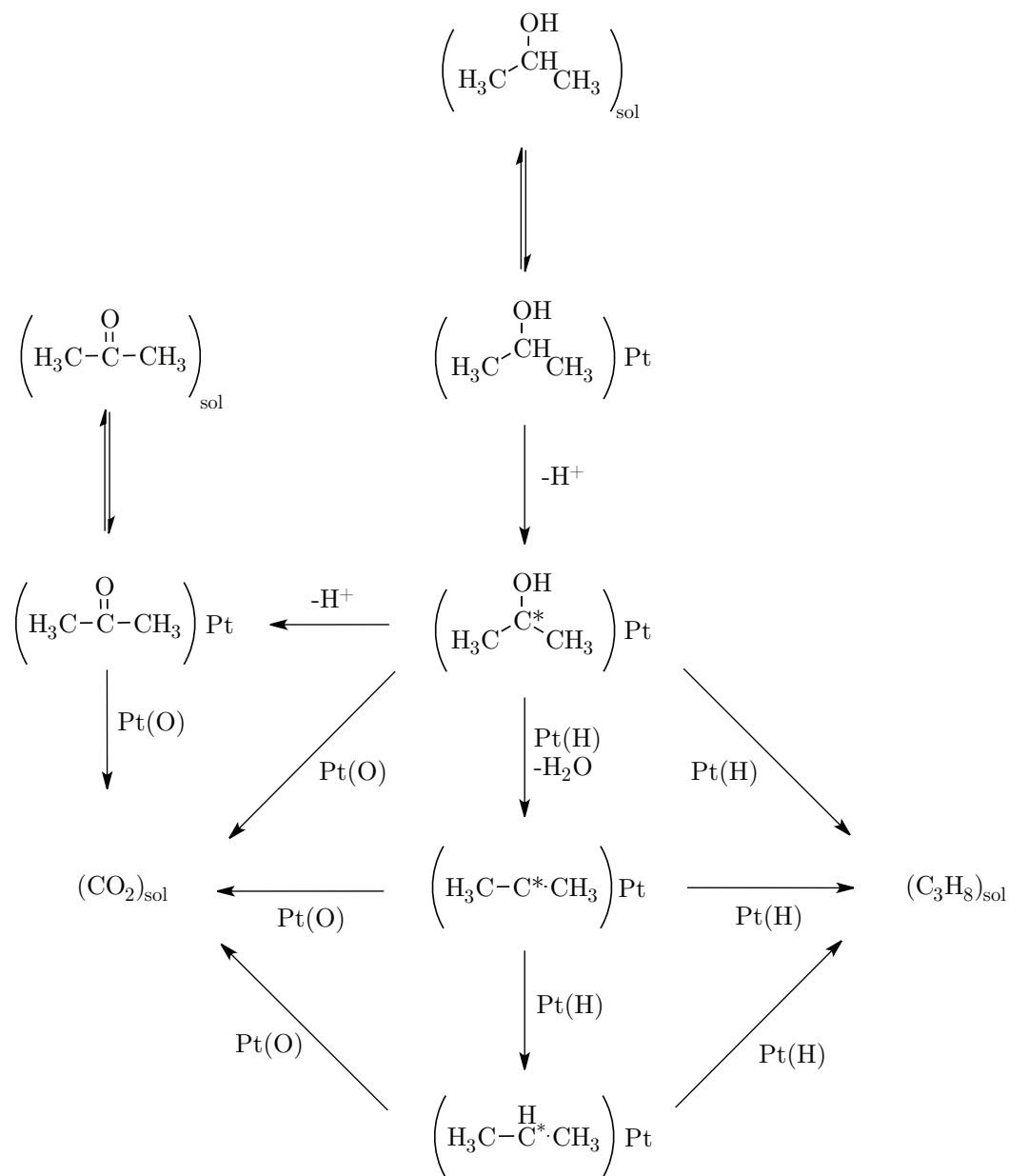
As discussed in Chapter 4, ruthenium enhances the rate of the oxidation of methanol through several effects; the bifunctional effect, an ensemble effect, and an electronic effect. Of these three, the bifunctional and ensemble effects arise from the presence of ruthenium on the surface, while the electronic effect can also arise from ruthenium that is in the bulk of the catalyst particle. Bulk alloys of platinum and ruthenium enhance the oxidation of 2-propanol (see Chapter 4), however, it is not well understood how this enhancement occurs nor is the rate determining process known.

The activity of submonolayers of ruthenium adsorbed on platinum has been intensely investigated by the Wieckowski group^[1-12] for use as a catalyst in the oxidation of methanol. The activity of these surfaces depends on the composition of the surface, and is largely enhanced through the bifunctional effect at low coverages of ruthenium. At high coverages of ruthenium, the reaction is inhibited due to the low activity of ruthenium towards the

dissociative adsorption of methanol. At low coverages of methanol the rate-determining oxidation of the carbon monoxide intermediate is enhanced by higher availability of adsorbed oxygen species. Similar fuel-cell grade catalysts have been studied by the Bergens group,^[13-17] using a novel method of preparation. Specifically, the addition of a ruthenium precursor, such as RuCl_3 , $\text{Ru}(1\text{-}5\text{-cyclooctadiene})(\eta^3\text{-C}_3\text{H}_5)_2$, or $\text{Ru}_4(\mu\text{-H})_4(\text{CO})_{12}$, to a platinum surface that has previously been treated with hydrogen to form a Pt-H_{UPD} monolayer, spontaneously deposits a controlled amount of ruthenium onto the platinum surface. These depositions are self-limiting, either by the availability of Pt-H_{UPD} or by poisoning from carbon monoxide.

The known mechanistic data for the oxidation of 2-propanol in acid has been extensively discussed in Chapter 1. The most consistent mechanism for the oxidation of 2-propanol was proposed by Pastor et al.,^[18] and is reproduced in Scheme 5.1 for convenience. In this mechanism, 2-propanol is oxidized to give either acetone or carbon dioxide. The major product is acetone at all potentials, but carbon dioxide forms at high potentials and when surface bound oxygen species are formed on the catalyst. As discussed in Chapter 2, a similar mechanism is believed to occur in alkaline electrolytes.

Platinum-ruthenium black is more active than platinum black towards the oxidation of 2-propanol at low potentials (see Chapter 4). The mechanism of this enhancement, however, is not known. One possibility is the bifunctional mechanism where the oxophilic ruthenium acts as a surface oxygen source for the oxidation of strongly bound intermediates to carbon dioxide, removing the strongly bound intermediate and providing more active sites for the oxidation of the fuel. The potential range which was studied for the oxidation of 2-propanol, however, appears to be inconsistent with the removal of such strongly



Scheme 5.1: Generally accepted mechanism for the oxidation of 2-propanol over platinum catalysts.

bound species, such as carbon monoxide, via the bifunctional mechanism (i.e., the sampled current voltammograms shown in Figure 4.5 (p. 129) peak at potentials that are significantly lower than potentials where carbon monoxide is oxidized from the surface (Figure 4.1, p. 121).

This chapter will focus on a detailed kinetic study of the oxidation of 2-propanol, using catalysts with well defined surface ratios of platinum and ruthenium. These catalysts were thoroughly characterized using X-ray Photoelectron Spectroscopy (XPS) to determine the chemical nature of the deposited ruthenium, Ultraviolet Photoelectron Spectroscopy (UPS) in order to determine if the electronic structures of the catalysts are different, and stripping of underpotentially deposited copper (Cu_{UPD}) to determine the surface composition. A novel three-dimensional analysis of the electrochemical data is presented, simultaneously extracting key thermodynamic and kinetic parameters such as the enthalpy of activation (ΔH^\ddagger), the transfer coefficient (α), and the apparent potential independent rate constant (k_{apparent}^0) from a multidimensional regression. Using these parameters, the rate determining step for the oxidation of 2-propanol will be proposed; a key mechanistic detail that has so far remained elusive regarding the mechanism of 2-propanol. Further, a transition state for the catalytic enhancement by ruthenium will be proposed, which provides evidence of a new mode by which the bifunctional mechanism enhances the oxidation of an alcohol.

5.2 Experimental

5.2.1 General

Nitrogen (Praxair, prepurified), KOH (Caledon, reagent grade), CuSO_4 (Caledon, reagent grade), H_2O_2 (EM Science, ACS Grade), RuCl_3 hydrate (Aithaca Chemical Corp.), and NafionTMsolution (ElectroChem inc., 5 wt% balanced with water) were used as-received from the supplier. Water from an in-house distilled water line was distilled once, then distilled again from alkaline KMnO_4 (Fisher Scientific) before use. 2-propanol (Fisher Scientific, suitable for electronic use) was freshly distilled before experiments.

The electrochemical cell is similar to that described in §2.2.1, with the exception of the working electrode (vide infra). Linear Sweep Voltammogram (LSV) and Electrochemical Impedance Spectroscopy (EIS) were performed using a Solartron SI 1287 electrochemical interface equipped with a Solartron SI 1260 impedance/gain-phase analyzer, controlled by the Corrware and Z-plot software packages. All potentials are reported on the Reference Hydrogen Electrode (RHE) scale, unless stated otherwise.

5.2.2 Preparation of platinum-ruthenium adatom catalysts

Platinum-ruthenium adatom catalysts were prepared by a spontaneous deposition method involving the oxidation of a M–H monolayer upon exposure to aqueous RuCl_3 , as reported by Cao and Bergens.^[14] Briefly, platinum black (Johnson Matthey, HiSPECTM-1000) was first cleaned with 3 vol% H_2O_2 and maintained in the remaining water. A typical ratio of platinum black to dilute peroxide was 0.0500 g catalyst to 10.0 cm^{-3} peroxide. The reactor was then

purged with nitrogen for 20 min, and then with nitrogen diluted hydrogen for 20 min, and then with pure hydrogen for 20 min to fully reduce the catalyst surface and form a M–H monolayer. Excess hydrogen was flushed from the reactor by purging with nitrogen for ca. 5 min, and then 5.0 cm⁻³ of freshly made 0.05 mol dm⁻³ RuCl₃ aqueous solution was cannula transferred into the reactor and maintained under a nitrogen atmosphere at bubbler pressure for 1 h. The catalyst was isolated by centrifuge, rinsed several times with water, and then dried in a vacuum desiccator. The procedure was then repeated to obtain catalysts with progressively higher loadings of ruthenium.

5.2.3 Working electrode preparation, conditioning, and characterization

The working electrode was a 0.125 cm² glassy carbon Rotating Ring Disk Electrode (RRDE) (Pine research instrumentation), with a NafionTM bound catalyst film (ca. 1 mg catalyst). The electrode was fabricated by first suspending the catalyst by ultrasound (1 h) in the appropriate amount of undiluted NafionTM solution to give a dry film that was 70 wt% catalyst. 10 μL of the suspension was then placed on the glassy carbon disk using a micropipette, and the film was dried in air. The catalyst loading was determined by mass difference, and the composition of the ink. The film was then annealed in an oven at 100 °C for 20 min, cooled in air, and assembled into the RRDE setup.

5.2.3.1 Platinum-ruthenium surface composition: Cu_{UPD} stripping

The ratio of ruthenium and platinum on the surface of the catalyst was determined by Cu_{UPD} stripping, as reported by Green and Kucernak.^[19] Briefly, the catalyst film prepared above was first conditioned in 0.1 dm³ of 0.5 mol dm⁻³

H₂SO₄ by potential cycling between -0.025 and 0.5 V at 5 mV s^{-1} at room temperature, until a stable response was observed. The baseline response (0.025 – 0.83 V) was then recorded at 2 mV s^{-1} . CuSO₄ · 5 H₂O solid was then added to give a concentration of $1 \times 10^{-3} \text{ mol dm}^{-3}$. Cu_{UPD} was deposited at 0.35 V for 30 min and with Rotating Disk Electrode (RDE) rotation ($\nu = 50 \text{ s}^{-1}$). Cu_{UPD} then stripped from the electrode by sweeping the potential from the deposition potential to 0.83 V at 2 mV s^{-1} . The signals from Ru–Cu_{UPD} stripping, and from Pt–Cu_{UPD} stripping, were determined assuming a symmetric voltammetric peak for the stripping of Ru–Cu_{UPD}. The Pt–Cu_{UPD} signal was obtained from subtracting the Ru–Cu_{UPD} from the total M–Cu_{UPD} voltammogram. An example of this analysis can be found in Figure 5.4 on p. 156. The composition of the surface was then determined by

$$\theta_{\text{Ru}} = \frac{Q_{\text{Ru-Cu}_{\text{UPD}}}}{Q_{\text{Ru-Cu}_{\text{UPD}}} + Q_{\text{Pt-Cu}_{\text{UPD}}}} \quad (5.1)$$

The real surface area of the catalyst was calculated assuming a fractional coverage of 1,^[19] and an atomic packing density of $1.51 \times 10^{15} \text{ atoms cm}^{-2}$,^[20] i.e.,

$$A_{\text{real}} = \frac{Q_{\text{Ru-Cu}_{\text{UPD}}} + Q_{\text{Pt-Cu}_{\text{UPD}}}}{420 \times 10^{-6} \text{ C cm}^{-2}} \quad (5.2)$$

5.2.3.2 X-ray Photoelectron Spectroscopy and Ultraviolet Photoelectron Spectroscopy

XPS and UPS spectra were collected by the staff members of the Alberta Centre for Surface Engineering and Science using a Axis 165 X-ray Photoelectron Spectrometer by Kratos Analytical. In the case of the XPS spectra, the excitation source was a monochromatic aluminum x-ray source (1486.69 eV); the source for the UPS measurements was the helium I line (21.21 eV) generated

from a helium lamp.

The samples were prepared by first mounting the powders on carbon tape, and reducing the surface under hydrogen. Specifically, the mounted samples were placed in a glass bomb and the system was degassed with nitrogen for 20 mins. The bomb was then purged with Hydrogen gas at room temperature, followed by pressurizing the system to 1 atm gauge pressure. The apparatus was isolated from the supply lines by use of a needle valve, and then heated to 60 °C in a water bath using a IKA RCT basic hotplate / magnetic-stirrer. The catalyst was reduced over the course of one hour, and then removed from the water bath and cooled to room temperature. Once cooled, the pressure of the bomb was reduced to ca. 1 psi gauge pressure, and the apparatus was stored in a glove box prior to collecting the XPS and UPS spectra. The sample stage was transported to the Alberta Centre for Surface Engineering and Science using a sample holder that is sealed with o-rings, and designed to deliver the samples into the instrument. Unfortunately, the port that the sample holder was designed to mate with is several substations away from the location of the XPS and UPS spectrometer; and the samples could not be successfully transferred throughout the entire apparatus. Instead, the samples were briefly exposed to air and loaded into the spectrometer using the standard port for XPS and UPS measurements.

High resolution XPS spectra were collected for platinum 4f (BE = 292–276 eV) and ruthenium 3d (BE = 84–66 eV), and UPS spectra of the valence band was collected between binding energies of –2 and 15 eV. The XPS spectra were fitted using a similar procedure as Kim et al.,^[21] who also studied the XPS spectra of platinum with submonolayers of ruthenium. Briefly, gaussian-lorentzian functions with asymmetric tailing were used, and the binding energies

were calibrated to the Pt $4f_{7/2}$ signal at 71.2 eV. The area ratios of the ruthenium $3d_{5/2}$ and $3d_{3/2}$ signals was set to 3:2, and the ratio of the of the platinum $4f_{7/2}$ and $4f_{5/2}$ was set to 4:3. Ruthenium signal assignments are consistent with those reported by Kim et al.^[21] for Ru^0 , RuO_2 , and RuO_3 at 280.3, 280.9, and 282.8 eV, respectively. An additional signal at 281.8 eV is consistent with the value reported for RuCl_3 by Folkesso;^[22] I cautiously assign this signal to RuCl_3 , as it seems unlikely that any residual RuCl_3 should remain after reduction with hydrogen (vide infra).

5.2.3.3 Variable temperature oxidation of 2-propanol

At a rotation rate of 50 s^{-1} , the catalyst film was first conditioned in 0.1 dm^3 of 1 mol dm^{-3} KOH by potential cycling between -0.25 and 0.5 V at 5 mV s^{-1} and at room temperature, until a stable response was observed. 0.77 cm^3 of freshly distilled 2-propanol was then added to the KOH electrolyte to give a 0.1 mol dm^{-3} 2-propanol solution in 1 mol dm^{-3} KOH electrolyte. The electrode was conditioned at -0.05 V for 60 s, and then left at Open Circuit Voltage (OCV) for 60 s to allow the electrode-electrolyte interface to equilibrate back to the bulk solution conditions. The potential was then scanned from the OCV to 0.0 V , followed by collecting a LSV between 0 and 0.5 V . The electrode was conditioned as before, and the LSV was collected again; this process was repeated until a total of four conditioning-LSV cycles were completed.

The resistance of the solution between the working electrode and the reference electrode was determined by EIS at a DC voltage of 0.05 V with a superimposed AC waveform (0.01 V amplitude, variable frequency). In addition to the setup used during the LSV, a fourth electrode was setup by connecting a $6.8\text{ }\mu\text{F}$ capacitor between the platinum ring of the RRDE and the RHE

electrode. This setup is known^[23] to reduce the capacitance and resistance contributions of the reference electrode in the EIS signal, which would otherwise cause progressively higher phase shifts at higher frequencies. The frequency of the AC signal was scanned from 20 Hz, to 2×10^6 Hz at 17 points decade⁻¹, with a 10 s integration time. The real impedance intercept at high AC frequencies was determined and then used to compensate the potentials of the LSV recorded previously. A detailed discussion on the principles of EIS can be found in the booklet by Vanysek,^[23] and in the textbook by Bard and Faulkner.^[24]

The bath temperature was then stepped between 25 and 65 °C at 10 °C increments, and the system was allowed to heat and equilibrate for 40 min at open circuit. The LSV and EIS experiments were then repeated at each temperature.

5.2.4 Multidimensional regression

Under the reaction conditions and potential ranges studied for this investigation (i.e., high convective mass-transfer, and moderate overpotentials), the reaction is assumed to be irreversible, and the concentrations of 2-propanol and acetone at the electrode-electrolyte interface are assumed to be near to that of the bulk electrolyte. Under these conditions, the Butler-Volmer current-overpotential equation (1.23, p. 20) can be written as

$$j = nFk^0 C^* e^{\frac{\alpha F \eta}{RT}} \quad (5.3)$$

or, upon substituting k^0 with $Ae^{\frac{-\Delta G^\ddagger}{RT}}$,

$$j = nFAe^{\frac{-\Delta G^\ddagger}{RT}} C^* e^{\frac{\alpha F \eta}{RT}} \quad (5.4)$$

Equation 5.4 can be rewritten in terms of ΔH^\ddagger and ΔS^\ddagger by using $\Delta G^\ddagger = \Delta H^\ddagger - T\Delta S^\ddagger$, giving

$$j = nFAe^{\frac{\Delta S^\ddagger}{R}} e^{-\frac{\Delta H^\ddagger}{RT}} C^* e^{\frac{\alpha F \eta}{RT}} \quad (5.5)$$

Finally, taking the natural logarithm and accounting for the temperature dependance of η (through E^0)* gives

$$\underbrace{\ln(j)}_{z=f(x,y)} = \underbrace{\ln(nFAC^*)}_{f(0,0)} + \frac{\Delta S^\ddagger}{R} - \frac{\Delta H^\ddagger}{R} \underbrace{\frac{1}{T}}_x + \frac{\alpha F}{R} \underbrace{\frac{\eta(T)}{T}}_y \quad (5.6)$$

From equation 5.6 it can be seen that $\ln(j)$ can be represented by a planar function, $f(\frac{1}{T}, \frac{\eta(T)}{T})$. The function has the gradients $\frac{\delta z}{\delta x} = -\frac{\Delta H^\ddagger}{R}$ and $\frac{\delta z}{\delta y} = \frac{\alpha F}{R}$, and has a constant value at $f(0,0)$ of $\ln(nFAC^*) + \frac{\Delta S^\ddagger}{R}$. Further, the apparent k^0 at T can be calculated from $\frac{\delta z}{\delta x}$ and $f(0,0)$ by

$$k^0(T) = \frac{e^{\left(\frac{\delta z}{\delta x}\right) \frac{1}{T}} e^{f(0,0)}}{nFC^*} \quad (5.7)$$

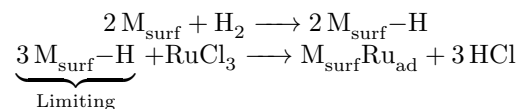
In this way, ΔH^\ddagger , α , and the apparent k^0 can be determined from a single 3-dimensional plot that simultaneously models the potential and temperature dependencies of the current density. This multidimensional analysis was coded in Python, using the regression functions in the SciPy^[26] statistics module.

* $\eta = E - E^0$. The values of E^0 range between 0.217 and 0.224 V, depending on the temperature. They are calculated using $E = -\frac{\Delta G}{nF}$, assuming the 2-propanol / acetone REDOX couple. ΔG is calculated using $\Delta G = \Delta H - T\Delta S$, and the tabulated thermodynamic constants published by the CRC.^[25] The temperature dependance of ΔH and ΔS are assumed to be negligible; that is to say that the heat capacities of the reactant and product solutions do not change appreciably.

5.3 Results and discussion

5.3.1 X-ray Photoelectron Spectroscopy

Figure 5.1 shows the high-resolution XPS spectra in the ruthenium binding energy region for a series of platinum-ruthenium adatoms catalysts, with different amounts of ruthenium on the surface. The catalysts were prepared by reduction of RuCl_3 by Pt-H_{UPD} (Scheme 5.2), using the method of Cao and Bergens.^[14] Specifically, platinum black (Johnson Matthey, HiSPECTM-1000) was cleaned in 1% hydrogen peroxide in water until all of the peroxide was consumed, and then maintained in the remaining water. The platinum black was then reduced by hydrogen, and the excess hydrogen was flushed from the reactor by purging with nitrogen. Freshly made 0.05 mol dm^{-3} RuCl_3 aqueous solution was then added to the catalyst and oxidized H_{UPD} , reductively depositing ruthenium on the surface. The reaction is designed to be self-limiting by the amount of H_{UPD} on the surface. The catalysts was rinsed several times with water to remove residual RuCl_3 , and isolated by centrifuge. The deposition procedure was repeated iteratively to produce catalysts with higher loadings of ruthenium.



Scheme 5.2: Reaction scheme for the preparation of platinum-ruthenium adatom catalysts. The scheme was repeated iteratively to prepare platinum-ruthenium adatom catalysts with varying concentrations of ruthenium on the surface.

Prior to collecting the XPS spectra, the platinum and platinum-ruthenium adatom catalysts were first reduced under hydrogen at 60°C and 1 atm gauge pressure. The catalysts were stored under nitrogen, and exposed to air while loading into the spectrometer. The spectra were fit similarly to the procedure of

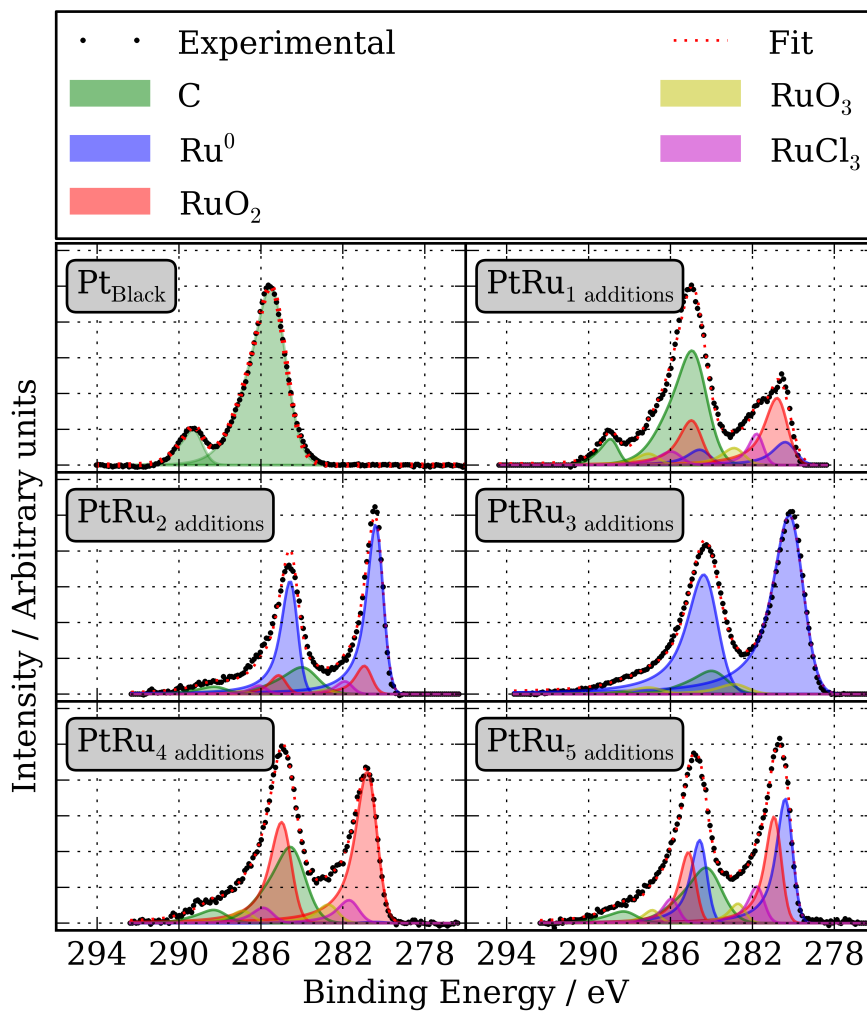


Figure 5.1: Ruthenium x-ray photoelectron spectra, and component fitting, for platinum and platinum-ruthenium catalysts with different amounts of ruthenium-atom on the surface. The results of this component analysis are summarized in Table 5.1.

Kim et al.,^[21] who studied the XPS spectra of ruthenium adatoms on Pt(111). Briefly, Gaussian-Lorentzian functions with asymmetric tailing were used, and the binding energies were calibrated to the Pt 4f_{7/2} signal at 71.2 eV. Table 5.1 summarizes the results of this component analysis. Upon one addition of ruthenium to platinum black, several new peaks appear in the XPS spectrum. These Ru 3d_{5/2} signals are centred at 280.4, 280.9, 281.8, and 282.9 eV, and have been assigned to Ru⁰, RuO₂, RuCl₃, and RuO₃, respectively. These are in excellent agreement with those reported by Kim et al.,^[21] who determined binding energies of 280.3, 280.9, and 282.8 eV for Ru⁰, RuO₂, and RuO₃ respectively. Although the peak at 281.8 is in excellent agreement with the value reported by Folkesso^[22] for RuCl₃, it seems unlikely that residual RuCl₃ would remain on the catalysts surface after reduction with hydrogen. This peak may instead be another ruthenium-oxide species, which is not presented in the XPS database provided by National Institute of Standards and Technology (NIST);^[27] indeed, this signal is absent in the catalysts which appear to be nearly completely reduced (PtRu₃ additions). Successive depositions of ruthenium to the catalysts (Scheme 5.2) results in a gradual increase in the intensities of the ruthenium components. The predominant ruthenium species is either Ru⁰ or RuO₂, depending on the catalysts. It is likely that the differences in the predominant species between catalysts results from differences in the time that the catalyst was exposed to air prior to loading into the spectrometer.

Figure 5.2 shows the platinum high-resolution XPS spectrum from the same catalysts studied in Figure 5.1. The spectra were fitted similar to that of ruthenium, with the exception that one enveloping function was used to account for surface oxidation. The results of this component analysis are summarized in Table 5.2. All signals were scaled to the Pt 4f_{7/2} signal at

Table 5.1: Summary of the ruthenium x-ray photoelectron spectra component fittings with different amounts of ruthenium-adatom on the surface.

Catalyst	C		Ru ⁰		RuO ₂		RuO ₃		RuCl ₃	
	BE (eV)	% _{comp} (%)	BE (eV)	% _{comp} (%)	BE (eV)	% _{comp} (%)	BE (eV)	% _{comp} (%)	BE (eV)	% _{comp} (%)
Pt _{Black}	285.5, 292.7	25.2								
PtRu(1 addition)	285.0, 288.0	16.1	280.4, 284.6	3.3	280.8, 285.0	3.3	282.9, 287.1	2.4	281.8, 286.0	3.0
PtRu(2 addition)	284.0, 288.3	5.1	280.4, 284.6	20.7	280.9, 285.1	3.4	282.8, 287.0	0.5	281.9, 286.1	1.5
PtRu(3 addition)	284.0, 288.3	2.8	280.2, 284.4	29.9	—	—	282.9, 287.1	1.6	—	—
PtRu(4 addition)	284.6, 288.3	13.3	280.4, 284.6	0.2	280.8, 285.0	24.6	282.9, 286.9	3.7	281.7, 285.9	3.7
PtRu(5 addition)	284.3, 288.3	6.1	280.4, 284.6	8.8	280.9, 285.1	8.1	282.7, 286.9	1.3	281.8, 288.3	6.1

71.2, an additional signal at 72.6 eV appeared in most of the samples, and was assigned to Pt(OH)₂. This assignment agrees well with the value of 72.4 eV reported by Hammond and Winograd.^[28] The dominant species is Pt⁰, which is indicative of surface oxidation rather than oxidation of the bulk material upon exposure to air. Differences in the amounts of Pt(OH)₂ closely resemble the differences in ruthenium oxidation discussed previously, and likely also results from differences in the time that the catalyst was exposed to air prior to loading in the spectrometer. The catalyst surface can therefore be viewed as metallic platinum and ruthenium, with varying degrees of surface oxidation. The catalysts may have some residual RuCl₃ adsorbed on the surface; however, as discussed above, it seems unlikely that RuCl₃ was not reduced under hydrogen.

Table 5.2: Summary of the platinum x-ray photoelectron spectra component fittings with different amounts of ruthenium-atom on the surface.

Catalyst	Pt		Pt(OH) ₂	
	BE (eV)	% _{comp} (%)	BE (eV)	% _{comp} (%)
Pt _{Black}	71.2, 74.5	74.4	72.6, 75.9	0.4
PtRu ₁ addition	71.2, 74.5	61.6	72.5, 75.8	3.9
PtRu ₂ additions	71.2, 74.5	64.8	72.6, 76.8	2.9
PtRu ₃ additions	71.2, 74.5	65.0	72.6, 76.9	0.4
PtRu ₄ additions	71.2, 74.5	51.3	72.6, 76.9	3.8
PtRu ₅ additions	71.2, 74.5	25.3	72.6, 76.9	1.9

5.3.2 Ultraviolet Photoelectron Spectroscopy

UPS was carried out on the catalysts to investigate how the addition of ruthenium adatoms may change the electronic structure of the catalyst's valence band. Figure 5.3 shows the UPS spectra of the platinum and platinum-ruthenium adatom catalysts with different amounts of ruthenium on the surface.

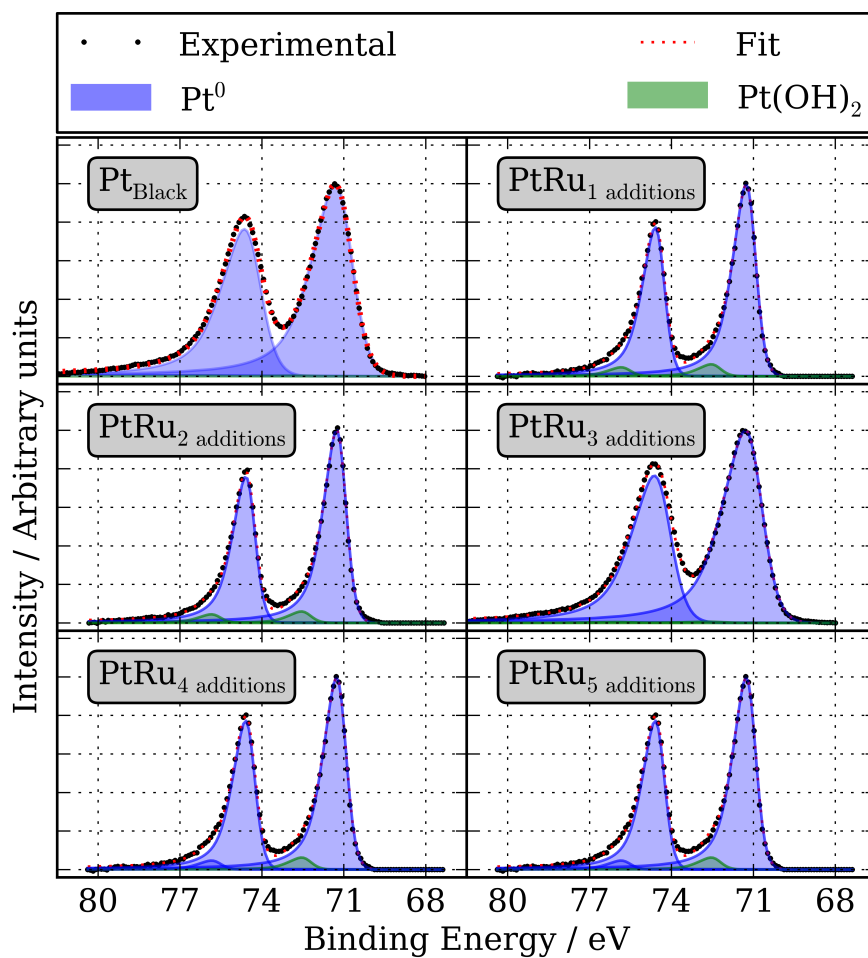


Figure 5.2: Platinum x-ray photoelectron spectra, and component fitting, for platinum and platinum-ruthenium catalysts with different amounts of ruthenium-atom on the surface. The results of this component analysis are summarized in Table 5.2.

To avoid changing the surface composition of the catalysts, the samples have not undergone argon sputtering. As shown by the XPS spectra, these catalysts have varying degrees of surface oxidation. As a result, changes in the band structure at binding energies that are more positive than 10 eV are likely due to differences in the extent of surface oxidation, or possibly from carbon adsorbents that have been deposited from the atmosphere or within the spectrometer. These features should therefore not be regarded as indicators of changes in the density-of-states of the reduced material.

As mentioned above, the XPS spectra of Pt_{Black} and PtRu_{3 additions} appear to be *nearly* completely reduced. Comparing the UPS spectra of these two catalysts, a clear change in the density of states near the Fermi edge (BE $\simeq 0$ eV) is observed. The d-band centres of PtRu_{3 additions} is shifted to higher binding energies by 0.3 eV relative to platinum. According to Hammer and Nørskov,^[29] the activity of a catalytic surface is directly related to the d-band centre of a material. These changes in reactivity result from a direct correlation between the energy of the d-band centre, and the energies of adsorption. Such trends have been used to explain the high activity of Pt₃M (M = Ni, Fe, Co) materials towards the reduction of oxygen.^[30-34] The fact that the d-band centre of PtRu_(3 additions) is different from Pt_{Black} suggests that an electronic effect may contribute to changes in the catalytic activity of of platinum-ruthenium adatom catalysts. Indeed, such proposals have already been made for platinum-ruthenium catalysts.^[4,5,35-37]

In order to provide more conclusive evidence for the electronic effect during the oxidation of 2-propanol over platinum-ruthenium electrocatalysts, however, more study of the electronic structure of the oxide-free catalysts are required.

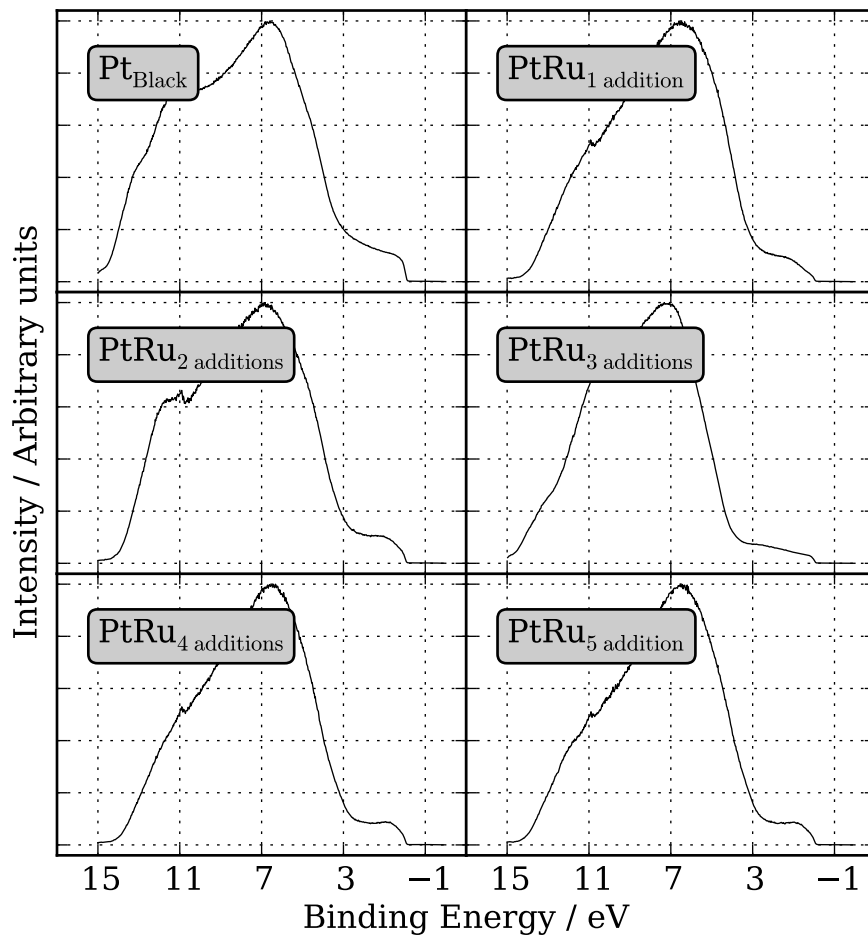


Figure 5.3: Ultraviolet photoelectron spectra of platinum and platinum-ruthenium catalysts, with different amounts of ruthenium-adatom on the surface.

5.3.3 Surface Composition

To get quantitative information of the fractional composition of the surface, Cu_{UPD} stripping was performed. Briefly, copper was underpotentially deposited from $1 \times 10^{-3} \text{ mol dm}^{-3} \text{ CuSO}_4$ in $0.5 \text{ mol dm}^{-3} \text{ H}_2\text{SO}_4$ at 0.35 V for 30 min . The Cu_{UPD} monolayer was then stripped from the surface by sweeping the potential of the electrode in the anodic direction. The voltametric wave was de-convoluted into $\text{Pt}-\text{Cu}_{\text{UPD}}$ and $\text{Ru}-\text{Cu}_{\text{UPD}}$ components by assuming a symmetric wave for $\text{Ru}-\text{Cu}_{\text{UPD}}$. Figure 5.4 shows the Cu_{UPD} stripping voltammograms for the platinum and platinum-ruthenium catalysts, and also shows the components of the wave resulting from stripping of $\text{Ru}-\text{Cu}_{\text{UPD}}$ and from $\text{Pt}-\text{Cu}_{\text{UPD}}$.

The fractional composition of the surface was calculated using 5.1, and the mass specific surface area of the catalysts was calculated using the total surface area determined from 5.2, and the mass of the catalyst deposit. Table 5.3 summarizes the results of these computations. Addition of ruthenium adatoms does not significantly change the mass specific surface area of the catalysts. For platinum black, the $\%_{\text{utilization}}$ calculated from the manufacturers specified mass-specific surface area ($27.0 \text{ m}^2 \text{ g}^{-1}$) is ca. 65%. The deviation from the manufacturers specified value likely results from the high NafionTM content of the catalyst layer (30% in this study). Although a lower loading of NafionTM will likely increase the $\%_{\text{utilization}}$, catalyst layers with 30% NafionTM were found to be more robust under the conditions used during the variable temperature oxidations of 2-propanol (vide infra). The improved robustness of the catalyst films deposited on a glassy carbon disks at high convection rates ($\omega = 50 \text{ s}^{-1}$) and at temperatures between 25 and 65°C was the deciding factor for the choice of this composition.

Figure 5.5 shows a plot of the mass-specific area of platinum versus the

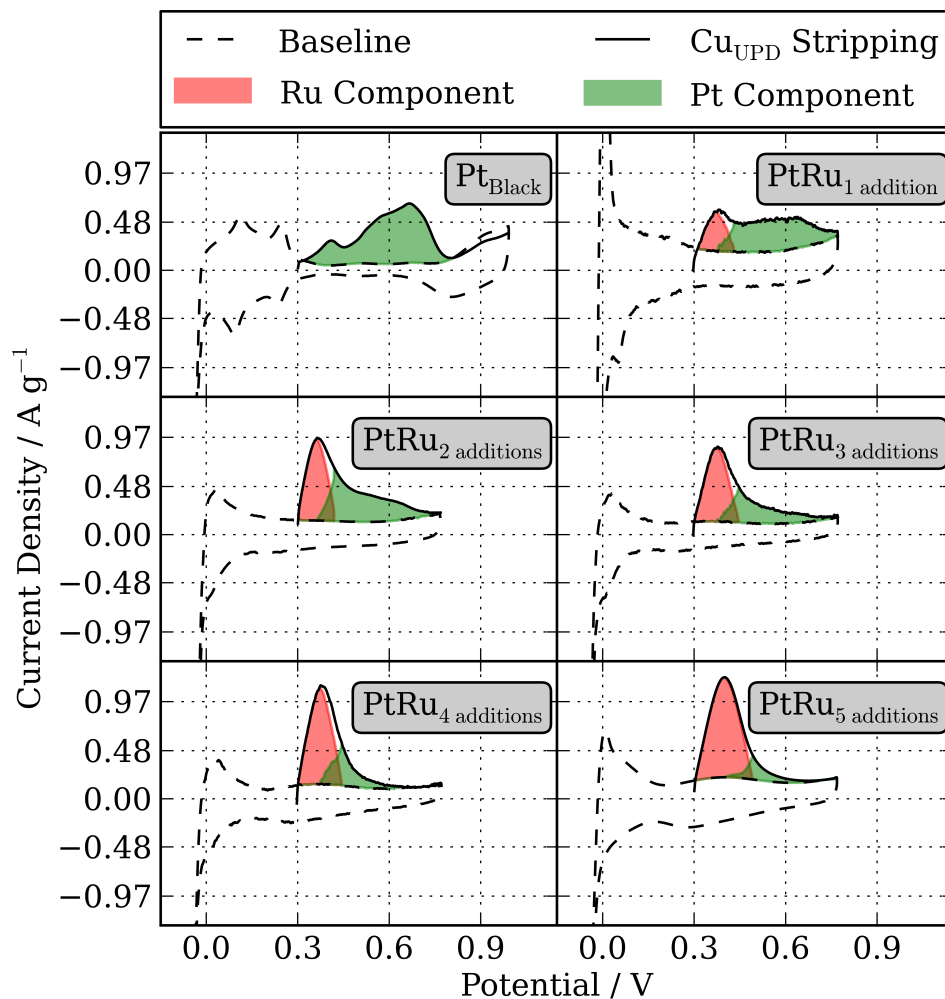


Figure 5.4: Stripping voltammetry of a underpotentially-deposited copper monolayer on platinum and platinum-ruthenium catalysts, with different amounts of ruthenium-atom on the surface. The components of the voltammogram due to stripping from ruthenium, and from platinum, have been deconvoluted assuming a symmetric wave for the stripping of Cu_{UPD} from ruthenium. $\nu = 2 \text{ mV s}^{-1}$

Table 5.3: Summary of the platinum and platinum-ruthenium Cu_{UPD} stripping component analysis.

Catalyst	Area			Θ_{Ru}
	Total ($\text{m}^2 \text{g}^{-1}$)	Pt ($\text{m}^2 \text{g}^{-1}$)	Ru ($\text{m}^2 \text{g}^{-1}$)	
Pt _{Black}	17.6	17.6	0.0	0.0
PtRu ₁ addition	16.9	13.0	4.0	0.23
PtRu ₂ addition	17.0	9.8	7.2	0.43
PtRu ₃ addition	15.8	6.9	8.9	0.56
PtRu ₄ addition	16.7	5.0	11.6	0.7
PtRu ₅ addition	15.6	2.3	13.3	0.85

mass-specific area of ruthenium for the adatom catalysts used in this study. The active area of platinum and ruthenium are linearly correlated, and the slope of the line is -1.13 . A slope of negative unity would imply that for every cm^2 of platinum surface area lost, one cm^2 of ruthenium surface area is gained. The fact the experimental slope is close to negative unity demonstrates that the platinum-ruthenium adatom catalysts have two-dimensional ruthenium deposits; i.e., the ruthenium is nearly exclusively on platinum atoms, and not on the previously deposited ruthenium atoms (three-dimensional growth). It is impossible to ascertain if this two-dimensional growth mechanism occurs during the deposition, or if the ruthenium atoms migrate either during the deposition, storage, or annealing of the catalyst film.

5.3.4 Variable temperature oxidations of 2-propanol

The rate of the oxidation of 2-propanol was studied by LSV between 0.0 and 0.5 V ($\nu = 5 \text{ mV s}^{-1}$) as a function of temperature and ruthenium surface coverage, using a RDE at high rotation rates (50 s^{-1}) and low concentrations of 2-propanol (0.1 mol dm^{-3}). The conditions of these experiments were selected to avoid the influences of surface poisoning by acetone oxidation, or by its

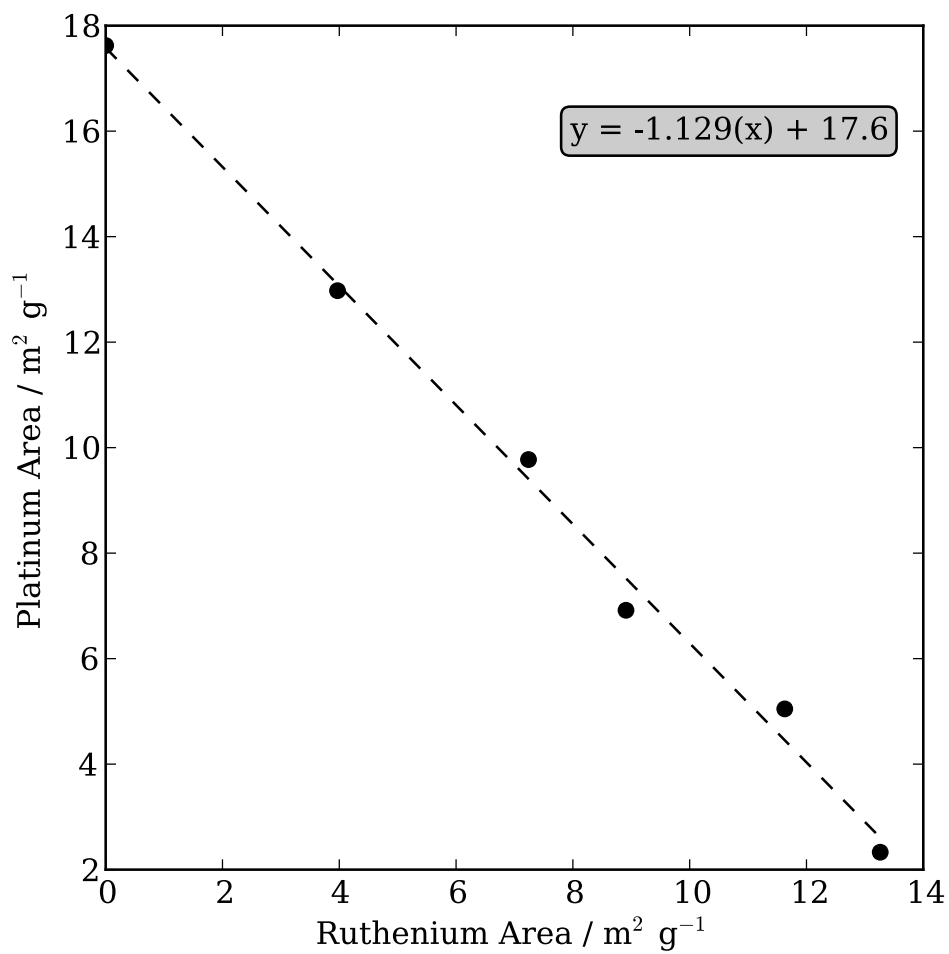


Figure 5.5: Active areas of platinum and ruthenium as determined by the stripping of underpotentially deposited copper for platinum-ruthenium adatom catalysts with varying degrees of ruthenium coverage.

adsorption. Specifically, platinum black is active towards the oxidation of acetone at potentials exceeding 0.175 V (see Chapter 4), and it inhibits the oxidation of 2-propanol. Well resolved three-dimension (potential,time) versus current plots (see Chapter 3) have shown that this inhibition is time dependent, and that there is an induction period of ca. 1 min before this inhibition becomes significant. The lower concentration of 2-propanol used in this study will result in lower concentrations of acetone produced at the electrode-electrolyte interface. Further, by keeping the timeframe of the LSV short (100 s), and by keeping the rate of mass transport high (i.e., remove acetone and supply 2-propanol) it is likely that poisoning by adsorbed acetone can be reduced, if not mitigated to a point where it will not be detected. Figure 5.6 shows the activity of the catalysts between 25 and 65 °C, under these reaction conditions. The real area of the catalyst deposit was calculated from the mass of the deposited film and the mass specific surface area determined by Cu_{UPD} stripping (see §5.3.3). This area was then used to normalize the currents to the real activity of the catalyst surface.

The activities of the platinum-ruthenium adatom catalysts are significantly different from platinum black. Specifically, the onset potential for the oxidation of 2-propanol is lowered from ca. 0.15 to 0.05 V upon a single addition of ruthenium adatoms. Subsequent additions of ruthenium further increase the activity of the catalyst at low potentials, up to a maximum of three additions. This increase in activity at low potentials is consistent with the high steady-state current densities reported for platinum-ruthenium black (see Chapter 4). Above three additions, the current density with respect to the baseline begins to decline. This effect is consistent with the existence of an optimum platinum:ruthenium surface ratio for the oxidation of 2-propanol. Such optimum

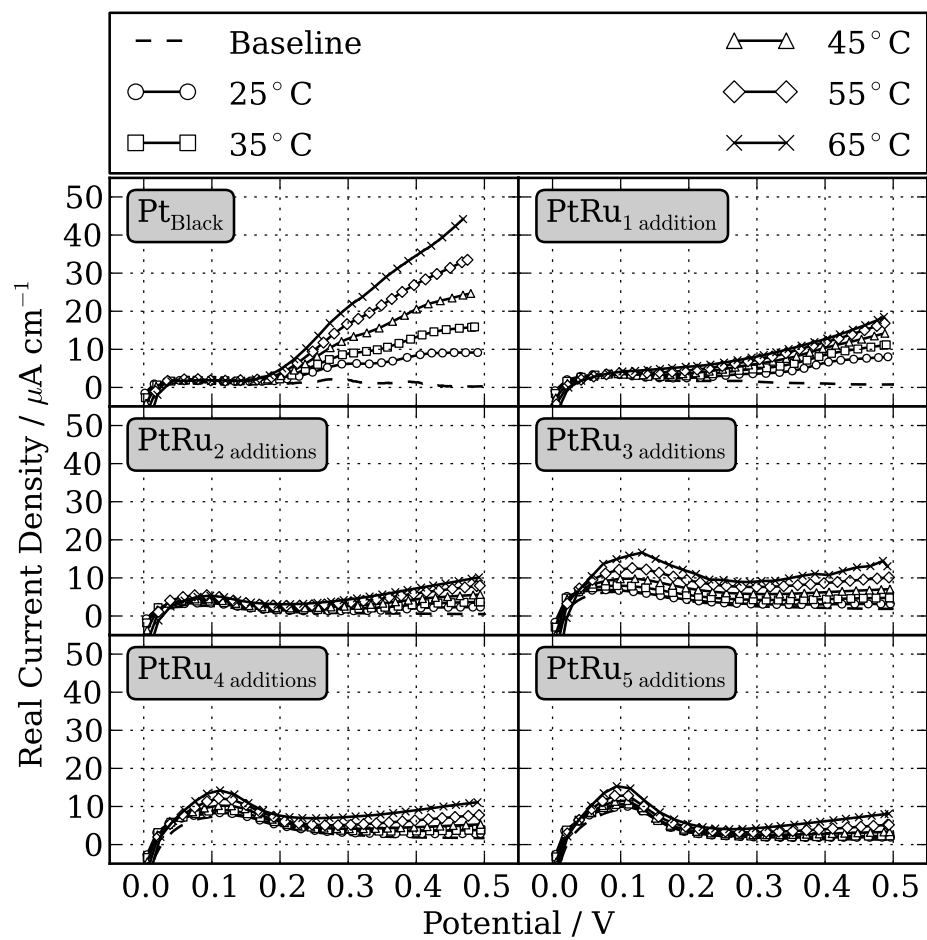


Figure 5.6: Linear sweep voltammetry of platinum and platinum-ruthenium adatom catalysts with and without 0.1 mol dm^{-3} 2-propanol in 1 mol dm^{-3} KOH as a function of temperature. $\omega = 50 \text{ s}^{-1}$, $\nu = 5 \text{ mV s}^{-1}$.

ratios are well known for the oxidation of methanol, and are dependant on the temperature of the system and the concentrations of the fuel (see §4.1.1).

Above 0.2 V, platinum is superior to platinum-ruthenium. Indeed, addition of ruthenium inhibits the reaction at potentials exceeding 0.2 V. This behaviour can be explained by the higher affinity of the surface towards the adsorption of oxygen species as the amount of ruthenium increases. Ruthenium is more oxophilic than platinum, and a fundamental feature of platinum-ruthenium catalysts is that the amount of oxygen-containing species at the surface increases as the amount of ruthenium increases. It has been proposed that the strongly bound oxygen species that are formed at high anodic potentials deactivate the catalyst towards the oxidation of alcohols at high potentials.^[38–40] The lower activity of the platinum-ruthenium adatom catalysts at high potentials and higher surface coverages is consistent with an inhibition by strongly adsorbed oxides.

As discussed above, the LSV and RDE parameters have been selected in such a way as to mitigate the formation of adsorbed acetone species that poison the catalyst surface. Further, as discussed in 5.2.4, under the conditions used in this study the reaction is assumed to be irreversible, and the concentrations of 2-propanol and acetone at the electrode-electrolyte interface are near that of the bulk electrolyte. Under these conditions, the Butler-Volmer current-overpotential equation is rewritten as

$$\underbrace{\ln(j)}_{z=f(x,y)} = \overbrace{\ln(nFAC^*)}^{f(0,0)} + \frac{\Delta S^\ddagger}{R} - \frac{\overbrace{\Delta H^\ddagger}^{\frac{\delta z}{\delta x}}}{R} \underbrace{\frac{1}{T}}_x + \frac{\overbrace{\alpha F}^{\frac{\delta z}{\delta y}}}{R} \underbrace{\frac{\eta(T)}{T}}_y \quad (5.6)$$

A plot of $(\frac{\eta(T)}{T}, \frac{1}{T})$ vs $\ln(j)$ is thereby planar with gradients of $-\frac{\Delta H^\ddagger}{R}$ and

$\frac{\alpha F}{R}$, and with the constant $f(0,0) = \ln(nFAC^*) + \frac{\Delta S^\ddagger}{R}$. The strict nature of the multidimensional regression requires careful selection of the potential region studied, as $\ln(j)$ must be linearly dependent on both of the independent variables. An advantage to the use of such a multidimensional analysis is that the concurrent fitting of both parameters increases the certainty of the gradients because the size of the dataset and the dimensionality of the model are larger than those of single dimensional regression. Further, since the data is simultaneously fit with respect to both potential and temperature, the resulting kinetic and thermodynamic values are valid over the entire potential and temperature region modelled. Treating the potential and temperature dependence separately *does not confirm* that the values obtained from the regression analysis reflect the system over the entire range of variables studied. Therefore, the multidimensional regression is more applicable in that the results *are correct over the entire range* of variables studied.

Figure 5.7 shows the results of the three-dimensional regression analysis of the data shown in Figure 5.6. Potential ranges were chosen to maximize the data set used within the regression analysis, and are therefore slightly different for each catalyst. Further, to mitigate the contributions of the reverse reaction, only potential ranges that were not significantly negative of $E^0(T)$ are considered[†]. Indeed, attempts to perform a similar regression analysis at potentials significantly below $E^0(T)$ were unsuccessful. The fact that the electrocatalytic behaviour at these lower potentials is not described by the planar function used in this study suggests that one or more of the assumptions made during its derivation is not longer valid. This potential region is also

[†]The values of E^0 range between 0.217 and 0.224 V, depending on the temperature. They are calculated assuming the 2-propanol / acetone REDOX couple, using the tabulated thermodynamic constants published by the CRC.^[25]

further complicated by surface REDOX processes such as the oxidation of H_{UPD} , and the oxidation of ruthenium to form surface oxygen species. It is also likely that at these lower potentials the 2-propanol to acetone reaction proceeds in the forward and reverse direction (see Chapters 2 and 4).

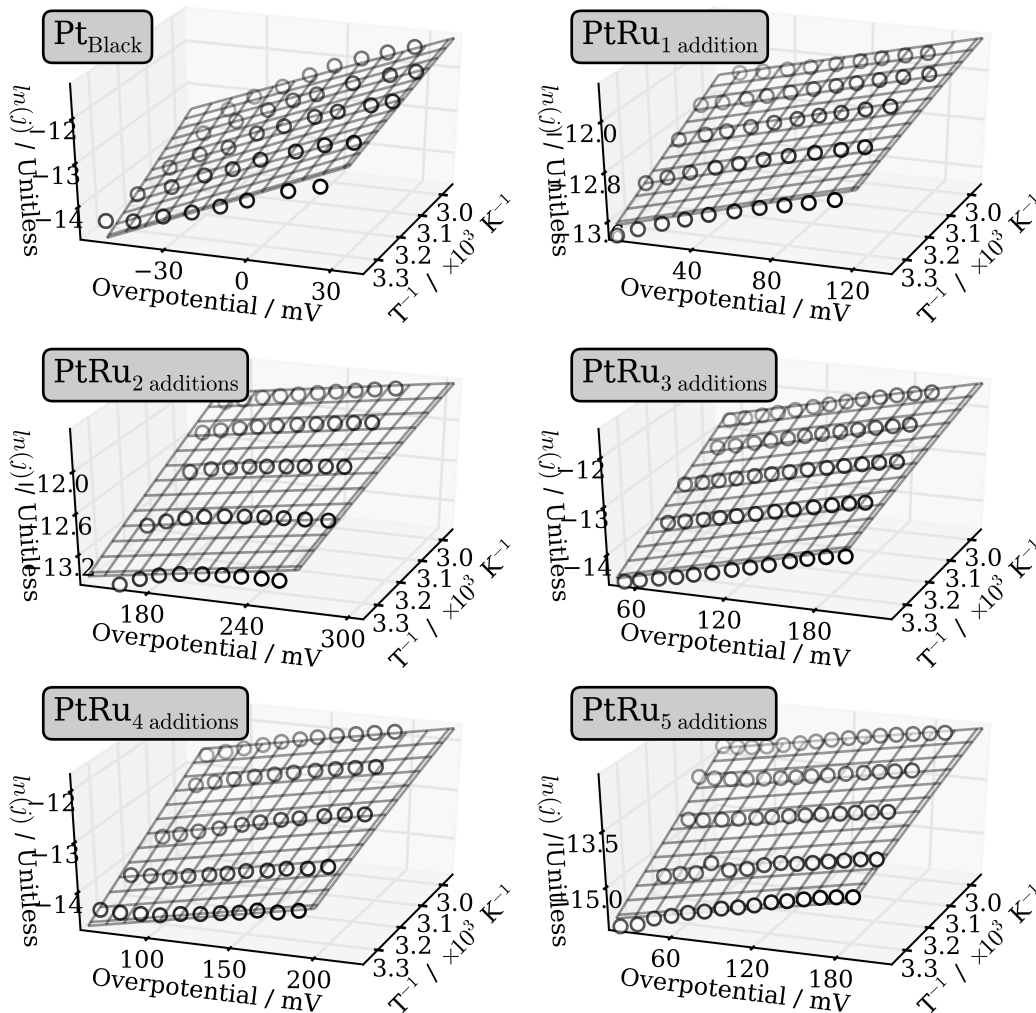


Figure 5.7: Three-dimensional regression analysis of the variable temperature linear sweep voltammetry of platinum and platinum-ruthenium adatom catalysts with and without 0.1 mol dm^{-3} 2-propanol in 1 mol dm^{-3} KOH. $\omega = 50 \text{ s}^{-1}$, $\nu = 5 \text{ mV s}^{-1}$.

Successful multidimensional regressions were achieved for all six catalysts at overpotentials near the equilibrium potential for the 2-propanol / acetone

REDOX couple. As discussed previously (§5.2.4), the apparent potential-independent rate constant (k^0), the enthalpy of activation (ΔH^\ddagger), and the transfer coefficient (α) can all be calculated from the fitting parameters using

$$\Delta H^\ddagger = -\frac{\delta z}{\delta x} \times R \quad (5.8)$$

$$\alpha = \frac{\frac{\delta z}{\delta y} \times R}{F} \quad (5.9)$$

and

$$k^0(T) = \frac{e^{\left(\frac{\delta z}{\delta x}\right) \frac{eF(0,0)}{R}}}{nFC^*} \quad (5.7)$$

Table 5.4 summarizes these parameters obtained from the three-dimensional regressions. Note that the values of $k_{apparent}^0$ are small; it is unclear at this time if these low values result from the unusually high loading of catalysts, low concentration of alcohol, or an intrinsic characteristic of the 2-propanol dehydrogenation reaction. The system may be far from saturation, and the catalysts may be under-utilized (i.e., catalysts particles further into the film are never reached by 2-propanol during voltammetry, but are accessed during the 30 min deposition of Cu_{UPD} for surface area measurements). These extreme conditions were chosen to avoid catalyst poisoning, but may have also inadvertently decreased the apparent rate constant relative to its true value.

Table 5.4: Summary of the kinetic parameters obtained from the three-dimensional regression analysis as a function of ruthenium surface composition.

Catalyst	Θ_{Ru}	α	$\sigma_\alpha \times 10^7$	ΔH^\ddagger (kJ mol ⁻¹)	$\sigma_{\Delta H^\ddagger}$ (kJ mol ⁻¹)	$k_{apparent}^0 \times 10^8$ (cm s ⁻¹)
Pt _{Black}	0.0	0.67	3	23.5	0.2	8.32
PtRu ₁ addition	0.23	0.22	3	24.8	0.2	5.94
PtRu ₂ additions	0.43	0.09	3	33.9	0.2	4.10
PtRu ₃ additions	0.56	0.09	3	38.2	0.2	1.99
PtRu ₄ additions	0.70	0.11	3	45.6	0.2	1.55
PtRu ₅ additions	0.85	0.19	3	54.4	0.2	0.567

Figure 5.8 plots the apparent rate constants tabulated in Table 5.4 versus the ruthenium surface composition of the catalysts. The magnitude of the apparent rate constant is linearly dependent on the composition of the surface. This linear dependence suggests that the total rate of the reaction is proportional to the surface area of each of its components. That is to say that

$$k_{apparent} \times A_{total} = (k_{Pt} \times A_{Pt}) + (k_{Ru} \times A_{Ru}) \quad (5.10)$$

The linear relationship between $k_{apparent}$ and Θ_{Ru} is made apparent by dividing 5.10 by A_{total} , giving

$$k_{apparent} = (k_{Pt} \times \Theta_{Pt}) + (k_{Ru} \times \Theta_{Ru}) \quad (5.11)$$

and then expressing Θ_{Pt} in terms of Θ_{Ru} . This substitution gives

$$k_{apparent} = k_{Pt} \times (1 - \Theta_{Ru}) + k_{Ru} \Theta_{Ru} \quad (5.12)$$

which upon rearranging gives the linear form

$$\boxed{k_{apparent} = k_{Pt} + \Theta_{Ru} \times (k_{Ru} - k_{Pt})} \quad (5.13)$$

From this treatment, the values of k_{Pt} and k_{Ru} are 8.1×10^{-8} ($s_{k_{Pt}} = 0.9 \times 10^{-8}$) and $-1 \times 10^{-8} \text{ cm s}^{-1}$ ($s_{k_{Ru}} = 1 \times 10^{-8}$), respectively. k_{Ru} is statistically the same as 0, suggesting that ruthenium is inactive towards the oxidation of 2-propanol at E^0 . The reason for the reduced reaction rate with increasing amounts of ruthenium is likely the dilution of the active platinum site.

Figure 5.9 plots the activation enthalpy for the oxidation of 2-propanol on platinum and platinum-ruthenium adatom catalysts as a function of the

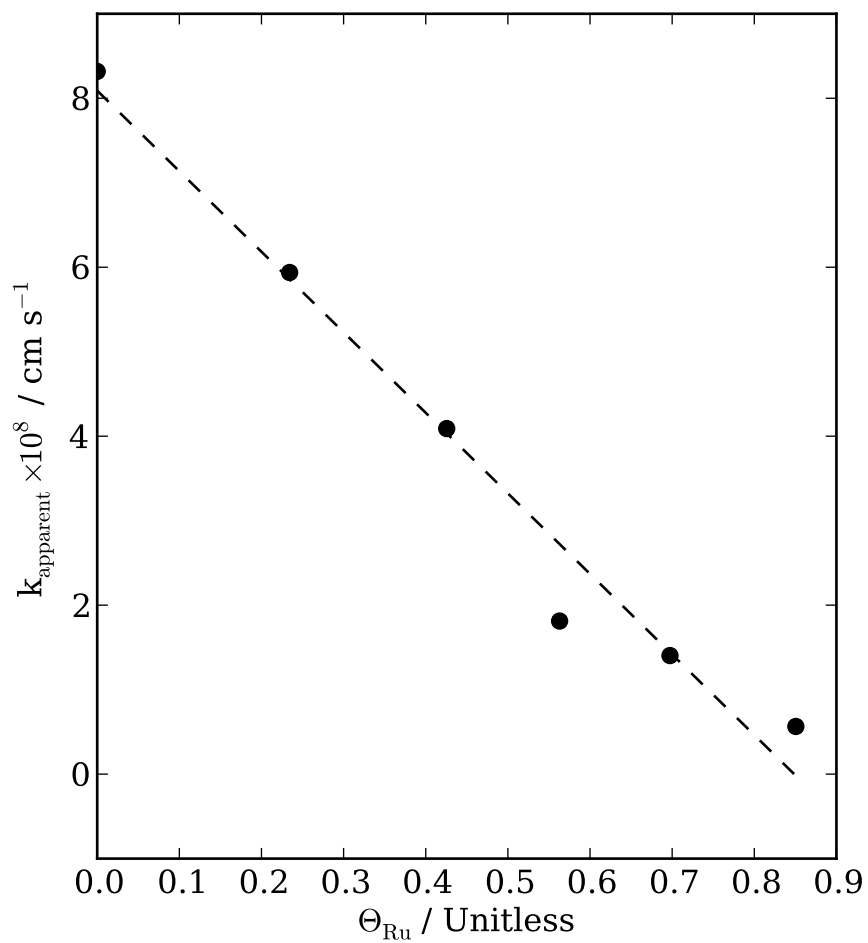


Figure 5.8: Apparent kinetic rate constant as a function of the fractional composition of the platinum-ruthenium adatom catalysts. $T = 298 \text{ K}$

ruthenium content of the surface. In the case of platinum-ruthenium adatom catalysts, the activation enthalpy is linearly dependent on the composition of the surface. The linearity implies that the reaction enthalpy can also be separated into components from platinum, and from ruthenium. Similar to the derivation of 5.13, the activation enthalpies dependence on surface composition can be describe by 5.14,

$$\Delta H_{\text{apparent}}^{\ddagger} = \Delta H_{\text{Pt}}^{\ddagger} + \Theta_{\text{Ru}} \times (\Delta H_{\text{Ru}}^{\ddagger} - \Delta H_{\text{Pt}}^{\ddagger}) \quad (5.14)$$

From this least squares fitting, $\Delta H_{\text{Pt}}^{\ddagger}$ and $\Delta H_{\text{Ru}}^{\ddagger}$ are 14 ($s_{\Delta H_{\text{Pt}}^{\ddagger}} = 2$) and 59 kJ mol⁻¹ ($s_{\Delta H_{\text{Ru}}^{\ddagger}} = 6$), respectively. Platinum black, however, does not follow the linear trend. This behaviour indicates that the activation process for the oxidation of 2-propanol over platinum-ruthenium adatom catalysts and over platinum black are different. Therefore the enthalpy of activation over platinum calculated from 5.14 should be regarded as the enthalpy of activation over *platinum in platinum-ruthenium* adatom surfaces. Interestingly, the enthalpy of activation over platinum in platinum-ruthenium adatom catalysts is lower than the enthalpy of activation over platinum in platinum black. The difference in $\Delta H_{\text{Pt}}^{\ddagger}$ is ca. 9 kJ mol⁻¹. Gale et al.^[41] studied the enthalpy of adsorption of 2-propanol on bare nickel, and oxide covered nickel. They found that on oxide covered surfaces, the enthalpy of adsorption increases by 8.4 kJ mol⁻¹ in the presence of oxides due to a hydrogen bonding interaction. The agreement between the value reported by Gale et al., and the difference in $\Delta H_{\text{Pt}}^{\ddagger}$ upon inclusion of ruthenium, suggests that the reduced enthalpy of activation may result from a hydrogen bonding interaction in the transition state that is not present on platinum black. As discussed previously, ruthenium is known to

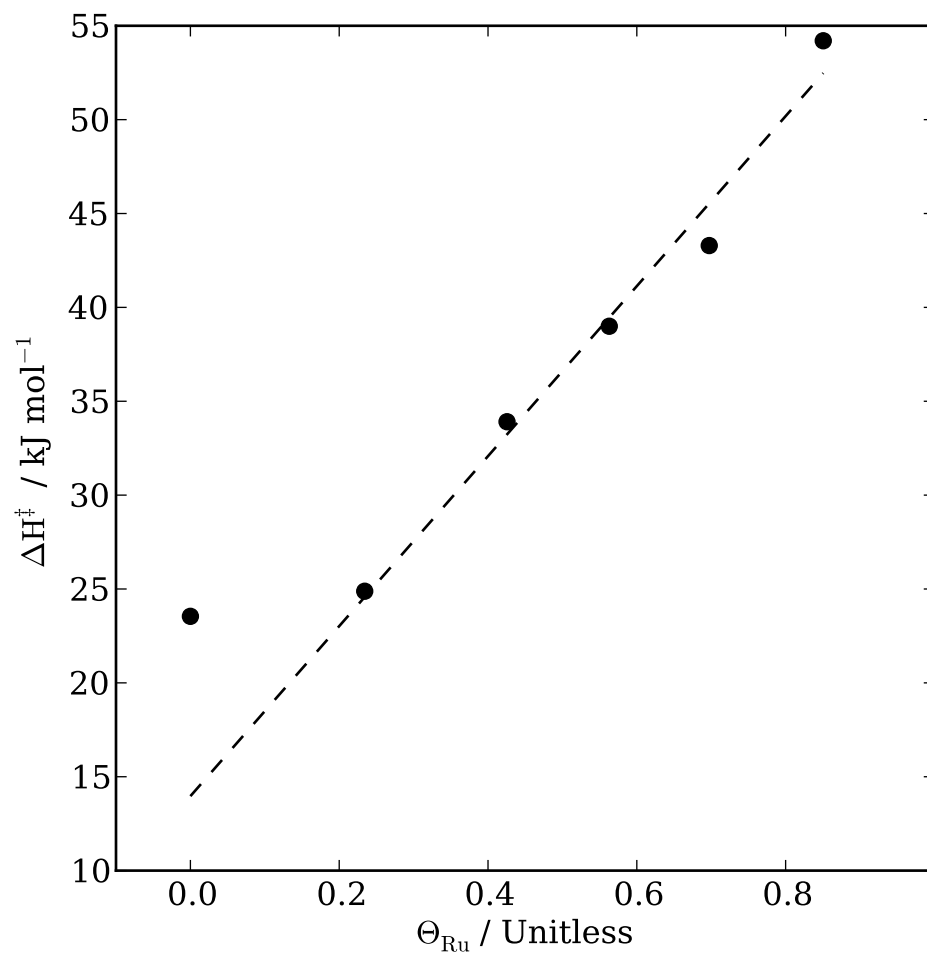
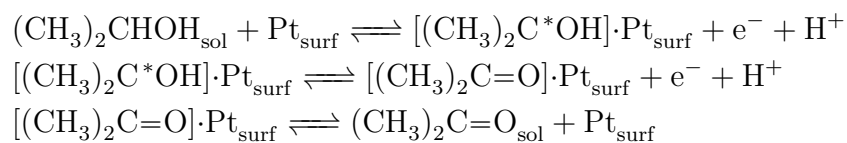


Figure 5.9: Activation enthalpy as a function of the fractional composition of the platinum-ruthenium adatom catalysts. $T = 298 \text{ K}$

form surface oxides and hydroxides at lower potentials than platinum. It seems reasonable to conclude that the reduced enthalpy of activation for the oxidation of 2-propanol over platinum in platinum-ruthenium adatom catalysts results from a hydrogen bonding interaction between an intermediate formed during the oxidation of 2-propanol, and a ruthenium oxide/hydroxide.

The enthalpy of activation calculated from 5.14 for the oxidation of 2-propanol when $\Theta_{Ru} = 1$ is 59 kJ mol^{-1} . This enthalpy of activation is consistent with rate limiting dissociative adsorption, involving the cleavage of a C–H and the formation of a Pt–H and a Pt–C bond. For example, Gasteiger et al.^[42] found that the enthalpy of activation for the destructive adsorption of methanol is 60 kJ mol^{-1} . As discussed previously, ruthenium oxides or hydroxides appear to be inactive towards the oxidation of 2-propanol. It therefore seems reasonable to conclude that at high surface coverages of ruthenium oxides or hydroxides, the reaction becomes limited by the destructive adsorption of 2-propanol.

Scheme 5.3 shows the elementary steps believed to occur during the oxidation of 2-propanol to acetone over platinum catalysts. The activation enthalpy for the oxidation of 2-propanol over platinum black is 23.5 kJ mol^{-1} , and the transfer coefficient is 0.67. The fact that the transfer coefficient is significantly different from 0 (typical values average are ca. 0.5) indicates a strong dependence of the rate determining step on potential, meaning that an electron transfer event is involved. Given that the activation enthalpy for the rate determining step over platinum black is significantly less than values indicative of rate determining destructive adsorption, it is likely that the rate determining step is the loss of the alcoholic proton from the adsorbed $(\text{CH}_3)_2\text{C}^*\text{OH}$ moiety. Upon addition of ruthenium to the surface, this step is stabilized by 9 kJ mol^{-1} , a value that is consistent with an additional hydrogen bonding interaction.

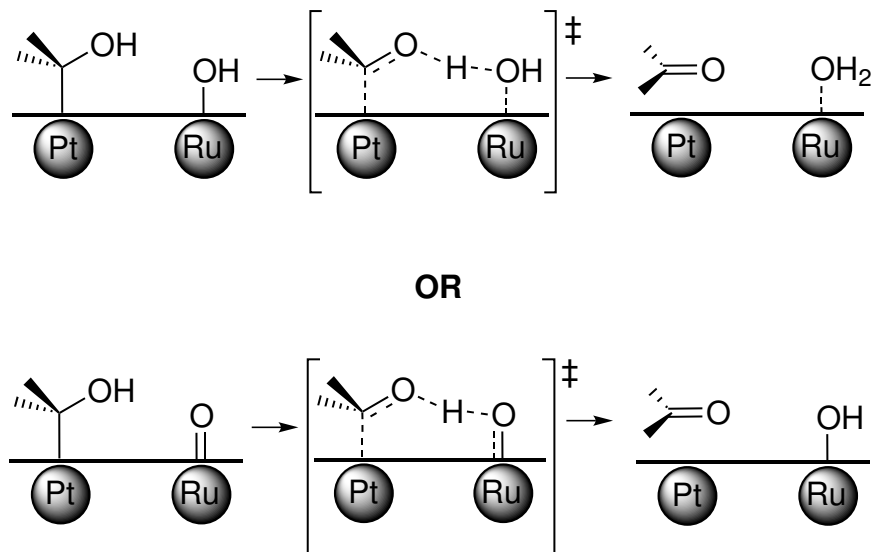


Scheme 5.3: Elementary steps for the oxidation of 2-propanol to acetone on metal electrodes.

Consistent with these results, I propose the following transition state for the oxidation of adsorbed $(\text{CH}_3)_2\text{C}^*\text{OH}$ on platinum ruthenium adatom catalysts (Scheme 5.4). In this transition state, a hydrogen bonding interaction is formed between the adsorbed $(\text{CH}_3)_2\text{C}^*\text{OH}$ intermediate and a ruthenium oxide, or hydroxide. The alcoholic proton is transferred to the ruthenium oxide or hydroxide, forming water or hydroxide that is adsorbed on ruthenium, and product acetone that can desorb from the surface. The water or hydroxide that is adsorbed on ruthenium can then be oxidized to adsorbed hydroxide or oxide, completing the catalytic cycle. One important consequence of this proposed transition state is that the second electron transfer event becomes decoupled from the rate determining step. Indeed, the transfer coefficients for the platinum-ruthenium adatom catalysts approach values that are close to 0 at intermittent coverages by ruthenium adatoms. This decrease in the transfer coefficient indicates that the rate determining process does not involve the transfer of an electron.

5.4 Conclusion

Platinum-ruthenium black is more active than platinum black at low potentials towards the oxidation of 2-propanol; however, the mode of this catalytic enhancement is not well understood. This chapter has made an attempt at



Scheme 5.4: Proposed transition state complex for the rate determining step during the oxidation of 2-propanol over platinum-ruthenium adatom catalysts.

elucidating this enhancement using platinum-ruthenium adatom catalysts that have well defined ratios of platinum and ruthenium on the surface. Variable temperature LSV was used to probe the reaction's dependence on temperature and potential, and a novel multidimensional regression was used to treat all of the data simultaneously. To the best of my knowledge, such multidimensional analysis has never been reported on experimental electrochemical data. The results of the regression give key thermodynamic and electrokinetic parameters, such as the enthalpy of activation (ΔH^\ddagger), the apparent potential independent rate constant ($k_{apparent}^0$), and the transfer coefficient (α).

From these parameters, it was found that ruthenium is essentially inactive towards the oxidation of 2-propanol at high potentials, likely due to the formation of strongly adsorbed oxygen species which are known to be inactive towards the oxidation of alcohols. A linear trend in ($k_{apparent}^0$) versus surface composition indicates that platinum is the active site for the oxidation of 2-propanol, and that at high coverages of ruthenium the reaction becomes rate

limited by the destructive adsorption of 2-propanol.

For platinum-ruthenium adatom catalysts, a linear trend exists between the surface composition and the activation enthalpy of the oxidation of 2-propanol. Platinum black does not follow this trend. Extrapolation of the linear trend reveals that the activation enthalpy over platinum in platinum-ruthenium adatom catalysts is lowered by 9 kJ mol^{-1} ; this value is consistent with the enthalpy of a hydrogen bonding interaction between 2-propanol and a surface oxide that was reported by Gale et al.^[41] To account for this extra stabilization in the rate determining step, a transition state was proposed where the adsorbed $(\text{CH}_3)_2\text{C}^*\text{OH}$ moiety is hydrogen bonded to a ruthenium-oxide, or ruthenium-hydroxide. This complex transfers a proton from the alcohol to the oxide or hydroxide, thereby reducing the oxide/hydroxide and oxidizing the adsorbate in a concerted fashion. The reduced oxide or hydroxide can then be oxidized to regenerate the non-protonated form, and acetone can desorb from the surface. An important consequence of this concerted surface REDOX reaction is that no net flow of electrons is required, and the rate limiting step becomes decoupled from the potential of the electrode. Indeed, it was found that the transfer coefficient approaches a value that is near 0 at moderate coverages of ruthenium and at high potentials, providing evidence for this decoupling. At low potentials, however, the extent of surface oxidation will be potential dependent, with higher concentrations of surface oxides and hydroxides occurring as the potential is increased until all of the ruthenium is oxidized. In this region low potential region, the rate of the reaction will be dependent on the potential of the electrode, insofar as it defines the extent of ruthenium oxidation. This interpretation is consistent with the potential dependence of the reaction rate at low potentials over platinum ruthenium

adatom catalysts, and on platinum-ruthenium bulk alloys (see Chapter 4).

The proposed mode of promotion by the ruthenium oxygen species is, in a way, different from the classical bifunctional effect. In the bifunctional mechanism for the oxidation of methanol over platinum-ruthenium, surface oxygen species that are formed on ruthenium are incorporated into the product carbon dioxide molecule.^[43] In the mode of promotion proposed in this study, the ruthenium oxygen species acts as proton acceptor during the rate determining loss of an alcoholic proton, reducing the ruthenium oxygen species and liberating the product. To the best of the author's knowledge, this is the first report of such a mode of catalytic enhancement by the bifunctional mechanism. These intriguing results warrant further investigations.

References

- [1] Chrzanowski, W.; Kim, H.; Wieckowski, A., Enhancement in methanol oxidation by spontaneously deposited ruthenium on low-index platinum electrodes. *Catalysis Letters* **1998**, *50* (1/2), pp. 69–75.
- [2] Spendelow, J.; Babu, P.; Wieckowski, A., Electrocatalytic oxidation of carbon monoxide and methanol on platinum surfaces decorated with ruthenium. *Curr. Opin. Solid. St. M.* **2005**, *9* (1-2), pp. 37–48.
- [3] Crown, A.; Moraes, I. R.; Wieckowski, A., Examination of Pt(111)/Ru and Pt(111)/Os surfaces: STM imaging and methanol oxidation activity. *Journal of Electroanalytical Chemistry* **2001**, *500* (1-2), pp. 333–343.
- [4] Tremiliosi-Filho, G.; Kim, H.; Chrzanowski, W.; Wieckowski, A.; Grzybowska, B.; Kulesza, P., Reactivity and activation parameters in methanol oxidation on platinum single crystal electrodes 'decorated' by ruthenium adlayers. *Journal of Electroanalytical Chemistry* **1999**, *467* (1-2), pp. 143–156.
- [5] Waszczuk, P.; Solla-Gullón, J.; Kim, H. S.; Tong, Y. Y.; Montiel, V.; Aldaz, A.; Wieckowski, A., Methanol Electrooxidation on Platinum/Ruthenium Nanoparticle Catalysts. *J Catal* **2001**, *203* (1), pp. 1–6.

- [6] Maillard, F.; Lu, G. Q.; Wieckowski, A.; Stimming, U., Ru-Decorated Pt Surfaces as Model Fuel Cell Electrocatalysts for CO Electrooxidation. *J Phys Chem B* **2005**, *109* (34), pp. 16 230–16 243.
- [7] Herrero, E.; Feliu, J. M.; Wieckowski, A., Scanning Tunneling Microscopy Images of Ruthenium Submonolayers Spontaneously Deposited on a Pt(111) Electrode. *Langmuir* **1999**, *15* (15), pp. 4944–4948.
- [8] Chrzanowski, W.; Wieckowski, A., Surface structure effects in platinum/ruthenium methanol oxidation electrocatalysis. *Langmuir* **1998**, *14* (8), pp. 1967–1970.
- [9] Chrzanowski, W.; Wieckowski, A., Ultrathin Films of Ruthenium on Low Index Platinum Single Crystal Surfaces: An Electrochemical Study. *Langmuir* **1997**, *13* (22), pp. 5974–5978.
- [10] Crown, A.; Wieckowski, A., Scanning tunneling microscopy investigations of ruthenium- and osmium-modified Pt(100) and Pt(110) single crystal substrates. *Phys Chem Chem Phys* **2001**, *3* (16), pp. 3290–3296.
- [11] Tong; Kim, H. S.; Babu, P. K.; Waszczuk, P.; Wieckowski, A.; Oldfield, E., An NMR Investigation of CO Tolerance in a Pt/Ru Fuel Cell Catalyst. *J Am Chem Soc* **2002**, *124* (3), pp. 468–473.
- [12] Park, K.-W.; Choi, J.-H.; Kwon, B.-K.; Lee, S.-A.; Sung, Y.-E.; Ha, H.-Y.; Hong, S.-A.; Kim, H.; Wieckowski, A., Chemical and Electronic Effects of Ni in Pt/Ni and Pt/Ru/Ni Alloy Nanoparticles in Methanol Electrooxidation. *J Phys Chem B* **2002**, *106* (8), pp. 1869–1877.
- [13] Cao, D.; Bergens, S. H., An organometallic deposition of ruthenium adatoms on platinum that self poisons at a specific surface composition. A direct methanol fuel cell using a platinum–ruthenium adatom anode catalyst. *Journal of Electroanalytical Chemistry* **2002**, *533* (1-2), pp. 91–100.
- [14] Cao, D.; Bergens, S. H., Pt-Ru adatom nanoparticles as anode catalysts for direct methanol fuel cells. *J Power Sources* **2004**, *134* (2), pp. 170–180.
- [15] Cao, D., A nonelectrochemical reductive deposition of ruthenium adatoms onto nanoparticle platinum: anode catalysts for a series of direct methanol fuel cells. *Electrochim Acta* **2003**, *48* (27), pp. 4021–4031.
- [16] Lee, C. E.; Bergens, S. H., Deposition of Ru Adatoms on Pt Using Organometallic Chemistry: Catalysts for Electrooxidation of MeOH and Adsorbed Carbon Monoxide. *J Phys Chem B* **1998**, *102* (1), pp. 193–199.
- [17] Lee, C.; Bergens, S. H., Deposition of Ru adatoms on Pt using organometallic chemistry: Electro-oxidation of methanol, ethanol, 1,2-ethanediol, and

- D-glucose over a Pt-Ruads surface optimized for oxidation of methanol. *J Electrochem Soc* **1998**, *145* (12), pp. 4182–4185.
- [18] Pastor, E.; Gonzalez, S.; Arvia, A. J., Electroreactivity of Isopropanol on Platinum in Acids Studied by DEMS and FTIRS. *J Electroanal Chem* **1995**, *395* (1-2), pp. 233–242.
- [19] Green, C.; Kucernak, A., Determination of the platinum and ruthenium surface areas in platinum-ruthenium electrocatalysts by underpotential deposition of copper. 2: Effect of surface composition on activity. *J Phys Chem B* **2002**, *106* (44), pp. 11 446–11 456.
- [20] Biegler, T.; Rand, D. A. J.; Woods, R., Limiting Oxygen Coverage on Platinized Platinum - Relevance to Determination of Real Platinum Area by Hydrogen Adsorption. *Journal of Electroanalytical Chemistry* **1971**, *29* (2), pp. 269–277.
- [21] Kim, H.; de Moraes, R.; Tremiliosi-Filho, G.; Haasch, R.; Wieckowski, A., Chemical state of ruthenium submonolayers on a Pt(111) electrode. *Surf Sci* **2001**, *474* (1-3), pp. L203–L212.
- [22] Folkesso, B., Esca Studies on Charge-Distribution in Some Dinitrogen Complexes of Rhenium, Iridium, Ruthenium, and Osmium. *Acta Chem Scand* **1973**, *27* (1), pp. 287–302.
- [23] Vanysek, P., Introduction to impedance. University of Calgary **1994**.
- [24] Bard, A. J.; Faulkner, L. R., *Electrochemical Methods*. Fundamentals and Applications, Hoboken, NJ: John Wiley & Sons, inc, **2001**.
- [25] Standard Thermodynamic Properties of Chemical Substances. In *CRC Handbook of Chemistry and Physics*, Haynes, W. M., ed., Boca Raton, FL: CRC Press/Taylor and Francis, **2010**.
- [26] Jones, E.; Oliphant, T.; Peterson, P.; others, SciPy: Open source scientific tools for Python **2001**.
- [27] Wagner, C. D.; Naumkin, A. V.; Kraut-Vass, A.; Allison, J. W.; Powell, C. J.; Rumble Jr., J. R., NIST Standard Reference Database 20, Version 3.5: NIST X-ray Photoelectron Spectroscopy Database **2007**, URL <http://srdata.nist.gov/xps/Default.aspx>.
- [28] Hammond, J. S.; Winograd, N., XPS spectroscopic study of potentiostatic and galvanostatic oxidation of Pt electrodes in H₂SO₄ and HClO₄. *Journal of Electroanalytical Chemistry* **1977**, *78* (1), pp. 55–69.
- [29] Hammer, B.; Nørskov, J., Theoretical surface science and catalysis-calculations and concepts. *Adv Catal* **2000**, *45*, pp. 71–129.

- [30] Greeley, J.; Stephens, I.; Bondarenko, A.; Johansson, T.; Hansen, H.; Jaramillo, T.; Rossmeisl, J.; Chorkendorff, I.; Nørskov, J., Alloys of platinum and early transition metals as oxygen reduction electrocatalysts. *Nat Chem* **2009**, *1* (7), pp. 552–556.
- [31] Stamenkovic, V. R.; Fowler, B.; Mun, B. S.; Wang, G.; Ross, P. N.; Lucas, C. A.; Markovic, N. M., Improved oxygen reduction activity on Pt₃Ni(111) via increased surface site availability. *Science* **2007**, *315* (5811), pp. 493–497.
- [32] Lima, F.; Zhang, J.; Shao, M.; Sasaki, K.; Vukmirovic, M.; Ticianelli, E.; Adzic, R., Catalytic activity - d-band center correlation for the O₂ reduction reaction on platinum in alkaline solutions. *J Phys Chem C* **2007**, *111* (1), pp. 404–410.
- [33] Toda, T.; Igarashi, H.; Uchida, H.; Watanabe, M., Enhancement of the electroreduction of oxygen on Pt alloys with Fe, Ni, and Co. *J Electrochem Soc* **1999**, *146* (10), pp. 3750–3756.
- [34] Paulus, U.; Wokaun, A.; Scherer, G.; Schmidt, T.; Stamenkovic, V.; Radmilovic, V.; Markovic, N.; Ross, P., Oxygen reduction on carbon-supported Pt-Ni and Pt-Co alloy catalysts. *J Phys Chem B* **2002**, *106* (16), pp. 4181–4191.
- [35] Koper, M.; Shubina, T.; van Santen, R., Periodic density functional study of CO and OH adsorption on Pt-Ru alloy surfaces: Implications for CO tolerant fuel cell catalysts. *J Phys Chem B* **2002**, *106* (3), pp. 686–692.
- [36] Iwasita, T.; Nart, F.; Vielstich, W., FTIR study of the catalytic activity of a 85: 15 Pt. Ru alloy for methanol oxidation. *Ber Bunsen Phys Chem* **1990**, *94* (9), pp. 1030–1034.
- [37] Frelink, T.; Visscher, W.; van Veen, J., Measurement of the Ru surface content of electrocodeposited PtRu electrodes with the electrochemical quartz crystal microbalance: Implications for methanol and CO electrooxidation. *Langmuir* **1996**, *12* (15), pp. 3702–3708.
- [38] Hayes, J. R.; Zeller, D.; Friesen, C., The Influence of Platinum Surface Morphology on the Electrooxidation of Methanol in Alkaline Solutions. In *ECS Trans*, ECS, **2008**, pp. 41–54.
- [39] Tripković, A. V.; Popović, K. D.; Lović, J. D., The influence of the oxygen-containing species on the electrooxidation of the C₁–C₄ alcohols at some platinum single crystal surfaces in alkaline solution. *Electrochim Acta* **2001**, *46* (20-21), pp. 3163–3173.

- [40] Hao Yu, E.; Scott, K.; Reeve, R. W., A study of the anodic oxidation of methanol on Pt in alkaline solutions. *Journal of Electroanalytical Chemistry* **2003**, *547* (1), pp. 17–24.
- [41] Gale, R.; Haber, J.; Stone, F., Adsorption calorimetry on granulated catalysts. A study of adsorption processes relating to isopropanol dehydrogenation. *J Catal* **1962**, *1* (1), pp. 32–38.
- [42] Gasteiger, H. A.; Markovic, N.; Ross Jr, P. N.; Cairns, E. J., Temperature-dependent methanol electro-oxidation on well-characterized Pt-Ru alloys. *J Electrochem Soc* **1994**, *141* (7), pp. 1795–1803.
- [43] Watanabe, M.; Motoo, S., Electrocatalysis by ad-atoms part II. Enhancement of the oxidation of methanol on platinum by ruthenium ad-atoms. *Journal of Electroanalytical Chemistry* **1975**, *60* (3), pp. 267–273.

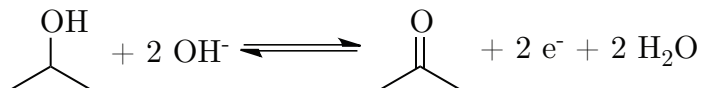
Chapter 6

Prototype alkaline direct 2-propanol fuel cell using platinum-ruthenium adatom catalyst

6.1 Introduction

As demonstrated in Chapter 3, the Alkaline Direct 2-Propanol Fuel Cell (AD2PFC) performs better than the Alkaline Direct Methanol Fuel Cell (ADMFC), presumably due to fewer strongly adsorbed intermediates forming on the surface during the oxidation, such as carbon monoxide. This rationale is consistent with the mechanistic data discussed in detail in §§1.3 and 2.1; specifically, methanol forms carbon monoxide as an intermediate during the oxidation of methanol,^[1-4] and it strongly inhibits the catalytic oxidation of methanol. 2-propanol, however, does not form carbon monoxide as an intermediate,^[5,6] but rather forms acetone as the final product of the oxidation in acidic^[5-10] and in alkaline^[11,12] electrolytes. Only small amounts of carbon dioxide have been observed, and it is believed that the dominant pathway is the dehydrogenation of 2-propanol to acetone (Scheme 6.1). Carbon dioxide reacts in stoichiometric side reactions with hydroxide, producing carbonates

that reduce the ionic conductivity of the electrolyte.



Scheme 6.1: Electrochemical oxidation of 2-propanol to acetone in alkaline media.

Platinum-ruthenium black is more active under steady-state conditions than platinum-black, and has a lower onset potential for the oxidation. As discussed in Chapter 4, the lower onset potential is proposed to result from the oxidation of the H_{UPD} monolayer at lower potentials on platinum-ruthenium black, initiating the destructive adsorption of 2-propanol at lower potentials. Indeed, Vannice et al.^[13] has shown that 2-propanol will not destructively adsorb onto platinum surfaces that are covered by hydrides in Ultra High Vacuum (UHV) environments, providing support for this proposal.

The promoting effect of surface ruthenium towards the oxidation of 2-propanol was explored in Chapter 5. It was found that oxidized ruthenium was inactive towards the destructive adsorption of 2-propanol, and that platinum is likely the site of destructive adsorption to form adsorbed $(\text{CH}_3)_2\text{C}^*\text{OH}$ or related species. The differences in the activation enthalpy between platinum and platinum-ruthenium adatom catalysts for the rate determining elimination of this species is lower for platinum-ruthenium adatoms catalysts with low coverages of ruthenium, by an amount that is consistent with a hydrogen bonding interaction. It was proposed that this extra stabilization of the transition state results from a hydrogen bonding interaction between the alcoholic proton of the adsorbate, and an adsorbed oxide or hydroxide.

The prevalence of metallic ruthenium, ruthenium oxides, and hydroxides, will be a function of the electrode potential. The study discussed in Chapter 5

could not resolve the complexities of the low potential region due to the evolving nature of the system under Linear Sweep Voltammogram (LSV) conditions. Here, this low potential region is characterized using similar platinum-ruthenium adatom electrodes under potential-step conditions. Further, this platinum-ruthenium adatom electrode will be fabricated into an operating prototype fuel cell, to see how the ruthenium adatom catalysts compare to the ruthenium-free catalysts.

6.2 Experimental

6.2.1 General

Nitrogen (Praxair, prepurified), hydrogen (Praxair, prepurified), oxygen (Praxair), KMnO_4 (Fisher, ACS grade), KOH (Caledon, reagent grade), and RuCl_3 hydrate (Aithaca Chemical Corp.) were used as received. Water from an in-house distilled water line was distilled a second time, and then distilled from alkaline KMnO_4 . 2-propanol (Fisher Scientific, suitable for electronic use) was freshly distilled before use. ESNS electrodes (silver plated nickel screen, 1.5 mg cm^{-2} platinum loading using 10% platinum on Vulcan XC-72) were pretreated as outlined in §§6.2.2, 6.2.3, and 6.2.4. All 3-electrode experiment potentials are reported versus the Reference Hydrogen Electrode (RHE), and all Fuel Cell (FC) experiments are reported as the cell potential. Measurements are not iR compensated.

6.2.2 Preparation of platinum-ruthenium adatom electrodes

Platinum-ruthenium adatom electrodes were prepared using the procedure discussed in §5.2.2, with the exception the 1 cm^2 piece of the ESNS electrode material (silver plated nickel screen, 1.5 mg cm^{-2} platinum loading using 10% platinum on Vulcan XC-72) was used in place of platinum black. Briefly, the electrode was first cleaned with 10 cm^{-3} of 3 vol% H_2O_2 , and maintained in the remaining water. The reactor was then purged with nitrogen for ca. 20 min, and then with nitrogen diluted hydrogen for ca. 20 min, and then with pure hydrogen for ca. 20 min to fully reduce the electrocatalyst and form a M–H monolayer. Excess hydrogen was flushed from the reactor by purging with nitrogen for ca. 5 min, and then freshly made RuCl_3 aqueous solution (3 mg RuCl_3) was cannula transferred into the reactor and maintained under a nitrogen atmosphere at bubbler pressure for 1 h. The electrode with rinsed several times triply distilled water, and its activity towards the oxidation of 2-propanol was investigated as outlined in 6.2.3.

After performing the 3-electrode experiments, deposition of ruthenium repeated as outline above on the same piece of the modified ESNS electrode material. The substrate was not, however, cleaned with 3% H_2O_2 between the electrochemical characterization and the addition of ruthenium. This deposition / electrochemical-characterization procedure was repeated several times to give electrodes with progressively higher loadings of ruthenium adatom on the surface.

6.2.3 Electrochemical characterization of platinum ruthenium adatom electrodes

Electrochemical experiments were performed using the setup described in §2.2.1. The working electrode was a 1 cm² ESNS electrode (silver plated nickel screen, 1.5 mg cm⁻² platinum loading using 10% platinum on Vulcan XC-72) that ruthenium adatoms had been deposited onto. Prior to the collection of any electrochemical data, the electrode was conditioned in a 1 mol dm⁻³ KOH / 1 mol dm⁻³ 2-propanol electrolyte at 60 °C by reducing the electrode at -0.1 V for 5 mins. Potential step experiments were then performed for 15 min per potential step, between 0 and 0.4 V, at 12.5 mV increments. Between the potential step experiments, the electrode was conditioned for 2 min at -0.1 V).

6.2.4 Operation of alkaline direct 2-propanol fuel cell using a platinum-ruthenium adatom anode

The fuel cell hardware was the same as that used in §3.2.3, and the cell was conditioned in a similar manner as before. Specifically, the electrodes were first conditioned under in 1 mol dm⁻³ KOH by sweeping its potential between -0.5 and 0.5 V at 5 mV s⁻¹ until a stable response was observed (ca. 60 cycles). The cathode was a 1.5 mg_{Pt} cm⁻² ESNS electrode, and the anode was either a 1.5 mg_{Pt} cm⁻² ESNS electrode or a PtRu_{adatom} electrode prepared using the procedures described in 6.2.3.

In the operating Direct 2-propanol Fuel Cell (D2PFC), the electrolyte was a 5 mol dm⁻³ potassium hydroxide solution at 70 °C; 100% 2-propanol was supplied to the anode compartment at 0.5 cm³ min⁻¹ and at room temperature. Dry oxygen was supplied to the cathode compartment at 300 cm³ min⁻¹ and at

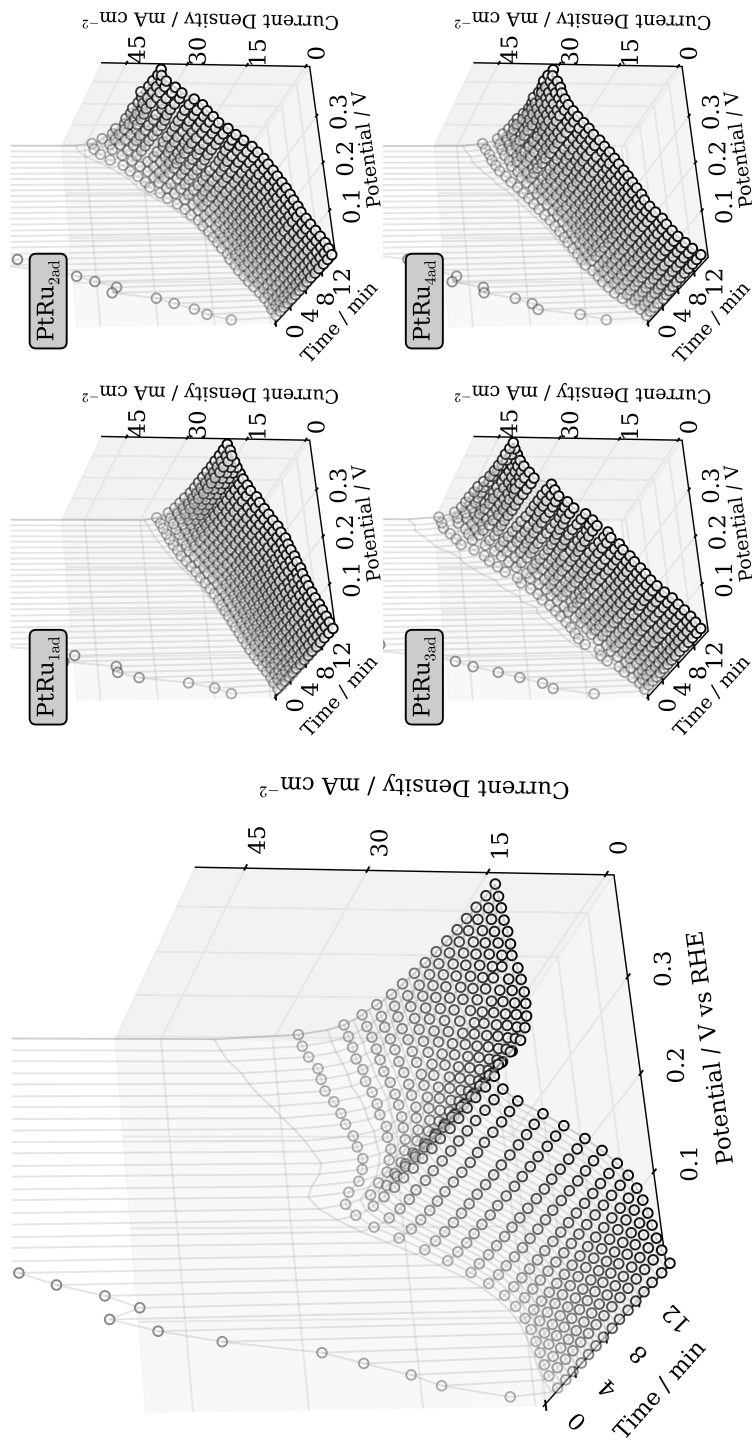
room temperature. Polarization curves were collected by stepping the current density using a logarithmic scale, to a maximum of 0.5 V cell potential. The cell potential was allowed to equilibrate for 30 s at each current density before recording the cell potential.

6.3 Results and discussion

Figure 6.1 shows the potential-time-current profile for the oxidation of 1 mol dm^{-3} 2-propanol in 1 mol dm^{-3} KOH over a series of ESNS electrodes that have progressively increasing amounts of ruthenium on the surface. The electrodes were prepared by the reductive deposition method reported by Cao and Bergens.^[14] In this procedure, ruthenium is reductively deposited from aqueous RuCl_3 by oxidizing a monolayer of H_{UPD} . This preparation scheme is designed to be self-limiting, with the deposition ceasing when the H_{UPD} is consumed. This deposition can be repeated iteratively, to produce catalysts with progressively higher loadings of ruthenium. For comparison, Figure 6.1 also shows the same set of experiments using the as-received platinum electrode. The electrochemical activity of the material changes significantly upon a single addition of ruthenium to the surface of the electrode. Specifically, the onset potential for the oxidation of 2-propanol is shifted to potentials that are only 12 mV above the RHE, and the activity of the catalyst at potentials lower than 0.125 V, or higher than 0.25 V, is significantly enhanced. Unlike the behaviour of the as-received platinum electrode, however, the low-potential current maximum is no longer observable. The absence of the current maximum is somewhat surprising, as it is observed for bulk platinum-ruthenium alloy catalysts (see Figure 4.5, p. 129). The apparent disappearance of the current maximum indicates that the mechanism of the reaction has changed. Further,

the higher current densities at low potentials indicates that the platinum-ruthenium adatom catalysts are more active than carbon supported platinum catalysts towards the oxidation of 2-propanol.

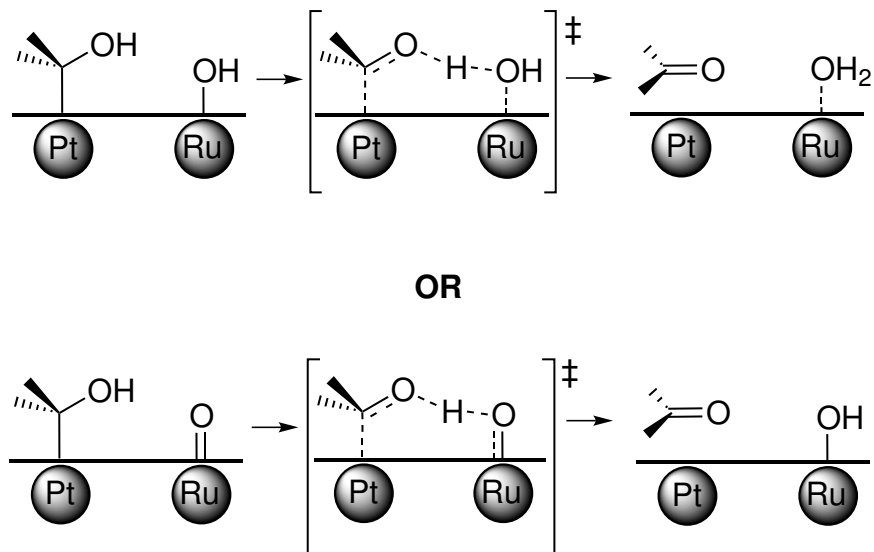
The first three additions of ruthenium to the catalyst increases its activity between 0 and 0.4 V. Upon the fourth deposition of ruthenium, however, the activity of the catalyst below 0.2 V continues to increase, but the activity above 0.2 V begins to decline. This behaviour is consistent with two different mechanisms occurring between 0.2 and 0.4 V; one that predominates at low potentials, and another or possibly both mechanisms operating at higher potentials. As discussed previously (see §4.1 and Chapter 5), oxidized ruthenium is inactive towards the oxidation of 2-propanol. At high coverages of ruthenium, and at potentials near 0.4 V, the reduced activity of these platinum-ruthenium adatom catalysts towards the oxidation of 2-propanol is consistent with the dilution of platinum, which is the active site responsible for the destructive adsorption of 2-propanol. At lower potentials, however, the activity of the catalyst is enhanced by ruthenium. This catalytic enhancement is consistent with a cooperative effect between the platinum and ruthenium sites during the oxidation of 2-propanol. As discussed in Chapter 5, this cooperative effect is believed to be a hydrogen bonding interaction between the adsorbed $(\text{CH}_3)_2\text{C}^*\text{OH}$ intermediate, and either a ruthenium oxide or a ruthenium hydroxide species (Scheme 6.2). The prevalence of these ruthenium species will be dependent on the extent that the surface is oxidized, and is therefore linked to the potential of the experiment. These oxides and hydroxides, although inactive towards the destructive adsorption of 2-propanol, enhance the rate determining step, and there is an optimum platinum:ruthenium ratio of the surface.



(a) Platinum electrode

(b) Platinum-ruthenium adatom electrode

Figure 6.1: (a) Current-time-potential profiles for the half-cell oxidation of 1 mol dm^{-3} 2-propanol / 1 mol dm^{-3} KOH over a 1.5 mgPt cm^{-2} ESNS electrode, and (b) the same study with progressively increasing amounts of ruthenium adatoms on the surface of the electrode. $T = 60 \text{ }^\circ\text{C}$.



Scheme 6.2: Proposed transition state complex for the rate determining step during the oxidation of 2-propanol over platinum-ruthenium adatom catalysts.

In addition to the kinetic factors discussed above, platinum-ruthenium surfaces also differ in their H_{UPD} stripping behaviour (Chapter 4). It has been shown that 2-propanol does not destructively adsorb onto a platinum surface that is covered by a monolayer of H_{UPD} .^[13] Further, the changes in the H_{UPD} stripping behaviour of platinum, platinum-ruthenium, and ruthenium blacks appear to correlate well with the onset potential for the oxidation of 2-propanol. The lower onset potential for the oxidation of 2-propanol over these platinum-ruthenium adatom electrodes is consistent with a reduction in the coverage of the electrode by H_{UPD} at lower potentials, facilitating the destructive adsorption of 2-propanol at lower potentials than over pure platinum.

Upon inspection of the current-time transients of platinum and of platinum-ruthenium adatom catalysts, it is also clear that the stability of the current-time transient is increased with the addition of ruthenium. Figure 6.2 shows the samples current voltammogram at 0.5, 3, 7.5 and 15 mins. As can be seen in these plots, the platinum-ruthenium catalysts reach a quasi-steady state

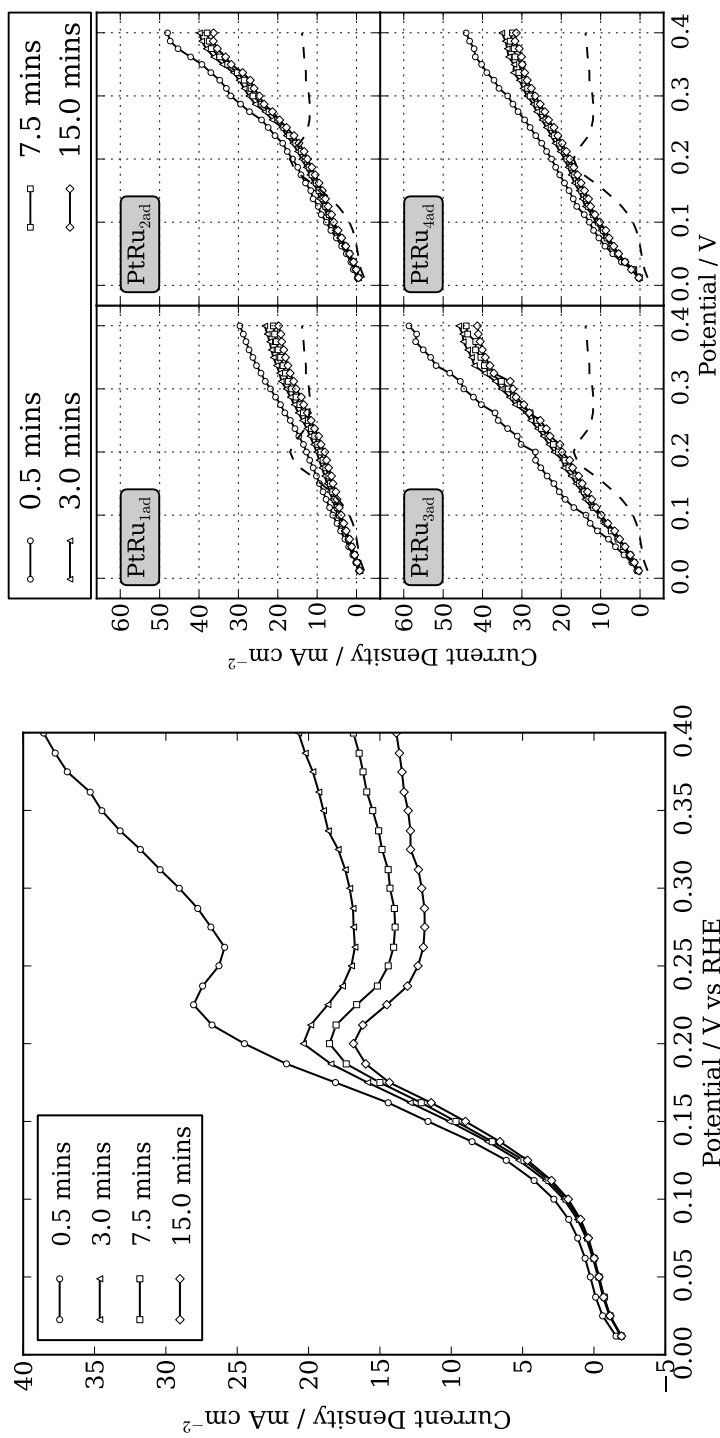
at relatively short times compared with platinum black. At high potentials, the current density of the platinum electrode is decreasing over time even after 7.5 min of oxidation, while the platinum-ruthenium adatom catalysts appear to be quite stable. This increase in stability is consistent with a decrease in the time dependence of the adsorbate coverage on the surface of the catalysts. As the reaction proceeds, platinum-ruthenium adatom catalysts have fewer adsorbates than platinum catalysts. In the case of the oxidation of 2-propanol, the adsorbate is believed to be acetone (see §§1.3.3.2 and 2.1.3); however, in Chapter 5 it was proposed that the rate-determining step is the oxidation of adsorbed $(\text{CH}_3)_2\text{C}^*\text{OH}$. The increased stability of the current-time transients suggest that the accumulation of adsorbed acetone, adsorbed $(\text{CH}_3)_2\text{C}^*\text{OH}$, or intermediates from the deeper oxidation of acetone to carbon dioxide is decreased on the platinum-ruthenium adatom electrodes. In chapter 5, it was proposed that ruthenium adatom catalysts enhance the oxidation of $(\text{CH}_3)_2\text{C}^*\text{OH}$ to acetone, and it follows that this enhancement will also decrease the prevalence of $(\text{CH}_3)_2\text{C}^*\text{OH}$ on the surface; however, this enhancement will also increase the amount of acetone at the electrode-electrolyte interface. It is therefore plausible that the adsorption strength of acetone is decreased on the platinum-ruthenium adatom catalysts (i.e., an electronic effect). Indeed, platinum-ruthenium adatom catalysts are known to form weaker bonding interactions with carbon monoxide.^[15-17] The synergistic bonding interaction in $\text{Pt}-\text{CO}$ and $\text{Pt}-(\eta^2-\text{Acetone})$ are somewhat similar; there is ligand to metal σ -type bonding, and metal to ligand π -type bonding. The similarity in the bonding, and the fact that the $\text{Pt}-\text{CO}$ bond strength is weaker on platinum-ruthenium surfaces, suggests that the $\text{Pt}-(\eta^2-\text{Acetone})$ bond may also be weaker on platinum-ruthenium adatom surfaces. Detailed studies on

the adsorption characteristics of acetone on these types of surfaces are required in order to explore this possibility. Finally, ruthenium is known to facilitate the oxidation of strongly bound intermediates to carbon dioxide by the bifunctional mechanism. It is also possible that the increased stability is due the removal of strongly bound intermediates formed during the deeper oxidation of acetone.

To see if the kinetic enhancements observed in the sampled current voltammetry equates to a higher performance AD2PFC, a prototype AD2PFC was constructed using the platinum-ruthenium adatom electrode as the anode. For this prototype cell, the anode chosen was made from the platinum-ruthenium adatom electrode with three depositions of ruthenium. The electrode was found to give the highest activity in the three-electrode experiments discussed previously. Figure 6.3 shows the performance of the AD2PFC using this anode, and using the as-received platinum substrate.

The polarization of the AD2PFC is significantly improved when the anode is replaced with the platinum-ruthenium adatom catalysts. First, at current densities just above 0 mA cm^{-1} , the cell potential is higher with the platinum-ruthenium adatom anode. This high potential at low current densities is consistent with the lower onset potential for the oxidation of 2-propanol over platinum-ruthenium adatom catalysts (see Figure 6.1). The higher current densities at potentials between the cell's Open Circuit Voltage (OCV) and 0.5 V is also consistent with the higher activity of the platinum-ruthenium adatom catalyst seen in Figure 6.1.

The current density at 0.5 V is significantly increased, by 32%, from 34.7 to 45.8 mA cm^{-2} . The improved polarization characteristics using the platinum ruthenium adatom anode increases the power density of the fuel cell by 41%, from 15.9 to 22.4 mW cm^{-2} . This significant increase in the power density of



(a) Platinum electrode

(b) Platinum-ruthenium adatom electrodes

Figure 6.2: Sampled current voltammograms at 0.5 (○), 3 (△), 7.5 (□) and 15 min (◇) for (a) the platinum electrode shown in Figure 6.1a, and (b) the platinum-ruthenium adatom electrodes shown in Figure 6.1b.

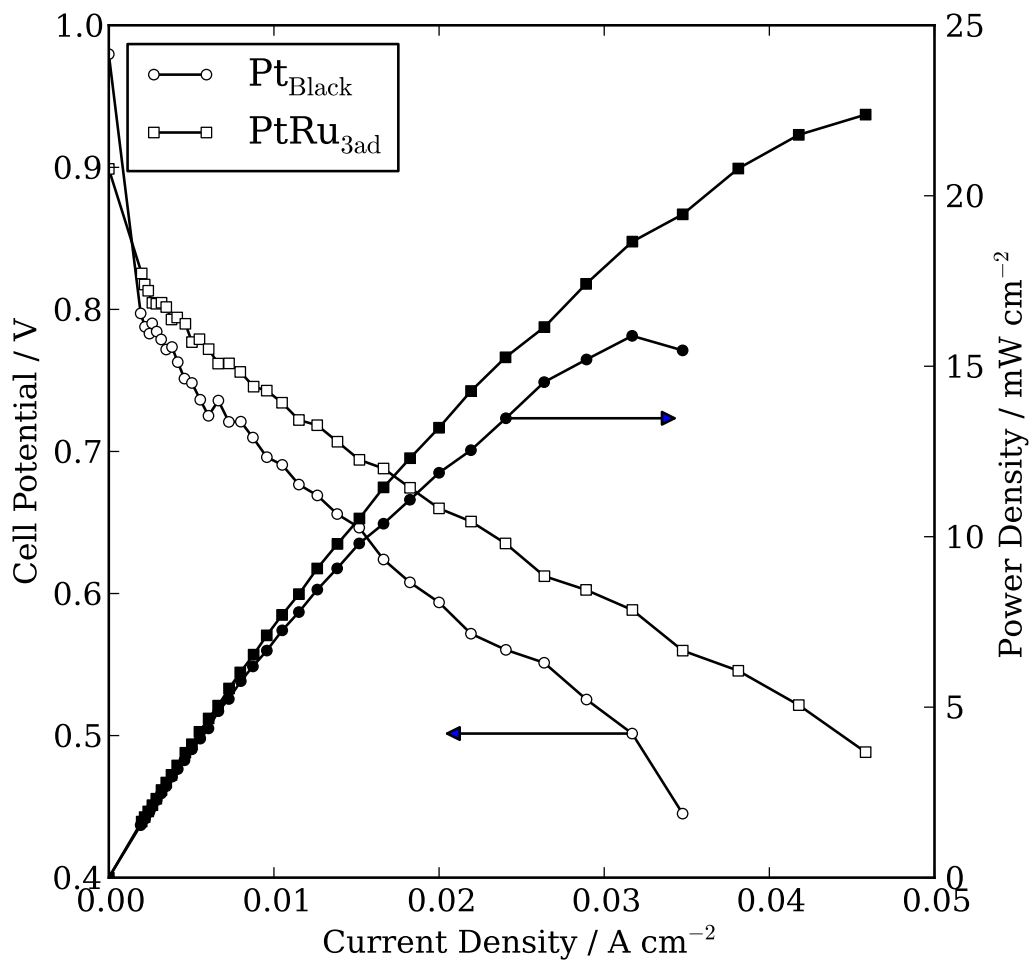


Figure 6.3: Polarization (\square, \circ) and power (\blacksquare, \bullet) curves for the same alkaline fuel cell 100% 2-propanol with either a $1.5 \text{ mg}_{\text{Pt}} \text{ cm}^{-2}$ ESNS anode (\circ, \bullet), or with the PtRu_3 additions anode (\square, \blacksquare). Temperature = 70°C ; alcohol flow rate = 0.5 mL min^{-1} ; dry $\text{O}_2 = 300 \text{ sccm}$; cathode = $1.5 \text{ mg}_{\text{Pt}} \text{ cm}^{-2}$ ESNS electrode.

the cell confirms that platinum-ruthenium adatom catalysts are superior to platinum only catalysts in the AD2PFC.

6.4 Conclusion

The low potential chronoamperometric oxidation of 2-propanol over platinum is enhanced by the addition of ruthenium adatoms to the surface of the catalysts. Using three-dimensional (potential,time) versus current plots, it was demonstrated that addition of ruthenium decrease the onset potential for the oxidation, and it also significantly improves the rate near 0.5 V. The lowered onset potential is consistent with the catalyst comparisons reported in Chapter 4, where it was proposed that addition of ruthenium, resulting in the oxidation of H_{UPD} at lower potentials, facilitates the destructive adsorption of 2-propanol at lower potentials. 2-propanol will not destructively adsorb onto H_{UPD} covered surfaces. Further, the enhanced rate of oxidation is consistent with a promoting effect by surface ruthenium. In Chapter 5, it was proposed that the rate determining step is the oxidation of adsorbed $(CH_3)_2C^*OH$ to acetone, and that ruthenium facilitates its oxidation by forming a hydrogen bonding interaction between the alcoholic proton and a ruthenium oxide or hydroxide, stabilizing the transition state and thereby increasing the rate of oxidation. Increasing the amount of ruthenium will increase the amount of ruthenium oxygen species present on the surface, and increase the likelihood of this hydrogen bonding interaction and thereby increase the kinetic rate of the oxidation.

Upon a fourth addition of ruthenium and at potentials near 0.5 V, the activity of the catalyst declines. The reduction in the rate of the reaction is consistent with the inactivity of oxidized ruthenium towards the destructive

adsorption of 2-propanol, and the decrease in activity is believed to result from a dilution of the platinum site which is the active site for the destructive adsorption. At low potentials, where the ruthenium is only partially oxidized, the fourth addition of ruthenium results in a more active catalyst; this increase is consistent with the promoting effect discussed above.

The higher activity of the platinum-ruthenium adatom catalyst results in significant increases in the performance characteristics of the AD2PFC. Indeed, the current density at 0.5 V cell potential increased by 32%, from 34.7 to 45.8 mA cm⁻², and the power density increased by 41%, from 15.9 to 22.4 mW cm⁻². This increase in performance results from the lowered onset potential for the oxidation of 2-propanol, and from the increased kinetic rate of oxidation.

The experiments are different from those presented in Chapter 5, as these chronoamperometry experiments allow the reaction to reach steady-state conditions, versus the LSV experiments which are changing and evolving over time.

References

- [1] Caram, J. A.; Gutiérrez, C., Cyclic voltammetric and potential-modulated reflectance spectroscopic study of the electroadsorption of methanol and ethanol on a platinum electrode in acid and alkaline media. *Journal of Electroanalytical Chemistry* **1992**, *323* (1-2), pp. 213–230.
- [2] Morallon, E.; Rodes, A.; Vázquez, J. L.; Pérez, J. M., Voltammetric and in-situ FTIR spectroscopic study of the oxidation of methanol on Pt (hkl) in alkaline media. *J Electroanal Chem* **1995**, *391* (1-2), pp. 149–157.
- [3] Spendelow, J. S.; Goodpaster, J. D.; Kenis, P. J. A.; Wieckowski, A., Methanol Dehydrogenation and Oxidation on Pt(111) in Alkaline Solutions. *Langmuir* **2006**, *22* (25), pp. 10 457–10 464.

- [4] Christensen, P.; Hamnett, A.; Linares-Moya, D., Oxygen reduction and fuel oxidation in alkaline solution. *Phys Chem Chem Phys* **2011**, *13* (12), pp. 5206–5214.
- [5] Leung, L.-W. H.; Chang, S.-C.; Weaver, M. J., Real-time FTIR spectroscopy as an electrochemical mechanistic probe. Electrooxidation of ethanol and related species on well-defined Pt (111) surfaces. *Journal of Electroanalytical Chemistry* **1989**, *266* (2), pp. 317–336.
- [6] Pastor, E.; Gonzalez, S.; Arvia, A. J., Electroreactivity of Isopropanol on Platinum in Acids Studied by DEMS and FTIRS. *J Electroanal Chem* **1995**, *395* (1-2), pp. 233–242.
- [7] Reis, R.; Martins, C.; Camara, G., The Electrooxidation of 2-Propanol: An Example of an Alternative Way to Look at In Situ FTIR Data. *Electrocatal* **2010**, *1* (2-3), pp. 1–6.
- [8] Sun, S.-G.; Lin, Y., Kinetics of isopropanol oxidation on Pt(111), Pt(110), Pt(100), Pt(610) and Pt(211) single crystal electrodes - Studies of in situ time-resolved FTIR spectroscopy. *Electrochim Acta* **1998**, *44* (6-7), pp. 1153–1162.
- [9] Sun, S.; Lin, Y., FTIR spectroscopic investigations of reaction mechanism of isopropanol oxidation on platinum single crystal electrodes. *Electrochim Acta* **1996**, *41* (5), pp. 693–700.
- [10] Gao, P.; Chang, S.-C.; Zhou, Z.; J Weaver, M., Electrooxidation pathways of simple alcohols at platinum in pure nonaqueous and concentrated aqueous environments as studied by real-time ftir spectroscopy. *Journal of Electroanalytical Chemistry* **1989**, *272* (1-2), pp. 161–178.
- [11] Santasalo-Aarnio, A.; Kwon, Y.; Ahlberg, E.; Kontturi, K.; Kallio, T.; Koper, M. T. M., Comparison of methanol, ethanol and iso-propanol oxidation on Pt and Pd electrodes in alkaline media studied by HPLC. *Electrochem Commun* **2011**, *13* (5), pp. 466–469.
- [12] Lin, H.; Chen, G.; Zheng, Z.; Zhou, J.; Chen, S.; Lin, Z., The adsorption and oxidation of isopropanol at platinum electrode in alkaline media. *Acta Phys-Chim Sin* **2005**, *21* (11), pp. 1280–1284.
- [13] Vannice, M. A.; Erley, W.; Ibach, H., A RAIRS and HREELS Study of Isopropyl-Alcohol on Pt(111). *Surf Sci* **1991**, *254* (1-3), pp. 12–20.
- [14] Cao, D.; Bergens, S. H., Pt-Ruadatom nanoparticles as anode catalysts for direct methanol fuel cells. *J Power Sources* **2004**, *134* (2), pp. 170–180.

- [15] Babu, P. K.; Kim, H. S.; Oldfield, E.; Wieckowski, A., Electronic Alterations Caused by Ruthenium in PtRu Alloy Nanoparticles as Revealed by Electrochemical NMR. *J Phys Chem B* **2003**, *107* (31), pp. 7595–7600.
- [16] Iwasita, T.; Nart, F.; Vielstich, W., FTIR study of the catalytic activity of a 85: 15 Pt. Ru alloy for methanol oxidation. *Ber Bunsen Phys Chem* **1990**, *94* (9), pp. 1030–1034.
- [17] Maillard, F.; Gloaguen, F.; Hahn, F.; Leger, J. M., Electrooxidation of Carbon Monoxide at Ruthenium–Modified Platinum Nano-particles: Evidence for CO Surface Mobility. *Fuel Cells* **2002**, *2* (34), pp. 143–152.

Chapter 7

Conclusions and future work

The Direct Alcohol Fuel Cell (DAFC) is a promising method for the production of energy from energy-rich hydrocarbon fuels. The efficiency that a DAFC harnesses the energy content of this fuel is a key concern if the DAFC is ever to become commercially viable. Typically, the acidic electrolyte DAFC has platinum-ruthenium at the anode, and platinum at the cathode. The reason for the predominance of platinum is its exceptionally high activity compared with other metals. The prohibitively high cost of platinum, however, remains a key hurdle that must be overcome if DAFC technology is ever to become commercially viable.

The Alkaline Fuel Cell (AFC) has several advantages over the acidic Fuel Cell (FC). Potentially the most attractive is that the cathodic reaction can be catalyzed by metals that are significantly cheaper than platinum, such as nickel, silver, and iron cobalt alloys. Further, the oxidation kinetics of many alcohols are known to be faster in base than in acid. One of the largest shortcomings of the AFC, however, is that they are intolerant towards carbon dioxide. Carbon dioxide is a byproduct of the oxidation of many alcohols, and will gradually carbonate the electrolyte in an Alkaline Direct Alcohol Fuel

Cell (ADAFC). Carbonation of the electrolyte significantly decreases the performance characteristics of the FC, and should be avoided.

2-propanol is an interesting candidate for use in an ADAFC. First, the major product formed during its oxidation is acetone, which will not react with the electrolyte in a stoichiometric side reaction, consuming the electrolyte. Second, the oxidation of 2-propanol to form acetone proceeds via a mechanism that does not involve the formation of strongly adsorbed species, and therefore proceeds at high kinetics rates and low overpotentials. This increase in kinetic rate results in an increase in the efficiency of the Alkaline Direct 2-Propanol Fuel Cell (AD2PFC) relative to the Alkaline Direct Methanol Fuel Cell (ADMFC), the latter of which produces adsorbed carbon monoxide as a surface stable poison.

In the preceding chapters it was shown that the oxidation of 2-propanol at low potentials is more facile in an alkaline electrolyte than in an acidic electrolyte, and a well defined low-potential current-maximum was observed during the steady-state oxidation of the fuel (Chapter 2). Perhaps even more important was that the activity of platinum towards the oxidation of 2-propanol within this potential range was significantly higher than its activity towards the oxidation of methanol. A prototype AD2PFC was shown to outperform the ADMFC under comparable conditions (Chapter 3), consistent with the higher activities observed in three-electrode experiments.

A brief study of platinum, platinum-ruthenium, and ruthenium blacks found that the low-potential maximum in stabilized-current density occurred over all three of these catalysts (Chapter 4). The onset potential for the oxidation was also found to decrease as the amount of ruthenium in the catalysts increased. It was proposed that this decrease in the onset potential resulted the oxidation of

H_{UPD} at lower potentials. 2-propanol will not destructively adsorb onto hydride covered surfaces. The magnitude of the low-potential maximum in stabilized-current density was significantly different between these three catalysts, with platinum-ruthenium giving current densities that were approximately three times higher than those observed for platinum.

The source of this catalytic enhancement was studied by Linear Sweep Voltammogram (LSV) using catalysts with well defined ratios of platinum and ruthenium on the surface (Chapter 5). A novel approach to the treatment of the temperature dependant electrokinetic data was implemented, where both of the independent variables were treated simultaneously using multidimensional regression. This treatment simultaneously gave the enthalpy of activation (ΔH^\ddagger), the apparent potential-independent rate constant (k_{apparent}^0), and the transfer coefficient (α), from a single model of the data. From the thermodynamic and electrokinetic parameters, it was proposed that the active site for the destructive adsorption of 2-propanol was platinum. Surface ruthenium was found to decrease the activation enthalpy of the rate determining step by an amount that is consistent with a hydrogen bonding interaction that is not present on platinum. A transition state complex was proposed to account for this stabilization, where an oxygen on ruthenium hydrogen bonds with the alcoholic proton of the adsorbed $(\text{CH}_3)_2\text{C}^*\text{OH}$ intermediate. The proton is then transferred to the ruthenium-oxygen species, producing acetone as a product and reducing the ruthenium-oxygen species. The reduced ruthenium-oxygen species is then oxidized, completing the catalytic cycle. This proposal has significant implications on the field of ruthenium promoted oxidation of alcohols. It is a new mode by which the bifunctional mechanism promotes the oxidation of an alcohol, and warrants further investigations. Additionally, this

mode of catalytic enhancement may be present using cheaper oxophilic metals such as tin, manganese, cerium, titanium, iron, cobalt, nickel, or copper, and they should be explored as promoters for the oxidation of 2-propanol.

Chapter 6 explored the utility of platinum-ruthenium adatom catalysts in an operating AD2PFC. It was found that the enhanced activity of these platinum-ruthenium adatom catalysts at low potentials results in higher power densities in the AD2PFC. In fact, the power density at 0.5 V cell potential increased by over 40% relative to the the platinum only cell. Further, three-electrode experiments showed that there is an optimum platinum:ruthenium surface ratio to achieve high current densities, and improved stability.

7.1 Future Work

Future work on the investigations presented throughout this thesis should focus on:

1. Validating of the multidimensional analysis used to determine the kinetic and thermodynamic parameters of electrochemical reactions. Specifically, well studied reactions (such as the REDOX chemistry of $\text{Ru}(\text{NH}_3)_6^{3+}$, $\text{Fe}(\text{CN})_6^{3-}$, or Ferrocene) should be investigated using the techniques developed in Chapter 5. The parameters obtained from the multidimensional analysis should then be compared with those currently accepted for the appropriate REDOX system.
2. The AD2PFC should be further investigated using an anion exchange membrane electrolyte. These systems should be thoroughly characterized in terms of their total efficiency, and net energy density. The long term stability of the AD2PFC should be evaluated, and the final product from

the oxidation of 2-propanol in alkaline electrolytes should be verified spectroscopically.

3. The mechanistic investigations for the oxidation of 2-propanol in alkaline electrolyte should be expanded to acidic electrolytes. Specifically, multidimensional analysis of the variable temperature oxidation of 2-propanol in acid using well defined platinum-ruthenium surfaces should be investigated.
4. Continuation of the mechanistic investigations for the oxidation of 2-propanol in alkaline electrolyte should focus on the exploration of alternative catalyst that are more cost effective than platinum, possibly palladium. Further, oxide supports based on tin, manganese, cerium, titanium, iron, cobalt, or nickel should be tested.
5. The possible influence of changes to the catalyst electronic structure must be determined. To this end, fully reduced platinum-ruthenium catalysts must be characterized by Ultraviolet Photoelectron Spectroscopy (UPS).
6. Detailed mechanistic investigations using single-crystal electrodes with different ratios of platinum and ruthenium on the surface should be carried out. Using these types of electrodes, the morphology of the deposited ruthenium (i.e., islands vs well-dispersed) can be more conclusively established using Scanning Tunneling Microscope (STM), and a detailed model of the electrokinetics that accounts for the different types of sites ($\text{Pt}_{\text{island}}$, $\text{Ru}_{\text{island}}$, $\text{PtRu}_{\text{island interface}}$, and $\text{PtRu}_{\text{dispersed}}$) should be developed.